

**FOULING AND ITS MITIGATION ON HEAT
EXCHANGER SURFACES BY ADDITIVES AND
CATALYTIC MATERIALS**

TENG KAH HOU

**A thesis submitted in partial fulfillment of the requirements
of Liverpool John Moores University for the degree of Doctor
of Philosophy**

**This research programme was carried out in collaboration
with University of Malaya, Malaysia**

June 2018

ORIGINAL LITERARY WORK DECLARATION

I, **TENG KAH HOU**, declare that this thesis titled, “FOULING AND ITS MITIGATION ON HEAT EXCHANGER SURFACES BY ADDITIVES AND CATALYTIC MATERIALS” and the work presented in it are my own. I confirm that:

- This work was done wholly or mainly while in candidature for a research degree at this University.
- Where any part of this thesis has previously been submitted for a degree or any other qualification at this University or any other institution, this has been clearly stated.
- Where I have consulted the published work of others, this is always clearly attributed.
- Where I have quoted from the work of others, the source is always given. With the exception of such quotations, this thesis is entirely my own work.
- I have acknowledged all main sources of help.
- Where the thesis is based on work done by myself jointly with others, I have made clear exactly what was done by others and what I have contributed myself.

Signed:



Date : 31 May 2018

FOULING AND ITS MITIGATION ON HEAT EXCHANGER SURFACES BY ADDITIVES AND CATALYTIC MATERIALS

ABSTRACT

Calcium carbonate (CaCO_3) fouling is the most commonly observed fouling phenomenon in cooling water applications. Fouling happens when a process uses cooling water supersaturated with mineral salt crystals (i.e. hard water). Precipitation deposits on heat transfer surfaces whenever these inversely-soluble salt crystals, like dissolved calcium ions, are exposed to high temperature. An online-monitoring system for fouling phenomena was studied experimentally using a mixture of sodium bicarbonate and calcium chloride for carbonate fouling salt in de-ionized water. The effects of different parameters such as surface temperature, flow velocity, and concentration on the calcium carbonate scale formation process were experimentally investigated by using the developed monitoring system. The calcium carbonate deposition rates on five different metal surfaces (Stainless steel 316, brass, copper, aluminum and carbon steel) were investigated. The surface was analyzed by analytical microscopy to investigate the morphology of the deposit layer. The results revealed that SS316 yielded the lowest deposition on the surface. Nowadays, hazardous chemical additives are often used to mitigate fouling but chemicals are expensive and pose problems to the environment. Physical water treatment (PWT), a non-chemical method is good alternative for fouling mitigation method. PWT using zinc and tourmaline as catalytic materials is presented in this research work. Fouling tests were conducted for verification of this PWT method. Artificially-hardened water at 300 mgL^{-1} was utilized as the fluid medium to form fouling deposits. The hard water flow velocities were varied from 0.15 ms^{-1} to 0.45 ms^{-1} and the artificially-hardened water temperature was maintained at $25 \text{ }^\circ\text{C}$ and the experimental time was set to 72 hours for each run. The results revealed that in the PWT-treatment case, the deposition of calcium carbonate particle is lower compared to those in the No-treatment case. Furthermore, mitigation of

calcium carbonate fouling by applying EDTA, EDTA-MWCNT and DTPA-MWCNT-based water nanofluids on heat exchanger surfaces were reported. Investigation of additive (benign to the environment) on the fouling rate of deposition was performed. Assessment of the deposition of calcium carbonate on the heat exchanger surfaces with respect to the inhibition of crystal growth was conducted by Scanning Electron Microscope (SEM). The results showed that the formation of calcium carbonate crystals can be retarded significantly by adding MWCNT-DTPA additives as inhibition in the solution. Moreover, investigation was extended by introducing a non-invasive-monitoring of concentrations of calcium hardness in cooling water. Investigation was conducted with a 2.5 GHz microwave cavity resonator. The principle of electric dipole moment theories were used to analyse the sample solution that occurs as a function of calcium ion content. The sample was centrally positioned in the electric field of the TM_{010} mode of a resonant cylindrical cavity. COMSOL simulation package was used to compare and validate the experimental cavity resonator frequency. Transmission signal (S_{21}) measurements via Vector Network Analyser (VNA) with different concentrations were investigated and observed linear relationship in amplitude with frequency changes. These research successfully introduce a novel technique of monitoring of water hardness concentration by using non-invasive microwave sensor.

ACKNOWLEDGEMENTS

First and foremost, I wish to express my sincere gratitude to my supervisors, Assoc. Prof. Kazi Md. Salim Newaz and Dr. Chew Bee Teng from University of Malaya, Malaysia, Prof. Ahmed Al. Shamma'a and Prof. Andy Shaw from Liverpool John Moores University, for all their invaluable advice and guidance of this research project and thesis. Working with them has been a fruitful learning and research experience.

I would also like to thank our research team in Malaysia, Ir. Dr. Abu Bakar Mahat, Dr. M.N.M. Zubir, Dr. Solangi Khalid, Dr. Samira Gharehkhani for their help on experimental design, and valuable suggestions. I would like to thank to my colleague Dr. Ahmad Amiri for his help on preparation of nanofluids and fruitful suggestions, which I experienced in all steps of my study. In addition, I would like to thank BEST research team in LJMU for all the support for sensor research, Dr. Patryk Kot, Mr. Vijahkumar, Dr. Montse, Prof. David Phillips and Dr. Mo. A final word of thank goes to all my lab mates over the past three and a half years. The writing of this thesis had been the most challenging undertaking of my life to date. I could not have completed this work without the support and help of many people. Special thanks to University of Malaya, High Impact Research (MOHE-HIR) grant (UM.C/625/1/HIR/MOHE/ENG/45-(D000046-16001), UMRG RP012A-13AET, PPP grant (PG109-2015A) and Institute Postgraduate Studies Units for Dual-PhD program, for providing the financial support and laboratory facilities.

Last but not the least, deepest thanks are extended to my family and my love Pick Khee for their support, encouragement and motivation throughout my PhD journey. They have encouraged me to achieve the best, and their support and faith in me during my hard times.

TABLE OF CONTENTS

ORIGINAL LITERARY WORK DECLARATION	ii
ABSTRACT	iii
ACKNOWLEDGEMENTS	v
TABLE OF CONTENTS	vi
LIST OF FIGURES	xii
LIST OF TABLES	xvii
LIST OF SYMBOLS AND ABBREVIATIONS	xviii
LIST OF APPENDICES	xx
CHAPTER 1: INTRODUCTION	1
1.1 Background of Study	1
1.1.1 Hard Water Characteristic	1
1.1.2 Sources of Water Hardness	1
1.1.3 Measurement & Classification of Water Hardness	2
1.1.4 Heat Exchangers	3
1.1.5 Fouling in Heat Exchangers	4
1.1.6 Cost Imposed Due to Fouling	4
1.1.7 Overall View of Fouling Effect to Industry	7
1.1.8 Current Technology Cleaning of Heat Exchanger	8
1.1.9 Potential and Application of Functionalize Nanofluids as Fouling Mitigation Approach	11
1.2 Problem Statements	12
1.3 Research Questions	12
1.4 Objectives of the Presented Research	12
1.5 Contribution of the Study	14
1.6 Layout of Thesis	15
CHAPTER 2: LITERATURE REVIEW	16
2.1 Background	16
2.2 Basic Principle of Fouling Mechanisms	18
2.2.1 Crystallization Fouling	18
2.2.2 Particulate Fouling	19
2.2.3 Chemical Reaction Fouling	19
2.2.4 Corrosion Fouling	19
2.2.5 Biological Fouling	20

2.3	Theoretical Background of Fouling.....	20
2.3.1	Solid Crystals.....	20
2.3.2	Fouling Process	21
2.3.3	Fouling Curve	25
2.3.4	Mechanism Scale Formation Process.....	27
2.3.5	Overview of Scale Deposition Formation on Surface.....	34
2.4	Fouling on Heat Exchanger Surfaces	34
2.4.1	Deposition of Calcium Carbonate	35
2.4.2	Scale Formation of Calcium Carbonate	36
2.4.3	Process Parameter Affecting Fouling.....	37
2.4.4	Previous Work of Fouling on Heat Exchanger.....	41
2.5	Fouling Mitigation and Control.....	43
2.5.1	Chemical Methods.....	44
2.5.2	Mechanical Methods	46
2.5.3	Physical Water Treatment	47
2.6	Summary.....	48
CHAPTER 3:	INSTRUMENT AND EXPERIMENTAL SETUP FOR FOULING ON DOUBLE PIPE HEAT EXCHANGER.....	49
3.1	Analysis Methods	49
3.1.1	Scanning Electron Microscopy (SEM).....	49
3.1.2	Energy Dispersive X-Ray Spectroscopy (EDS).....	50
3.1.3	X-Ray Powder Diffraction	50
3.1.4	Transmission Electron Microscopy.....	51
3.1.5	Fourier Transform Infrared Spectroscopy	53
3.1.6	Electric Conductivity.....	53
3.1.7	Surface Roughness Measurement.....	54
3.1.8	Electronic Weighting Balance	54
3.1.9	KD2-Pro	55
3.2	Description of the Experiment.....	57
3.2.1	Experimental System.....	57
3.2.2	Design and Construction	60
3.2.3	Test Section	60
3.2.4	Reservoir Tank	61
3.2.5	Magnetic Gear Pump.....	62

3.2.6	Inverter	63
3.2.7	Electromagnetic Flow Meter	64
3.2.8	Differential Pressure Transducers	65
3.2.9	Cooling Unit	67
3.2.10	Heater	69
3.2.11	Power Control.....	70
3.2.12	Thermocouple.....	71
3.2.13	SCADA & Programmable Logic Controller	72
3.2.14	Data Logging System	74
3.2.15	Calcium Hardness Detection	75
3.3	Data Reduction, Calibration, Experimental Work, Observation and Analysis	76
3.3.1	Experimental System.....	76
3.3.2	Data Reduction – Heat Transfer Coefficient.....	77
3.3.3	Data Reduction – Fouling Resistance.....	78
3.3.4	Weight Deposition Reduction	79
3.3.5	Calcium Hardness Reduction	80
3.4	Summary.....	82
CHAPTER 4: INVESTIGATION OF DOUBLE-PIPE HEAT EXCHANGER FOULING AND FOULING MITIGATION.....		83
4.1	Introduction	83
4.2	Experimental Work	84
4.2.1	Apparatus.....	84
4.2.2	Test Specimens.....	87
4.2.3	Data Acquisition.....	88
4.2.4	Experimental Procedures.....	89
4.2.5	Measurement and Characterization	91
4.3	Results and Discussion.....	91
4.3.1	Data Validation and Reproducibility.....	91
4.3.2	Fouling on Various Surface Materials.....	94
4.3.3	Fouling under Effect of Velocity.....	97
4.3.4	Fouling under Effect of Hot Inlet Temperature.....	98
4.3.5	Fouling under Effect of Concentration.....	100
4.3.6	Visualization of the Fouling Test Section and Crystal Morphology.....	104

4.3.7	Fouling Mitigation by using Catalytic Material	108
4.4	Summary.....	111
CHAPTER 5: NANOFUIDS PREPARATION FOR FOULING MITIGATION, EXPERIMENT AND ANALYSIS		112
5.1	Introduction	112
5.2	Experimental Work	112
5.2.1	Chemical-assisted Functionalization and Preparation of MWCNT- EDTA Water based Nanofluids and MWCNT-DTPA Water based Nanofluids	112
5.2.2	Functionalization Analysis of DTPA-treated MWCNT.....	114
5.2.3	Test Set-up.....	117
5.2.4	Test Specimens	118
5.2.5	Experimental Procedures.....	119
5.2.6	Measurement and Characterization	120
5.2.7	Fouling Characteristics	120
5.3	Results and Discussion	121
5.3.1	Effect Concentration of the EDTA and MWCNT-EDTA.....	121
5.3.2	Effect Concentration of MWCNT-DTPA	123
5.3.3	Fouling Resistance.....	125
5.3.4	Effect of Additives on the Scale Morphology of CaCO ₃ Crystal.....	129
5.3.5	Thermal Analysis.....	132
5.4	Summary.....	134
CHAPTER 6: IMPLEMENTATION OF A NON-INVASIVE SENSOR FOR ASSESSING WATER-HARDNESS IN HEAT EXCHANGERS IN REAL-TIME.....		135
6.1	Introduction	135
6.2	Literature Review	135
6.2.1	Microwave Fundamentals	135
6.2.2	On-line Monitoring of Water Quality.....	136
6.3	Experimental Design and Methodology.....	139
6.3.1	Microwave Theory and Application.....	139
6.3.2	Design of Cylindrical Microwave Cavity Resonator	140
6.3.3	Sample Preparation.....	142
6.3.4	Data Acquisition and Analysis	143

6.3.5	Numerical Simulation.....	144
6.4	Results and Discussion.....	145
6.4.1	Effect of Concentration	145
6.4.2	Effect of Different Cations and Anions in Water Hardness.....	148
6.4.3	Repeatability of the Technique and Validation of the Experiments.....	150
6.5	Numerical Investigation on using EMW Sensor to Detect Water Hardness	151
6.5.1	Introduction	151
6.5.2	Water Hardness Properties	153
6.5.3	Numerical Simulation.....	154
6.5.4	Meshing Validation	155
6.5.5	Material Assignment and Boundary Condition.....	157
6.5.6	Numerical Procedure	157
6.5.7	Results and Discussion.....	158
6.6	Summary.....	162
CHAPTER 7:	TWO PHASE FLOW HEAT TRANSFER AND FOULING EXPERIMENT UNDER NON-BOILING CONDITION.....	164
7.1	Introduction	164
7.2	Literature Review	165
7.2.1	Multiphase Flow Patterns.....	165
7.2.2	Detection of Two-Phase Flow Regimes.....	166
7.3	Description of the Experiment.....	167
7.3.1	Experimental System.....	167
7.3.2	Heat Transfer Test Section	170
7.3.3	Component Used	172
7.4	Results and Discussion.....	177
7.4.1	Test Rig Validation.....	177
7.4.2	Two-Phase Flow Experiment	179
7.4.3	Two-Phase Flow System with Different Regimes	183
7.5	Two Phase Flow Heat Transfer	185
7.5.1	Constant Average Wall Temperature of 45 °C and 0.2 m/s Water Velocity	185
7.6	Two-Phase Flow Fouling	186
7.6.1	Fouling Resistance and Total Deposition.....	186

7.6.2	Visualization of Fouled Test Section	188
7.7	Summary.....	189
CHAPTER 8: CONCLUSIONS AND RECOMMENDATION		190
REFERENCES		194
LIST OF PUBLICATIONS AND PAPERS PRESENTED		210
APPENDIX		212

LIST OF FIGURES

Figure 1.1:	Equilibrium reactions describe the formation/dissolving calcium carbonate scales. (Demény et al., 2016)	2
Figure 1.2:	Classification of industrial heat exchanger. ("Heat Exchangers," 2013)	3
Figure 1.3:	Overall view of fouling effect (H Müller-Steinhagen, Malayeri, & Watkinson, 2011).....	7
Figure 2.1:	Overall views of 5 X 5 matrix of fouling mechanisms.....	16
Figure 2.2:	Fouling processes (S. N. Kazi, Duffy, & Chen, 2010).	22
Figure 2.3:	Net results of a deposition and removal process (Zhao & Chen, 2013).	22
Figure 2.4:	Typical fouling curves (H. Müller-Steinhagen, M. R. Malayeri, & A. Watkinson, 2005).....	26
Figure 2.5:	Effect of temperature on an inverse solubility salt solution (Bott, 1995).	28
Figure 2.6:	Types of nucleation.....	29
Figure 2.7:	Free energy changes associated with homogeneous and heterogeneous mechanism (Brar, France, & Smirniotis, 2001).....	30
Figure 2.8:	Wetting angle (Yuan & Lee, 2013).	31
Figure 2.9:	Overview of scale deposition formation on surfaces (Zahid Amjad, 2007).	34
Figure 2.10:	Solubility of calcium carbonate in water as function of temperature. (Helalizadeh, Müller-Steinhagen, & Jamialahmadi, 2000).	35
Figure 2.11:	Summary of primary chemical scale inhibition mechanism (Nguyen, Roddick, & Fan, 2012).	45
Figure 3.1:	Schematic layout of a scanning electron microscopy (Collett, 2007).....	50
Figure 3.2:	Working principles of XRD (Bunaciu, UdriŞtioiu, & Aboul-Enein, 2015).....	51
Figure 3.3:	Schematic layout of TEM.....	52
Figure 3.4:	Photography of Perkin Elmer-spectrum 100 model FT-IR.....	53
Figure 3.5:	A model of Mitutoyo SJ-210 portable surface roughness tester.....	54
Figure 3.6:	Electronic Weighing Balance.....	55
Figure 3.7:	Schematic Setup of KD2 Thermal Properties Analyser.....	56
Figure 3.8:	Comparison between distilled water and previous data.....	56
Figure 3.9:	Coupons of different materials on heat exchanger surfaces.....	60
Figure 3.10:	Schematic drawing of double pipe heat exchanger with metal pipes located centrally as an inner tube.....	60
Figure 3.11:	Overview dimensions of double pipe heat exchanger.....	61
Figure 3.12:	Jacketed Stainless steel tank of cylindrical shape with a capacity of 40 litres for solution flow tank.....	62
Figure 3.13:	Araki EX-100RM magnetic driven seal-less chemical pump.....	62
Figure 3.14:	Hoffman Muller inverter used to control both pumps' speed.....	63
Figure 3.15:	Photograph of the Electromagnetic flow meter used for cold flow line (left) and hot flow line (right).....	64

Figure 3.16:	Photographs of the Differential Pressure Transducers.....	66
Figure 3.17:	WiseCircu - WCR-P30 Refrigerator Bath Circulator.....	68
Figure 3.18:	Air cooled industrial chiller used in experiment.....	69
Figure 3.19:	Double ended tubular heater immersed in hot tank for heating purposes.....	70
Figure 3.20:	WinCC interface for control and monitoring of the experiments setup.....	70
Figure 3.21:	Photograph of the Thermocouple calibrator.....	72
Figure 3.22:	Thermocouple testing.....	72
Figure 3.23:	Photograph of the PLC system attached with the scada system.....	73
Figure 3.24:	Data logging system for experiment.....	74
Figure 3.25:	Apparatus for EDTA titration.....	75
Figure 3.26:	Colour change from wine red to clear blue.....	75
Figure 3.27:	DR2800 spectrophotometer used to conduct water hardness cuvette test.....	76
Figure 4.1:	Double pipe heat exchanger experimental test rig.....	86
Figure 4.2:	Coupons installation of different materials on heat exchanger surfaces.	87
Figure 4.3:	Composition of catalytic materials composes of zinc and tourmaline.	88
Figure 4.4:	Validation of the experimental run results with standard equations...93	
Figure 4.5:	Reproducibility of the experimental run results under same conditions.....	94
Figure 4.6:	Total depositions on different heat exchanger materials at 50 °C and 25 °C at hot and cold water inlet respectively, 0.15 m/s solution flow and 300 mg/l concentration.....	95
Figure 4.7:	Deposition rate as the function of time on different heat exchanger materials.....	96
Figure 4.8:	Fouling resistances as the function of time based on different heat exchanger materials at 50 °C and 25 °C at hot and solution inlet respectively, 0.15 m/s solution flow velocity and 300 mg/l concentration.....	96
Figure 4.9:	Images of calcium carbonate deposition on different metal surfaces. 97	
Figure 4.10:	Calcium carbonate depositions as the function of time under different velocity conditions on SS316L, 50 °C hot water inlet, 25 °C solution inlet and 300 mg/l concentration.....	98
Figure 4.11:	Total depositions on SS316L under effect of temperature, at 25 °C solution inlet, 0.15 m/s solution flow velocity and 300 mg/l concentration.....	99
Figure 4.12:	Fouling resistance of deposition on SS316L under effect of hot inlet temperature at 25 °C solution inlet, 0.15 m/s solution flow velocity and 300 mg/l concentration.....	99
Figure 4.13:	Fouling resistance of deposition on SS316L under effect of concentration at 50 °C and 25 °C at hot and solution inlet respectively and 0.15 m/s solution flow velocity.	101

Figure 4.14:	Total depositions on SS316L under effect of concentration, at 50 °C and 25 °C at hot and solution inlet respectively and 0.15 m/s solution flow velocity.	101
Figure 4.15:	Image (a) and crystal morphology (b & c) of calcium carbonate formation at 300 mg/l, 50 °C and 25 °C at hot and solution inlet respectively and 0.15 m/s solution flow velocity.	102
Figure 4.16:	Image (a) and crystal morphology (b & c) of calcium carbonate formation at 400 mg/l, 50 °C and 25 °C at hot and solution inlet respectively and 0.15 m/s solution flow velocity.	103
Figure 4.17:	Image (a) and crystal morphology (b & c) of calcium carbonate formation at 500 mg/l, 50 °C and 25 °C at hot and solution inlet respectively and 0.15 m/s solution flow velocity.	103
Figure 4.18:	Deposition on brass material.	104
Figure 4.19:	Deposition on copper material.	105
Figure 4.20:	XRD analyses of the deposited materials.	106
Figure 4.21:	SEM analyses of the deposited materials.	107
Figure 4.22:	SEM and EDS analyses of the deposited materials on carbon steel.....	107
Figure 4.23:	Total deposition of calcium carbonate between PWT and Non-PWT cases.	108
Figure 4.24:	SEM images of 1500x – 10000x of calcium carbonate crystal under non-PWT case.	109
Figure 4.25:	SEM images of 1500x – 10000x of calcium carbonate crystal under PWT case.	110
Figure 4.26:	EDS analysis for calcium carbonate deposition under PWT case.	110
Figure 4.27:	XRD analyses for calcium carbonate deposition under PWT case.	111
Figure 5.1:	Schematic layout functionalization procedure of MWCNT with EDTA.	114
Figure 5.2:	Schematic layout functionalization procedure of MWCNT with DTPA.	114
Figure 5.3:	Fourier transform infrared spectroscopy (FTIR) spectra of MWCNT-OH and DTPA-treated MWCNT.	115
Figure 5.4:	Raman spectra of MWCNT-OH and DTPA-treated MWCNT.	117
Figure 5.5:	TEM images of DTPA-treated MWCNT.	117
Figure 5.6:	Schematic diagram of the experimental set-up.	118
Figure 5.7:	Deposition of fouling under effect of concentration at inlet temperature of 60 °C for EDTA and MWCNT-EDTA.	123
Figure 5.8:	Deposition of fouling and corrosion effect under effect of additives MWCNT-EDTA treatment.	123
Figure 5.9:	Deposition of fouling under effect of concentration at inlet temperature of 60 °C for MWCNT-DTPA.	125
Figure 5.10:	Fouling resistances under influence of EDTA additive at inlet temperature of 60 °C with 300 mg/l CaCO ₃	126
Figure 5.11:	Fouling resistances under influence of additive at inlet temperature of 60 °C with 300 mg/l CaCO ₃	126

Figure 5.12:	Fouling resistances under influence of additive at inlet temperature of 60 °C with 300 mg/l CaCO ₃	128
Figure 5.13:	SEM images of 250–1000x of calcium carbonate crystal under no treatment case.	130
Figure 5.14:	SEM images of 250-1000x of calcium carbonate crystal under effect of 0.015% MWCNT-EDTA.	130
Figure 5.15:	SEM images of 250-1000x of calcium carbonate crystal under effect of 0.015%wt MWCNT-DTPA.....	131
Figure 5.16:	Crystal morphology of CaCO ₃ under effect of 0.03wt% additives concentration.....	132
Figure 5.17:	Crystal morphology of CaCO ₃ under effect of 0.045wt% additives concentration.....	132
Figure 5.18:	Thermal Conductivity of MWCNT-EDTA based water nanofluids at weight concentrations of 0.015, 0.030 and 0.045 %.....	133
Figure 5.19:	Thermal Conductivity of MWCNT-DTPA based water nanofluids at weight concentrations of 0.015, 0.030 and 0.045 %.....	134
Figure 6.1:	Electromagnetic spectrum. (Rao, 2015)	136
Figure 6.2:	EMW cavity resonator measurement system used in experiment. ...	141
Figure 6.3:	COMSOL model of the aluminium cavity resonator showing the distribution of the electric field magnitude in TM ₀₁₀	142
Figure 6.4:	Microwave measurements under different CaCl ₂ concentration.	145
Figure 6.5:	Frequency shifts at varying CaCl ₂ concentrations.....	146
Figure 6.6:	Amplitude changes for varying CaCl ₂ concentration.....	146
Figure 6.7:	Variation of dielectric constants under different concentrations.	147
Figure 6.8:	Variation of dielectric loss under different concentrations of CaCl ₂	148
Figure 6.9:	Frequency spectrum measurements for different chloride based cations.	149
Figure 6.10:	Frequency spectrum measurements for different calcium based anion.....	150
Figure 6.11:	Comparison of simulated and experimental results.....	151
Figure 6.12:	Repetitive of frequency measurements for de-ionized water.	151
Figure 6.13:	Model schematic of the cylindrical cavity.....	155
Figure 6.14:	Different meshes used in this simulation, (a) coarse mesh, (b) normal mesh, (c) fine mesh, and (d) extra fine mesh.....	156
Figure 6.15:	Boundary conditions for the analysed model.	157
Figure 6.16:	Comparison of simulated frequency spectrum data with experimental frequency spectrum data.	158
Figure 6.17:	S ₂₁ spectrum analysis for different hardness concentrations in the solution.....	161
Figure 6.18:	Comparison amplitude changes of simulated and experimental results under effect of different concentration of CaCl ₂	162
Figure 7.1:	Different flow regimes for horizontal flow. (Flouros, Iatrou, Yakinthos, Cottier, & Hirschmann, 2015).....	166
Figure 7.2:	Schematic layout of two-phase flow experimental system.....	167

Figure 7.3:	Schematic representation of the cavity sensor along with the coupling structures.	168
Figure 7.4:	Sectional view of the experimental test section.	171
Figure 7.5:	High temperature heating tapes wrapping around test section for constant heat flux (Edwards & Bindra, 2017).	172
Figure 7.6:	PerfectION combination calcium electrode used in our experimental set-up (Athavale et al., 2017).	173
Figure 7.7:	Peristaltic pumps used to feed chemical to maintain 500 mg/l calcium carbonate concentration throughout experiment.	173
Figure 7.8:	VNA used to analyse the transmitted signal under effect of two-phase and fouling condition.	174
Figure 7.9:	Ni hardware for LabVIEW program.	175
Figure 7.10:	Control panel for constant wall temperature control.	175
Figure 7.11:	Automation chemicals dosing system	176
Figure 7.12:	Validation of heat transfer coefficient with available literature review.	178
Figure 7.13:	Validation of friction factor with available literature review.	178
Figure 7.14:	Repetitive for single phase flow by using EMW sensor.	179
Figure 7.15:	S ₂₁ signal spectrum for different water fractions from 1-6 GHz in 4000 points.	179
Figure 7.16:	S ₂₁ signal spectrum for different water fractions from 2-3 GHz in 4000 points.	180
Figure 7.17:	S ₂₁ signal spectrum for different water fractions from 4.5 - 6 GHz in 4000 points.	180
Figure 7.18:	S ₂₁ spectrum signal under effect of temperature from 2.2 – 2.8 GHz.	181
Figure 7.19:	S ₂₁ spectrum signal under effect of temperature from 5.2-5.9 GHz.	182
Figure 7.20:	Statistical analysis results for different water fraction at 5.45 GHz.	183
Figure 7.21:	3 different flow regimes of plug, semi-slug and slug flow.	183
Figure 7.22:	S ₂₁ signal under effect of 0.2 m/s water velocity and 0.1 m/s air velocity (Plug Flow)	184
Figure 7.23:	S ₂₁ signal under effect of 0.2 m/s water velocity and 0.2 m/s air velocity (Semi-Slug Flow)	184
Figure 7.24:	S ₂₁ signal under effect of 0.2 m/s water velocity and 0.3 m/s air velocity (Slug Flow)	184
Figure 7.25:	Overall Heat Transfer Coefficient against air flow velocity curve.	185
Figure 7.26:	Fouling resistance as the function of time based on different air velocity input at constant $\Delta T = 15\text{ }^{\circ}\text{C}$, 0.2 m/s water flow and 500 mg/l concentration.	186
Figure 7.27:	Total deposition on test section surface under effect of air velocity input, at constant $\Delta T = 15\text{ }^{\circ}\text{C}$, 0.2 m/s water flow and 500 mg/l concentration.	187
Figure 7.28:	Deposition on test section surface under effect of air velocity input [(a) clean pipe surface, (b) 0.0 m/s air velocity & (c) 0.3 m/s air velocity], at constant $\Delta T = 15\text{ }^{\circ}\text{C}$, 0.2 m/s water flow and 500 mg/l concentration	188

LIST OF TABLES

Table 1.1:	Table of standard measurement and classification of water hardness.(Ohara & Reid, 1973)	2
Table 1.2:	Estimated fouling costs incurred in some countries (2005 estimation).....	6
Table 2.1:	Properties of calcite and aragonite. (de Leeuw & Parker, 1998).....	36
Table 2.2:	Summary of mineral fouling research conducted from 1968 to current.	41
Table 3.1:	Specification and errors of the measuring instruments and sensors used in the present experiments.	59
Table 3.2:	A summary of fouling experimental conditions for heat transfer and pressure loss studies.....	59
Table 3.3:	Physical properties of different heat exchanger materials at 300 K. ...	61
Table 3.4:	Specification of the magnetic driven pump.....	63
Table 3.5:	Technical specification for V8 series inverters.....	64
Table 3.6:	Technical specification of Electromagnetic Flow Meter.....	65
Table 3.7:	Flow meter calibration data.	65
Table 3.8:	Standard specification of the Differential Pressure Transducers.....	66
Table 3.9:	Calibration condition.	67
Table 3.10:	Static pressure test.	67
Table 3.11:	Differential pressure test.....	67
Table 3.12:	Specifications of the refrigerated bath.....	68
Table 3.13:	Specification of air cooled industrial chiller.....	69
Table 3.14:	Specification of LCK327 cuvette test.....	82
Table 4.1:	Details of insulated materials.....	85
Table 4.2:	Physical properties and R_a of different heat exchanger materials at 300 K.....	88
Table 5.1:	Fourier transform infrared interpretation of the MWCNT-OH and MWCNT-EDTA.	115
Table 6.1:	List of samples for monitoring and analysis of water hardness.....	142
Table 6.2:	List of samples for monitoring and analysis of anion effects in water hardness.....	143
Table 6.3:	List of samples for monitoring and analysis of cation effects in water hardness.....	143
Table 6.4:	Electric conductivity and permittivity of different water hardness concentrations.	154
Table 6.5:	Relative permittivity, relative permeability and electrical conductivity of aluminum and polyvinyl chloride.....	154
Table 6.6:	Grid independence tests inside an empty cavity for the electromagnetic wave model.....	156
Table 6.7:	Modes formed in the cylindrical cavity and their associated eigen frequencies	159
Table 7.1:	Specification of flexible heating element	172

LIST OF SYMBOLS AND ABBREVIATIONS

DW	Distilled water
od	Inside pipe outer diameter (mm)
id	Inside pipe inner diameter (mm)
OD	External pipe outer diameter (mm)
ID	External pipe inner diameter (mm)
RTD	Resistance temperature detector
PLC	Programmable logic controller
W_s	Weights of the deposited scale (g)
W_f	Weights of the fouled coupon (g)
W_I	Weights of the initial coupon (g)
R_f	Fouling resistance ($m^2.K/W$)
U_{fouled}	Overall heat transfer coefficient for the fouled case ($W.m^{-2}.K^{-1}$)
$U_{initial}$	Overall heat transfer coefficient for the initial case ($W.m^{-2}.K^{-1}$)
Q	Rate of heat gain (W)
A	Total heat transfer surfaces (m^2)
ΔT_{LMTD}	Log mean temperature difference which was determined from the measured temperatures at the inlet and outlet of hot and solution water (K)
$T_{hot,in}$	Temperature at hot inlet (K)
$T_{hot,out}$	Temperature at hot outlet (K)
$T_{cold,in}$	Temperature at cold inlet (K)
$T_{cold,out}$	Temperature at cold outlet (K)
Nu	Nusselt number
Re	Reynolds number
Pr	Prandtl number
f	friction factors
VNA	Vector network analyser
EM	Electromagnetic
EMW	Electromagnetic wave
S_{11}	Reflection coefficient
S_{21}	Transmission coefficient
ϵ'	Dielectric constant
ϵ''	Dielectric loss
f_{nml}	Resonant frequency a TM_{nm0}

c	Velocity of light
μ_r	Relative permeability of the material
ϵ_r	Relative permittivity of the material
D	Depth of the cavity
p_{mn}	m th root of the Bessel function of the n th order
b	Radius of the cavity.
V_c	Volume of cavity resonator
V_s	Volume of under test dielectric sample
f_s	Shifted frequency
Q_{LS}	Q-value for the sample inside the cavity resonator
Q_{L0}	Q-value for the empty cavity resonator loaded with coupling loop
f_0	Resonant frequency
Δf	Bandwidth of the reflection curve
RF	Radio Frequency
TM_{010}	Fundamental operation mode for Transverse Magnetic
S_{21}	Transmission coefficient
Q	Quality factor

LIST OF APPENDICES

- APPENDIX A: PROGRAM-LOGIC-CONTROL (PLC) OVERVIEW AND POWER DISTRIBUTION
- APPENDIX B: DATA ACQUISITION AND CONTROL IN LABVIEW PROGRAM
- APPENDIX C: CLEANING OF THE TEST SECTION

CHAPTER 1: INTRODUCTION

1.1 Background of Study

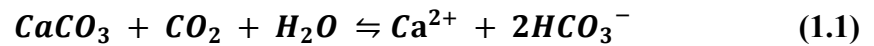
1.1.1 Hard Water Characteristic

Water is the most commonly used cooling fluid in industrial systems, such as in heat exchangers, cooling towers, and boilers. Depending on the quality and availability of fresh water supply, the recirculating cooling water systems contain varying amounts of solids suspended or dissolved, most likely both of them (Karagiannis & Soldatos, 2008). Hard water is water that has high mineral content (in contrast with “soft water”). It’s generally not harmful to one’s health, but can pose serious problems in industrial settings. Therefore, hard water handling is one of the major concerns in industrial environments. A solution of an inverted-solubility salt in contact with a hot surface can attain supersaturation by the inverted solubility effect and deposit scale on the hot surface. It causes serious problems by reducing the heat exchanger’s performance, costly breakdowns in boilers, cooling towers, and other equipment that handles water. Thus, it is important to keep the hardness of cooling water at a lower level to avoid decreasing the performance of the heat exchanger (Vidojkovic et al., 2013).

1.1.2 Sources of Water Hardness

Water’s hardness is determined by the concentration of multivalent cations in the water. Multivalent cations are cations (positively charged metal complexes) with a charge greater than 1+. Usually, the cations have the charge of 2+. Common cations found in hard water include Ca^{2+} and Mg^{2+} . These ions enter a water supply by leaching from minerals within an aquifer (Gros, 2013). Common calcium-containing minerals are calcite and aragonite. A common magnesium mineral is dolomite (which also contains calcium). Rainwater and distilled water are soft, because they only contain few ions

(Thomas, 2010). The following equilibrium reaction describes the dissolving/formation of calcium carbonate (Equation 1.1):



Calcium carbonate scales formed in water-heating systems are called limescale. Figure 1.1 demonstrates the formation and dissolving of calcium carbonate scale.

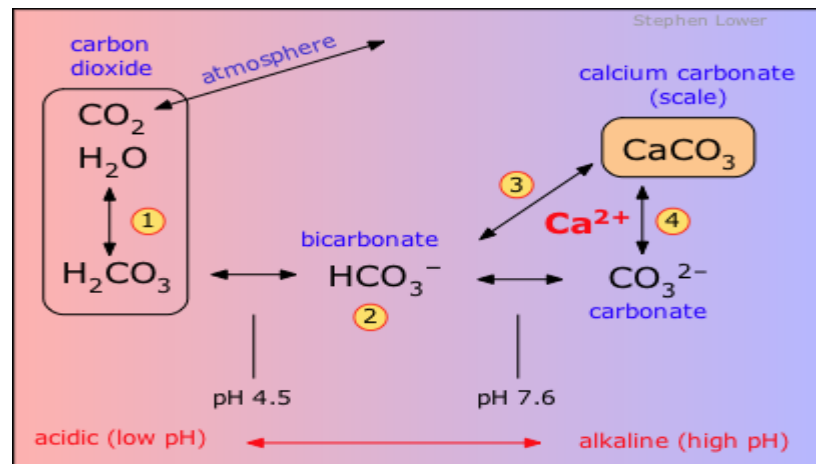


Figure 1.1: Equilibrium reactions describe the formation/dissolving calcium carbonate scales. (Demény et al., 2016)

1.1.3 Measurement & Classification of Water Hardness

Table 1.1 shows the total water hardness in sum of the molar concentrations of Ca²⁺ and Mg²⁺, in mole/L or mmole/L units.

Table 1.1: Table of standard measurement and classification of water hardness.(Ohara & Reid, 1973)

Classification	Hardness in mg/L	Hardness in mmol/L	Hardness in dGH ^o dH
Soft	0-60	0-0.6	0-3.36
Moderately Hard	61-120	0.61-1.2	3.42-6.72
Hard	121-180	1.21-1.80	6.78-10.08
Very Hard	≥181	≥1.81	≥10.14

1.1.4 Heat Exchangers

An industrial heat exchanger is heat-transfer equipment that utilizes a thermal energy exchange process between two or more medium available at different temperatures. Industrial heat exchangers are applied in various industrial applications such as power plant generation, petroleum oil and gas industry, chemical processing plant, transportation, alternative fuels, cryogenics, air conditioning and refrigeration, heat recovery, and other industries. In addition, heat exchangers are the equipment always closely related to our daily life, for example evaporators, air preheaters, automobile radiators, condensers, and oil coolers. In most heat exchangers, a heat-transfer surface separates the fluid which incorporates a wide range of different flow configurations to achieve the desired performance in different applications. Heat exchangers could be classified in many different ways. Generally, industrial heat exchangers have been classified according to construction, transfer processes, degrees of surface compactness, flow arrangements; pass arrangements, phase of the process fluids, and heat-transfer mechanisms as seen in Figure 1.2.

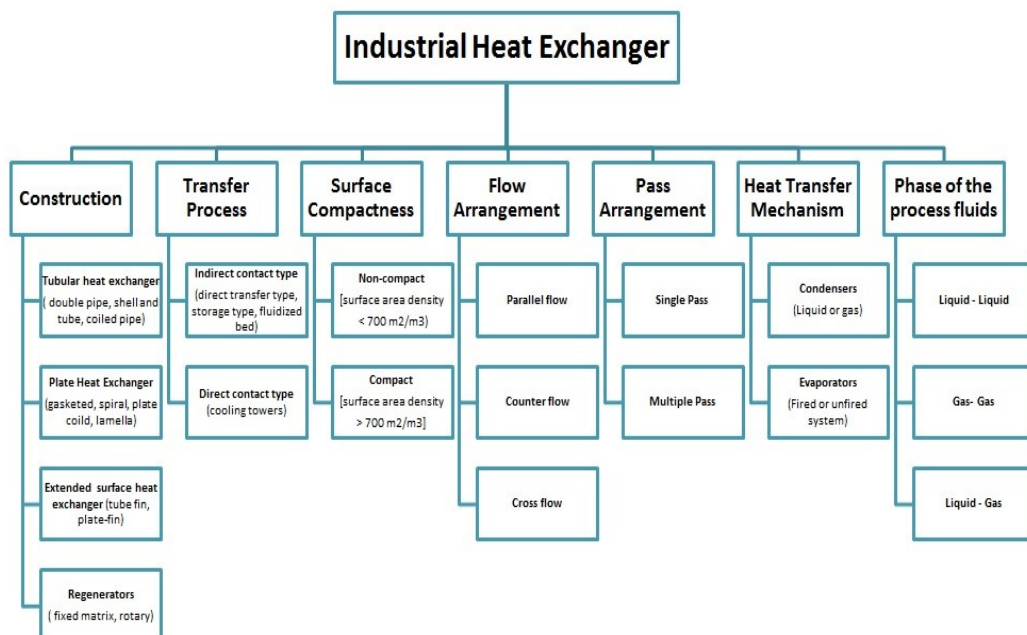


Figure 1.2: Classification of industrial heat exchanger. ("Heat Exchangers," 2013)

1.1.5 Fouling in Heat Exchangers

Fouling can be defined in the simplest way as undesired deposition or sedimentation on heat transfer surfaces which may reduce the effectiveness of the equipment. Thus, the operational capacity is more likely to be negatively affected as well (Hans, 2010). Some of the typical deposits that appear on heat exchanger surfaces are mineral substances such as calcium carbonate (CaCO_3), calcium sulfate (CaSO_4) and calcium silicate (CaSiO_2). These depositions create a layer that is proven to resist the rate of heat transfer in heat exchangers mainly due to the very low thermal conductivity (i.e. $2.9 \text{ Wm}^{-1} \text{ K}^{-1}$) of the mineral salts (Patnaik, 2003). This occurrence decreases efficiency and increases pressure drop and maintenance cost. For those reasons, engineers need to pay heed to the effects of fouling on heat exchangers when designing work is done.

1.1.6 Cost Imposed Due to Fouling

Fouling is ubiquitous and creates tremendous operational losses to industry. As reported in China in 2006, an analysis was reported that the economic loss due to boiler and turbine fouling in its utilities amounted to 4.68 billion USD, which is about 0.169% of the country's GDP (Walker et al., 2012). The loss is initially a consequence of inefficient heat transfer, damage to instrumentation (in particular under-deposit), flow blockages, increased pressure drop, flow redistribution inside components, flow instabilities, premature failure of electrical heating elements, and a large number of other often unanticipated problems.

As an example, "normal" fouls at a conventionally fired 500 MW (net electrical power) power station unit account for output losses of the steam turbine of 5 MW and more (Walker et al., 2012). In a 1,300 MW nuclear power station, typical losses could be 20 MW and up (up to 100% if the station shuts down due to fouling-induced component degradation). In seawater desalination plants, fouling may reduce the gained output ratio by two-digit percentages (the gained output ratio is an equivalent that puts the mass of

generated distillate in relation to the steam used in the process). The extra electrical consumption in compressor-operated coolers is also easily in the two-digit area. In addition to the operational costs, also the capital increases because the heat exchangers have to be designed in larger sizes to compensate for the heat-transfer loss due to fouling. To the output losses listed above, one needs to add the cost of down-time required to inspect, clean, and repair the components (millions of dollars per day of shutdown in lost revenue in a typical power plant), and the cost of actually doing this maintenance. Finally, fouling is often a root cause of serious degradation problems that may limit the life of components or entire plants.

Apart from the high cost imposed by the heat exchanger fouling, the fouling-related costs involved are also reported as the following (Ghaffour, Missimer, & Amy, 2013; Walker et al., 2012):

1. Capital expenditure

Excessive surface area required to overcome the heavy fouling conditions, costs for stronger foundation, provision for extra spaces, extra devices and increased transportation and installation costs.

2. Energy costs

Costs for extra fuel required if fouling leads to extra fuel burning in heat exchanging equipment to overcome the effect of fouling.

3. Maintenance costs

Costs for removal of fouling deposits, costs for chemicals, or other operating costs for antifouling devices.

4. Cost of production loss

Planned or unplanned plant shutdowns due to fouling in heat exchangers can cause large production losses. These losses are often considered to be the main cost of fouling and very difficult to pre-estimate.

5. Extra environmental management cost

Cost of disposing of large amounts of chemical/additives used for fouling mitigation.

Huge fouling costs are reported in different countries. Steinhagen et al. reported about the fouling costs in term of Gross Domestic Product (GDPs) for some countries as presented in Table 1.2 (H. MÜLLer-Steinhagen, M. R. Malayeri, & A. P. Watkinson, 2005).

Table 1.2: Estimated fouling costs incurred in some countries (2005 estimation).

Country	Fouling Cost US \$ million	GDP (1984) US \$ billion	Fouling costs % of GDP
USA	3,860-7,000	3,634	0.12-0.22
	8,000-10,000		0.28-0.35
Japan	3,062	1,225	0.25
West Germany	1,533	613	0.25
UK	700-930	285	0.20-0.33
Australia	260	173	0.15
New Zealand	35	23	0.15
Total Industrial World	26,850	13,429	0.20

1.1.7

Overall View of Fouling Effect to Industry

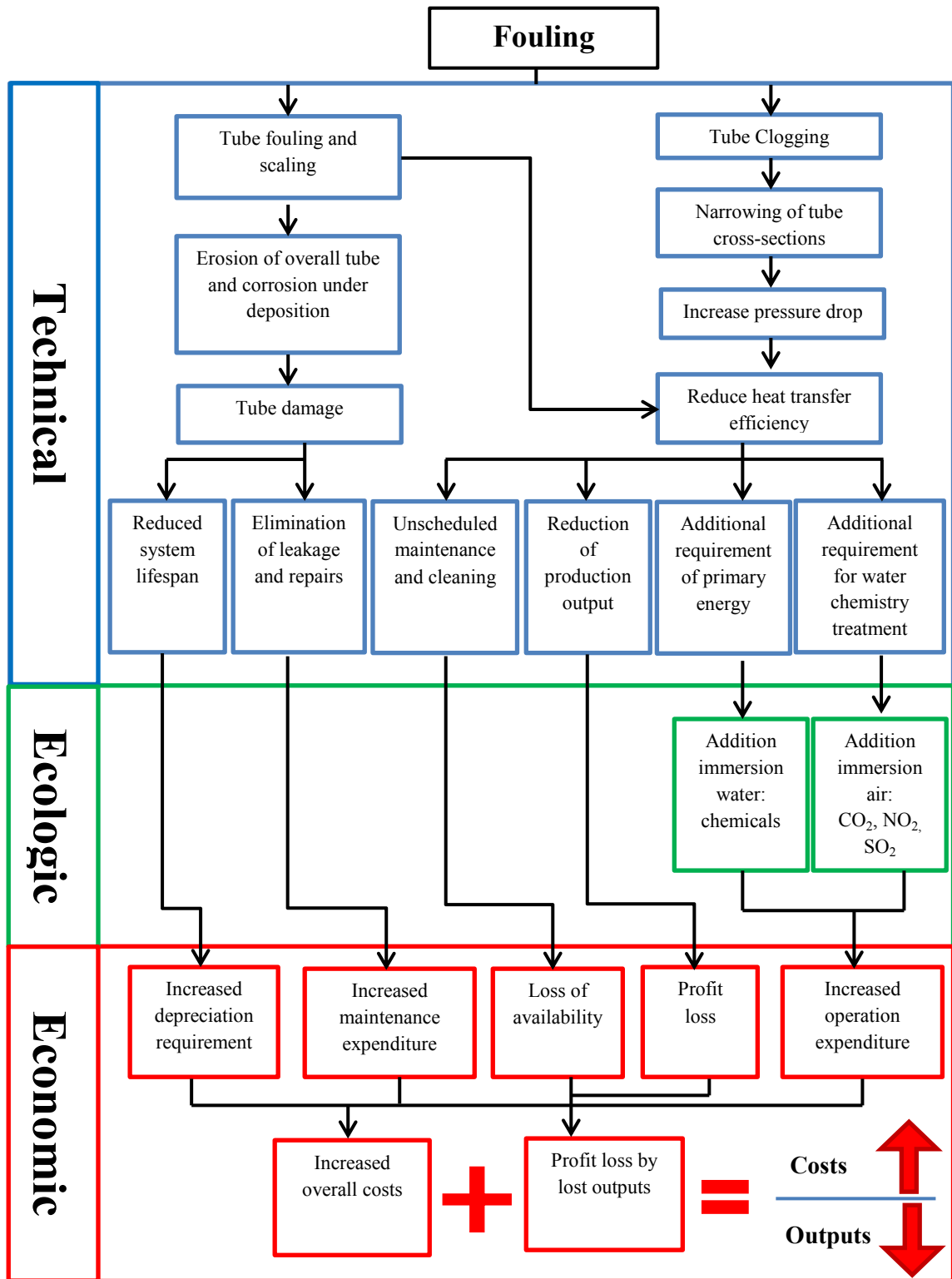


Figure 1.3: Overall view of fouling effect (H Müller-Steinhagen, Malayeri, & Watkinson, 2011)

Figure 1.3 demonstrates the overview of fouling in industrial operation. The figure explained the fouling effect included 3 main parts which are technical, ecological and

economical. The figure explained the main negative impacts on fouling are increased overall industrial operation cost and depreciation of equipment efficiency leading to profit loss by lost output.

1.1.8 Current Technology Cleaning of Heat Exchanger

In order to maintain or restore efficiency of the heat exchanger, it is often necessary to clean the heat exchangers. Methods of cleaning may be classified into two groups; on-line and off-line cleaning (H. MÜLLer-Steinhagen et al., 2005). In some applications, the cleaning can be done on-line to maintain acceptable performance without interruption of operation. In other cases, off-line cleaning must be used.

1.1.8.1 On-line Cleaning

On-line cleaning generally utilises a mechanical method designed for only tube sides and requires no disassembly. The advantages of on-line cleaning are the continuity of service of the heat exchanger with the hope that no cleaning-mandated downtime will occur. However, it adds extra cost of a new heat exchanger installation or the large cost of retrofits and there is no assurance that all the tubes would be cleaned sufficiently.

I. Circulation of sponge rubber balls (Hans Müller-Steinhagen, 2000)

The technique is capable of preventing the accumulation of particulate matter, biofilm formation, and scale and corrosion product deposition. It is only applicable to flow through the inside of tubes.

II. Two phases of the ferrous sulphate treatment. The first phase involves the initial laying down of the protective film. The second phase involves the maintenance of the film, which would be otherwise destroyed by the shear effects of flow.

III. Chlorination used for combat bio-fouling (Rajagopal, Van der Velde, Van der Gaag, & Jenner, 2003)

IV. Scale inhibitors (Choi, You, & Kim, 2002; Y.-P. Lin & Singer, 2005; J Macadam & S Parsons, 2004)

V. Magnetic devices (J Macadam & S Parsons, 2004; Parson, S.J. Judd, Stephenson, S.Udol, & Wang, 1997; Parsons, Wang, Judd, & Stephenson, 1997)

VI. Sonic Technology (S. Lin & Chen, 2007)

High and low frequency sound emitters (horns) are used to relief fouling problems on heat exchangers. The use of sound is much less effective in sticky and tenacious deposits that are generally associated with slugging.

VII. On-line chemical cleaning (X. D. Chen, Li, Lin, & Özkan, 2004) by injection of chemical solutions into the process stream for the cleaning purposes.

VIII. The use of radiation (Park et al., 2003)

Radiation sterilisation of microbial-laden water, the use of ultra violet light and Gamma rays have been considered for a long time.

1.1.8.2 Off-line Cleaning

An alternative to on-line cleaning is to stop the operation and clean the heat exchanger. Off-line cleaning can be classified into off-line chemical cleaning or by mechanical means. The cleaning method preferred is without the need to dismantle the heat exchangers, but usually it is necessary to have access to the inside surfaces. It would be prudent to consider the installation of a “standby” heat exchanger, thereby providing the opportunity to clean the fouled heat exchanger while at the same time maintain the production.

- **Off-line Mechanical Cleaning**

- a. Tube drilling and rodding (Hans Müller-Steinhagen, 2011)

Devices may be applied to the rotating shaft including drills, cutting and buffing tools and brushes that may be made from different materials, e.g.

steels or nylon, brasses depending on the tube material and the nature of the deposit.

b. Cleaning with explosives

Use of controlled explosions, where the energy to remove the deposits, is transmitted by a shock wave in the air adjacent to the surface to be cleaned, or by the general vibration of tubes brought about the explosion. It is a relatively new innovation introduced in boiler plant cleaning. It is possible to begin the cleaning process while the structure is still hot.

c. Thermal shock (Wilson, 2005)

Changes in temperature, particularly rapid changes, cause cracking of the foulant layer with the possibility of flaking. This technique is similar to steam soaking. The water flushing carries away the dislodged material and it is repeated until clean surfaces are obtained

- Off-line Chemical Cleaning

a. Inhibitor hydrofluoric , hydrochloric, citric, sulphuric acid or EDTA (chemical cleaning agent) for iron oxides, calcium/magnesium scale (foulant) etc. cleaning (Madaeni & Samieirad, 2010). Inhibitor hydrofluoric acid is by far the most effective agent but cannot be used if deposits contain more than 1% w/v calcium.

b. Chlorinated or aromatic solvents followed by washing are suitable for heavy organic deposits e.g. tars and polymers (foulant) (Arhancet, 1999).

c. Alkaline solutions of potassium permanganate (Spicher & Skrinde, 1963) or steam-air decoking (Clavenna et al., 2006) are suitable for cleaning carbon (foulant) deposition.

1.1.9 Potential Application of Functionalized Nanofluids in Fouling Mitigation Approach

Nanofluids are suspensions obtained from dispersing different nanoparticles in host fluids to enhance thermal properties. In general, the size of a nanoparticle spans the range between 1 and 100nm. These are next-generation heat transfer fluids and introduced as heat exchanging fluids. They have better thermal properties than conventional heat transfer fluids. Over the past two decades, nanofluids have exhibited remarkable improvements in thermal conductivity and heat transfer coefficient which could reduce overall plant power consumption and costs of application in heat exchangers. Nanofluids are increasingly utilized in different heat exchangers to optimize energy consumption. Hence, discovery of suitable nanofluids having improved heat transfer properties and high thermal conductivity has become challenging. Several studies have reported the results of thermal conductivity of metal oxide based water nanofluids (e.g. aluminium oxide, SiO₂, TiO₂, CuO) in the last decade. Recently, significant investigations into the use of carbon-based nanomaterials, such as single wall carbon nanotube (CNT), multi-wall carbon nanotube (MWCNT), graphene oxide (GO) and graphene nanoplateles (GNP) to make nanofluids were reported in the literature review. New research specifies the carbon based nanofluids that could provide higher thermal conductivity enhancement in comparison to other tested nanofluids. Successful employment of nanofluids supports the current trend towards component miniaturization by enabling the design of small and light heat exchanger systems.

In addition, research is ongoing to investigate functionalized nanoparticles in various applications, such as enhancement of stabilization, eliminating heavy metal from industrial wastewater, etc. Fouling is a well-known problem in most heat exchanger equipment. Therefore, further investigation should be conducted to bring nanofluids to a

state where application is applicable on an industrial scale, at the same time, eliminating or reducing the fouling problems.

1.2 Problem Statements

- 1 Water with high Ca^{2+} contents causing fouling and the deposited white solid on the surface of heat exchangers lower the heat transfer effectiveness and shorten its life.
- 2 Untreated water circulation in industrial heating or cooling process system creates tremendous scale build-up which requires expensive chemical treatment to maintain efficient operation in industry.
- 3 Contemporary practice using hazardous chemicals for de-scaling are harmful to the environment and costly as well.
- 4 Production time is lost when systems are shut down for de-scaling. Eventually production loss leads to increment of production costs.
- 5 Contemporary practice is to use the traditional manual methods in industry comprising of plant operators or technicians conducting scheduled chemical tests for heat transfer liquid analysis which are time consuming and inefficient.

1.3 Research Questions

Fouling introduce undesired thermal resistance on heat transfer surface, so the present research has taken in hand to monitor fouling online and retard rate of deposition on heat exchangers. Thus, in this research the following quarries are taken into consideration.

- 1 What particular particles have deposited on heat exchangers surface and detrimental the heat transfer efficiency?
- 2 What and how industrial process parameters effect on deposition growth?

- 3 What alternative methods benign to environment potential to mitigate fouling?
How these methods mitigate fouling?
- 4 How to control water quality effectively in industrial? Is that possible to
implement an on-line monitoring and control for water quality throughout
industrial operations?

1.4 Objectives of the Presented Research

The aim of the research is to investigate the industrial process parameter effect on fouling deposition and thereby introduce the green environmental methods to reduce fouling in heat exchangers. On top of that, the new and novel online approach for monitoring the process of fouling could be introduced for implementation in industrial applications. The online approach refers to measure the parameters and analyse data in situ instead of sample analysis in the laboratory and take decision on adjusting process parameters.

The main objectives of this research can be summarized as follows:

1. To fabricate an experimental test rig for on-line monitoring of fouling experiments and water hardness monitoring by a novel non-destructive electromagnetic wave signal technique in real time.
2. To evaluate the effect of fouling deposition under influence of different materials, temperatures, velocities and concentrations.
3. To explore effective catalytic material and novel green additives having environmental friendly character as variable means to inhibit fouling and compare to the contemporary practice.
4. Simulation of the use of electromagnetic wave for water hardness detection and compare the numerical data with the experimental results for validation.

5. To evaluate the heat transfer efficiency and fouling deposition by varying different multiphase flow phenomena.

1.5 Contribution of the Study

A unique on-line monitoring experimental test rig for fouling deposition research was designed and constructed. A series of fouling deposition studies for different conditions were conducted which includes temperature effect, velocity effect, concentration effect, different flow regimes and different metal surfaces effects. This research data could be useful for consideration as heat exchanger design references in the near future.

The build-up of scale leads to decreased operating efficiency due to the increase in tube wall temperature and increase energy consumption. Chemical additives are often used to mitigate this problem in contemporary practice. With the increasing environmental consciousness in society, an environmentally friendly method in mitigation fouling is highly encouraged instead of relying on chemical additives which are expensive and not environmentally friendly. Explorations of different novel techniques in mitigating fouling were reported in this research, including the exploration of effective catalytic material having environmentally friendly character and novel green additives materials as means to inhibit fouling. These environmentally friendly approach findings could possibly be used as a replacement for the chemical method used in mitigation fouling at present.

Furthermore, a novel non-destructive electromagnetic wave sensor technique to detect water hardness in the water cooling industry system has potential to be implemented in the industry system as an on-line and reliable monitoring system.

1.6 Layout of Thesis

The thesis starts with an overview of heat exchangers, problems and impact of fouling in heat exchangers, current technology and potential approach to inhibit fouling problems. In chapter 2, a summary of previous literature on double pipe heat exchangers, principles and categories of fouling, formation mechanism, parameters affecting fouling, fouling mitigation, control and monitoring will be presented. Following into chapter 3, the instrument, the experimental setup, test section and calibration of the instrument are discussed. In addition, the methods of data reduction, uncertainty analysis of the experimental set-up and validation of the test section well discussed too. Investigation of double pipe heat exchanger fouling and its mitigation will be discussed thoroughly in Chapter 4. Chapter 5 discusses the nanofluids preparation for fouling mitigation experiments and analysis. Chapter 6 contains the design and implementation of a non-invasive real time microwave sensor for assessing water-hardness in heat exchanger whereas Chapter 7 discusses the fouling under two-phase flow conditions. Summary of the work done and proposed recommendation for future work will be discussed in Chapter 8. Appendix A contains discussion about calibration and PLC program of the experimental test rig. Appendix B describes the data acquisition and in the last Appendix C the cleaning procedure is elucidated.

CHAPTER 2: LITERATURE REVIEW

2.1 Background

Fouling has been an object of research since the 1980s. (Epstein, 1983) was the first to attempt to explain and verify fouling by summarizing the fouling process in a 5 X 5 fouling matrix. This approach is a major area of interest within the field of different aspects of the fouling process. Figure 2.1(a) shows the five different aspects of fouling mechanisms in the matrix column and the five rows show the sub-processes involved with it. Over the period of time, the 5 X 5 fouling matrix was further improved as reflecting the progress level of understanding as shown in Figure 2.1(b) by (Bohnet, 1987). Recently, researchers have shown an increased interest in this research area, and the evidence of experts in various aspects of the field involved in the Heat Exchanger Fouling and Cleaning XI conferences held in Ireland in 2015. Throughout the years, many gaps in fouling research seem to be filled. Figure 2.1(c) shows that a large and growing body of literature has investigated in particular the transport research area. So far, however, there has been little discussion about the attachment, removal and ageing areas. Although some research has been carried out on attachment and removal areas, there is still very little scientific understanding on this approach.

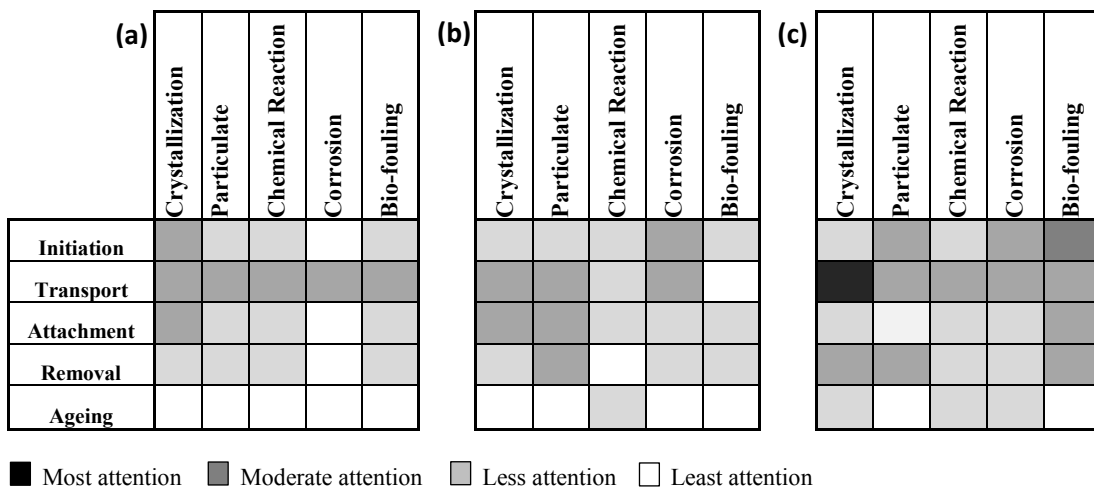


Figure 2.1: Overall views of 5 X 5 matrix of fouling mechanisms.

Fouling has been described as the major unresolved problem in heat transfer applications. There are numerous reasons why the fouling problem has not been solved to date. There is divergence between the researchers on the research findings on the mechanisms involved in producing the deposits such as an understanding of the foulant precursors, location of the reaction taking place (whether these are in the tube surface or bulk of the fluid) and surprisingly even the chemical structure of the species that constitutes the fouling deposits is unclear. However, there is agreement on the fact that mitigation of fouling in industrial heat exchangers can only be achieved if a superior comprehension of the basic science is accomplished

Several review articles were reported on fouling of heat transfer surfaces, (Bott, 1995; Ghaffour et al., 2013; Jitka MacAdam & SimonA Parsons, 2004; H Müller-Steinhagen et al., 2011; J.W. Mullin, 2001; Sadeghinezhad et al., 2014; Zhao & Chen, 2012) and more specifically on calcium carbonate fouling formation (Altay, Shahwan, & Tanoğlu, 2007; T. Chen, Neville, & Yuan, 2005; J. W. Morse, Arvidson, & Lüttge, 2007; Pääkkönen, Riihimäki, Simonson, Muurinen, & Keiski, 2012; Sunagawa, 2005).

This chapter aims to present a clear picture to the reader with the basic principle in fouling science, beginning with the fouling mechanism (Section 2.2) with particular focus on calcium carbonate crystallization fouling (Section 2.3) and the sub-processes involved in fouling (Section 2.4). Furthermore, a description of the process parameters affecting fouling and the relationship between the process parameters (Section 2.4) and the potential fouling mitigation approach, control and on-line monitoring (Section 2.5) have been incorporated. Finally, an overall review of the fouling process presented in (Section 2.6).

2.2 Basic Principle of Fouling Mechanisms

Fouling refers to undesired accumulation of solid material (by-products of the heat transfer processes) on heat exchanger surfaces, which results in additional thermal resistance to heat transfer, thus reducing exchanger performance. The fouling layer also blocks the flow passage and increases surface roughness, which either reduces the flow rate in the exchanger or increases the pressure drop or both. Fouling in heat exchangers is a very complex phenomenon and its negative impact translates into billions of dollars every year worldwide and is being investigated with considerable effort. Many types of fouling can occur on the heat transfer surfaces. The generally favoured scheme for the classification of the heat transfer fouling is based on the different physical and chemical processes involved. Nevertheless, it is convenient to classify the fouling main types as sub-section below.

2.2.1 Crystallization Fouling

Crystallization fouling is the deposition of dissolved salts onto the heat transfer surface due to the saturated solution (J.W. Mullin, 2001). Generally, it occurs with aqueous solutions and other liquids of soluble salts whose solubility characteristic changes with temperature beyond the saturation point. When the solution is heated, the deposition of inverse solubility salts will precipitate and deposit on the heat transfer surface. This phenomenon is usually called “scaling” and its deposited layers generally are hard and tenacious. Crystallization fouling is most common fouling found in industrial heat transfer processes when seawater, untreated water, aqueous solution of caustic soda, geothermal water, brine, and other salts are used in the heat exchanger. The formation of nuclei on the surface is the primary source followed by crystal growth during precipitation in the crystallization phenomenon (J. W. Mullin, 2001a).

2.2.2 Particulate Fouling

Particulate fouling is also known as “sedimentation” fouling. The suspended particles in the process streams deposit onto the heat transfer surfaces due to gravity (Henry, Minier, & Lefèvre, 2012). Most often, this type of fouling involves deposition of corrosion products dispersed in fluids, clay and mineral particles in river water, suspended solid in cooling water, soot particles of incomplete combustion, deposition of salts in desalination systems, deposition of dust particles in air coolers, particulates in fire-side (gas side) fouling of boilers, etc (R Sheikholeslami, 2000).

2.2.3 Chemical Reaction Fouling

Chemical reaction fouling is defined as deposition of one or more chemical reactions between reactants contained in the bulk fluids. Most of the time the surface materials themselves are not participant in the reaction, however, they may be contributing to fouling by acting as a catalyst as in cracking, coking, polymerization, and autoxidation. The fouling precursors such as protein and asphaltenes could be induced due to the thermal instabilities of chemical species. Generally, this fouling happens over a wide temperature range from ambient to over 1,000 °C but is more prominent at higher temperature. Chemical reaction fouling is found in many different process industries, for example, oil refining, petrochemical industries, cooling of oils and gas, vapour-phase pyrolysis, polymerization of process monomers and so on. Moreover, fouling on heat transfer surface by biological fluid may incorporate with complex heterogeneous chemical reaction and physicochemical processes (A. P. Watkinson & D. I. Wilson, 1997).

2.2.4 Corrosion Fouling

Corrosion fouling is a process involving heat transfer surface and the fluid stream to produce a corrosion product by chemical or electrochemical reaction. It changes the heat transfer surface characteristic and deposition on it. Corrosion fouling could occur

in two different ways. First, corrosion products accumulate and adhere to the surface providing resistance to heat transfer. Secondly, corrosion products may be transported as particulate material from the corrosion site and be deposited as particulate fouling on the heat transfer surface in another side of the system. Corrosion fouling is prevalent in many applications where chemical reaction fouling takes place and the protective oxide layer is not formed on the surface. It is of significant importance in the design of the condenser and boiler of a fossil fuel-fired power plant (E. F. C. Somerscales, 1997).

2.2.5 Biological Fouling

Biological fouling is the growth of microorganism/macroorganism, attachment and accumulation on the heat transfer surfaces. Generally it is called “Biofouling” and is a common problem in water streams. Biofouling could be categorized into two different types: microbial and macrobial. Microbial fouling is accumulation of microorganisms such as bacteria, algae, fungi, moulds etc. On the other hand, macrobial fouling is the deposition of macroorganism such as barnacles, mussels, vegetation and clams which are commonly found in seawater. Biofouling is generally in the form of biofilm which is filamentous, uneven and deformable but very difficult to remove (Guo, Ngo, & Li, 2012).

2.3 Theoretical Background of Fouling

2.3.1 Solid Crystals

According to the definition provided by (Lacmann, 1998), the characteristic of a true solid crystal consists of a rigid lattice of ions, atoms, or molecules . These crystals are categorized into seven different systems: regular, tetragonal, orthorhombic, monoclinic, triclinic, trigonal and hexagonal. Rapid crystallization from supersaturated solutions often causes the formation of fluffy treelike crystals named dendrites. Dendrites are formed most commonly during the early stage of crystallization; at later stages a more normal uniform growth takes place and the pattern may be obliterated. Mechanical and

chemical properties of crystalline materials are altered by the imperfection in crystals. Surface defects can greatly affect the crystal growth process. There are 3 main types of lattice defect which are point, line and surface. Point defect is described as a unit missing in a lattice which can be occupied by impurities and consequently lead to distortion of the crystal and influence its crystal structure stability. Line defect can be due to edge or screw distortion and resulting in the regular crystal structure throughout the whole solid whereas surface imperfections including mismatch of crystal boundaries produces crystalline materials mechanical or thermal stresses.

2.3.2 Fouling Process

Fouling is a dynamic process and always defined as the formation and accumulation of unwanted materials deposit onto the processing equipment surfaces as shown in Figure 2.2. (Epstein, 1983) considered that each of five generic types of fouling (crystallization, particulate, chemical reaction, corrosion and biological) comprise into five different stages. These five stages can be summarized as initiation of fouling, transport to the surface, attachment to the surface, removal from the surface and ageing at the surface (J.W. Mullin, 2001). The overall fouling process is usually considered to be the net result of two simultaneous sub processes; a deposition process and a removal process as shown in Equation 2.1 and Figure 2.3.

$$\frac{dm_f}{dt} = m_d - m_r \quad (2.1)$$

Where, $\frac{dm_f}{dt}$, m_d and m_r are the net deposition, deposition and removal rates respectively.

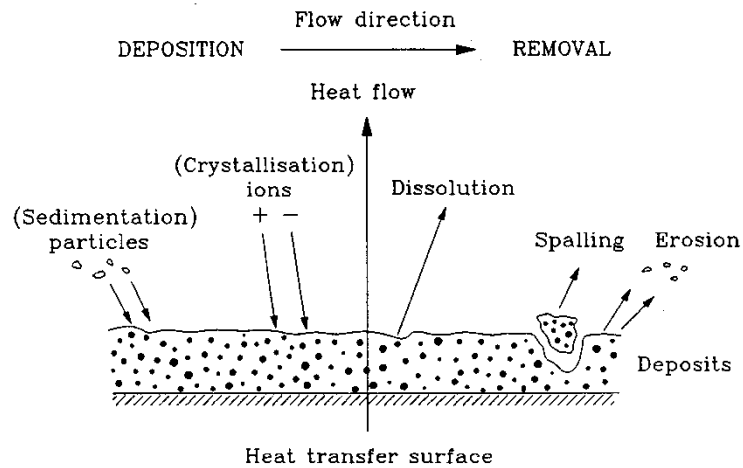


Figure 2.2: Fouling processes (S. N. Kazi, Duffy, & Chen, 2010).

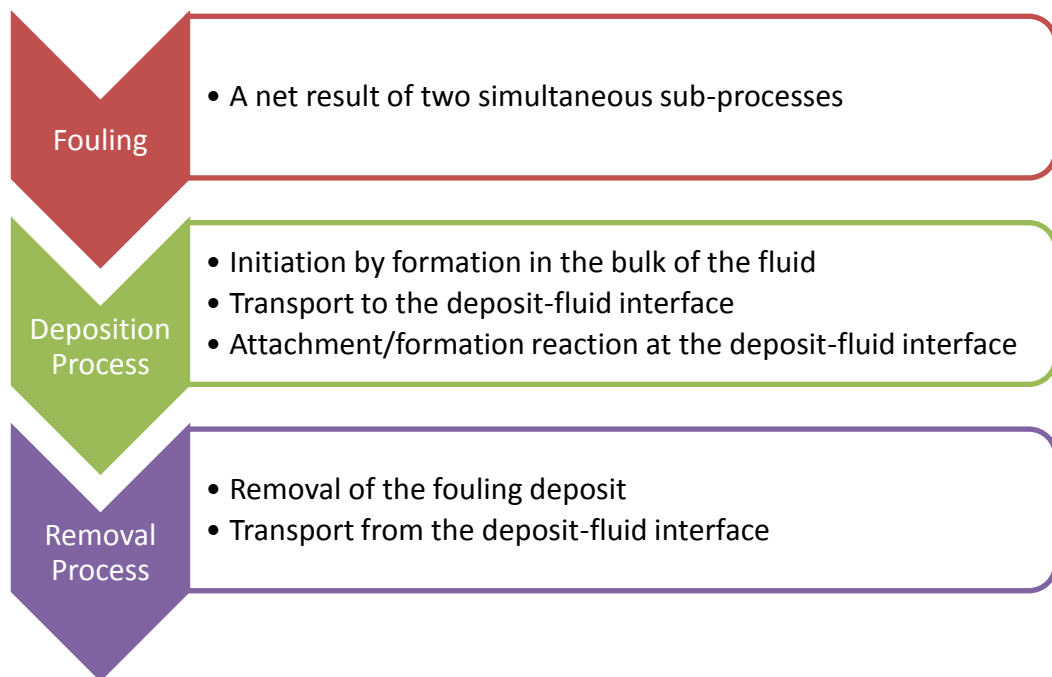


Figure 2.3: Net results of a deposition and removal process (Zhao & Chen, 2013).

2.3.2.1 Initiation

An initiation of fouling is a first occasion of a fouling process which is followed by a delay period or induction period. In the induction period, the surface is conditioned. The literature reported on (Awad, 2011) has highlighted that an induction period of a certain time duration is normally present during which the conditions that promote subsequent

fouling are established. Among these are the establishment of a surface temperature, surface finish, roughness, surface coating, scalant concentration, velocity gradient, etc. During the induction period, nuclei for crystallization of deposits are formed. The basic mechanism involved during this period is heterogeneous nucleation whereby the higher nucleation rate tends to lower the induction period. In addition, (E. Somerscales & Knudsen, 1981) has demonstrated that low-energy surfaces (unwetable) exhibit a longer induction period than those of high-energy surfaces (wetable).

(Geddert, Augustin, & Scholl, 2011) reported that the increasing degree of supersaturation will decrease the induction period. Whereas in chemical reaction fouling, (A. Watkinson & D. Wilson, 1997) reviewed the literature about the induction period and show that it appears to decrease when the temperature increases, as generally, all fouling mechanisms have a shorter induction period if exposed to the rough surfaces due to the ease of nucleation and adhesion onto the heat transfer surface (Herz, Malayeri, & Müller-Steinhagen, 2008).

Moreover, the duration of the induction period is not only related to the nature of the surface (surface roughness/energy) but also process conditions such as fluid velocity and surface temperature.

2.3.2.2 Transport

Based on 5 X 5 matrix in Figure 2.1, the existing literature on all the sub-process fouling is extensive and focuses particularly on transport mechanism since mid-1980s. It can be concluded that transport mechanism gained a remarkable level of understanding across all fouling mechanism types. In all reaction mechanisms, the fouling precursors (foulants) must be transported by convective mechanisms from the bulk of the fluid toward the zone across the boundary layer in which they are converted

into deposits by attachment or adhesion to the heat transfer surface (Lau & Ismail, 2009).

Transport mechanism is accomplished by a number of phenomena including diffusion, sedimentation, and thermophoresis. The local deposition flux m_d on a surface can be expressed by the Equation 2.2.

$$m_d = h_D(C_b - C_w) \quad (2.2)$$

Where, C_b and C_w are reactant concentrations in the bulk fluid and in the fluid adjacent to the surfaces whereas h_D is the convective mass transfer coefficient, which could be evaluated from Sherwood number, $h = h_D L / D$, where L is a characteristic length (m) and D is mass diffusivity (m^2/s).

In a study conducted by (Watkinson, 2007), it was shown that if the transport step controls the overall rate of deposition then the fouling rate should only be a weak function of surface and bulk temperature. The fouling rate should increase with velocity, linearly in turbulent flow and more weakly in laminar flow.

2.3.2.3 Attachment

After the transportation of foulant from bulk fluid toward the surface across the boundary layer, the deposits attach or adhere to the heat transfer surface and among themselves. Overall, factors affecting adhesion include surface energies, surface temperature, and shear force acting at the surface, as well as the nature and composition of previously deposited layers. The scale layer grows gradually with time after the salt ions approaching the surface are attracted to each other. In a study of the investigation into nucleation and growth orders, (Packter, 1968) reported that under the influence of electromagnetic forces between foulant, it started to adhere onto the surface to form nucleation and finally accumulate.

2.3.2.4 Removal

Deposition is always defined as the net results between deposition and removal of the scalant up to the steady growth of deposition on the heat transfer surface. Up to now, removal mechanisms are relatively poorly understood in comparison with deposition mechanisms (Uyak, Akdagli, Cakmakci, & Koyuncu, 2014). As generally, shear force near the boundary of heat transfer surface between deposited scales and fluid, plays a vital role for removal. Shear force near the interface is guided by a few different parameters such as viscosity of the fluid, surface roughness and velocity gradient near the surface. (Epstein, 1981) described the removal mechanism performed through the dissolution, erosion and spalling. Moreover, (Paz, Suárez, Eirís, & Porteiro, 2012) have recently reported on the critical local wall shear stress around cylindrical probes fouled by diesel exhaust gases .

2.3.2.5 Aging

With the commencement of deposition aging starts. In the aging stage, under the effect of higher wall temperature over extended periods of time, the fouling layer exhibits transformation of crystals either physically or chemically which alters the structure and properties of the deposits. Alteration of these crystals may change its mechanical properties such as mechanical strength between the scalant accumulation. Aging plays an important role in industrial operations especially in the scheduling management for cleaning strategies throughout the industry.

2.3.3 Fouling Curve

The overall process of fouling is represented by the fouling factor, R_f (fouling resistance) which is a well-known measurement for the capacity of the operating heat exchanger.

The fouling curve used to illustrate the various modes of fouling with reference to time.

Figure 2.4 shows the typical fouling curves. It generally can be classified into three categories, (A) Linear, (B) Falling, and (C) asymptotic.

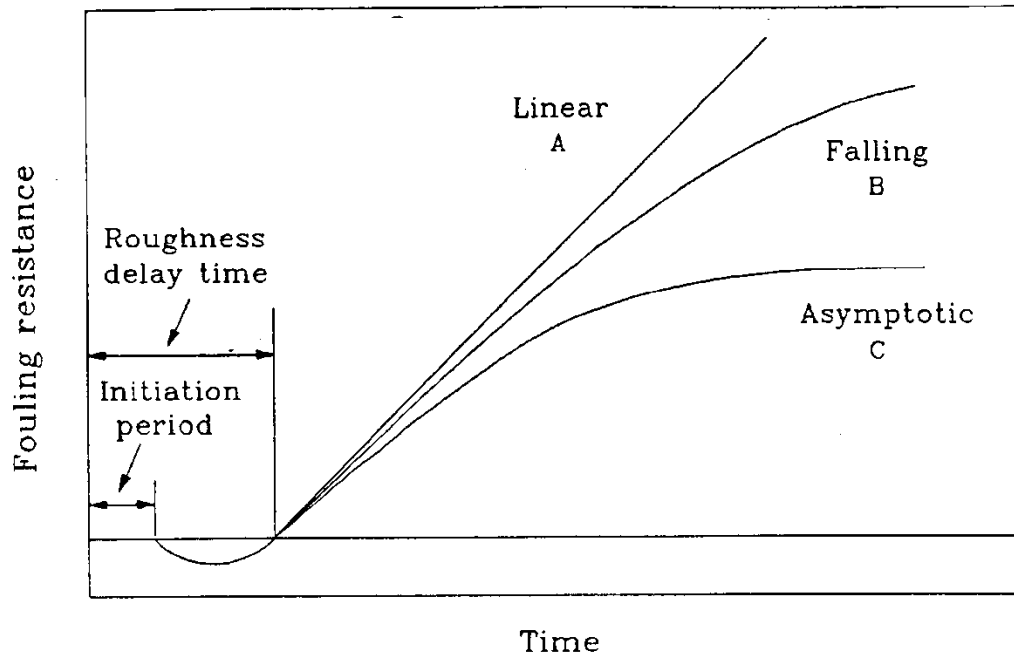


Figure 2.4: Typical fouling curves (H. Müller-Steinhagen, M. R. Malayeri, & A. Watkinson, 2005).

Initiation period or time delay in heat exchanger fouling is considered the time when there is no deposition for some time after a clean heat exchanger is incorporated into operation. The initial growth of deposit results in an increment in the heat transfer coefficient rather than a decrease. It is due to the changing flow characteristic near the boundary wall in which the deposition penetrates the viscous sub-layer and results in the enhancement of the turbulence of the film heat transfer coefficient at the solid/liquid interface.

Several lines of evidence suggest that negative fouling resistance exists at the initial stage of fouling deposition (Awad, 2011; Geddert et al., 2011; S. N. Kazi, G. G. Duffy, & X. D. Chen, 2012). This process lasts until the additional heat transfer resistance overcomes the advantages of increased turbulence.

2.3.4 Mechanism Scale Formation Process

There are three simultaneous factors which influence the precipitation of a crystalline substance from a solution onto the heat transfer surface: supersaturation, nucleation and sufficient contact time. Finally, there is the crystal growth on the heat transfer surface.

2.3.4.1 Supersaturation

The main driving force for any crystallization process is the “supersaturation” condition near the heat transfer boundary surface. The supersaturation condition is achieved by having a concentration greater than that of a saturated solution, the one is in equilibrium with the soluble solid phase. Since supersaturated solutions are thermodynamically unstable, nucleation and crystal growth occurs as a step to bring the solution back to equilibrium (Bott, 1995). The degree of supersaturation, S , is often described as a ratio of the bulk concentration to the saturation concentration; the degree of driving force, Δu , can be generalized by the difference of the chemical potentials between solid and liquid phases. Hence, the function of supersaturation can be express in Equation 2.3.

$$\Delta u = k_B T \ln(S + 1) \quad (2.3)$$

where k_B is the Boltzmann constant ($J \cdot K^{-1}$) and T is the absolute temperature (K).

There are two different types of salts distinguished by their change solubility with temperature. Normal solubility salts are the salts whose solubility increases with temperature increase, such as sodium chloride, potassium chloride, potassium nitrate and potassium sulphate. These salts may crystallise on cooling. In contrast, inverse solubility salts have reduced solubility as temperature rises and are more likely to form a deposit if the saturated solution is being heated, for example, calcium carbonates, calcium sulphate and silica. In 1995, T.R. Boot et al. published a book in one chapter of which they described how the inverse solubility salt solution transforms into crystal under the supersaturation condition. As shown in Figure 2.5, it demonstrated a solution

at point A on heating reaches the saturation point B at temperature T_1 before turning supersaturated at C, a metastable point corresponding to temperature T_2 . The solution moves toward point D on the curve on further heating.

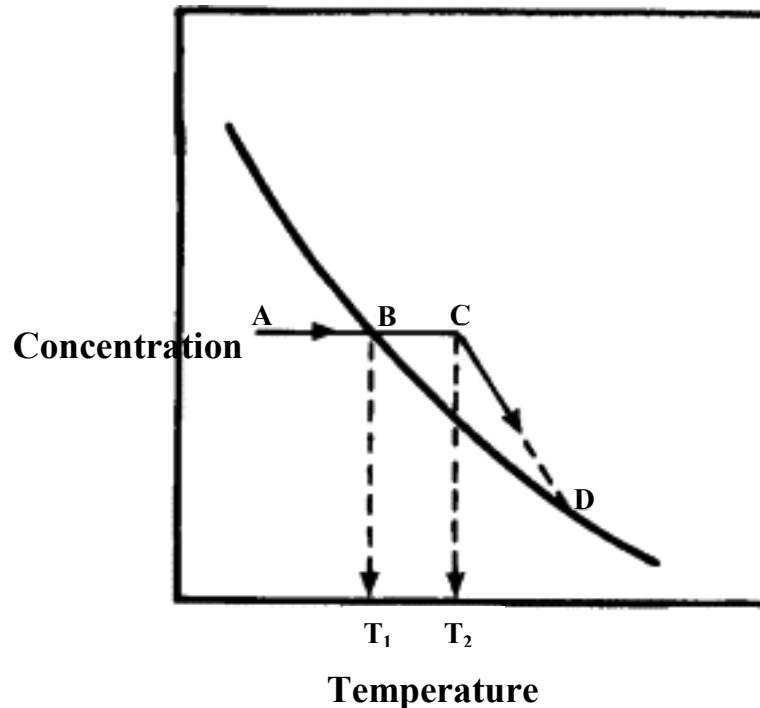


Figure 2.5: Effect of temperature on an inverse solubility salt solution (Bott, 1995).

2.3.4.2 Nucleation

(Giulietti, Seckler, Derenzo, Ré, & Cekinski, 2001) define the nucleation as the smallest form of stable aggregates of the crystalline phase in a crystallization system. The first stage of scale formation is nucleation, which happens with minimum supersaturation of the scale-forming compound established in the liquid layer adjacent to the exposed surface. (J. W. Mullin, 2001a) summarize the nucleation process as tabulated in Figure 2.6. Nucleation is categorized in two types which are primary and secondary. Primary crystallization occurs when they do not contain crystalline matter. It grows under the situation whereby crystallites are spontaneously formed from bulk solution (homogeneous) or induced by foreign particles (heterogeneous). On the other hand, secondary crystallization happens when nuclei are generated in the existing crystals.

Homogeneous nucleation can be established in controlled experiments by associating with pure solution. However, it is unlikely to take place in industrial systems. Generally, the condition of supersaturation alone cannot be a sufficient reason for a system to start crystallization. The first experiment realisation that nucleation on a surface proceeds mostly by heterogeneous mechanisms was reported by (Brown, 1988).

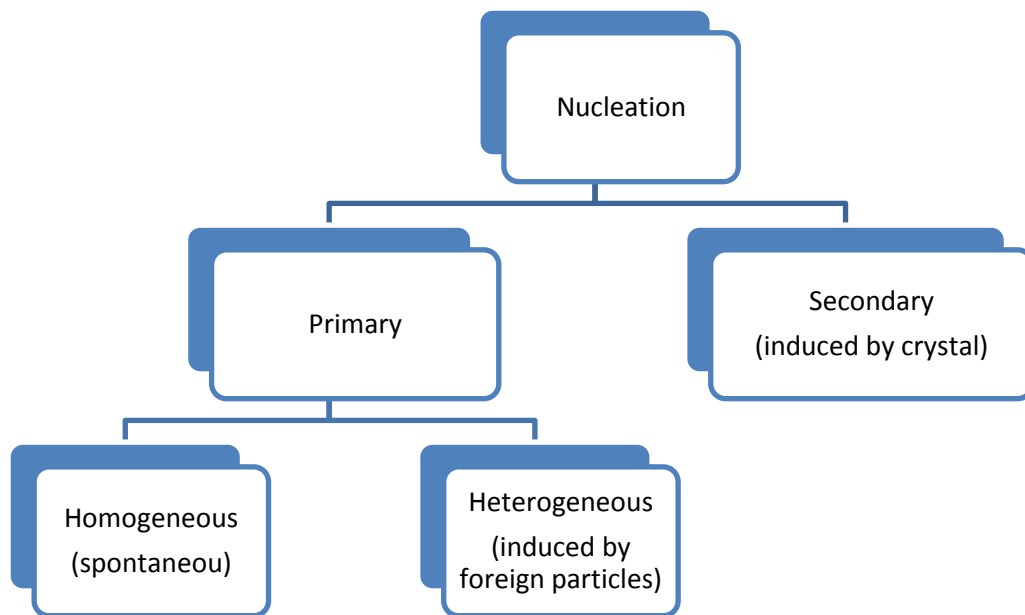


Figure 2.6: Types of nucleation.

Heterogeneous nucleation occurs much more often than homogeneous nucleation. Heterogeneous nucleation applies to the phase transformation between any two phases of gas, liquid, or solid, typically for example, condensation of gas/vapour, solidification from liquid and bubble formation from liquid. Heterogeneous nucleation forms at preferential sites such as phase boundaries, surfaces (of containers, bottles, etc.) or impurities like dust. At such preferential sites, the effective surface energy is lower, thus diminishing the free energy barrier and facilitating nucleation. Surfaces promote nucleation because of wetting – contact angles greater than zero between phases facilitate particles to nucleate. The free energy needed for heterogeneous nucleation is equal to the product of homogeneous nucleation and a function of the contact angle (θ) as shown in Equation 2.4:

$$\Delta G_{heterogeneous} = \Delta G_{homogeneous} + f(\theta) \quad (2.4)$$

Where

$$f(\theta) = \frac{2 - 3\cos\theta + \cos^3\theta}{4}$$

$$0 \leq f(\theta) \leq 1.0$$

for $\theta = 180^\circ$, $f(\theta) = 1$, indicating no wetting of the surface, and thus no catalysis by the surface and the crystallization falling into the case of homogeneous nucleation.

for $\theta = 0^\circ$, $f(\theta) = 0$, indicating full wetting, fully catalysed and no barrier for nucleation at surface.

The barrier energy needed for heterogeneous nucleation is reduced as show in Figure 2.7.

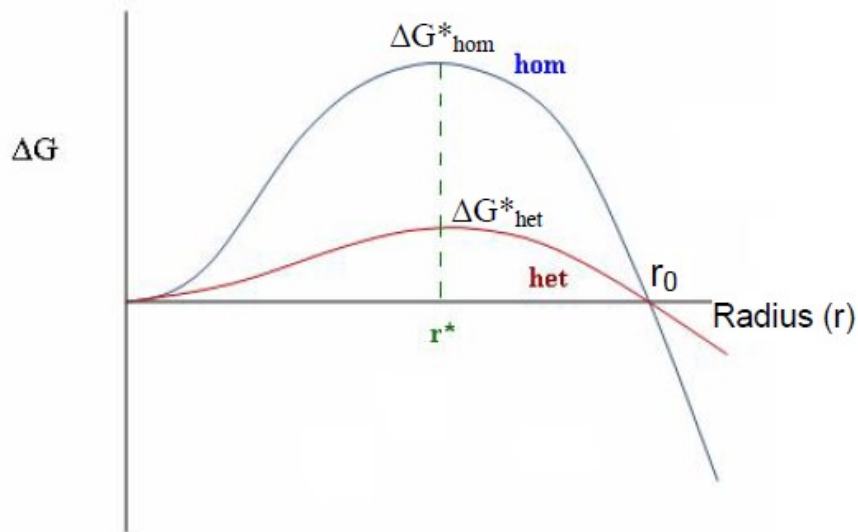


Figure 2.7: Free energy changes associated with homogeneous and heterogeneous mechanism (Brar, France, & Smirniotis, 2001).

The wetting angle determines the ease of nucleation by reducing the energy needed as shown in Figure 2.8.

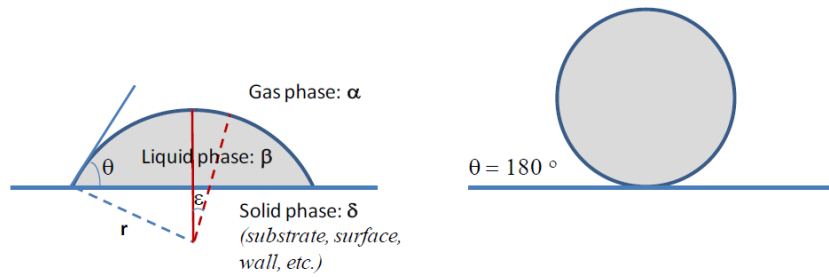


Figure 2.8: Wetting angle (Yuan & Lee, 2013).

$$\gamma_{\alpha\beta} = (\text{gas} - \text{liquid}), \gamma_{\alpha\delta} = (\text{gas} - \text{solid}), \gamma_{\beta\delta} = (\text{liquid} - \text{solid})$$

Consider a droplet of liquid on a flat surface with fixed volume. The total surface energy of the system is a function of the shape of the droplet.

The diagram above shows two different shapes of the same volume, but of different surface area leading to different surface energy:

$$G_s = \gamma_{\alpha\beta} A_{\alpha\beta} + \gamma_{\alpha\delta} A_{\alpha\delta} + \gamma_{\beta\delta} A_{\beta\delta}$$

where $A_{\alpha\beta}$, $A_{\alpha\delta}$ and $A_{\beta\delta}$ are areas of $\alpha\beta$, $\alpha\delta$ and $\beta\delta$ interfaces, respectively.

Therefore, the condition near the boundary surface (surface temperature, degree of supersaturation, pressure, and hydrodynamic conditions) (Zhao & Chen, 2013) as well as factors involving the attachment of scale to the surface (surface material and roughness) have great impact on the rate of deposit formation at the initial stage (Gunn, 1980; S.-T. Liu & Nancollas, 1970).

2.3.4.3 Contact Time

Scaling process is not sufficient to be initiated only by the condition of supersaturation near the boundary surface. A number of active centres where nucleation may occur or be induced should be created first. Deposits will accumulate as soon as stable nuclei have been formed on the surface.

(Hoang, Ang, & Rohl, 2011) and (Muryanto, 2002) carried out an investigation of crystallisation and scaling process of calcium sulphate in a maximum of 16 hours. Their results indicated that the fouling curve is generally close to a linear model regardless of the pipe material and diameter. In contrast, (S. N. Kazi et al., 2010) reported an asymptotic model in the fouling curve for an experimental work of calcium sulphate fouling in 70 hours. It presented a picture of the investigation time playing a significant role in the fouling process. It is due to the fact that the investigation time was not long enough and the linear relationship might be only a part of the actual curve of the fouling process.

2.3.4.4 Crystal Growth

The stable nuclei which referred to particles larger than the critical size started to grow into visible crystal size as soon as they were formed in a supersaturation system. Different theories exist in the literature to explain this crystal growth process which included surface energy theory, adsorption layer theory, and diffusion-reaction theory.

2.3.4.4.1 Surface Energy Theory

(Gibbs, 1961) was the first to develop the surface energy theory on the crystal growth. His research concluded that the total free energy of a crystal is in equilibrium with the surrounding crystal at constant pressure and temperature would be minimum for a given volume. It illustrates that the equilibrium shape of a crystal is very much related to the free energy of the crystal surfaces. However, the surface energy theory hasn't been generally accepted due to the lack of sufficient evidence.

2.3.4.4.2 Adsorption Layer Theory

Numerous studies have attempted to explain crystal growth by adsorption layer theory. It described that a crystallizing substance unit loses one degree of freedom and is free to migrate between the crystal layer and bulk solution when it approaches the crystal face. Atom, ion, or molecules link to the lattice in positions where attractive forces are

greatest and stepwise build-up continues until the whole plane face is completed. (Burton, Cabrera, & Frank, 1951) developed a kinetic theory of crystal growth based on the relationship between crystal growth G and supersaturation ratio S as in Equation 2.5.

$$G = A(S - 1)^2 \tanh\left(\frac{B}{S-1}\right) \quad (2.5)$$

where A and B are constant depending on temperature.

2.3.4.4.3 Diffusion-Reaction Theory

(Noyes & Whitney, 1897) research work was the first approach to introduce the diffusion-reaction theory on the crystal growth, in which they considered the deposition of solid on a surface is a diffusional process. They also believed the crystallization process is a reverse of dissolution and occurs under the influence of concentration in solution near the solution and bulk. Up to now, a number of studies have reported this theory on the deposition on a surface. It suggested that crystal growth is in two stages in the mass deposition: transportation of solute molecule to the boundary surface (diffusion process) and arrangement of solute molecule in first order reaction into crystal lattice (reaction process) as shown in Equation 2.6 and Equation 2.7 respectively.

$$\text{Diffusion} \quad : \quad \frac{dm}{dt} = k_d A_s (C - C_i) \quad (2.6)$$

$$\text{Reaction} \quad : \quad \frac{dm}{dt} = k_r A_s (C_i - C_s) \quad (2.7)$$

where $\frac{dm}{dt}$ = rate of mass deposited in time t , A_s is a surface area, and C and C_i are solute concentration in the bulk solution and at the interface, respectively ; C_s is equilibrium saturation concentration, k_d = concentration of mass transfer by diffusion, and k_r is rate constant for the surface reaction (integration) process.

2.3.5 Overview of Scale Deposition Formation on Surface

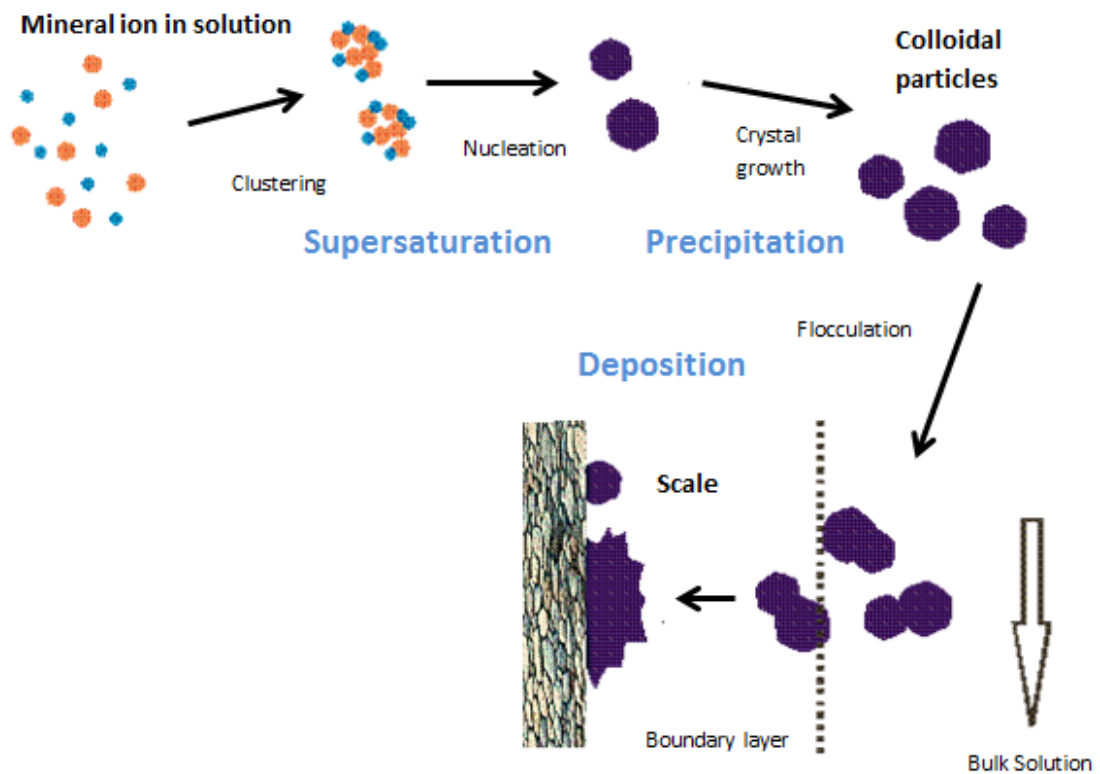


Figure 2.9: Overview of scale deposition formation on surfaces (Zahid Amjad, 2007).

Figure 2.9 described an overview of scale formation on surfaces. At first, mineral ion in the solution will be clustering whenever supersaturation condition within the bulk solution is reached. Following, nucleation started on surfaces and gradually growth into crystal size and forming colloidal particles. Finally, the colloidal particles deposited onto the surfaces.

2.4 Fouling on Heat Exchanger Surfaces

The deposited scales on heat exchangers create a severe reduction in heat transfer capacity in water processing industries (Morra, 2000). Moreover, scale build-up also causes changes in tube diameter, which significantly decrease the flow rate or increase the pressure drop across the heat transfer equipment. This problem is quite severe and is further exacerbated by the rough surface of the deposit. Fouling has been proven a

serious problem burdening the industry with costs and losses in production of hundreds of millions of dollars every year (Gleick, 2003).

The equipment life can considerably be improved by incorporating a proper and green environment mitigation approach. Therefore, there is a pressing need for solutions from both an economical and environmental point of view.

2.4.1 Deposition of Calcium Carbonate

(Bott, 1997) reported that in cooling water applications, scale deposition can form with the presence of small traces of salts such as CaCO_3 , CaSO_4 and CaC_2O_4 . One of the most common fouling is calcium carbonate form of scale. Calcium carbonate scale can be categorized into two crystal structures: calcite and aragonite. Calcite having a hexagonal crystal shape with a specific gravity of 2.71. Aragonite on the other hand has a rhombic crystal shape with specific gravity 2.94. Calcium carbonate is an inversely soluble salt against temperature as seen in Figure 2.10. Since all three forms of calcium carbonate have an inverse solubility characteristic, their solubility in water will decrease as temperatures increase. Therefore, the saturation concentration will decrease near the heated wall surface and gradually trigger the crystallization fouling of calcium carbonate near the heat transfer surface. Table 2.1 summarizes the properties of calcite and aragonite.

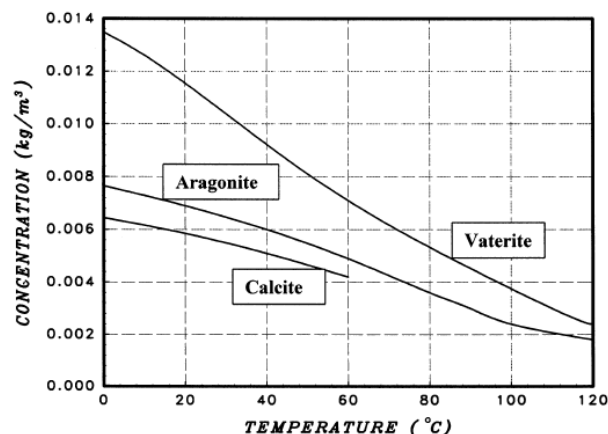




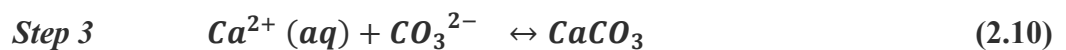
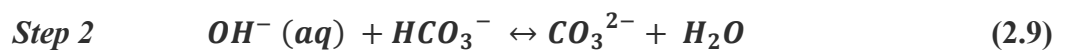
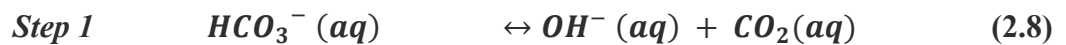
Figure 2.10: Solubility of calcium carbonate in water as function of temperature. (Helalizadeh, Müller-Steinhagen, & Jamialahmadi, 2000).

Table 2.1: Properties of calcite and aragonite. (de Leeuw & Parker, 1998)

	Calcite	Aragonite
Specific gravity	2.71	2.94
Crystal form		
	Hexagonal	Orthorhombic
Microscopic visualization	Round shape	Needle shape
Exact Mass	100.0869 g/mole	
Appearance	White powder	
Melting point	825 °C	1339 °C
Solubility in water	0.00015 mol/l (25 °C)	
Solubility product, K_{sp}	4.8×10^{-9}	
Acidity (PK_{sp})	1.59	

2.4.2 Scale Formation of Calcium Carbonate

(Snoeyink & Jenkins, 1980) stated that the main source of fouling in cooling water systems is the precipitation of calcium carbonate. Since water contains bicarbonate ions and not carbonate ions, the following three-step reactions describe the actual process of CaCO_3 precipitation:



The first reaction dissociates bicarbonate ions into hydroxide ions and carbon dioxide in aqueous form. One can expect a local increase in pH values due to the presence of hydroxide ions. The carbon dioxide gradually evolves into gaseous form over time in open cooling-tower systems and escapes from water, leaving a surplus of hydroxide

ions and raising the pH of the circulating water to above 7.0. Due to the excess of hydroxide ions, the pipe surface becomes negatively charged, attracting positively charged calcium ions and eventually making an “electric double layer” near the pipe wall. Moreover, a new reaction takes place between the hydroxide and bicarbonate ions as shown in the second reaction, which produces carbonate ions. Once the carbonate ions are produced, they react spontaneously with calcium ions to form calcium carbonate scale on the heat exchanger surface (Cho, Lee, Kim, & Suh, 2004).

Calcium carbonate formation is highly affected by pH value of the solution. The natural form of calcium carbonate can be calcite, aragonite and vaterite (R. Sheikholeslami, 1999).

Below pH 5.8, carbonate acid will exist whereas above pH 8.8 carbonate ions form. Between these 3 pH values, bicarbonate ions will exist in the water. To determine the saturation point of calcium carbonate, Driving Force Index (DFI) is used (Wang, 2005) :

$$DFI = \frac{[Ca^{2+}][CO_3^{2-}]}{K_{sp}} \quad (2.11)$$

$[Ca^{2+}]$ = concentration of calcium ion

$[CO_3^{2-}]$ = concentration of carbonate ion

DFI < 1.0 = calcium carbonate is supersaturated

DFI > 1.0 = calcium carbonate is under saturated

2.4.3 Process Parameter Affecting Fouling

2.4.3.1 Fluid Flow Velocity

Fluid flow velocity of the process plant is one of the important parameters affecting fouling. Over the years, different literature has been reporting the effect of velocity on the rate of deposition. (Hasson, Avriel, Resnick, Rozenman, & Windreich, 1968) were

the first to conduct an experiment to examine the effect of velocity on deposition. They reported that an increase in velocity of fluid flow would increase the rate of calcium carbonate formation. They demonstrated the higher velocities increase the deposition rate by diminishing the diffusional resistance. In contrast (P Walker & R Sheikholeslami, 2003) research argued that there is a decrease of deposition thickness with the increased velocity in the fully developed turbulent flow. It is due to the increment of the removal rate near the boundary surface which results in higher shear force near the solid-liquid interface. Numerous researchers also demonstrated that the velocity contributes to a higher shear force for removal rate and resulting lower deposition thickness.

2.4.3.2 Surface Temperature

Temperature has significant effects on the scale formation. A diversity of opinions of the temperature effect on fouling have been reported in the literature review. These literature reviews included the “positive, negative, or has no effect on the fouling rates” (Awad, 2011). This variation provides a huge interest among researchers to investigate the temperature effect. In 1985, (Budz, Karpiński, & Nuruć, 1985) investigated the effect of temperature on crystallization in a fluidized bed crystallizer. They revealed that increased temperature results in a lower nucleation rate. In contrast, (Chenoweth, 1990) reported that fouling build-up tends to be slower when the temperature is low and usually these deposits are easily removable. It is also supported by (Zahid Amjad, 2000) who described that it is more practical to follow as the temperature increases, expecting more fouling due to the scaling tendencies, faster reaction, crystal formation, “baking on” effect, and increased corrosion rate.

2.4.3.3 Surface Roughness

The literature review illustrated that the surface roughness is supposed to have the following effects: (1) The provision of “nucleation sites” that encourage the laying

down of the initial deposits (Yu, 2007). (2) The creation of turbulence effects within the flowing fluid and, probably, instabilities in the viscous sub-layer (P. Kukulka, Kukulka, & Devgun, 2007). In (S. N. Kazi et al., 2010) experiments have been reported that a better surface finish has been shown to influence the delay of fouling and ease cleaning. Similarly, non-wetting surfaces delay fouling. Similar results have been reported to support these findings (Hou et al.) in experiments which investigated protein crystallization under effect of surface roughness. They revealed rough surfaces encourage particulate deposition and provide a good chance for deposit sticking. After the initiation of fouling, the persistence of the roughness effects will be more a function of the deposit itself. In addition, (Demadis, 2003) experiments suggest that even smooth surfaces may become rough in due course due to scale formation, formation of corrosion products, or erosion.

2.4.3.4 Surface Materials

The selection of surface material is significant to deal with fouling. In a previous study (J Macadam & SA Parsons, 2004), different surface materials were found to be related to calcium carbonate deposition fouled on the materials surfaces. They found that copper fouled the most in the fouling experiment conducted for stainless steel, copper and aluminium scale formation and in the order copper > aluminium > steel. Following on from that, (S. Kazi, Duffy, & Chen, 2009) investigated the calcium sulphate deposition on copper, brass, stainless steel and aluminium. They reported that the extent of fouling on different metal surfaces increased with thermal conductivity of the metal (copper > aluminium > brass > stainless steel). Carbon steel is one of the common materials incorporating in industrial. Although its natural characteristic is to be relatively highly corrosive compared to copper and brass, it is the least expensive material among the others (Chigondo & Chigondo, 2016). Therefore, it would be of interest to investigate the fouling effect on carbon steel as well. Copper is the best

thermal conductivity material used in heat transfer application. However, it exhibits biocidal effects in water attacked by biological organisms including sulphate-reducing bacteria which would dramatically increase the fouling. In addition, copper alloys are prohibited in high pressure steam power plant heat exchangers, since the corrosion deposits of copper alloys are transported and deposited in high-pressure steam generators and subsequently block the turbine blades (E. Somerscales, 1990). Glass, polymer and Teflon tubes often resist fouling and/or improve cleaning but they have low thermal conductivity which is not applicable in heat transfer applications.

2.4.3.5 Impurities and Suspended Solids

As reported by (Davey & Garside, 2000), growth morphology can be affected by supersaturation, temperature, as well as impurities. Interruption of small amounts of impurities can initiate or substantially increase fouling. They can either deposit as a fouling layer or act as catalysts to the fouling processes. In crystallization fouling, the presence of small particles of impurities may initiate the deposition process by seeding. Sometimes impurities such as sand or other suspended particles in cooling water may have a scouring action, which will reduce or remove deposits (Bott, 1990). Suspended solids promote particulate fouling by sedimentation or settling under gravitation onto the heat transfer surfaces.

2.4.3.6 pH

Solution pH values have been studied corresponding to their effect on fouling. pH values play an important role in determining the fouling rate mainly on crystallization fouling. At neutral state (pH 7), fouling seems to occur the least. When the solution is either acidic or alkaline, the result will differ significantly. Below pH 6, only calcium sulphate is detected using X-ray powder diffraction (XRD) method. At higher pH value, both calcium carbonate and calcium sulphate foul at different percentages for every pH value. However, the highest strength of crystals formed at middle and upper layers is at

pH 7 and followed by pH 6. Although at these two pH values scaling will be less likely to occur, the crystallization occurrence will be very strong in terms of molecular bond. Conclusively, pH can significantly affect crystallization fouling (Höfling, Augustin, & Bohnet, 2004).

2.4.4 Previous Work of Fouling on Heat Exchanger

Fouling has been a challenge that has yet to be completely overcome. The main fouling in focus is crystallization fouling. Over the years, many researches have been carried out mainly into mineral fouling as tabulated in Table 2.2.

Table 2.2: Summary of mineral fouling research conducted from 1968 to current.

References	Hasson et al. (1968) (Hasson et al., 1968)	Sheikholeslami and Watkinson (1986) (R Sheikholeslami & Watkinson, 1986)	Bansal and Muller-Sheinhagen (1993) (Bansal & Muller-Steinhagen, 1993)
Concentration (ppm)	110-575	600-700	250-1000
Flow velocity (m/s)	0.25 - 0.82	0.30 - 0.80	0.25 - 0.85
Foulant	Calcium Carbonate	Calcium Carbonate	Calcium Sulfate
Surface material	Copper	Copper	Copper
Analysis Method	Fouling resistance	Fouling resistance	Fouling resistance
Results	Investigation of CaCO ₃ in an annular heat exchanger, scale layer growth increase with the flow velocity but decrease with surface temperature.	Investigation of CaCO ₃ on plain and externally finned heat exchanger tubes. They reported that fouling resistance reduce when flow velocity increase.	Investigation of crystallization fouling in plate heat exchanger. They concluded that fouling resistance was drop when velocity increases.

Table 2.2: Summary of mineral fouling research conducted from 1968 to current – continued

References	Lee and Cho (2002) (S. H. Lee & Cho, 2002)	Kazi et al. (2012) (S. Kazi, G. Duffy, & X. Chen, 2012)	Current Research
Concentration (ppm)	230-1120	3000-3600	300 - 500
Flow velocity (m/s)	0.60 - 1.50	0.26 – 1.3	0.15 – 0.45
Foulant	Calcium Carbonate	Calcium Sulfate	Calcium Carbonate
Surface material	Copper	Copper, Brass and Stainless Steel	Copper, Aluminium, Brass, Carbon Steel and Stainless Steel
Analysis Method	Fouling resistance and photo visualization	Fouling resistance ,photo visualization and SEM	Fouling resistance, real time video recorder, photo visualization and SEM
Results	Experimentally studied the velocity effect on electronic anti fouling technology to mitigate mineral fouling in enhanced tube heat exchanger. They concluded that the characteristics of the fouling mechanism are reduced due to fluid velocity increase in a heat exchanger.	Experiment studied the effect of velocity on heat exchanger and concluded that fouling resistance and crystal size reduce when velocity increase. In addition, higher foulant concentration promote higher deposition rate.	Experiment studied the effect of velocity on double pipe heat exchanger. They concluded that fouling resistance and crystal size reduce when velocity increase. Foulant concentration, surface temperature and different materials alter the scale deposition.

(Sudmalis & Sheikholeslami, 2000) put their efforts into studying fouling for pure salt in the last 50 years. It is very important to study this particular condition especially when its purpose is to determine two important facts. The first is regarding fouling mechanism for salts in mixing condition. It is probable that salts will foul differently in pure and impure state. The second is to determine whether there is a minimum amount

of impurities in salt that can affect thermodynamic and kinetic properties of original salt. If this doubt is true, then the data for pure salt will be useless in determining behaviour of mixing salt.

(Middis, Paul, Müller-Steinhagen, & Duffy, 1998) added fibres in the precipitation and found it effective in reducing fouling even the when the addition is in small proportion (0.05 mass percent). (S. N. Kazi, Duffy, & Chen, 2013) conducted similar experiments using fibre suspension of long softwood and short hard wood fibres at different concentrations. They reached a point where no fouling appeared when 0.25 mass percent of concentration was used. The experiment was then terminated after 46.5 days of constant-no-fouling condition.

(Quan, Chen, & Ma, 2008) used a method of forced convection to study its effect on fouling. They used dynamic monitoring apparatus of fouling resistance. They found that increasing fluid velocity will increase the fouling rate and asymptotic fouling resistance and decrease the induction period. In addition alkalinity and temperature of the solution will increase crystallization and particulate fouling.

(Dydo, Turek, & Ciba, 2003) analysed the scaling of Nano filtration system with $\text{CO}_3^{2-}/\text{SO}_4^{2-}$ molar ratio ranging from 0.05 to 2.8×10^{-3} . They identified both bulk and surface crystallization mechanism and also informed that fouling is affected by water quality.

2.5 Fouling Mitigation and Control

In 1993, (Steinhagen, Müller-Steinhagen, & Maani, 1993) revealed the problems and cost due to heat exchanger fouling in New Zealand industries. They outlined the most effective steps taken during the design of heat exchangers in industrial applications.

- i.) Selection of a suitable heat exchanger type
- ii.) Optimize industrial operating condition e.g. higher flow velocities
- iii.) Optimize heat exchanger design

In recent years, numerous methods have been developed to control fouling. These methods can be classified as chemical methods, mechanical methods and physical water treatment methods.

2.5.1 Chemical Methods

There are four essential methodologies for CaCO_3 scale control: (a) support of low operational pH (b) utilization of sequestrates (c) upkeep of low cycles of focus, and (d) utilization of scale inhibitors (Schoenitz, Grundemann, Augustin, & Scholl, 2015). Utilization of corrosive acid is a powerful approach to avoid calcium carbonate fouling development by keeping up a low pH. However, it raises worries because of its hazardous nature and the capability of accelerating metal erosion. The utilization of sequestering specialists is too excessive for open recycling water applications. Scale inhibitor use is a generally acknowledged practice and includes expansion of moment measures of scale inhibitors in the recycling water (Zhang, Hou, Sheng, Deng, & Xie, 2006). These added substances contain phosphonate and/or carboxylate amasses, and can be monomeric or polymeric. They work at threshold levels, since the inhibitor concentration ratio is extremely high (Rubasinghege & Grassian, 2013). It is believed that they perform “threshold inhibition” by a surface adsorption mechanism involving Langmuir adsorption. Adsorption onto the CaCO_3 crystal surface(s) causes inhibition (or delay) of crystal growth at the very early stages. On the topic of scale inhibition mechanism, three possible inhibitor mechanisms involved in scale inhibition were summarized by Liu et al. (X. Liu et al., 2012) as shown in Figure 2.11.

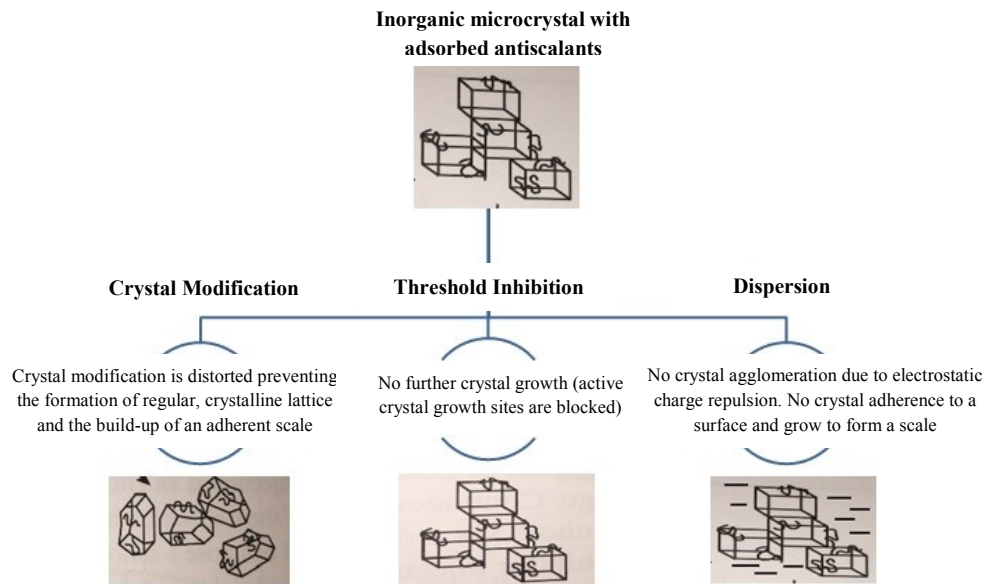


Figure 2.11: Summary of primary chemical scale inhibition mechanism (Nguyen, Roddick, & Fan, 2012).

Scale inhibitors are a group of chemicals that are capable of reducing the rate of scale formation and precipitation. The function of scale inhibitors is to prevent the scale mineral crystal growth (Z. Amjad, 2006). Application of scale inhibitors is by far the major scale control technique, the overall goal of the inhibitor treatment is to provide the longest possible protection against scale formation before another treatment is necessary (Frenier). As reported by Davey and Garside (R.Davey, 2000) , the growth morphology can be affected by supersaturation, solvent, temperature and additives. The inhibitors can alter crystal surface properties and influence the electrical double layers causing change in nucleation, growth retardation, agglomeration, and morphology (Hasson, Shemer, & Sher, 2011). Each face of the crystal has a different surface lattice structure and a different distribution of adsorption sites. The additives absorb onto the crystal surface, changing the charge of the surface and the associated electrical double layer, which in turn alters the dispersion properties. This varies the shape of the growing crystals (De Yoreo & Vekilov, 2003). The attractive features of these chemical additives such as ease of handling, relatively low cost, low dose rates, avoidance of corrosion

problems arising from the use of mineral acids, and ability to impact on hard scale formation have made their use widespread (Kavitha, Vasudevan, & Prabu, 2011).

Several chemical additives can be used to control scaling, but those that are used at present introduce hazards to the environment (S. N. Kazi et al., 2010; H. Müller-Steinhagen, M. R. Malayeri, & A. P. Watkinson, 2009). Therefore, investigators have tried to explore green additives, such as carboxyl methyl cellulose (CMC), cationic inulin polymer (cations), poly-allylamine hydrochloride (PALAM), and more environmentally benign additives (Z Amjad & Zuhl, 2008). A comprehensive study was done by Tung A. Hoang et al. (Hoang, Ang, & Rohl, 2009) of nine organic additives including EDTP, NTMP NDPA, HEDP, HEDP, NPDA, EDTA, NTA, citric acid and tartaric acid on the formation of calcium sulphate in a pipe system using a multiple flow system. The results revealed that a low concentration of additives can retard the growth of calcium sulphate scale on the pipe walls.

2.5.2 Mechanical Methods

(Pritchard & Freyer, 1988) generally categorized mechanical methods into two categories according to their ways of reaction. (1) Brute force methods such as high-pressure jets, lances, drill etc. (2) Mild methods such as brushes and sponge ball. (H Müller-Steinhagen et al., 2011) summarized the mechanical methods developed in recent years very much related to the process parameters such as flow velocity, flow direction, heat transfer surfaces, turbulence promoters and transport of cleaning devices through tubes. The deposits which are not strongly adhering to the surface can be removed by increasing the flow velocity. (Hans Müller-Steinhagen, 2010) reported that at higher flow velocity, the wall shear stress increases and causes more removal of deposits from the surface.

In addition, wood pulp fibres at various concentrations have mitigated fouling and reduced the deposition rate, showing that the life of a heat exchanger could be

prolonged. Middis et al. [28] have reported that the addition of small amounts of fibre into a calcium sulphate solution could create a reasonable reduction in the growth rate of the fouling deposition. They found that the fibres reduce the deposition rate by preventing the reactants from reaching the surface and also by continuous physical collision with the heat transfer surface. Kazi et al. [29] have extended their work by introducing a large pipe diameter, a larger heated section and a different pipe material, to represent conditions more relevant to industrial situations and found similar results. They have also noticed that with the rise of fibre concentrations, the fouling rate reduces for a longer period. No fouling occurred at 3.6 g/l $\text{CaSO}_4 \cdot 2\text{H}_2\text{O}$ concentration with 0.15% fibre concentration for 11 days [28, 30]. The study of fouling on different metal surfaces in a shear field approaches the reality of heat exchangers used in industry.

2.5.3 Physical Water Treatment

Physical water treatment (PWT) methods have been proposed to solve fouling problems and include the use of permanent magnets (Parsons et al., 1997), catalytic material alloys (G. J. Lee, Tijjing, Pak, Baek, & Cho, 2006), solenoid coil devices (L. D. Tijjing, Kim, Lee, Kim, & Cho, 2010) and natural fibres (S. N. Kazi et al., 2013). The major advantage of the PWT method is because of its eco-friendly environmental characteristic (Ashraf et al., 2013).

Numerous studies have been carried out to investigate the efficacy of catalytic alloys in solving calcium carbonate scaling by controlling scale formation from dissolved impurities. Macadam and Parsons (2004) investigated the effectiveness of calcium carbonate precipitation using copper and zinc (Tang, Meng, Liang, Nie, & Li, 2010). They observed that 5mgL^{-1} of zinc reduces fouling by 35%, which indicates that zinc is an effective inhibitor. Tai and Chien (2002) and Tao (2006) showed that the induction period could be prolonged by adding magnesium ions in the fouling solution (Tai & Chien, 2003). Yang (2002) discovered that the addition of 2mgL^{-1} of zinc retards

deposition of calcium carbonate fouling in the system significantly (Yang, Liu, Gu, Ding, & Shen, 2002). Based on the findings of previous studies, it is evident that crystallization fouling is significantly influenced by a variety of parameters (Alahmad, 2008). For example, the operating conditions (flow velocity, wall and bulk temperatures) (D. J. Kukulka & Devgun, 2007), solution properties (salt, degree of supersaturation) (R. W. Morse & Knudsen, 1977) as well as the geometry of the system (thickness of the laminar boundary layer, shear forces) (B. Thonon, 1999) influence the formation of the deposition layer on the heat transfer surface. In general, it is not possible to investigate the effects of all crystallization fouling factors, and the investigation needs to be limited within a specific scope. Nevertheless, it is imperative to investigate the influence of such factors in order to inhibit crystallization fouling as well as provide a detailed model of the fouling process.

2.6 Summary

The formation of mineral scales is a complex and not fully understood problem faced in industrial sector. There are numerous mineral depositions, such as calcium carbonate, calcium sulphate and silica which can be formed in processes where water is used. Presently, discrepancy exists in calcium sulphate fouling data in the literature and other depositions salts have not been fully understood yet. The major efforts are to determine process parameters effect on calcium carbonate deposition such as temperature, velocity, concentration and surface materials.

In addition, fouling deposition problems impact to the economy is a serious concern, still there is lack of awareness in concerned authorities. Therefore the present chapter will promote the overview and raise awareness of concerned organisations about seriousness of this problem and application of possible mitigation approach.

CHAPTER 3: INSTRUMENT AND EXPERIMENTAL SETUP FOR FOULING ON DOUBLE PIPE HEAT EXCHANGER

3.1 Analysis Methods

Characterization of nanofluids and fouling particles is an important task to understand and verify the findings of the experimental results. Details of the methods are stated and discussed in the following section.

3.1.1 Scanning Electron Microscopy (SEM)

Scanning Electron Microscopy (SEM) is a non-destructive and versatile method used to observe the crystal morphology of fouling particles (e.g. calcium carbonate) on the piping surface materials. It can produce images of sample surfaces and cross sections of membrane up to 1000x and even 10000x magnification and 10 kV scanning voltage. The surface of the solid being analysed must be conductive, and thus the fouled calcium carbonate on metallic piping surfaces is suitable for this analysis. SEM analysis in this study was performed using a JEOL JSM-6460LA Scanning Electron Microscope (SEM). The fouled coupon sample to be characterized was placed onto an aluminium sample holder with double sided carbon tape as adhesive before analysis. Figure 3.1 illustrates the schematic layout of a scanning electron microscope. The working principle of SEM is using electrons instead of light to generate an electron beam. The specific area of surfaces under investigation is scanned and focused by this electron beam. When an electron beam strikes on a sample, a large number of signals are generated and detected signal by the x-ray detector and then converted to an image of sample as a surface topography (Goldstein et al., 2012).

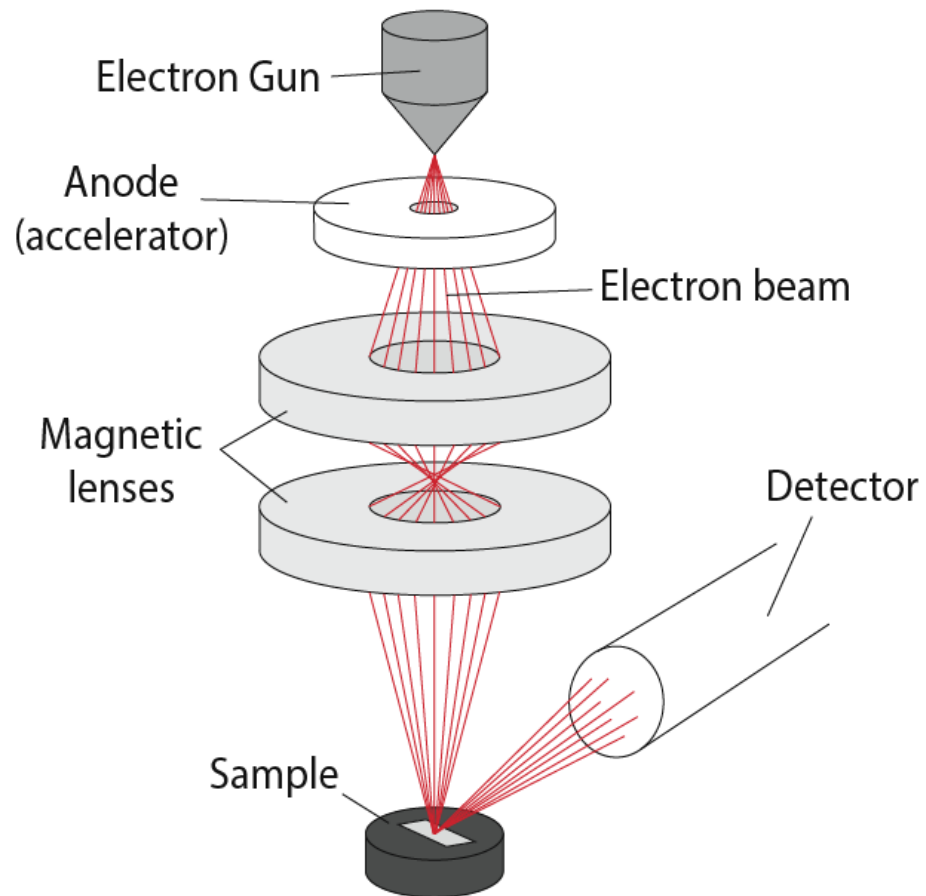


Figure 3.1: Schematic layout of a scanning electron microscopy (Collett, 2007).

3.1.2 Energy Dispersive X-Ray Spectroscopy (EDS)

Energy-dispersive X-ray spectroscopy (EDS) is an analytical technique used for chemical characterisation or elemental analysis of samples. It relies on an interaction of some source of X-ray excitation and a sample. Its characterization capabilities are due in large part to the fundamental principle that each element has a unique atomic structure allowing a unique set of peaks on its electromagnetic emission spectrum (which is the main principle of spectroscopy).

3.1.3 X-Ray Powder Diffraction

X-Ray diffraction analysis is used to identify the fouled crystal compound deposited on the surface to investigate the types of the crystalline elementals. Different crystals have

different d spacing. Therefore by measuring the d spacing, different compounds can be identified. Crystals from each experiment were analysed. The test sample for this analysis was made up from very fine powder obtained by crushing the crystals from the surfaces before the sample was spread on the surface of the sample holder using pieces of glass to minimize the effect of preferred orientation on the XRD pattern. XRD-6000 Shimadzu X-Ray Diffractometer with $\text{CuK}\alpha$ radiation generated at 30 mA and 40 kV was used in this experiment. Step scans are performed from $10 - 70^\circ 2\theta$ at $0.02^\circ 2\theta$ steps, integrated at a rate of 1.2 second per step.

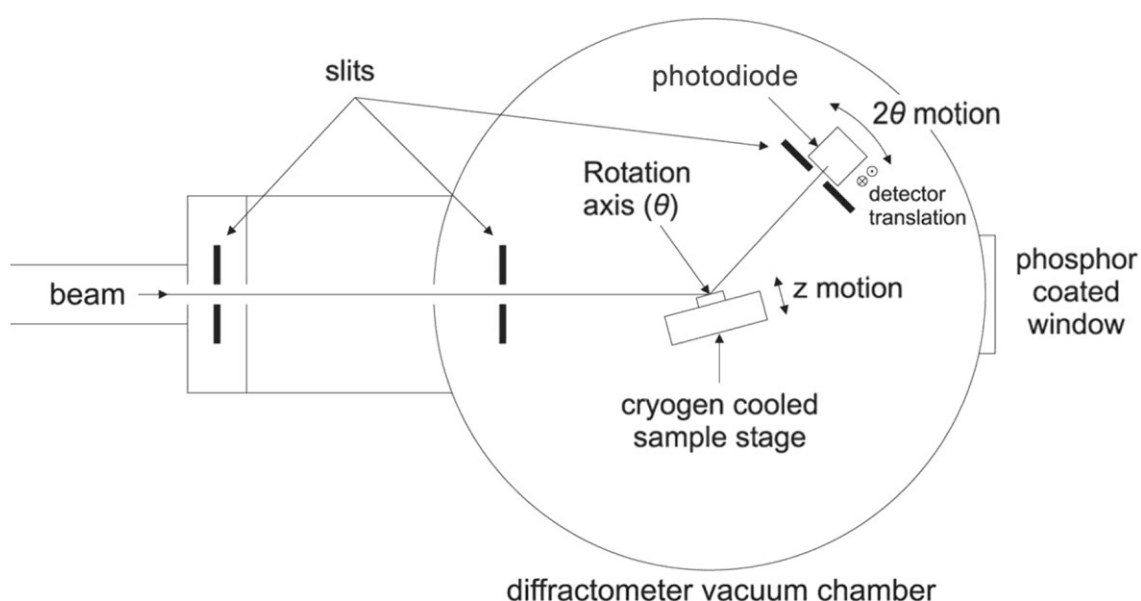


Figure 3.2: Working principles of XRD (Bunaciu, UdrişTioiu, & Aboul-Enein, 2015).

As seen in Figure 3.2, the main working principle of XRD is using Bragg's Law. A detector detects the X-ray signal and converts the signal by analysing the changing angle between the X-ray source and the sample.

3.1.4 Transmission Electron Microscopy

Transmission electron microscopy (TEM) is the primary technique to verify the dimensions of a single particle and to identify agglomerations of particles. The electron beam can be used to observe the features at the nanometer level. The samples must be dried out of solution in order to be attached to the carbon matrix and placed in the

vacuum chamber of the TEM; therefore the particles are not exactly in the colloid state and agglomeration might occur during drying. However, TEM can be used in combination with dynamic light scattering to acquire exact sizing in nanofluid form. Another drawback of TEM is the cost and time investment needed to prepare and view the sample. It was decided to perform some initial imaging as a feasibility study. Transmission electron microscopy (TEM) measurements were conducted on a CARL ZEISS-LIBRA120 microscope. The TEM operates on the same basic principle as the SEM. When an electron beam is passed through a thin-section specimen of material, the electrons are scattered. A sophisticated system of electromagnetic lenses focuses the scattered electrons into as image or a diffraction pattern, or a nano-analytical spectrum. Figure 3.3 shows the schematic layout of TEM.

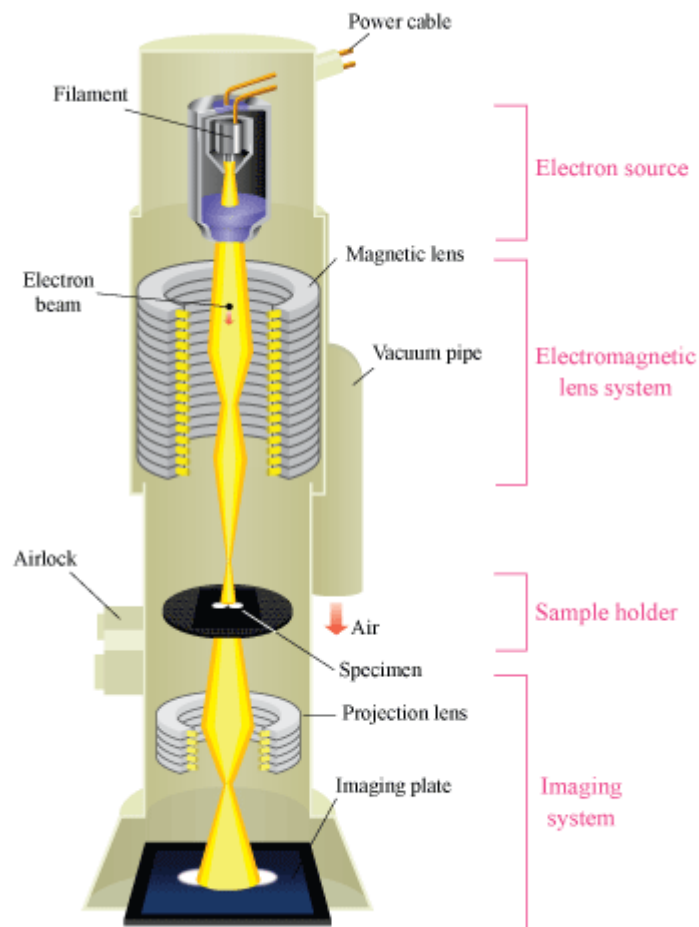


Figure 3.3: Schematic layout of TEM.

3.1.5 Fourier Transform Infrared Spectroscopy

Fourier transform infrared spectroscopy (FT-IR) samples were prepared by grinding a very low concentration of dry material with potassium bromide (KBr) to form a very fine powder. FTIR Analysis is an analytical technique used to identify organic, polymeric and inorganic materials. This powder is then compressed into a thin pellet which can be analysed. Functional groups on the basis of the carbon nanotube surface were analysed by Fourier Figure 3.4 illustrates the Transformation Infrared Spectrometer (Perkin Elmer-spectrum100 model FT-IR) at the wave ranges of 4000-400 cm^{-1} .



Figure 3.4: Photography of Perkin Elmer-spectrum 100 model FT-IR.

3.1.6 Electric Conductivity

Electrical conductivity of the nanofluids both as functions of loading and fluid temperature were measured using AB200 pH/Conductivity Meter (Fisher Scientific). The conductivity meter has a measuring range between 0 and 500 mS/cm and a resolution of 0.1%. Prior to the measurements, the meter was calibrated using the buffer solutions of known electrical conductivities. Measurements were taken by using ~ 40 ml of the nanofluid sample in a beaker which is located in an isothermal bath, with the

conductivity probe immersed in it. At each temperature, the measurements were repeated 5 times, and the average value was taken.

3.1.7 Surface Roughness Measurement

A model of Mitutoyo SJ-210 portable surface roughness tester was used to make measurements on the piping test section before the fouling study as seen in Figure 3.5. The 2.4-inch colour graphic back-lit LCD provides excellent readability and an intuitive display that is easy to use. Up to 10 measurement conditions and one measured profile can be stored in the internal memory. All the collected data complies with the applicable international standards concerning definition and calculation of the values of surface roughness parameters. In addition to calculation results, sectional calculation results and assessed profiles, bearing curves and amplitude distribution curves can be displayed.

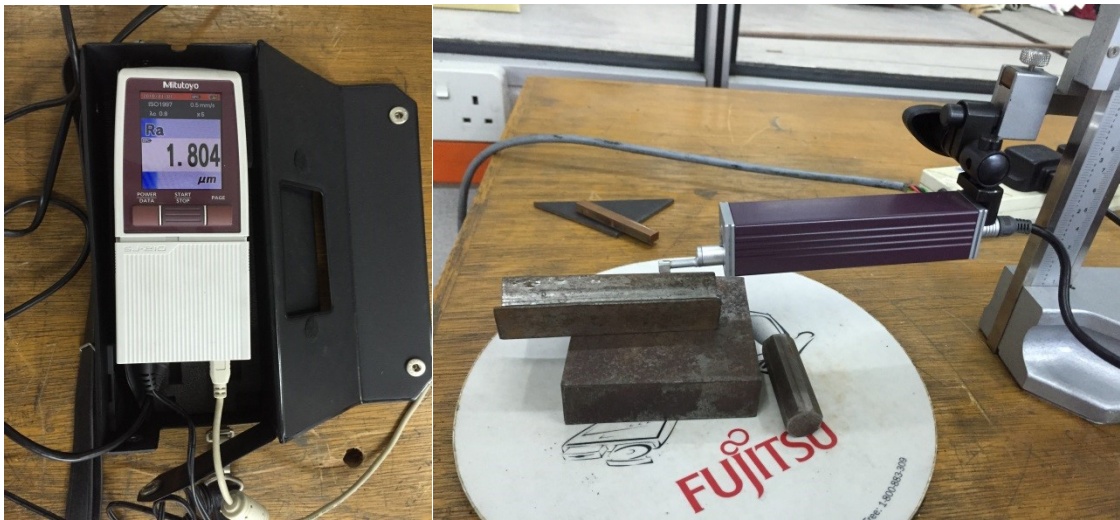
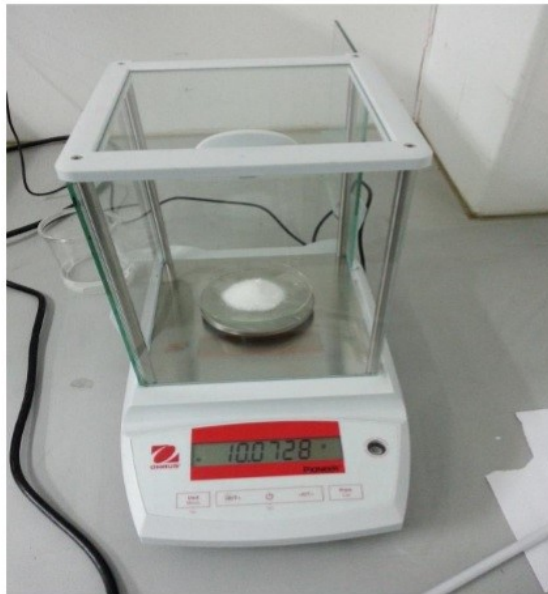


Figure 3.5: A model of Mitutoyo SJ-210 portable surface roughness tester.

3.1.8 Electronic Weighting Balance

Electronic weighting balance was used to measure the weight of chemical required for the solution preparation. In addition, the weight deposition on the coupon surface before and after the fouling test was performed by measuring the weight difference on this electronic weighing balance. The high accuracy of the balance obtained a precise

reading of the measurement. Figure 3.6 illustrates the specification of the electronic weighing balance.



Model Number	JA-500
Type	Laboratory Balance
Power Supply	100-220V
Display Type	Large LCD
Rated Load	500g
Accuracy	0.0001/0.01g

Figure 3.6: Electronic Weighing Balance.

3.1.9 KD2-Pro

Thermal conductivity of the nanofluids is one of the important properties to be characterized in this study. In order to characterize the enhanced thermal conductivity, an inexpensive commercially available system was introduced for the measurement of the thermal conductivity (Mehrali et al., 2014). The Decagon Devices KD2 thermal properties analyser (KD2 Pro, Decagon Devices, Inc. USA) is used for nanofluids at room temperature as a first check. The accuracy of the KD2 is given as 5% margin of error by the manufacturer over a span of temperatures from 0 to 60°C. However it is found, through trial and error, that the KD2 operates very accurately if the probe is set up perfectly vertical and an isothermal bath is used to maintain the sample at 25°C. These techniques prevent convection problems and the external boundary effect problems as well. A schematic of the KD2 setup with the isothermal bath is shown in Figure 3.7.

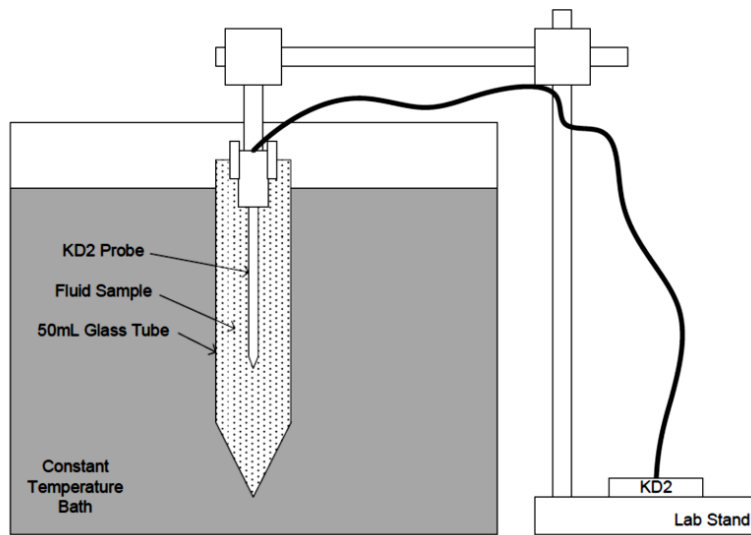


Figure 3.7: Schematic Setup of KD2 Thermal Properties Analyser.

Thermal conductivity measurements in this work were done based on the Transient Hot-wire (THW) method and the analyser device used has 5% margin of error between 5°C and 50°C (Mehrali et al., 2014). THW methods is a standard transient dynamic technique based on the measurement of the temperature rise in a defined distance from a linear heat source (hot wire) embedded in the test material (Roder, 1981) The thermal conductivity measurements for distilled water are within 2-4% of previously reported data (Buongiorno et al., 2009) as shown in Figure 3.8 The thermal conductivity measurements were repeated ten times and the average values were reported.

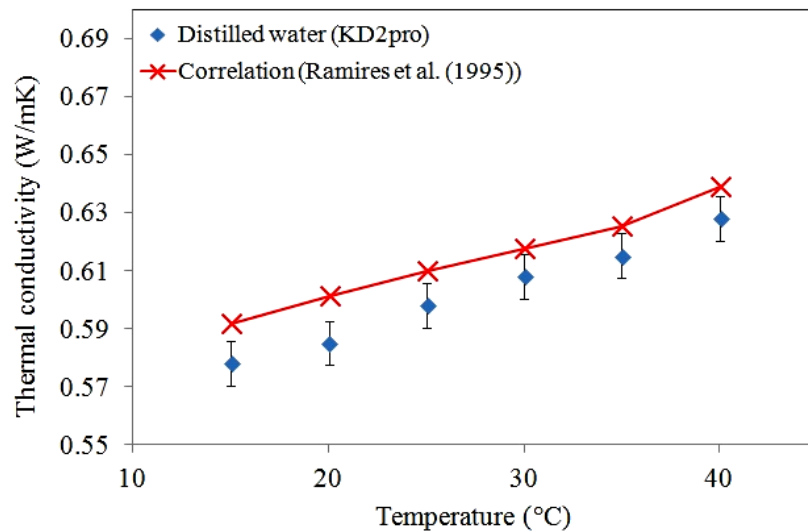


Figure 3.8: Comparison between distilled water and previous data.

3.2 Description of the Experiment

3.2.1 Experimental System

The experimental test rig basically consists of a double-pipe heat exchanger 1300 mm in length and specially designed to minimize corrosion effect which will affect experiments accuracy. For this reason HDPE has been employed for all the ancillary piping and fittings in contact with artificial hard water, as well as for the main heat exchanger which consists of outer pipe made of acrylic tubes for clear visualization and inner tube of different materials to be tested. In order to examine the heat transfer conditions, metallic tubes were heated from inner tube by a distilled water closed system to maintain a tube surface temperature equal to prescribe bulk temperature. The hot water temperature set point was 50 °C with a difference through the inner tube of only 0.5 °C, this being achieved by employing a flow rate of 1m/s through the inner tube, giving a high thermal capacitance to the hot fluid. Cooling artificial hard water flows in one pass through the heated tubes, as fouling is formed on the outer surface and its flow rate is automatically regulated to maintain a prescribed flow velocity. Flow-meter sensors were calibrated periodically to ensure a relative error not greater than 5%. Resistance thermometer (RTDs) are 0.1 °C accurate, and were also frequently intercalibrated; then, the observed measurements were corrected accordingly. RTDs were calibrated via the use of an Ametek temperature calibrator (AMETEK Test & Calibration Instruments, Denmark). All measurement instruments were connected to the SCADA system for the continuous monitoring and recording of the temperature data by WINCC software at the workstation. SCADA system composes of PLC used for control and monitoring. On the other hand, WINCC software is an interface program used as interpretation software for data collection.

Taking into account that the type and rate of fouling will be dependent on the specific characteristics of the cooling artificial hard water, climatology and other operating

conditions of every industrial cooling water system, in situ studies must be made. Consequently, the experimental test rig was arranged for the Programmable Logic Controller (PLC) control system to achieve the desired constant parameters.

In order to obtain a better understanding of the effect of catalyst material for the fouling progression, a set of experiments was designed. Tests over periods of about 72 hours were carried out to evaluate the effect of catalyst material on crystallization fouling development. A set of experiments were examined with comparison of treatment and no-treatment cases of catalyst material.

Flow velocity was maintained nearly constant throughout the experiment, with a Coefficient of Variation (standard deviation/average value) less than 10 %. Physical and chemical properties of the cooling artificial hard water, such as pH, conductivity and salinity registered minimal variations. Such stable environmental conditions together with the capabilities of the experimental test rig, helped obtain meaningful and congruent data.

Throughout the experiments, the signals of the sensor were automatically recorded: cooling water temperature (in and out), flow rate and pressure drop, as well as the inlet and outlet bulk temperature in the cooling water artificial hard water. From all these measured variables, on-line instantaneous data was obtained for computing the increment of heat transfer resistance due to fouling development.

The overall heat transfer resistance (sum of conductive and convective resistance) is expressed by the reciprocal of the overall heat transfer coefficient and can be easily determined for each tube. The resistance due to fouling is then determined by calculating the difference in fouling resistance between fouled and clean conditions.

The specification and the accuracy of the measuring instruments and sensors used in the present experimental setup are presented in Table 3.1. Table 3.2 tabulated the summary of fouling experimental conditions for heat transfer and pressure loss studies.

Table 3.1: Specification and errors of the measuring instruments and sensors used in the present experiments.

Measured parameter	Instrument and sensor type	Operating	Signal Output	Error
Temperature	RTD (PT-100) sensor	0-200 °C	n/a	± 0.1 °C
Fluid flow rate	Electromagnetic flow meter (NFLO-KF700)	0.03m/s ~ 12m/s	4-20 mA	± 0.5 %
Fluid pressure drop	Different pressure transmitter (DPT) (YOKOGAWA EUA110E)	0-200 mbar	4-20 mA	± 0.075 %
Cooling Unit	WiseCircu, Refrigerated circulating bath, Industrial Chiller	2.2kW – 8 kW	n/a	± 0.1 °C
Heating unit	Immersion Tube Heating coil	4 kW	n/a	± 0.1 °C

Table 3.2: A summary of fouling experimental conditions for heat transfer and pressure loss studies.

Fluid types	Artificial hard water (CaCO ₃),
Concentration	300mg/l , 400mg/l, 500mg/l
Test section material	Stainless Steel, Aluminum, Carbon Steel, Copper and Brass
Velocity range	0.15m/s ,0.30m/s, 0.45m/s
Solution Bulk Temperature	25°C
Hot flow line temperature	50°C ,60°C, 70°C

3.2.2 Design and Construction

Some basic requirements are developed as a design consideration for the double pipe heat exchanger loop. These requirements are generated in order to meet our research goal: some to simulate heat exchanger condition, some to meet existing equipment and lab requirements and finally some limitation condition.

3.2.3 Test Section

The experimental pipes are 1300mm in length with a wall thickness of 2.11 mm and outer diameter of 12.7mm. Five metal pipes (copper, aluminium, brass, carbon steel and stainless steel 316) with the same dimensions were used in these experiments. It can be seen in Figure 3.9, the coupons were installed in the middle of the test section. A double pipe heat exchanger was fabricated as shown in Figure 3.10. Metal pipes were located centrally in an acrylic pipe with dimensions of 47.1mm outer diameter and 42.7mm inner diameter. An overview of double pipe heat exchanger dimensions can be seen in Figure 3.11. Characterizations of the fouling deposition on the surfaces were conducted after completion of the fouling test.



Figure 3.9: Coupons of different materials on heat exchanger surfaces.

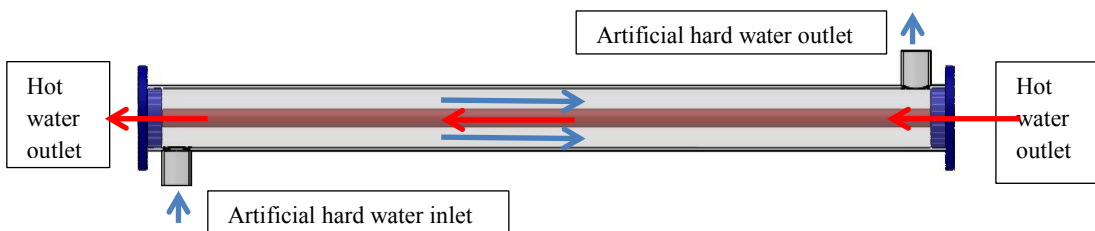


Figure 3.10: Schematic drawing of double pipe heat exchanger with metal pipes located centrally as an inner tube.

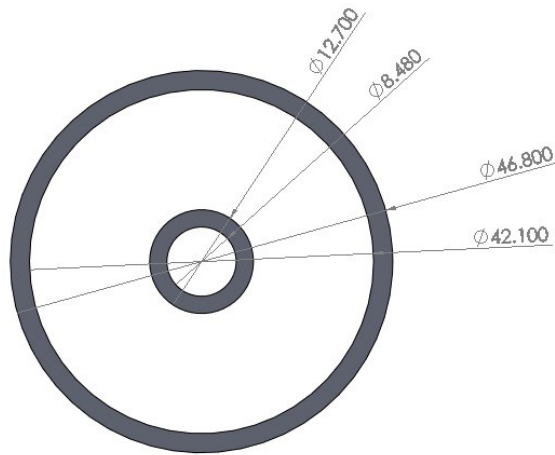


Figure 3.11: Overview dimensions of double pipe heat exchanger.

The smooth test specimen pipes (Table 3.3) were used in the as-received condition but before installing in the test rig, they were cleaned by rubbing with a water-soaked cloth and flushing with hot water to remove any deposition of grease and oil.

Table 3.3: Physical properties of different heat exchanger materials at 300 K.

Materials	Properties at 300 K			
	ρ (kg/m ³)	C_p (J/kg.K)	K (W/m.K)	R_a (μ m)
Aluminum	2702	903	250	2.16
Brass	8530	380	109	2.18
Stainless Steel	8238	468	16	1.27
Copper	8960	385	401	2.22
Carbon Steel	7850	502	90	2.34

3.2.4 Reservoir Tank

The reservoir is a Jacketed Stainless steel tank of cylindrical shape with a capacity of 20 litres and 40 litres for hot flow tank and solution flow tank respectively. The reservoir tanks are kept 30 cm above the gear pumps so that the gear pumps have adequate inlet

flow to avoid cavitation. At the bottom of the reservoir a pipe connects to the gear pump while at the top there is a bypass line, return line and top stirrer for mixing fluid inside the tank as presented in Figure 3.12.

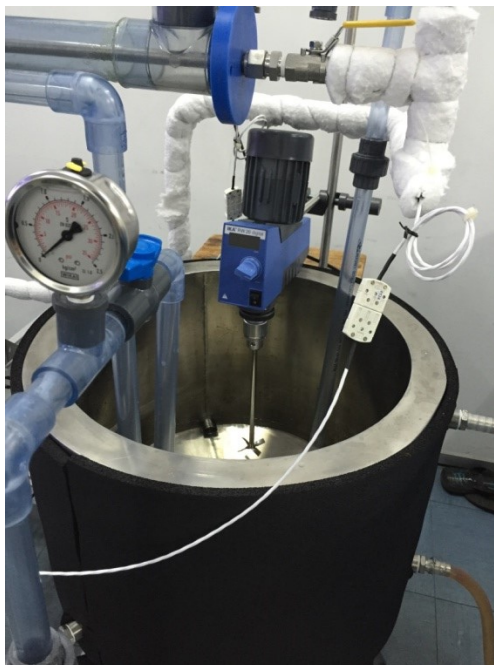


Figure 3.12: Jacketed Stainless steel tank of cylindrical shape with a capacity of 40 litres for solution flow tank.

3.2.5 Magnetic Gear Pump

Two gear pumps (Araki EX-100RM magnetic driven seal-less chemical pump – Figure 3.13) was used in the solution flow loop and hot flow loop to circulate the solution throughout the system.



Figure 3.13: Araki EX-100RM magnetic driven seal-less chemical pump.

It is rated for a maximum flow of 120 litre per minutes and max head of 8.6 meter. This pump is capable of operating at variable speed with the maximum rated speed of 2800 rpm. The suction side of the pump is connected to the reservoir. The pump is capable of operating with water up to 80 °C due to the shaft seal limitation. After rough estimation of the total loop pressure losses and acknowledgement of the pump characteristic curve, it is found that the pump should be capable to reach our desired velocity throughout the system. Therefore, the pump is deemed usable for the experiment. Table 3.4 shows the pump specification used in these experiments.

Table 3.4: Specification of the magnetic driven pump.

Type	Hose connected		Threaded connected		Max Capacity	Max Head	Temperature	Motor		
	Inlet	Outlet	In/Out	Union				Output	Input	Phase
EX-100RM	26mm	26mm	G1	20	120 L/min	8.6 m	0-80 °C	260W	245W	1

3.2.6 Inverter

Hoffman Muller inverters were used to control the speed of the pumps in the hot flow loop and solution flow loop respectively as shown in Figure 3.14.



Figure 3.14: Hoffman Muller inverter used to control both pumps' speed.

The specifications of the inverters are presented in Table 3.5.

Table 3.5: Technical specification for V8 series inverters.

Items	Contents
Model	HM-V8A11P5B
Input	AC, 1PH, 230V, 50/60Hz
Output	3PH, 1.5kW, 7A, 0-650Hz

3.2.7 Electromagnetic Flow Meter

N-FLO-25 Electromagnetic flow meter was used to measure fluid flow rate (see Figure 3.15) throughout the experiment. A magnetic flow meter is a volumetric flow meter which does not have any moving parts and is ideal for wastewater applications or any dirty liquid which is conductive or water based. Magnetic flow meters are also ideal for applications where low pressure drop and low maintenance are required.

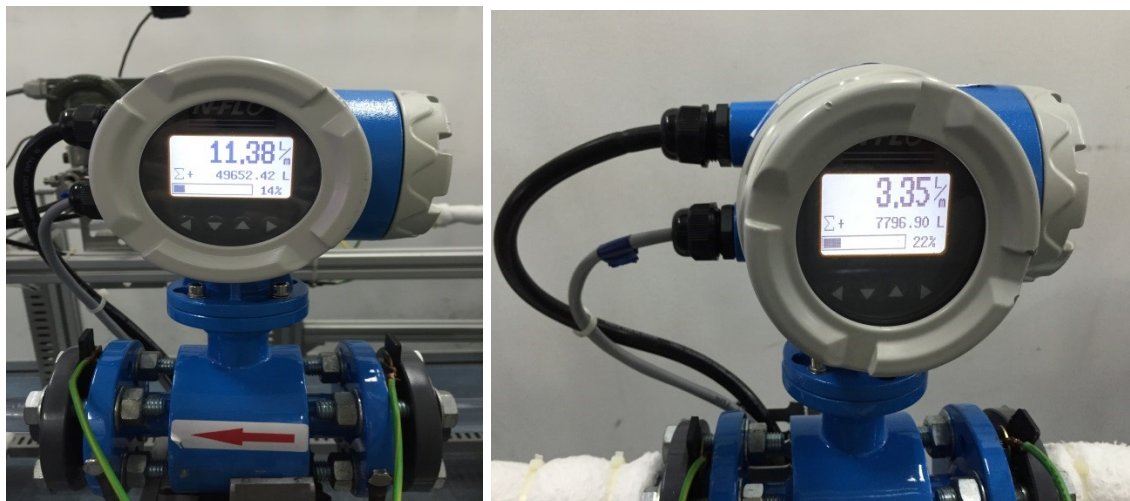


Figure 3.15: Photograph of the Electromagnetic flow meter used for cold flow line (left) and hot flow line (right).

The operation of a magnetic flow meter or mag meter is based upon Faraday's Law, which states that the voltage induced across any conductor as it moves at right angles

through a magnetic field is proportional to velocity of the conductor. The technical specifications are presented in Table 3.6.

Table 3.6: Technical specification of Electromagnetic Flow Meter.

Items	Contents
Model	N-FLO-25 Electromagnetic Flow Meter
Sensor Range	DN10- DN3000
Measurement flow range	0.03m/s – 12m/s
Measurement Accuracy	±0.5%
Repeatability	±0.1%
Application temperature	-20 °C – 80°C
Minimum conductivity of measured liquid	5µs/cm
Lining	Teflon (PTFE)
Measuring electrodes	Hastelloy C4 standard

As stated above, the flow meters were calibrated before being supplied by the manufacturer, as shown in Table 3.7.

Table 3.7: Flow meter calibration data.

Flow (m ³ /hr)	Volume (L)	Actual(L)	Error (%)	Repeatability (%)
0.3	15.980	16.015	0.22	0.165
1.5	61.911	61.911	0.00	0.062
3	123.601	123.646	0.04	0.037

3.2.8 Differential Pressure Transducers

The smart YOKOGAWA differential pressure transmitter (Model: EJA110E) with accuracy of ±0.075% of span connected to the inlet and outlet of the test section was used in this experiment (see Figure 3.16).

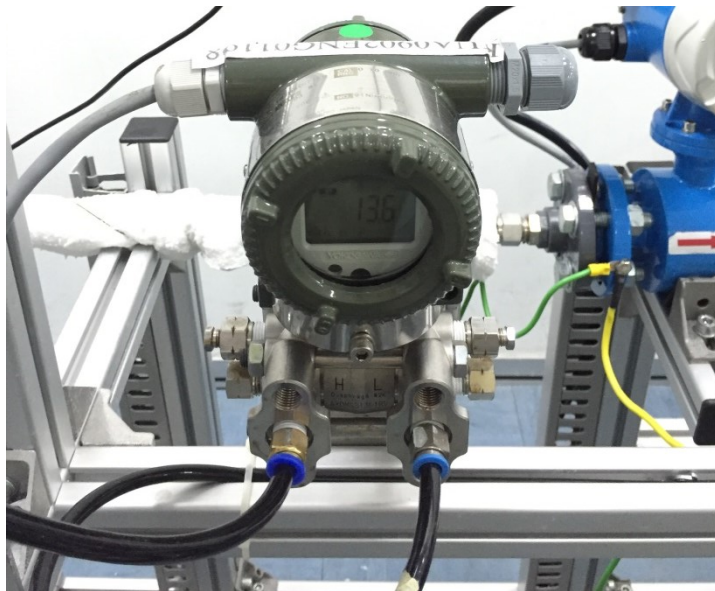


Figure 3.16: Photographs of the Differential Pressure Transducers.

The standard specifications of the Differential Pressure Transducers are presented in Table 3.8. The calibration condition, static pressure test and differential pressure test are presented in Tables 3.9 to Table 3.11, respectively.

Table 3.8: Standard specification of the Differential Pressure Transducers.

Items	Contents
Model	EJA110E
Process Fluid	Liquid, Gas or Vapour
Application	Differential Pressure, Gauge Pressure, Absolute Pressure
Measuring Range	0.5 to 20 Kpa (5-200mbar)
Accuracy	± 0.075% of span
Stability	± 0.15% of URL for 2 years
Working Temperature	-25 to 95°C
Max. Pressure	20 Kpa
Body Material	SS 304
Diaphragm	SS 316L

Table 3.9: Calibration condition.

Ambient temperature	Grounding resistance	Relative humidity	Calibration Range
20°C	>200MΩ	60%	0 ~ 20KPa

Table 3.10: Static pressure test.

Differential Pressure Value	Static Pressure = 4.00 MPa			
	1 ATM	Error (%)	4MPa	Error (%)
0.0 KPa	4.000 mA	0.000	4.012 m A	0.075
50.0 KPa	20.003 mA	0.019	20.000 mA	0.000

Table 3.11: Differential pressure test.

D/P value (KPa)	Output	Zero to F.S.	Error (%)	F.S. to Zero	Error (%)
0.0	4.00 mA	3.998 mA	-0.012	4.009 mA	0.056
5	8.00 mA	7.991 mA	-0.056	7.997 mA	-0.019
10	12.00 mA	11.992 mA	-0.050	11.992 mA	-0.050
15	16.00 mA	15.990 mA	-0.062	15.999 mA	-0.006
20	20.00 mA	19.997 mA	-0.019	19.992 mA	-0.050

3.2.9 Cooling Unit

3.3.5.1 Refrigerated Bath Circulator

A refrigerated bath circulator (WiseCircu- WCR-P30) shown in Figure 3.17 was used to maintain our desired heat input by circulating the cooling fluid inside the jacketed tank.

This refrigerator bath has:

1. RS232C Interface for Remote Monitoring and Controlling with PC
2. Stainless steel bath (#304) for superior durability & High Thermal Efficiency.
3. Powerful circulation pump to ensure temperature uniformity between internal and external circulation.
4. Locking mode supported for experimental safety

5. Simplest Control by Jog-Shuttle Switch (Patent pending) and Digital LCD display.
6. Storage functions for repeated applications in the laboratory under identical conditions.



Figure 3.17: WiseCircu - WCR-P30 Refrigerator Bath Circulator.

The specifications of the refrigerated bath are listed in Table 3.12.

Table 3.12: Specifications of the refrigerated bath.

Items	Contents
Capacity & Models	30L, WCR-P30
Temp. Range & Accuracy	-25°C ~ +150°C, ± 0.1°C
Temp. Resolutions	0.1°C-Display & Control
Temp. uniformity & Probe	± 0.2°C at -10°C, PT100
Heating Power	2.2kW
Refrigerator	7/8 HP
Cooling capacity at +20°C	631 W
at 0°C	429 W
at -20°C	284 W
Refrigerant	CFC-Free (R-404A) Refrigeration System

3.3.5.2 Air Cooled Industrial Chiller

A higher capacity with better performance air cooled industrial chiller (XC-05ACI) was used to maintain experiments' temperature in the desired ranges for long running hours.

The air cooled chiller was equipped (Figure 3.18) with safety protection and error

indication system with figure intellectualized temperature controls, which can accurately measure and control temperature within the range of 5°C- 35°C. Table 3.13 gives the specification of the chiller used for the experimental setup.



Figure 3.18: Air cooled industrial chiller used in experiment.

Table 3.13: Specification of air cooled industrial chiller.

Items	Contents
Cooling capacity	12040 Kcal/h
Compressor	All-closed vorticity
Compressor power	4.4 Kw
Refrigerant	R22
Chiller water pump power	0.75 Kw
Max flow rate of chilled water	120 L/min
Cooling fan power	0.5 Kw
Water tank capacity	68 L

3.2.10 Heater

The hot water tank was heated by a double-ended tubular heater. Hot water fluid circulates by pumping into the hot flow line and heating up the test section. The heater has a specification of 940 W, 13 W/in², 240 V and maximum exposure temperature of 982 °C. The versatility of this tubular heater means it can be used in virtually the entire range of air heating and immersion processes. A photograph of the heater used in the

experimental set-up is presented in Figure 3.19. This heater is then connected to a PLC system for regulating the amount of heat input to the hot water tank.



Figure 3.19: Double ended tubular heater immersed in hot tank for heating purposes.

3.2.11 Power Control

WINCC software was used to control the power supply and to record the data which was connected with the SCADA system. The maximum power output of 20 A and output voltage of 0-240 V was used to regulate the voltage. A snapshot of the WINCC software and SCADA system to control the power supply is shown in Figure 3.20.

Details of the power distribution are illustrated in Appendix A.

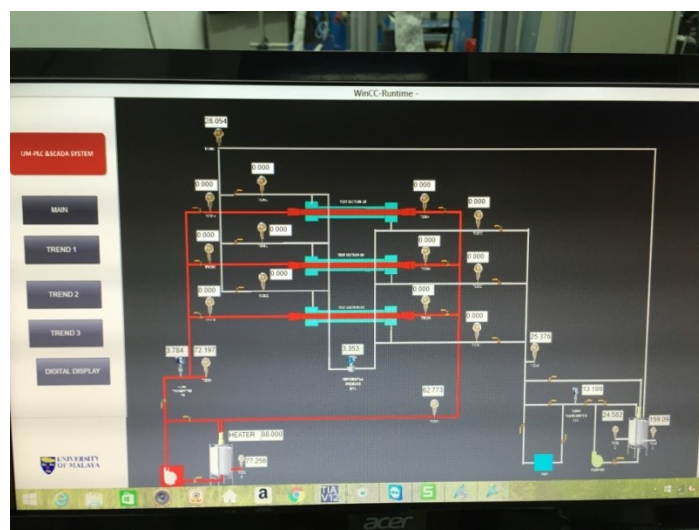


Figure 3.20: WinCC interface for control and monitoring of the experiments setup.

3.2.12 Thermocouple

Thermocouples were used throughout the experiment for the measurement of temperature. The thermocouples were used for the bulk fluid inlet and outlet (bulk) temperatures, hot fluid inlet and outlet temperature, solution tank and hot water tank temperature. It was a RTD sensor (PT-100) thermocouple with 3 mm sheath diameter and 100 mm length. The tip of the thermocouple was inserted into the middle of the flow path of the fluid. The thermocouple was then attached to the data acquisition unit where the bulk temperature was recorded and analysed.

Another type of thermocouple used is type-K thermocouples from Omega (Model: TJ36-CASS-032U-6). The metal transition barrel provides a solid mounting surface and the PFA insulated lead wire is a cost-effective solution for environmental temperatures to 260 °C. This type-K thermocouple has 1 mm sheath diameter and 150 mm length. The thermocouples come specified from the manufacturer to have ± 1 °C accuracy. All thermocouples are calibrated in the technical sense and they are tested with standard temperatures to ensure no manufacturing or connection flaws are creating erroneous readings. The heat transfer results are directly affected by the temperature measurements. Thus, all the thermocouples (Type-K and RTD sensor) used in this experiment must be calibrated to determine their accuracy. The thermocouples are calibrated in two ways:

1. 650SE - Reference Temperature Calibrator

The system gives significant improvement in the calibration accuracy up to ± 0.04 °C with the use of the external reference sensor. Axial homogeneity in the calibration well is important, as the typical thermo-sensitive element of a sensor can vary from 5 mm to 60 mm. The actual temperature in the well could inherently deviate from the ideal temperature as a function of the proximity to the bottom of the well Figure 3.21.

2. The thermocouples were immersed in a well-mixed boiling-water bath which was at 100.16 °C for the laboratory pressure and a well-mixed ice-water bath maintained was at 0 °C (see Figure 3.22).



Figure 3.21: Photograph of the Thermocouple calibrator.

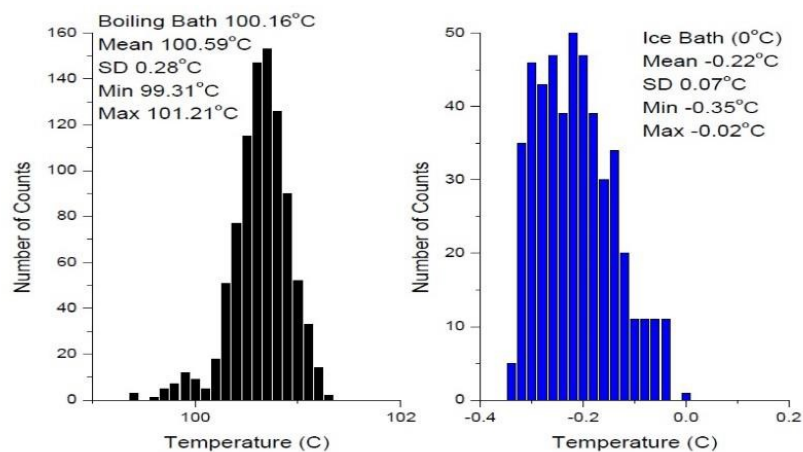


Figure 3.22: Thermocouple testing.

3.2.13 SCADA & Programmable Logic Controller

A SCADA (Supervisory Control and Data Acquisition) system simply refers to the layers of software and infrastructure that sit between a digital screen, and any control or measuring device. SCADA is used to issue control commands to remote devices like valves, pumps or heater, read values from those devices, and analyse device data accordingly. SCADA systems can be small in order to manage field devices that are in close proximity inside a single facility, or expand to handle devices that are spread

across vast geographical areas (like sensors on oil pipes). SCADA exist almost everywhere in this day and age. For examples, in an oil rig, SCADA is what allows the operators and engineers to control temperatures and pressure of the oil pipes by interfacing with measuring and control devices on these pipes. A PLC (Programmable Logic Controller) is a control device that is smart and can be programmed to make sophisticated decision. PLCs are very popular because of their intelligence. In current research, PLC is connected to the SCADA software to allow monitoring and control as shown in Figure 3.23. For a PLC overview refer to the Appendix A.



Figure 3.23: Photograph of the PLC system attached with the scada system.

3.2.14 Data Logging System

Data for the inlet and outlet temperatures for solution flow and hot flow, flow rate and frictional pressure drop are logged using a SCADA data acquisition system (WINCC) and recorded using a Hewlett Packard personal computer. All the results were recorded by transmitting 4-20 mA signals via PLC to the software. The program was set in recording mode of every 10 minutes interval and continuous up to 4320 minutes for each of the experiments. Fouling process is a slow reaction process. Therefore, 10 minutes interval is set and sufficient data is collected to interpret the fouling condition. Figure 3.24 shows an example of set value for one of the experiments.

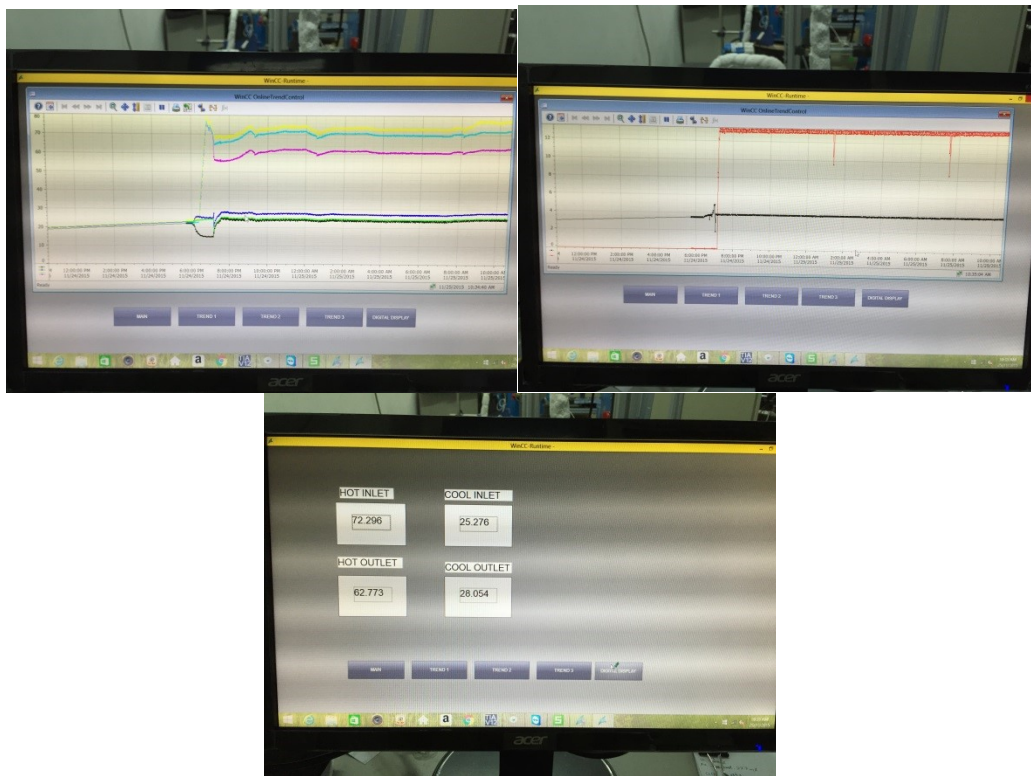


Figure 3.24: Data logging system for experiment.

3.2.15 Calcium Hardness Detection

3.2.15.1 A Set of Apparatus for EDTA Titration

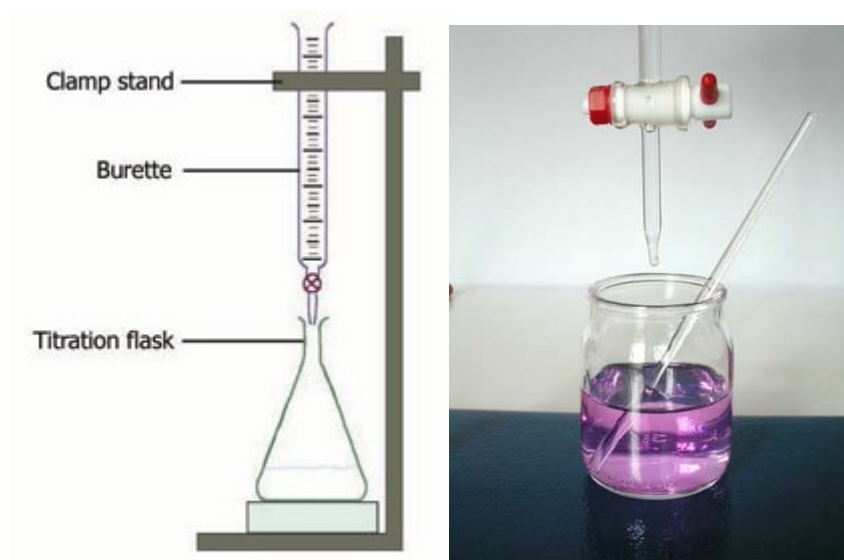


Figure 3.25: Apparatus for EDTA titration.

The titration method was used in this experiment by set of apparatus as shown in Figure 3.25 to measure the concentration of calcium carbonate (CaCO_3) in the solution, gram/litre. The solution is titrated with standard 0.01 M EDTA ($\text{Na}_2\text{H}_2\text{Y}$) solution until the colour changes from wine red to clear blue shown in Figure 3.26.

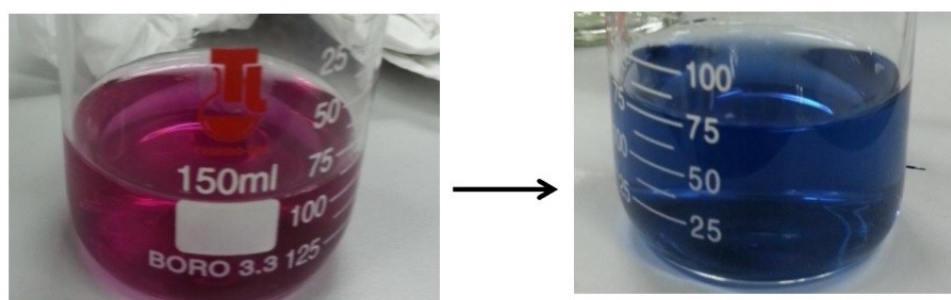


Figure 3.26: Colour change from wine red to clear blue.

3.2.15.2 Calcium Hardness Cuvette Test

The LCK 327 Cuvette test was an alternative way used to determine the calcium contents of the samples. LCK Cuvette Tests are automatically measured correctly with high precision and safety. A DR2800 spectrophotometer as shown in Figure 3.27 was used to identify the cuvette test from its barcode (IBR+); it rotates the cuvette and takes 10 measurements and calculates the calcium contents results immediately in mg/L. This method is easy to use, simple and well-designed to prevent errors from occurring.



Figure 3.27: DR2800 spectrophotometer used to conduct water hardness cuvette test.

3.3 Data Reduction, Calibration, Experimental Work, Observation and Analysis

3.3.1 Experimental System

In this chapter the methodology of determining the heat transfer coefficient, friction factor, fouling resistance, weight of deposited particles and calcium hardness determination is described. The experimental procedure and data reductions are discussed with the experimental results being validated for distilled water against the standard equations, such as the Gnielinski, Pak and Choy, Mangai and Dittus–Boelter for turbulent flow. Furthermore, for the pressure drop the results were compared and correlated with Power law, Blasius and Petukhov in turbulent flow conditions. The main

purpose of this validation was to ensure that the experimental setup can provide accurate measurements with water before any test is conducted on the fouling study.

3.3.2 Data Reduction – Heat Transfer Coefficient

Fouling thickness across the heat exchanger surfaces is uneven due to the nature of the phenomenon. It is because fouling deposition is a very complex and inconsistent process. Hence, in the present research, the localized heat transfer measurements were not applied. The average heated wall temperature and bulk temperature of the foulant liquid were considered to evaluate the effective heat transfer coefficient at the section. Figure 3.10 shows the schematic of the double-pipe heat exchanger test section showing the heat transfer between two fluids from which the heat transfer coefficient is calculated by Equation 4.4. All the measurements were taken at constant hot inlet temperature, cold inlet temperature and data were taken by steady state conditions at the chosen velocity, surface temperature and bulk temperature. The hot inlet temperature was fixed at 50 °C and 25 °C at cold inlet by automation control of heater and industrial chiller. The velocity was systematically increased, log mean temperature differences were recorded using the data acquisition system for heat transfer and fouling study. The temperature profile between hot fluid and cold fluid are calculated using Equation 4.1 and 4.2.

$$Q_h = M_h C_{p_h} \Delta T_h \quad (4.1)$$

Where, Q_h is the thermal energy transfer of hot flow section (J/s), M_h is the mass flow rate of hot flow (kg/s), C_{p_h} is the specific heat constant (J/kg.K) and ΔT_h is the temperature different of hot inlet and hot outlet (K).

$$Q_c = M_c C_{p_c} \Delta T_c \quad (4.2)$$

Where, Q_c is the thermal energy transfer of cold flow section (J/s), M_c is the mass flow rate of cold flow (kg/s) and ΔT_c is the temperature different of cold inlet and cold outlet (K).

The overall thermal energy between two fluids was calculated by using Equation 4.3.

$$Q_{overall} = \frac{Q_h + Q_c}{2} \quad (4.3)$$

These overall heat transfer coefficients were calculated by using the Equation 4.4.

$$Q_{overall} = hA\Delta T_{LMTD} \quad (4.4)$$

Where, $Q_{overall}$ is the thermal energy of heat transfer section (J/s), h is the overall heat transfer coefficient (W/m².K), $A = 2 \pi r l$, is the total surface area of the heat transfer section (m²) and ΔT_{LMTD} (Equation 4.5) is the log mean temperature difference which was determined from the measured temperatures at the inlet and outlet of hot and solution water (K):

$$\Delta T_{LMTD} = \frac{(T_{h,out} - T_{c,in}) - (T_{h,in} - T_{c,out})}{\ln \left[\frac{(T_{h,out} - T_{c,in})}{(T_{h,in} - T_{c,out})} \right]} \quad (4.5)$$

3.3.3 Data Reduction – Fouling Resistance

Fouling resistance R_f (m².K/W) throughout the experimental tests to monitor fouling behaviour on metal surface as seen in Equation 4.6.

$$R_f = \frac{1}{U_{fouled}} - \frac{1}{U_{initial}} \quad (4.6)$$

Where, U_{fouled} is the overall heat transfer coefficient for the fouled case (W/m².K) and $U_{initial}$ is the overall heat transfer coefficient for the initial clean condition (W/m².K).

The deposited scale hardness of the solution was measured by EDTA complexometric titration method.

3.3.4 Weight Deposition Reduction

3.3.4.1 Coupons' Weight

A comparison of coupons' weight before and after scaling tests was conducted. The amount of deposited calcium carbonate scale on the coupon was determined by using the Equation 4.7.

$$W_s = W_f - W_I \quad (4.7)$$

Where, W_s , W_f and W_I are weights of the scale deposited (g), fouled coupon (g) and initial coupon (g), respectively. The crystal morphology of the scale deposits was characterized by x-ray diffraction analysis (XRD) and scanning electron microscopy (SEM). In addition, the elemental analysis was checked by energy dispersive spectroscopy (EDS). Optical images and photographs were obtained to visually differentiate the fouling deposition on different tested surfaces.

3.3.4.2 Deposition on Surfaces

The dissolving salt method is applied to calculate the total amount of calcium carbonate deposited on the test section pipe of the heat exchanger. After the fouling test run, the test section pipe is dismantled from the heat exchanger. At this phase of study, the test section is removed carefully to avoid the test section being scratched on the surface and affecting the readings of the deposited calcium carbonate. Then the procedure is to dissolve the calcium carbonate that attached on the test section surface in HCl and dilute into 1 L distilled water and use a soft brush to clean the surface and collect the solution into a beaker. Clear solution must be observed before the sample is taken for titration. EDTA-complexometric titration method was used to calculate the concentration of the calcium carbonate salt forming crystalline deposition on the test section pipe.

3.3.5 Calcium Hardness Reduction

3.3.5.1 EDTA Complexometric Titration

Complexometric titration with EDTA (Ethylene Diamine Tetra Acetic Acid) has been used for the analysis of dissolved CaCO_3 in the solution and suspension. To perform the test for quantitative analysis of dissolved calcium ion in the solution, several reagents and solution are required for the titration such as EDTA solution, Eriochrome black T solution, ammonia-ammonium chloride buffer solution pH 10 and magnesium complex of EDTA. The preparation procedure of the reagents is stated here below:

1. EDTA solution (0.01 M): Dissolve 3.722 g of analytical reagent grade of disodium dihydrogen ethylene diamine tetra acetic acid in distilled water and dilute to 1000 ml.
2. Eriochrome black T solution: Dissolve 200 mg of the solid in solution consisting of 15 ml of triethanolamine and 5 ml of absolute ethanol. Solution should be kept in the refrigerator when not in use or be freshly prepared every two weeks.
3. Ammonia-ammonium chloride buffer solution, pH 10: Dilute 570ml of aqueous NH_3 (sp. Gr. 0.90) and 70 g of NH_4Cl to approximately 1 litre of dilute solution with distilled water.
4. Magnesium complex of EDTA, 0.1M: to 37.2 g of EDTA ($\text{Na}_2\text{H}_2\text{Y}\cdot 2\text{H}_2\text{O}$) in 500 ml of distilled water, add an equivalent quantity 24.65 g of magnesium sulphate ($\text{MgSO}_4\cdot 7\text{H}_2\text{O}$). Introduce a few drops of phenolphthalein followed by sufficient sodium hydroxide to turn the solution faintly pink. Dilute the solution to 1 litre. When properly prepared, portions of this solution should assume a dull violet colour when treated with pH 10 buffer and a few drops of Eriochrome black T (Erio T) indicator in this solution. Furthermore a single drop of 0.01 M Mg^{2+} should cause a change to red. The composition of the

solution should be adjusted by addition of Mg^{2+} or Na_2H_2Y until these criteria are met.

All the reagents were prior prepared before the titration. 25 ml of fouling solution were taken into a 250 ml conical flask and diluted with 25 ml of distilled water. 2 ml of pH 10 buffer solution, 1 ml of 0.1 M magnesium chelate solution (mg-EDTA) and 3-4 drop of Erio T indicator were added following the sequence. Titrate with standard 0.01 M EDTA (Na_2H_2Y) solution until the colour changes from wine red to clear blue. No tinges of reddish blue should remain at the equivalent point.

1ml of 0.01M EDTA = 0.4008 mg Ca^{2+}

After obtaining the amount of Ca^{2+} in the solution, $CaCO_3$ concentration is calculated

3.3.5.2 Calcium Hardness Cuvette Test

The LCK 327 cuvette test was performed to analyse the dissolved $CaCO_3$ in the solution and suspension. To perform the test, the standard procedure is listed below:

- 1.) Insert sample cuvette into DR2800 spectrophotometer.
- 2.) Remove sample cuvette. Drop 0.2 ml of water sample into the same cuvette.
Close cuvette, invert a few times and thoroughly clean the outside of the cuvette.
- 3.) After 30 sec insert sample cuvette again.
- 4.) Remove sample cuvette. Drop 0.2 ml of masking solution B (LCK 327 B) and repeat the procedure #2.
- 5.) After 30 sec insert sample cuvette again.

The results for calcium hardness displayed onto the LCD screen. Table 3.14 summarizes the specification of LCK327 cuvette test.

Table 3.14: Specification of LCK327 cuvette test.

Description	Water Hardness, Calcium/Magnesium
Instrument	DR 2800
Measuring range	5-100 mg/L Ca ²⁺ , 3-50 mg/L Mg
Method	Metalphtalein
Storage condition	15 – 25 °C

3.4 Summary

In summary, characterization of nanofluids and fouling particles conducted in details with the help of analysis instruments such as SEM and TEM for measurement of crystal size and shape, XRD for elements analysis, FTIR for functionalization of nanofluids, Mitutoyo SJ-210 for surface roughness analysis, AB200pH for electric conductivity measurements and KD2-Pro for thermal conductivity analysis. In addition, description of the experimental setup has been presented in details with all the technical specification for each of the instruments, hardware and software used. Finally, data reduction methods are explained in details in each of the section for ease of understands in analysis of fouling research.

CHAPTER 4: INVESTIGATION OF DOUBLE-PIPE HEAT EXCHANGER FOULING AND FOULING MITIGATION

4.1 Introduction

An experimental setup of a double pipe heat exchanger fouling test rig was built to investigate the mineral scales on different heat exchanger pipe surfaces. Progressive fouling deposition on different material surfaces under similar solution conditions were observed and analyzed. Measurable data on the progressive build-up of scale deposits, deposition rate, as well as the composition and crystal morphology of the deposits were studied after each experimental run by analyzing the deposited scale on the test pipes. In this research the artificial calcium carbonate deposit on different material surfaces is considered as it is one of the major constituents of most scales found in heat exchanging equipment. Fouling on different smooth test pipes was investigated in the centrally located larger concentric pipe heat exchanger. Uniform flow condition near the pipe surface was maintained by constant flow rate throughout the system. The calcium carbonate deposition rates on five different metal surfaces (Stainless steel 316, brass, copper, aluminum and carbon steel) were investigated. The results illustrated in an upward trend for fouling rate with time on the tested specimens. The deposition on the surfaces showed a linear growth with the enhancement of thermal conductivity of the metals. However, deposition on carbon steel metal surfaces did not follow the typical linear trend of thermal conductivity over deposition as its surface was altered by corrosion effects. In addition, temperature, velocity, and concentration effects on fouling deposition were investigated on the SS316 metal surface.

On top of it, mitigation of calcium carbonate scaling by physical water treatment (PWT) in an operating double pipe heat exchanger using zinc and tourmaline as catalytic materials is presented in this chapter. The PWT is defined as a non-chemical effective fouling retardation method which exhibits promising protection to protect the

environment and maintain a green environment. Catalytic materials such as (zinc and tourmaline) are capable of tackling fouling problems. Experiments were conducted in this chapter to verify this method. Artificially hardened water at 300 mg/L was used as the cooling water for deposit analysis. The velocity of the cooling water (i.e. hard water) was varied from 0.15 to 0.45 m s⁻¹ and bulk temperature of the solution was maintained at 25 °C. The results showed that the reduction in calcium carbonate formation for the case with PWT was higher compared to those without PWT.

4.2 Experimental Work

4.2.1 Apparatus

The schematic diagram of the experimental apparatus is presented in Figure 5.1. The apparatus consists of two flow loops with two separate tanks containing artificial fouling solution (blue line) and hot water (red line) respectively with a test section (Heat exchanger). The hot flow loop comprises of a frequency controlled magnetic gear pump, N-Flow 25 magnetic flow meter, pipes of different metal surfaces and a thermostatically controlled heater to maintain the heater tank at a constant hot inlet temperature (50 ± 0.5 °C). The hot line outside the test section is insulated thoroughly to prevent heat loss along the flowing line. Also, the cold flow loop contains a jacketed artificial fouling solution tank, frequency controlled magnetic gear pump, transparent HDPE piping for flowing line, Burkert inline paddle wheel flow meter, RW20 digital stirrer and a chiller to maintain the artificial fouling solution at a constant cold inlet temperature (25 ± 0.5 °C). The cold line magnetic gear pump (Araki Magnet Pump) has the specifications of 2800 rpm, 1.1 amps, 260 W motor and of capacity 120 L/minute, with maximum head of 8.6m.

The test section is a counter current double pipe heat exchanger with the length of 130 cm. In this exchanger, the hot water flows into the pipe and cold artificial fouling solution in the annular space of the pipe. The inside pipe is made of different metals

with the same dimensions (outer diameter of 12.7 mm and inner diameter of 8.48 mm). The outer pipe is of transparent HDPE piping with the inner diameter (ID) of 42.1 mm and outer diameter (OD) of 46.8 mm.

The inlet and outlet temperatures in the hot and cold lines were measured at the inlet and outlet of the test section, respectively, via installing 4 RTD sensors. A PLC program data acquisition system was installed for collecting data and automatically maintaining hot and cold inlet sections at the specified temperatures. The pressure drop variation in both the lines across the test section was measured by using a YOKOGAWA Differential Pressure Transmitter (0-200 mbar). During the fouling test, the volume flow rate, pressure drop, inlet and outlet temperatures for hot and cold lines were recorded.

In order to demonstrate the main differences between the heat transfer characteristics of clear and fouled situations, the hot line pipe was fully insulated and cold line pipe made of HDPE piping which is good to minimize the heat loss to the environment. The details data of the insulated materials are listed in Table 4.1 below:

Table 4.1: Details of insulated materials.

Insulation Thickness (t)	Insulation Thermal Conductivity(k_s)	Heat Transfer coefficient for the outside of insulation	Emissitivity of the insulation (ε)
25 mm	0.038W/m.K	10 W/m ² .K	0.8

In addition, mitigation approach was conducted by incorporating catalytic material to minimize fouling deposition on the heat transfer surfaces. The fouling experiment was run to compare with and without PWT treatment to verify the effectiveness of catalytic materials in solving the fouling problem in a double pipe heat exchanger.

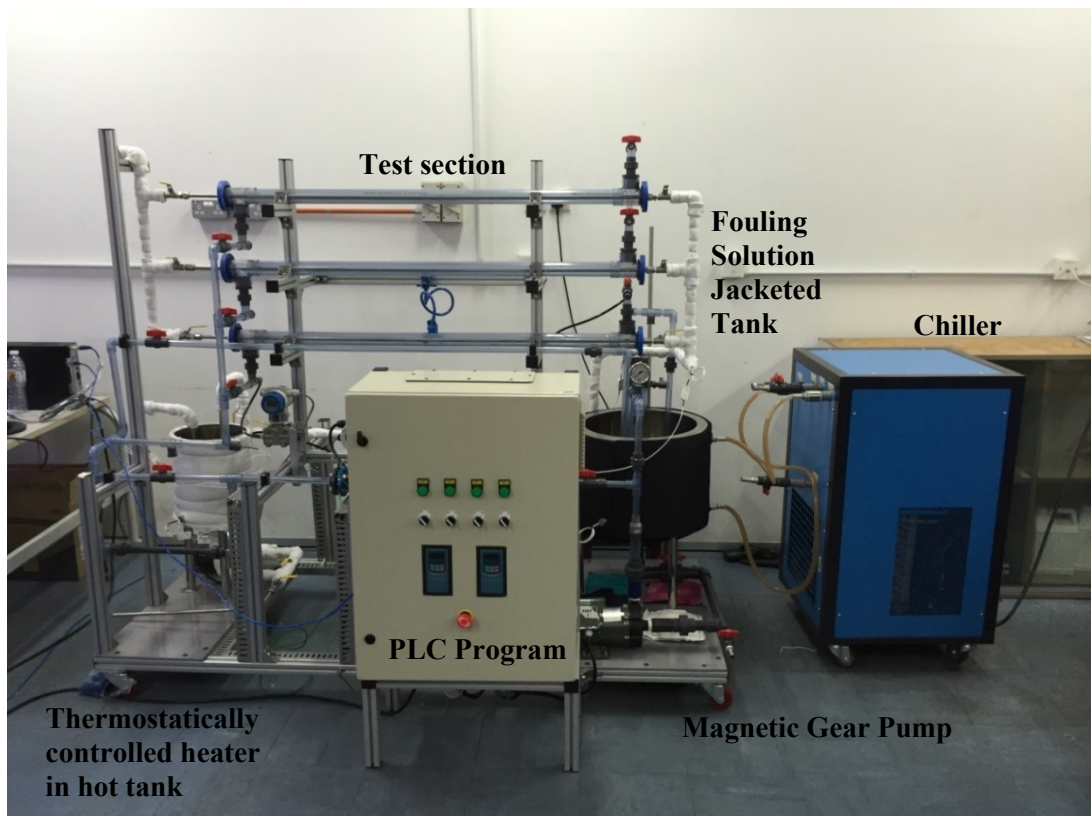
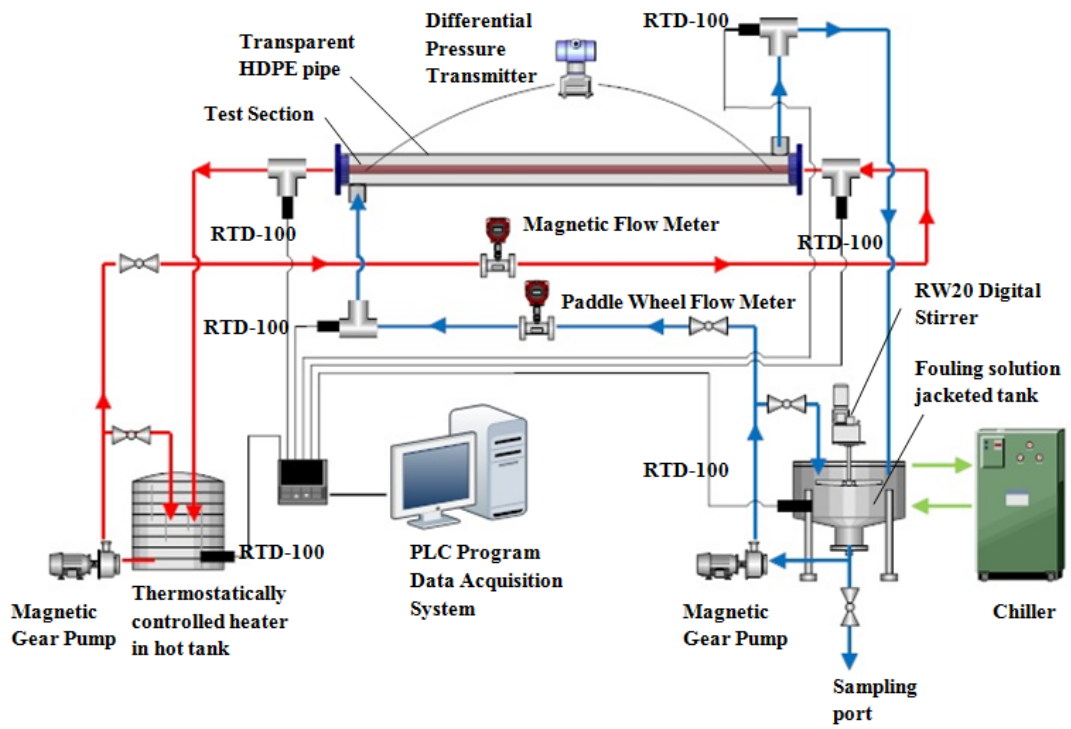


Figure 4.1: Double pipe heat exchanger experimental test rig.

4.2.2 Test Specimens

The experimental pipes are 1300 mm in length with a wall thickness of 2.11 mm and outer diameter of 12.7 mm. Five metal pipes (copper, aluminum, brass, carbon steel and stainless steel 316) with the same dimensions were used in these experiments. The test section pipe and coupon were connected in same material by precise machining of inner and outer thread respectively as the connector. As can be seen in Figure 4.2, the coupons were installed in the middle of the test section. Characterizations of the fouling deposition on the surfaces were conducted after completion of the fouling tests.

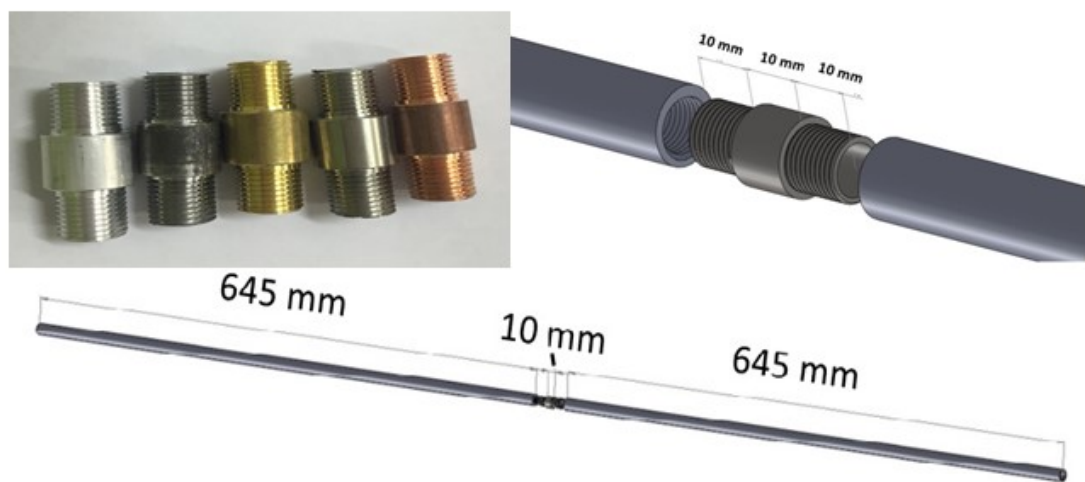


Figure 4.2: Coupons installation of different materials on heat exchanger surfaces.

The smooth test specimen pipes (Table 4.2) were used in the as-received condition but before installing in the test rig, they were cleaned by rubbing with a water-soaked cloth and flushing with hot water to remove any deposition of grease, oil, etc.

Table 4.2: Physical properties and R_a of different heat exchanger materials at 300 K

Materials	Properties at 300 K			
	ρ (kg/m ³)	C_p (J/kg.K)	K (W/m.K)	R_a (μ m)
Stainless Steel	8238	468	16	1.27
Carbon Steel	7850	502	90	2.34
Brass	8530	380	109	2.18
Aluminum	2702	903	250	2.16
Copper	8960	385	401	2.22

Figure 4.3 illustrates the geometrical configuration of the unit and shows a perforated cylindrical casing made of zinc having hollow tourmaline cylindrical rods as packed material. The outermost casing made of aluminium.

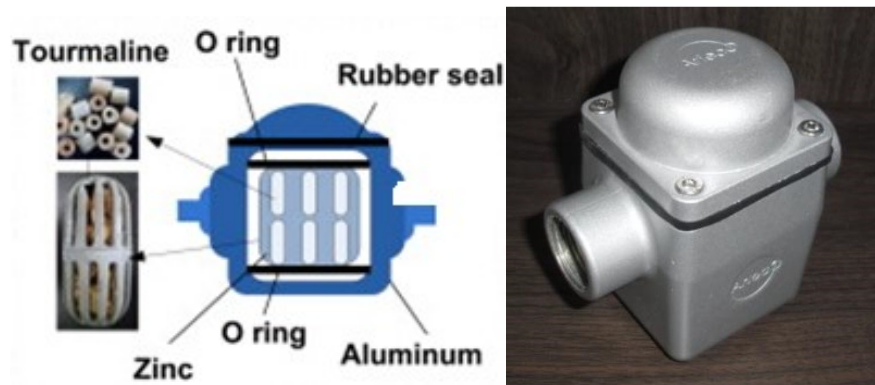


Figure 4.3: Composition of catalytic materials composes of zinc and tourmaline.

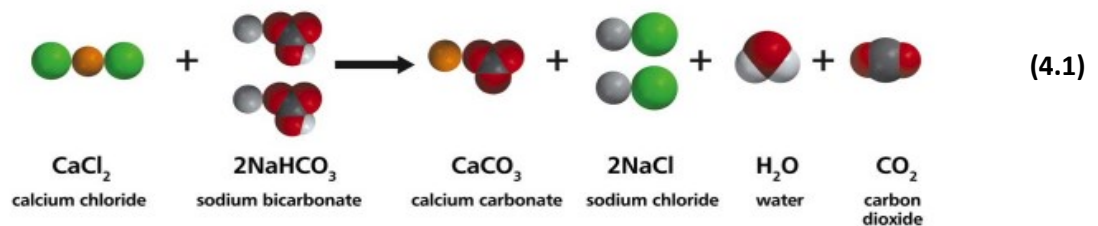
4.2.3 Data Acquisition

A programmable logic controller (PLC) was installed and a software WinCC was employed to record the inlet and outlet temperatures of hot water passing through the pipe, the mean temperature of tanks, inlet and outlet of artificial solution temperatures passing through the annular pipe, differential pressure between annular pipe and flow rates of hot line and solution line. All the temperatures were measured using the RTD-

100 sensors. Also, the differential pressure and flow rates were recorded by a transmitting 4-20 mA signal via PLC to the software. The program was set in recording mode of every 10 minutes interval and continuous up to 4320 minutes (S. N. Kazi et al., 2010).

4.2.4 Experimental Procedures

Experiments on fouling rate, fouling resistances and total deposition formed on different heat exchanger surfaces by varying parameters were conducted by means of the fouling test experiment. A leakage test was performed prior to the experimental runs to ensure the suitability and validity of the setup and working conditions. Next, the experimental setup was cleaned by circulating distilled water and chemical cleaning agents (Decon 90) to ensure reproducibility of data in each of the experimental runs. Artificial fouling solution was prepared at 300 mg/l CaCO_3 from the proportionate amount of calcium chloride (CaCl_2) and sodium bicarbonate (NaHCO_3) powders diluted in distilled water to accelerate the scaling effect in a short period of time. Equation 4.1 illustrates the calcium carbonate formation from the reaction between calcium chloride and sodium bicarbonate in water (L. D. Tijng et al., 2011).



The velocity of the artificial fouling solution flow varied from 0.15 to 0.45 m/s and the velocity of the hot water flow running through the inner tube was maintained constant at 1m/s. The temperature of hot flow loop was set at a constant inlet value of 50 ± 0.5 °C and cold flow loop was set at 25 ± 0.5 °C. The solution hardness was maintained at a

constant value of 300 ± 30 mg/L throughout the experiments and the hardness of the solutions were measured by EDTA complexometric titration method. The stirrer in the solution tank was operated at 475 rpm to ensure a smooth mixing condition in the artificial fouling solution tank.

As a common correlation, Equation 4.2 was used to calculate the fouling resistance, R_f , throughout the experimental tests and to monitor fouling behaviour on the surface of metal.

$$R_f = \frac{1}{U_{fouled}} - \frac{1}{U_{initial}} \quad (4.2)$$

Where, U_{fouled} and $U_{initial}$ are the overall heat transfer coefficient for the fouled case and the overall heat transfer coefficient for the initial clean condition, respectively. These overall heat transfer coefficients were calculated by using the Equation 4.3.

$$Q = UA\Delta T_{LMTD} \quad (4.3)$$

where Q is the thermal energy of heat transfer section, U is the overall heat transfer coefficient, $A = 2 \pi RL$, is the total surface area of the heat transfer section and ΔT_{LMTD} (Equation 4.4) is the log mean temperature difference, which was determined from the measured temperatures at the inlet and outlet of hot and solution water:

$$\Delta T_{LMTD} = \frac{(T_{h,out} - T_{c,in}) - (T_{h,in} - T_{c,out})}{\ln \left[\frac{(T_{h,out} - T_{c,in})}{(T_{h,in} - T_{c,out})} \right]} \quad (4.4)$$

The deposited scale hardness of the solution was measured by EDTA complexometric titration method.

4.2.5 Measurement and Characterization

The technique of dissolving salt was applied to calculate the total amount of calcium carbonate deposited on the test section pipe of the heat exchanger. After 72 hours fouling test run, the test section pipe was dismantled from the heat exchanger. At this phase of study, test section was removed carefully to avoid the test section being scratched on the surface and affecting the readings of the deposited calcium carbonate. Then the calcium carbonate that attached on the test section surface in HCl was diluted into 1L distilled water and a soft brush was used to clean the surface and then the solution was collected into a beaker. A clear solution must be observed before the sample is taken for titration. The EDTA-complexometric titration method was used to calculate the concentration of the calcium carbonate crystalline deposition salt on the test section pipe. The coupons were removed carefully from the test pipe for characterization of the deposits. The crystal morphology of the scale deposits were characterized by x-ray diffraction analysis (XRD) and scanning electron microscopy (SEM). In addition, the elemental analysis was checked by energy dispersive spectroscopy (EDS). Optical images and photographs were obtained to visually differentiate the fouling deposition on different tested surfaces (J. W. Morse et al., 2007).

4.3 Results and Discussion

4.3.1 Data Validation and Reproducibility

A set of initial experiments were prior performed for water as the base fluid to assess the reliability and accuracy of the experimental setup. The experimental results of distilled water for double pipe heat transfer were compared with the results from standard equation. The empirical correlation of Gnielinsky, Maiga, DittusBelter and Pak & Cho were selected for comparison with the obtained results especially for the test of accuracy of the setup in the turbulent region.

The Nusselt number, friction factor, and Reynolds number are presented in Equation.

- a) The Nusselt number is defined by Equation 4.5

$$Nu = \frac{hD}{k} \quad (4.5)$$

- b) The friction factor is defined by Equation 4.6

$$f = \frac{\Delta P}{\left(\frac{L}{D}\right)\left(\frac{\rho v^2}{2}\right)} \quad (4.6)$$

- c) The Reynolds number is defined by Equation 4.7

$$Re = \frac{\rho v D}{\mu} \quad (4.7)$$

- d) The Prandtl number is defined by Equation 4.8

$$Pr = \frac{\mu C_p}{k} \quad (4.8)$$

Figure 4.4 illustrates the validation of the experimental results by correlating with the following equations:

Maiga et al. (El Bécaye Maïga et al., 2006) (Equation 4.9)

$$Nu = 0.085 Re^{0.71} Pr^{0.35} \quad (4.9)$$

Dittus and Boelter (Dittus & Boelter, 1985) (Equation 4.10)

$$Nu = 0.023 Re^{0.8} Pr^{0.4} \quad (4.10)$$

Pak and Cho (Pak & Cho, 1998) (Equation 4.11)

$$Nu = 0.021 Re^{0.8} Pr^{0.5} \quad (4.11)$$

Gnielinski equation (Gnielinski, 1975) (Equation 4.12)

$$Nu = \frac{\left(\frac{f}{8}\right)(Re-1000)Pr}{1+12.7\left(\frac{f}{8}\right)^{0.5}\frac{2}{(Pr^3-1)}} \quad (4.12)$$

Where, the friction factor is

$$f = (0.78 \ln Re - 1.64)^{-2}$$

The data were also reproduced and the results are showing a good agreement between the two similar runs as presented in Figure 4.5. The current setup shows that the experimental test rig yielded a promising result for conducting the fouling tests.

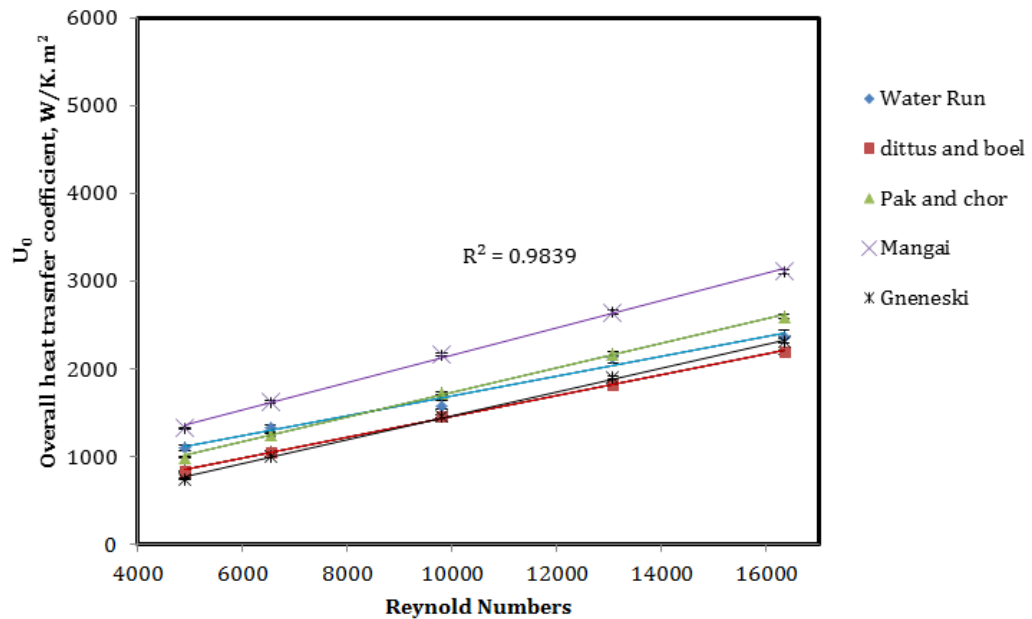


Figure 4.4: Validation of the experimental run results with the standard equations.

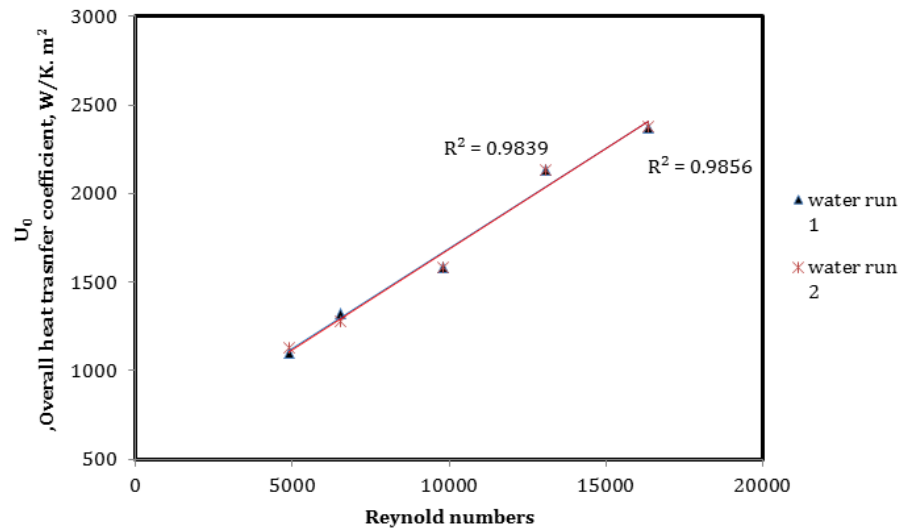


Figure 4.5: Reproducibility of the experimental run results under the same test conditions.

4.3.2 Fouling on Various Surface Materials

The effect of these metals' nature (copper, aluminium, carbon steel, brass and stainless steel 316) on the deposition of calcium carbonate scale was studied in a series of experiments (Ruelo et al., 2013; L. Tijning et al., 2013). The total depositions after fouling tests on different heat exchanger metal surfaces are shown in Figure 4.6. It can be seen that copper and stainless steel-316 show the greatest and lowest quantities of deposition, constituting 841.68 and 190.38 mg, respectively.

As seen in Figure 4.7, the calcium carbonate depositions on five different heat exchanger surfaces as a function of time are presented. The sequence of deposition is copper > aluminium > carbon steel > brass > stainless steel. Figure 4.8 illustrates the fouling resistance under the effect of different materials; it is observed that the deposition tends to be asymptotic which is consistent with pipe flow investigations for all the materials. Kazi et al. obtained similar results for the deposition of calcium sulphate on different heat exchanger materials which were consistent with the values of their thermal conductivities (S. Kazi, 2012).

The effect of various heat exchanger surface materials on surface deposition has been mentioned in several studies (Alahmad, 2004) in which the deposition on substrates was consistent with their thermal conductivity values, i.e. copper > aluminium > brass > stainless steel. The experimental results appear to correlate well with thermal conductivity for copper, aluminum, brass and stainless steel, which implies the increase in the deposition with thermal conductivity enhancement.

Moreover, this research indicates that the carbon steel material didn't follow the thermal conductivity trends where it is expected to yield lower fouling deposition compared to brass. As seen in Figure 4.8, the fouling resistance of carbon steel material at about 1,500 min is dramatically increased and overtakes the fouling resistance of brass and moves nearer to the aluminium. Severe corrosion on the carbon steel was observed and it is believed that the deposition on carbon steel metal surfaces was altered by this corrosion effect (promoted by the rough surfaces). Figure 5.9 (a-d) shows the crystallization deposition on the different materials and Figure 5.9 panel (e) shows the corrosion fouling on carbon steel surface after 72 hours exposure at 300 mg/L aqueous calcium carbonate concentration and at 0.15 m/s velocity.

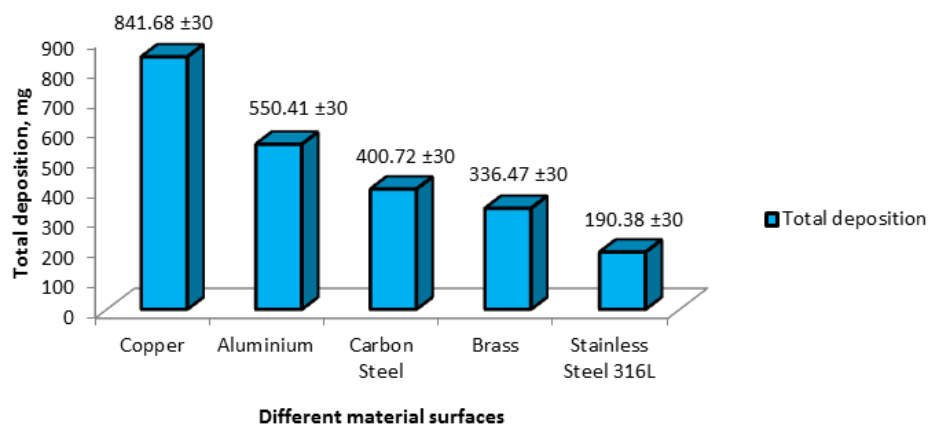


Figure 4.6: Total depositions on different heat exchanger materials at 50 °C and 25 °C at hot and cold water inlet respectively, 0.15 m/s solution flow and 300 mg/l concentration.

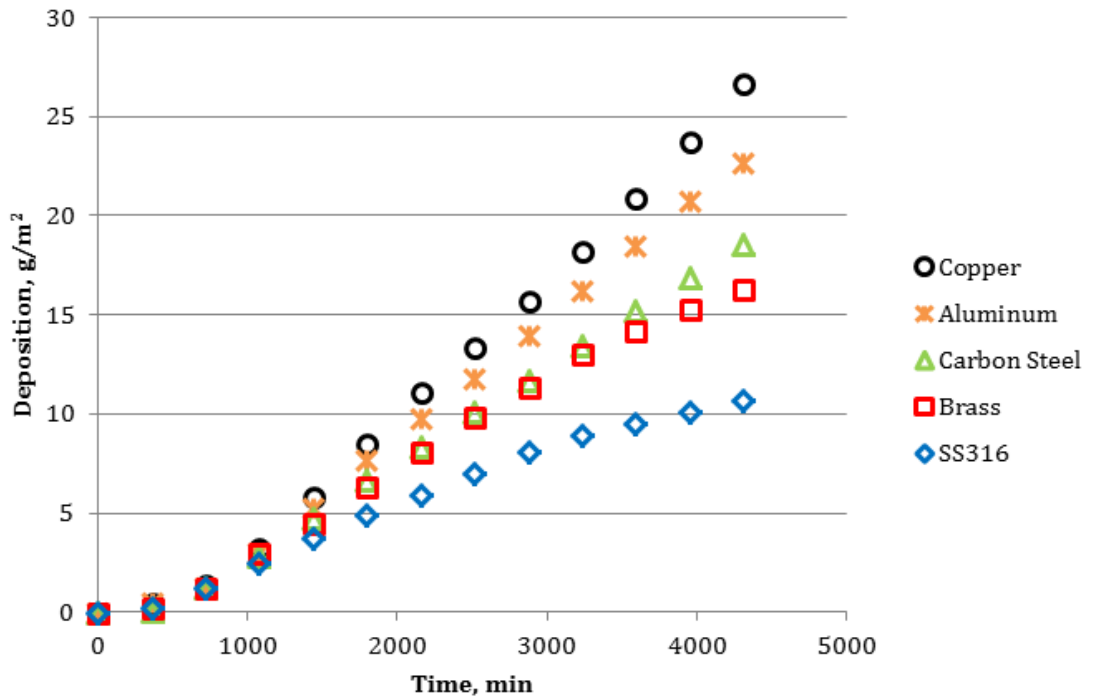


Figure 4.7: Deposition rate as the function of time on different heat exchanger materials.

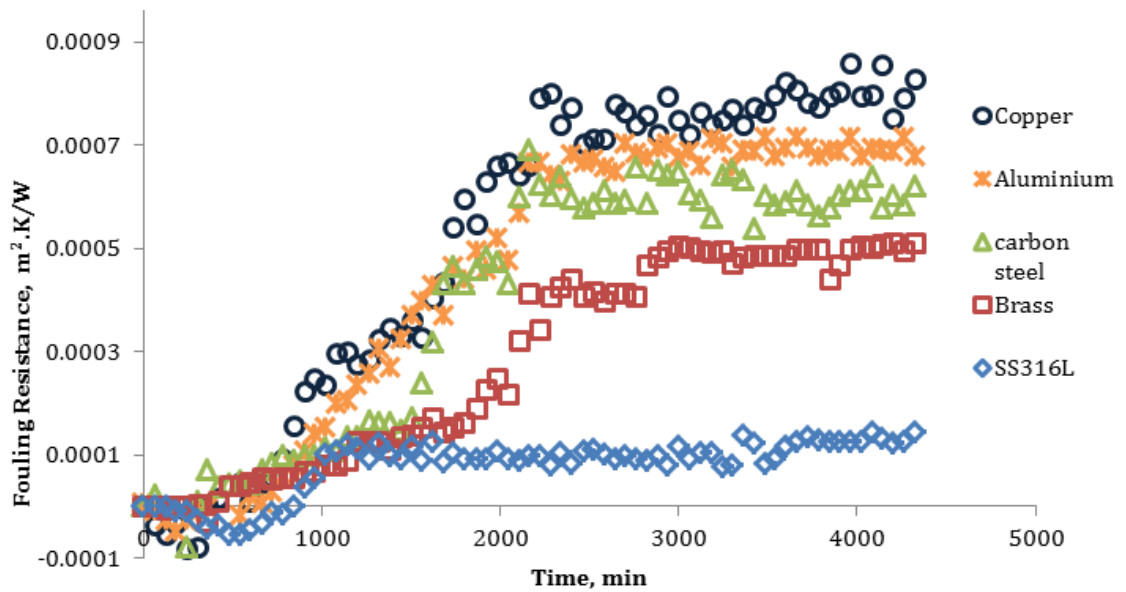


Figure 4.8: Fouling resistances as the function of time based on different heat exchanger materials at 50 °C and 25 °C at hot and solution inlet respectively, 0.15 m/s solution flow velocity and 300 mg/l concentration.

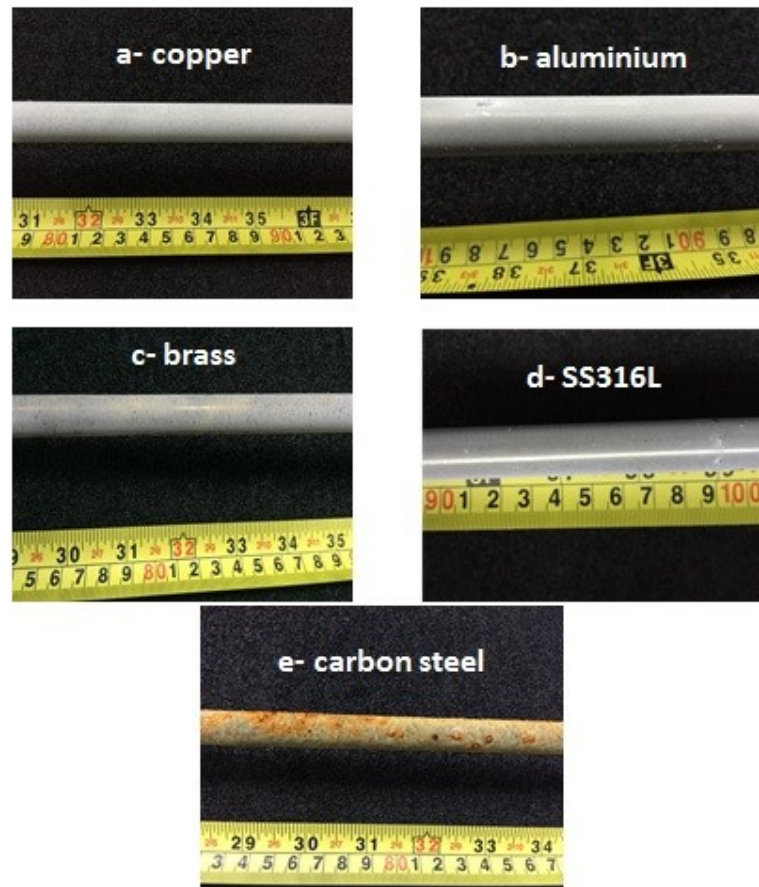


Figure 4.9: Images of calcium carbonate deposition on different metal surfaces.

4.3.3 Fouling under Effect of Velocity

Fouling tests of water hardness of 300 mg/L CaCO₃ at different flow velocities (0.15 - 0.45 m/s) were conducted. Figure 4.10 illustrates the results of the flow velocity effect on the fouling deposition rate. It can be observed the deposition rate of CaCO₃ at low velocity is clearly higher than that at high velocity. Several researchers have reported the same results (Awad, El-Samad, Gad, & Asfour; Hoang et al., 2011), suggesting the great effect of velocity on the fouling deposition. It was caused by the significant removal of scale particles from the fouling deposition formation due to increase of shear stress near the boundary wall of metal surfaces at the liquid-solid interface (Alahmad, 2008; Ceylan & Kelbaliyev, 2003; P. Walker & R. Sheikholeslami, 2003).

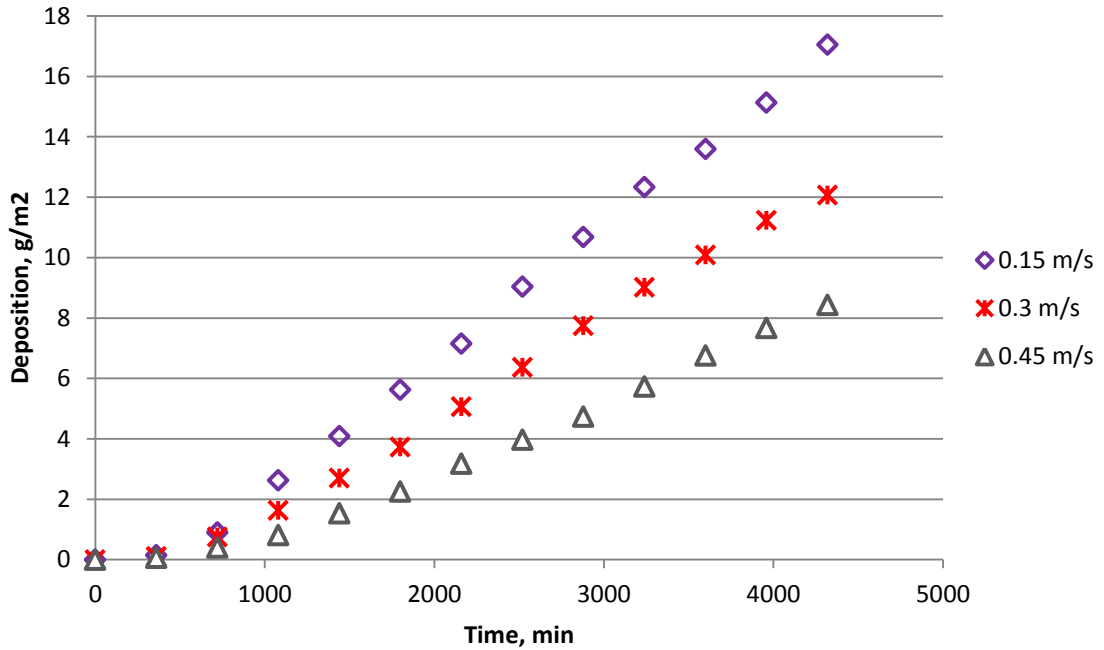


Figure 4.10: Calcium carbonate depositions as the function of time under different velocity conditions on SS316L, 50 °C hot water inlet, 25 °C solution inlet and 300 mg/l concentration.

4.3.4 Fouling under Effect of Hot Inlet Temperature

Fouling under the effect of inlet temperature was conducted on stainless steel 316L at the constant velocity of 0.15 m/s. Calcium carbonate is an inversely soluble salt against temperature. Hence, it can be predicted that the composition of calcium carbonate scale deposits can be influenced by varying temperature (D. J. Kukulka & Devgun, 2007; Yang et al., 2002). As it can be seen in Figure 4.11, higher inlet temperature induces higher total deposition on the SS316 material. In addition, longer induction period of scale formation at 50 °C in comparison to that at 70 °C was reported in Figure 4.12. It indicates that the induction period of fouling depends strongly on the temperature. The same results were reported by Mullin (J. W. Mullin, 2001a) by expressing the relationship between induction period and temperature in Equation 4.13.

$$\log(T_{int}^{-1}) = A - \frac{E_a}{2.303RT} \quad (4.13)$$

where E_a is the molar activation energy for nucleation (J/mol), R is the universal gas constant, which is 8.3145 J/K.mol and A is a constant value.

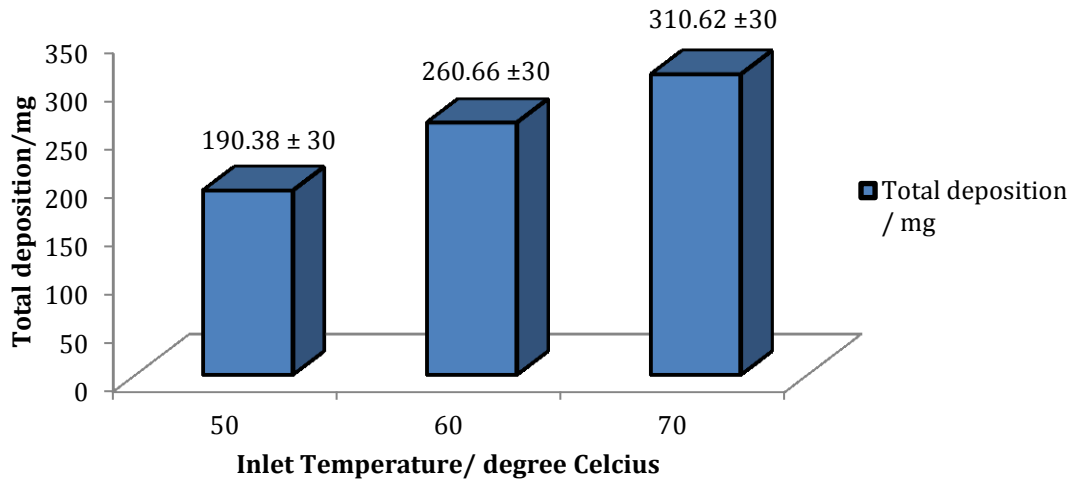


Figure 4.11: Total depositions on SS316L under effect of temperature, at 25 °C solution inlet, 0.15 m/s solution flow velocity and 300 mg/l concentration.

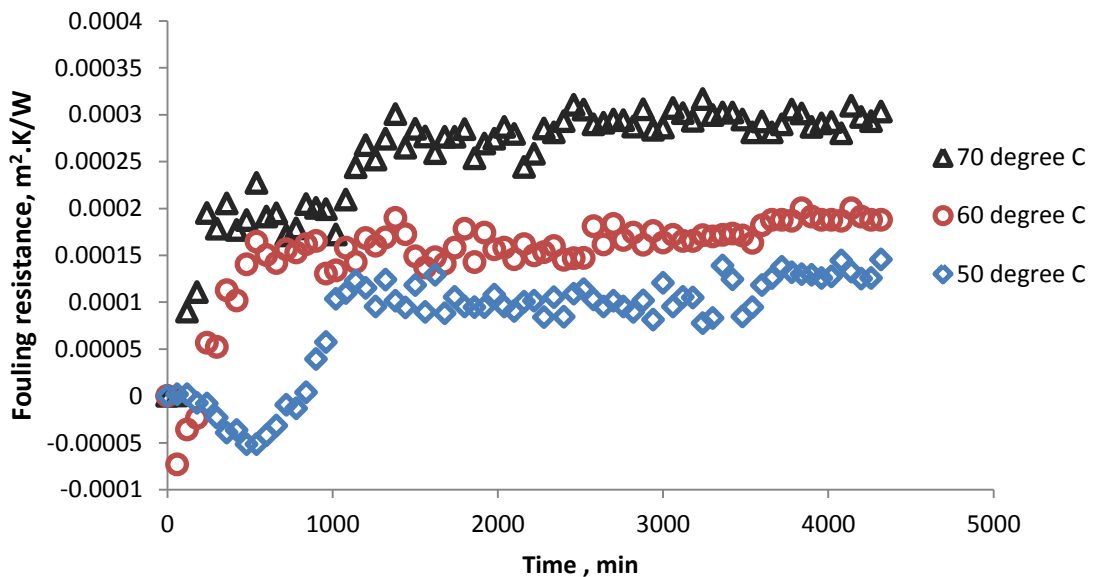


Figure 4.12: Fouling resistance of deposition on SS316L under effect of hot inlet temperature at 25 °C solution inlet, 0.15 m/s solution flow velocity and 300 mg/l concentration.

4.3.5 Fouling under Effect of Concentration

A fouling rate experiment under the effect of hardness concentration was conducted in this double pipe heat exchanger. Kazi et al. reported that a high concentration of calcium sulphate has a significant impact of deposition on different materials (S. Kazi et al., 2012). So, it can be predicted that the high concentration of calcium carbonate will form high deposition on the test section pipe. Figure 4.13 shows that a concentration of 500 mg/l experienced shortest induction period for a scale layer to form in less than one hour. It shows that the scale deposition layer formed quickly compared to other fouling solution concentrations and indicates that the induction period of the fouling depends strongly on concentration. At the end of the experiment, hardness concentration at 500 mg/l shows the highest fouling resistance resulting in the lowest heat transfer rate in the system.

Figure 4.14 shows total fouling deposition on the heat exchanger test section surface at different fouling solution concentrations. By comparing 3 different fouling solution concentration, it shows that the highest weight fouling is reported at 500 mg/l fouling solution concentration. This is because the high concentration solution that circulates in the heat exchanger provided a high tendency region for calcium carbonate solution to form in solid state. The lowest deposition weight is at 300 mg/l. It is because of the low concentration and less calcium carbonate particles tend to be deposited on the heat transfer the surface.

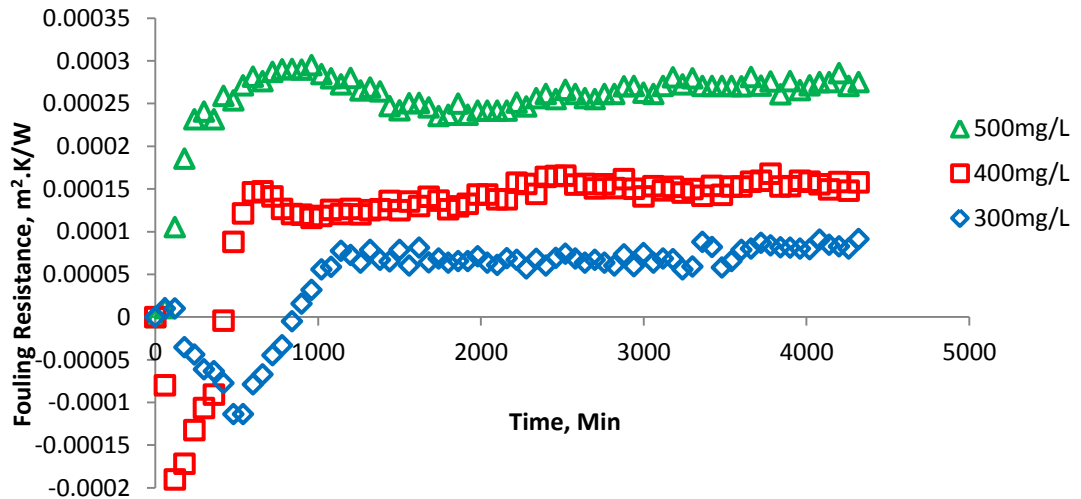


Figure 4.13: Fouling resistance of deposition on SS316L under effect of concentration at 50 °C and 25 °C at hot and solution inlet respectively and 0.15 m/s solution flow velocity.

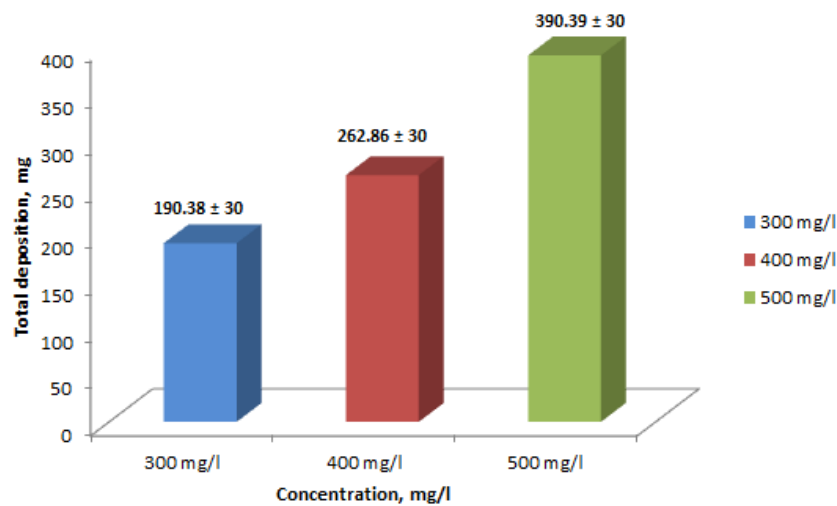


Figure 4.14: Total depositions on SS316L under effect of concentration, at 50 °C and 25 °C at hot and solution inlet respectively and 0.15 m/s solution flow velocity.

For crystal morphology analysis, scanning electron microscope (SEM) observation was conducted on the samples. As seen in Figure 4.15 & 4.16, at concentration of 300 mg/l and 400 mg/l, calcite type structures which have sharp cubic edges and orthorhombic crystal structure were observed. It can be seen clearly, the crystal morphology is relative smaller crystal size in 300 mg/l (about 15 μm) is observed compare to crystal size in

400 mg/l (about 25 μm). This crystal structure type enhances the structure to form a robust fouling layer. For 500 mg/l, the crystal structure is a bit different from the other samples. Figure 4.17 shows the crystal morphology of calcium carbonate formation at 500 mg/l for temperatures of 50 $^{\circ}\text{C}$ and 25 $^{\circ}\text{C}$ and constant solution flow velocity of 0.15 m/s. The salt structure behaviour looks slightly like air-pore because the porosity can be observed in panel (b). The crystal structure is the same as the others but the difference is only the size of the block. The amorphous CaCO_3 appears to be metastable and aggregate into larger spherical particles (about 45 μm). The crystals simultaneously grow larger and accumulate to form a CaCO_3 fouling layer. The blunt cubic edge will make the structure less robust compared to the sharp cubic structure. It is believed the deposition occurs in 500 mg/l is a mix between particulate and crystalline based on SEM image observation.

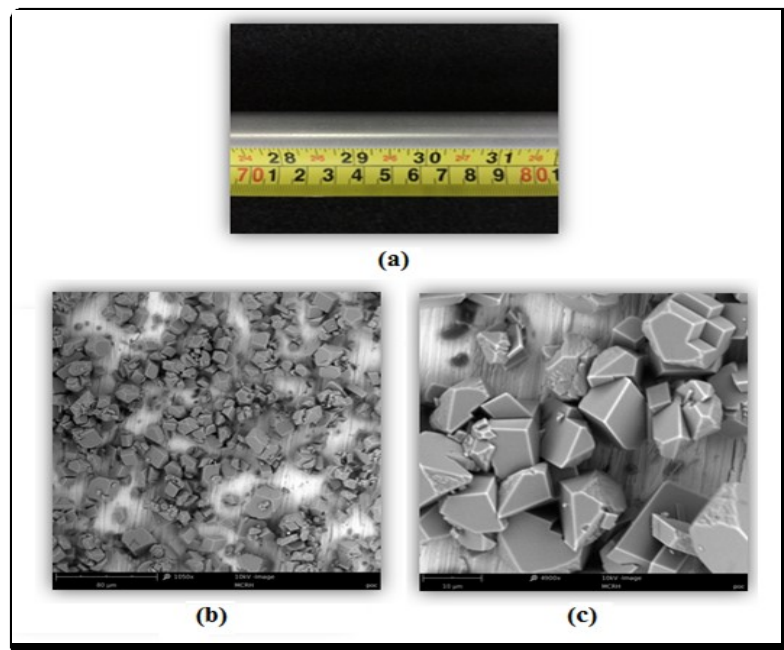


Figure 4.15: Image (a) and crystal morphology (b & c) of calcium carbonate formation at 300 mg/l, 50 $^{\circ}\text{C}$ and 25 $^{\circ}\text{C}$ at hot and solution inlet respectively and 0.15 m/s solution flow velocity.

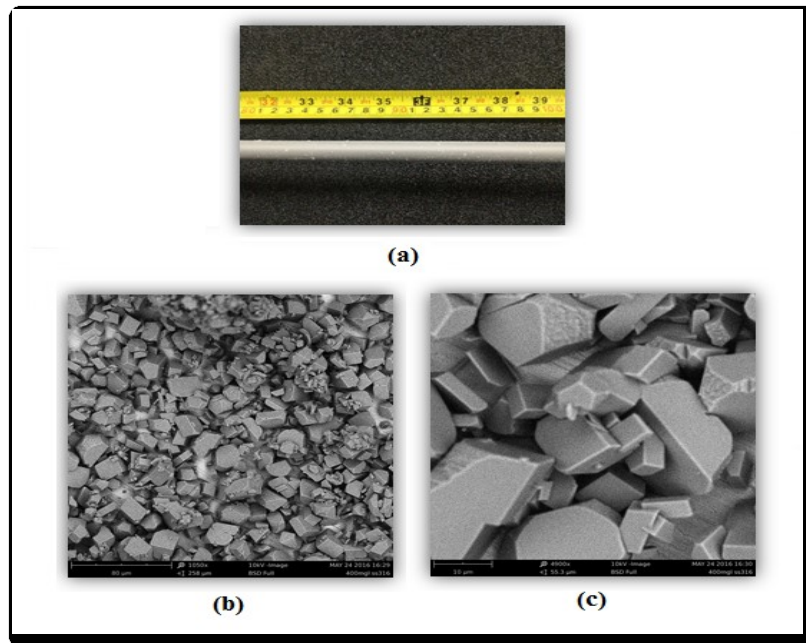


Figure 4.16: Image (a) and crystal morphology (b & c) of calcium carbonate formation at 400 mg/l, 50 °C and 25 °C at hot and solution inlet respectively and 0.15 m/s solution flow velocity.

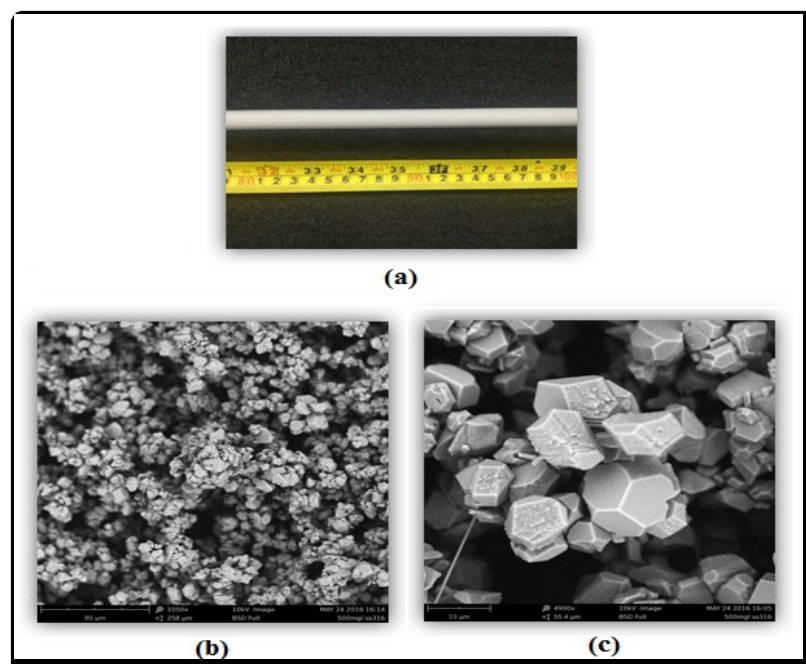


Figure 4.17: Image (a) and crystal morphology (b & c) of calcium carbonate formation at 500 mg/l, 50 °C and 25 °C at hot and solution inlet respectively and 0.15 m/s solution flow velocity.

4.3.6 Visualization of the Fouling Test Section and Crystal Morphology

Figures 4.18 and 4.19 show the deposition on brass and copper materials respectively. Note that only white deposition formed and no corrosion effects were observed on SS316 and aluminium after the fouling test. However, the deposits formed on the brass surfaces have green and reddish stains along with white encrustation of calcium carbonate, which indicate that the chemical reaction took place and hence some chemical fouling was observed as seen in Figure 4.18. Deposits formed on the copper pipe surface were observed similarly with the green layer along with white deposits as seen in Figure 4.19. It happened due to the effect of chemical fouling and crystallization. Similar results were reported by Kazi et al. on calcium sulphate deposition (S. N. Kazi et al., 2013). Moreover, it was observed that carbon steel suffered severe corrosion after the fouling test. A combination of crystallisation fouling and corrosion fouling was observed on the carbon steel surface. In a nutshell, it could be concluded that industrial cooling waters are a corrosion contributor to heat exchanger surfaces where there are combinations of various effects on fouling.

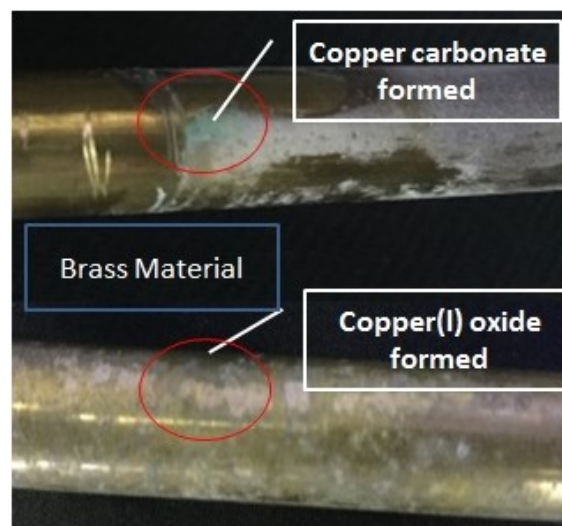


Figure 4.18: Deposition on brass material.

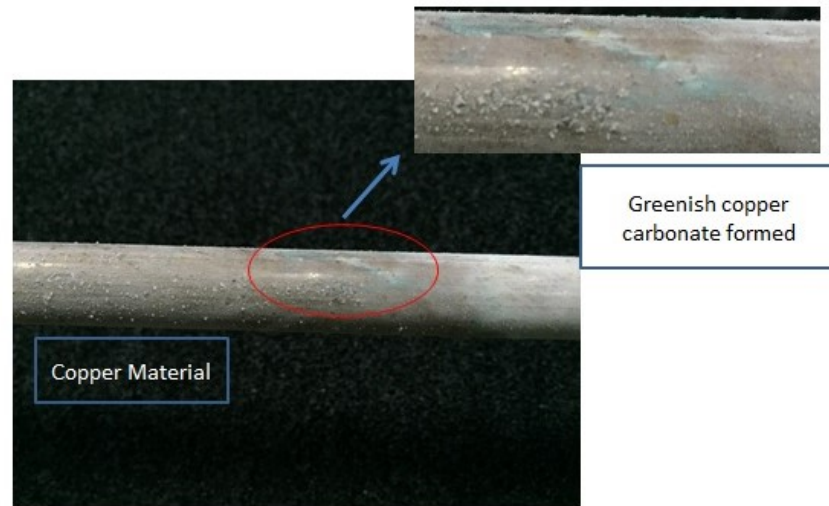


Figure 4.19: Deposition on copper material.

Figure 4.20 presents the x-ray diffraction spectrum (XRD) of the deposited materials on copper, aluminium, brass, SS316, and carbon steel, respectively. First it can be seen that the characteristic peaks at $2\theta \sim 29.3^\circ$, 23.1° , 36.1° , 39.4° , 47.5° , and 48.7° verified the presence of calcite in all the substrates (Palanisamy, Sanjiv Raj, Bhuvanewari, & Subramanian, 2016). Also, all the metals exhibit the presence of a duplex mixture containing calcite and vaterite and the lack of aragonite is obvious (Gopi & Subramanian, 2012). Insignificant peaks of vaterite were observed at $2\theta \sim 26.7^\circ$ and 31.4° . It is noteworthy that copper and carbon steel demonstrate an oxidation phase, represented by copper carbonate and Iron oxide hydroxide peaks, respectively. Also, due to high intensities of the peaks of the metal substrate, the CaCO_3 polymorphic peaks were subdued and it made deconvolution difficult. We know that the metal intensities were five to six times stronger than the CaCO_3 peaks due to which some of the peaks were subdued and sometimes missed in Figure 4.20. Overall, pure calcite elements were the dominant component deposited on the surface of different metals.

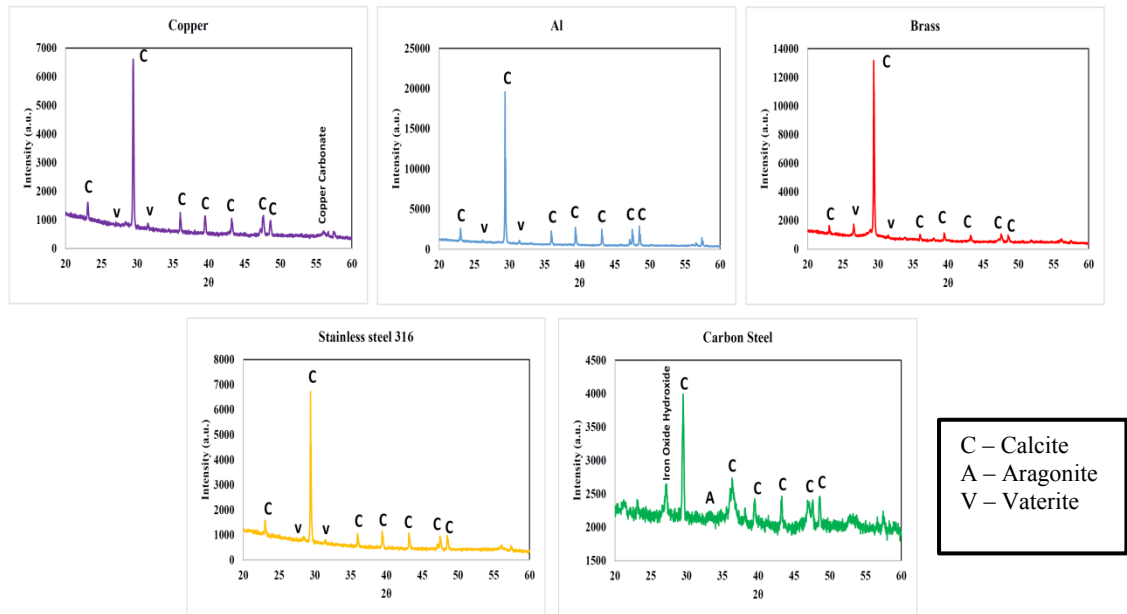


Figure 4.20: XRD analyses of the deposited materials.

Figure 4.21 (a-e) shows SEM images taken from calcium carbonate deposition on SS316, brass, aluminium, and copper and the corrosion products with calcium carbonate fouling on carbon steel. It can be clearly seen that the growth of crystal structure size is following the total deposition trends in which copper is (about 40 μm) > aluminium (about 37.33 μm) > brass (about 20.36 μm) > stainless steel 316 (about 15 μm). These results are supporting the theory of crystal structure size which could determine the fouling deposition rate on the surfaces (J. W. Mullin, 2001b). On the other hand, SEM images of carbon steel show the combination of calcite and the corrosion products.

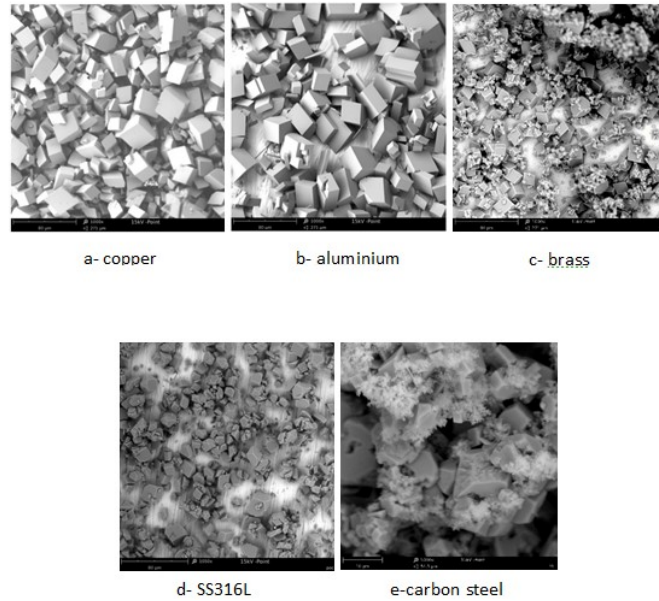


Figure 4.21: SEM analyses of the deposited materials.

Figure 4.22 shows the energy dispersive spectroscopy (EDS) of the combination of corrosion fouling and crystallization fouling on carbon steel materials. Point 1 has reported the composition on iron oxide whereas point 2 shows the deposition of the calcite layer in between the iron oxides.

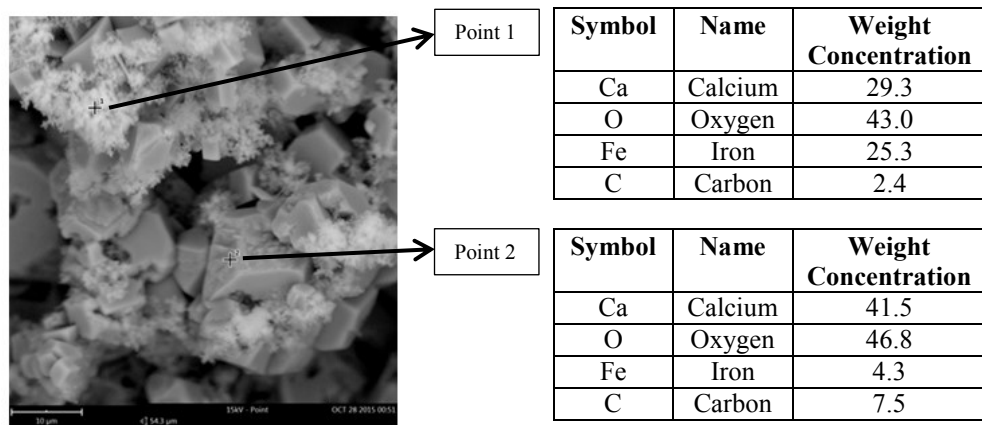


Figure 4.22: SEM and EDS analyses of the deposited materials on carbon steel.

4.3.7 Fouling Mitigation by using Catalytic Material

4.3.7.1 Calcium Content in Scale

Figure 4.23 shows the results of analyses of scale deposition of calcium carbonate on the SS316 metal surfaces. Calcium hardness was measured by EDTA complexometric titration method from time to time to analyse the deposition in function of time. The same technique of dissolving salt is applied for both PWT and non-PWT cases at 300 mg/L. It can be observed that the system without PWT has higher calcium carbonation deposition compared to that with PWT. The highest deposition is obtained at 0.15 m/s for both cases. These results show that the operation of the double pipe heat exchanger can be prolonged by reducing calcium carbonate deposition as in the PWT cases. The results are promising and indicate that the PWT method is capable of improving the efficiency and productivity of industries by reducing the breakdown frequency of the industrial plant. We can observe that the total deposition of calcium carbonate is relatively low for all the cases applied, for all velocities when it is treated with PWT. Moreover, velocity of flow contributes to the removal of scale particles near the boundary wall, which is believed to be due to the increase of shear stress on metal surfaces.

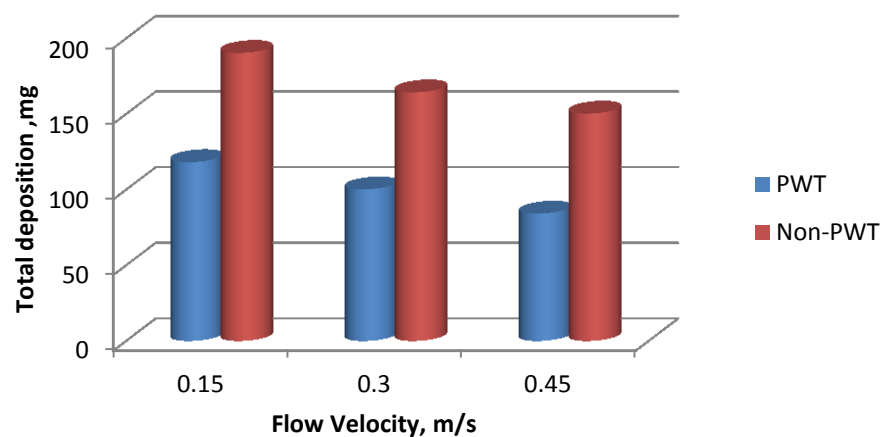


Figure 4.23: Total deposition of calcium carbonate between PWT and Non-PWT cases.

4.3.7.2 Crystal Morphology and XRD Analysis of Calcium Carbonate for PWT-Treatment and Non-PWT Cases

Figure 4.24 and Figure 4.25 show crystal morphology of a calcium carbonate structure formed on metal surface for both PWT-treatment and Non-PWT cases, at flow velocity of 0.15 m/s and hot temperature inlet of 50 °C respectively. It can be clearly seen from the SEM images that the deposited calcium carbonate on the hot transfer surfaces was transformed from calcite form into aragonite form. Calcite is reported to be the most thermodynamically stable phase at room temperature and under normal atmospheric pressure (Lyklema, 2005). Under non-PWT cases, we observed a metastable calcite form deposited on the metal surfaces of approximately 15 μm size.

Compared to the PWT-treatment case, the deposited calcium carbonate appears in aragonite form which is often reported to be the first phase to precipitate out of solution (F Manoli & Dalas, 2000). In addition, the crystal structure size of the deposited calcium carbonate in aragonite form (about 2 μm) on the hot transfer surface is significantly smaller compared to the non-PWT case.

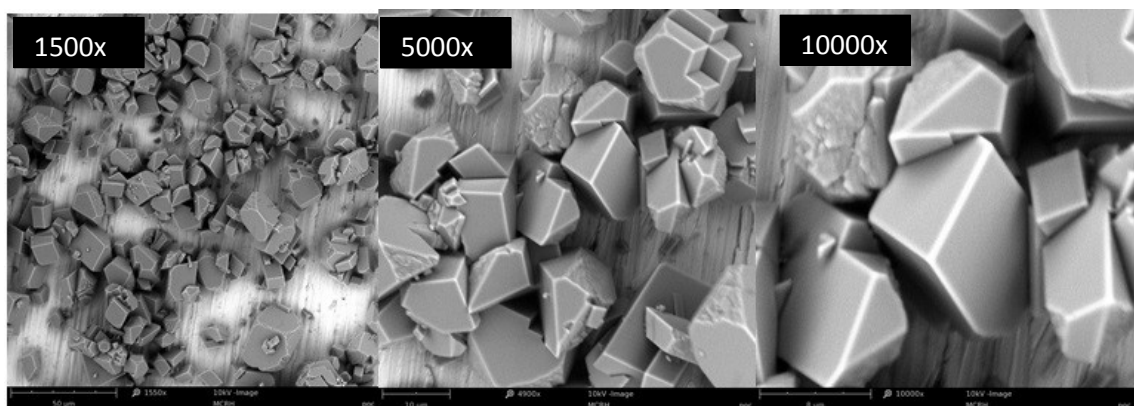


Figure 4.24: SEM images of 1500x – 10000x of calcium carbonate crystal under non-PWT case.

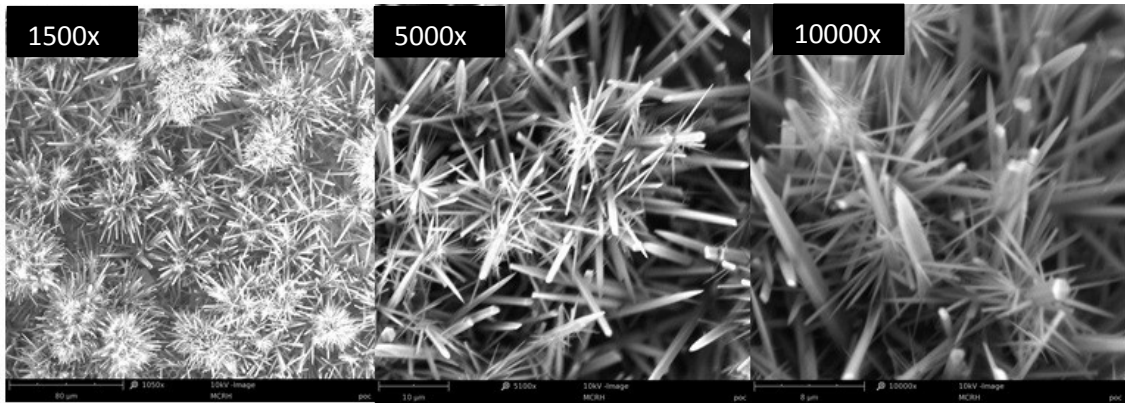
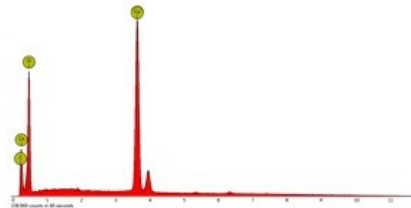
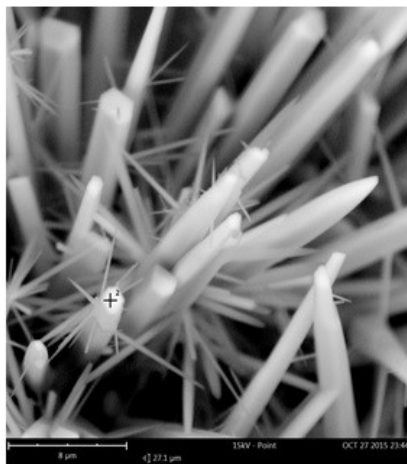


Figure 4.25: SEM images of 1500x – 10000x of calcium carbonate crystal under PWT case.

Figure 4.26 and Figure 4.27 illustrate the energy dispersive spectroscopy (EDS) and XRD of the crystallization fouling on PWT case. Point shows the deposition of pure aragonite form the hot transfer surface.



Element Number	Element Symbol	Element Name	Weight Concentration	Error
20	Ca	Calcium	30.7	0.0
8	O	Oxygen	58.7	0.0
6	C	Carbon	10.7	0.8

Figure 4.26: EDS analysis for calcium carbonate deposition under PWT case.

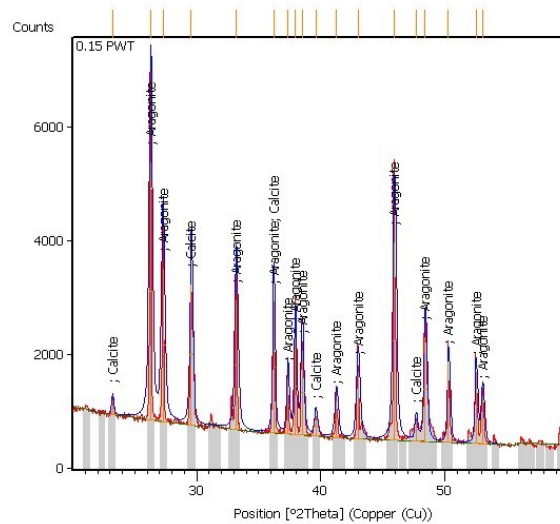


Figure 4.27: XRD analyses for calcium carbonate deposition under PWT case.

4.4 Summary

In these experiments, several variable parameters (velocity, temperature, concentration and materials effect) were studied systematically. In summary, it is observed that the calcium carbonate deposition on the surfaces has linearly increased with the thermal conductivity of the metal. However, deposition on carbon steel metal surfaces did not follow the linear trend of thermal conductivity as it has been altered by the corrosion effects. Temperature has a great effect on the total deposition as well as the induction period of fouling deposition formed on the metal surfaces. In addition, velocity plays a vital role in reducing the fouling deposition thickness. These findings could be good references to use in designing systems and heat exchangers with enhanced performance and lifespan which are topics to be addressed in the future research.

Furthermore, the results show that fouling deposition can be reduced by implementing PWT, whereby zinc and tourmaline are used as the catalytic materials. However, regeneration of catalytic materials for continuous capability to mitigate fouling needs to be addressed in the future research before the implementation of catalytic material in industrial applications can be verified for reliable performance.

CHAPTER 5: NANOFLUIDS PREPARATION FOR FOULING MITIGATION, EXPERIMENT AND ANALYSIS

5.1 Introduction

Mineral scale deposition on heat exchanging surfaces increases the thermal resistance and reduces the operating service life. The effect is usually intensified at higher temperatures due to the inverse temperature solubility characteristics of some minerals in the cooling water. Scale formation builds up when dissolved salts crystallize from the solution onto the heated surface, forming an adherent deposit. It is very important for heat transfer applications to cope with the fouling problems in industry. In this present study, a set of fouling experiments was conducted to evaluate the mitigation of calcium carbonate scaling by applying EDTA, EDTA-treated MWCNT-based water nanofluids, and DTPA-treated MWCNT-based water nanofluids on heat exchanger surfaces. Investigations of these additives (benign to the environment) on fouling rates of deposition were performed. 300 mgL^{-1} of artificially-hardened calcium carbonate solution was prepared as a fouling solution for deposit analysis. Assessment of the deposition of calcium carbonate on the heat exchanger surface with respect to the inhibition of crystal growth was conducted by Scanning Electron Microscope (SEM).

5.2 Experimental Work

5.2.1 Chemical-assisted Functionalization and Preparation of MWCNT-EDTA Water based Nanofluids and MWCNT-DTPA Water based Nanofluids

Hydroxyl-functionalized multi-walled carbon nanotubes (MWCNT-OH) with an outer diameter of 8-15 nm, lengths of 30 nm, and purity > 95% were obtained from Nanostructured & Amorphous Materials, Inc. (NanoAmor). All analytical grade chemicals were purchased from the Sigma-Aldrich Co. Recently, a new mechanism for the direct esterification of carboxylic acids and alcohols catalysed by zirconium(IV) salts was suggested by Ishihara et al. (Ishihara, Nakayama, Ohara, & Yamamoto, 2002).

Regarding the synthesis of MWCNT-EDTA, in a typical experiment, MWCNT-OH (50 mg), $ZrCl_4$ (0.2 mol%), and EDTA (50 mg) were poured into an agate mortar and ground for 5 min. Then, the mixture was poured into a vessel filled with 200 ml of tetrahydrofuran (THF) and sonicated for 2 h at 50 °C until a uniform suspension was obtained. During the sonication, 5 ml of toluene were added drop by drop to the suspension to complete the esterification reaction. Subsequently, the mixture was placed on a stirrer and continuously agitated at 80 °C for 24 h. After the mixture cooled to room temperature, it was centrifuged and washed more than 20 times with water, THF, and methanol to remove any unreacted materials.

To prepare EDTA-treated MWCNT-based water nanofluid, the functionalized MWCNT with EDTA in a known amount of water as a base fluid was sonicated for nearly 30 min using a sonicator. Unsurprisingly, the MWCNT-EDTA was dispersed easily in water. Figure 5.1 shows the functionalization procedure of MWCNT-OH with EDTA. The easily-miscible EDTA functionalities can explain the higher dispersion of the functionalized MWCNT. MWCNT-EDTA-based water nanofluid with weight concentrations of 0.015, 0.030, and 0.045 % was synthesized.

The same procedure was repeated by replacing EDTA into DTPA to synthesise the MWCNT-EDTA in the same weight concentration. Figure 5.2 illustrates the functionalization procedure of MWCNT-OH with DTPA.

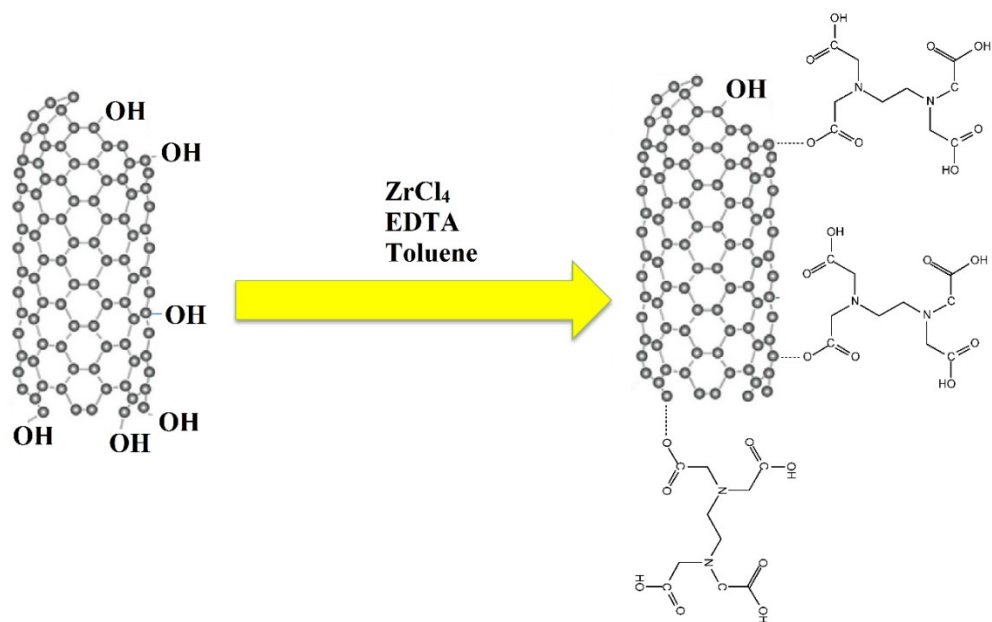


Figure 5.1: Schematic layout functionalization procedure of MWCNT with EDTA.

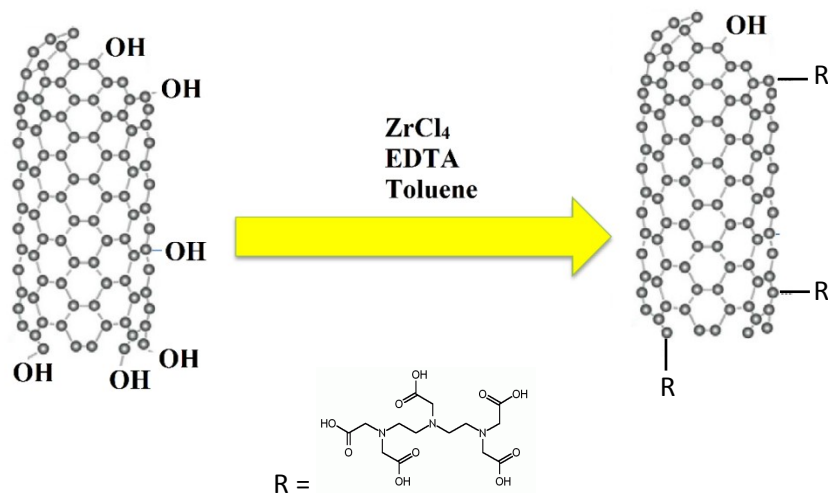


Figure 5.2: Schematic layout functionalization procedure of MWCNT with DTPA.

5.2.2 Functionalization Analysis of DTPA-treated MWCNT

Figure 5.3 presents the Fourier transform infrared spectroscopy (FTIR) spectra of MWCNT-OH as pristine material and DTPA-treated MWCNT. Also, the detailed lists

of peaks along with their interpretations are given in Table 5.1. It can be seen that both of the materials illustrate significant peaks in their spectra, however the number of peaks increases after the functionalization procedure.

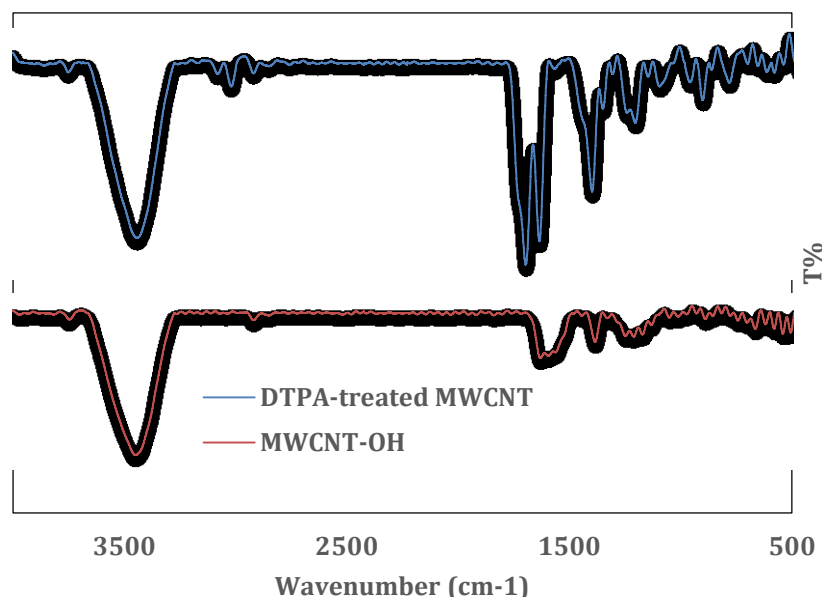


Figure 5.3: Fourier transform infrared spectroscopy (FTIR) spectra of MWCNT-OH and DTPA-treated MWCNT.

Table 5.1: Fourier transform infrared interpretation of the MWCNT-OH and MWCNT-EDTA.

MWCNT-OH	DTPA-treated MWCNT	Interpretation
Peak(cm^{-1})		
3448.56	3441.53	O–H stretching vibration
	3018.62 and 3079.61	C–H stretching vibration
	1695.63	–C=O stretching vibration (Ester band)
1629.88	1634.6	–C=O stretching vibration (Carboxylic Acid)
1384.07	1397.75	O–H bending vibration
	1349.00	CH ₂ bending vibration
	1305.85	C–N stretching vibration
1247.75	1203.29	C–O stretching vibration
1210.88	1146.03	C–O stretching vibration
1171	1093.84	C–C stretching vibration

The FT-IR spectra of both materials show some similar peaks at the range of 3440-3450, 1629-1635, 1200-1250 and 1090-1170 cm^{-1} , which were attributed to the O-H, C=O, C-O and C-C stretching vibrations on the MWCNT generated by the attachment of the -OH groups. After MWCNT with DTPA, some new peaks are appeared in the spectrum of DTPA-treated MWCNT. The main peak at 1695.63 cm^{-1} can be assigned to C=O stretching vibration after esterification. Also, the peak at 1305.85 cm^{-1} corresponds to the stretching vibration of C-N. In addition, two other peaks, one at 3018.62 cm^{-1} and one at 3079.61 cm^{-1} , are consistent with the sp^3 C-H and sp^2 C-H, respectively, which resulted from MWCNT decoration with DTPA. It can be seen that there is a peak at 1349.00 cm^{-1} , which was attributed to the C-H bending vibration.

Raman characterization is a strong measurement for analysing structure, sp^2 and sp^3 hybridized carbon atoms in carbon-based nanomaterials, functionalization, and exfoliation by following alterations in hole and electron doping (Amiri, Ahmadi, et al., 2015; Amiri, Shanbedi, et al., 2015). The Raman spectra of the MWCNT-OH and DTPA-treated MWCNT are presented in Figure 5.4. While the MWCNT-OH is weak in terms of D intensity, the fairly strong D bands in the DTPA-treated MWCNT sample can be seen at 1350 and 1578 cm^{-1} , respectively. The ratio of the intensities of the D-band to those of the G-band (I_D/I_G) is the amount of sp^3 -hybridized carbon relative to sp^2 -hybridized carbon. In functionalization of carbon-based materials, the higher intensity ratio of I_D/I_G indicates the higher disordered carbon. The I_D/I_G ratio of DTPA-treated MWCNT was relatively higher than that of MWCNT-OH, which confirmed the successful functionalization via a DTPA.

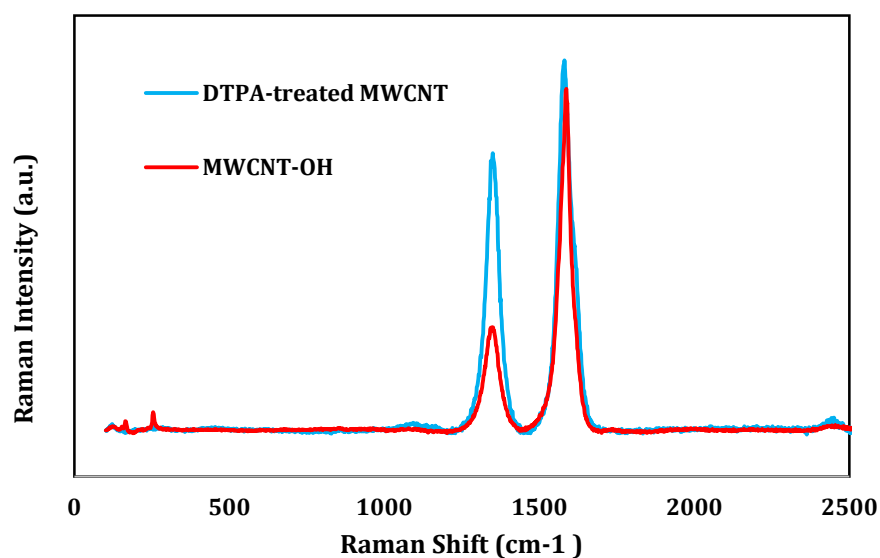


Figure 5.4: Raman spectra of MWCNT-OH and DTPA-treated MWCNT.

TEM images of the DTPA-treated MWCNT are shown in Figure 5.5. In these images, one can see multi-walled CNT (few-walled CNT) with relatively cylindrical shape and diameter less than 15 nm. It can also be seen that there is no unzipping with low-diameter MWCNT.



Figure 5.5: TEM images of DTPA-treated MWCNT.

Characterisation of EDTA-treated MWCNT is not performing in this research as has been reported by Ishihara et al.(Ishihara et al., 2002).

5.2.3 Test Set-up

Figure 5.6 demonstrates the experimental setup employed in this research work. Discussion on the equipment and instruments, experimental setup and the experimental

procedure are presented in this section. The experimental setup consisted of two rotary flow meters, WiseCircu refrigerated bath circulator with temperature controlled, hot water bath circulator, K-type thermocouples, solution tank made of Perspex material, test specimens with coupon (SS-316) and data acquisition system (Graphtec Midi Logger GL220) (Amiri, Shanbedi, et al., 2015).

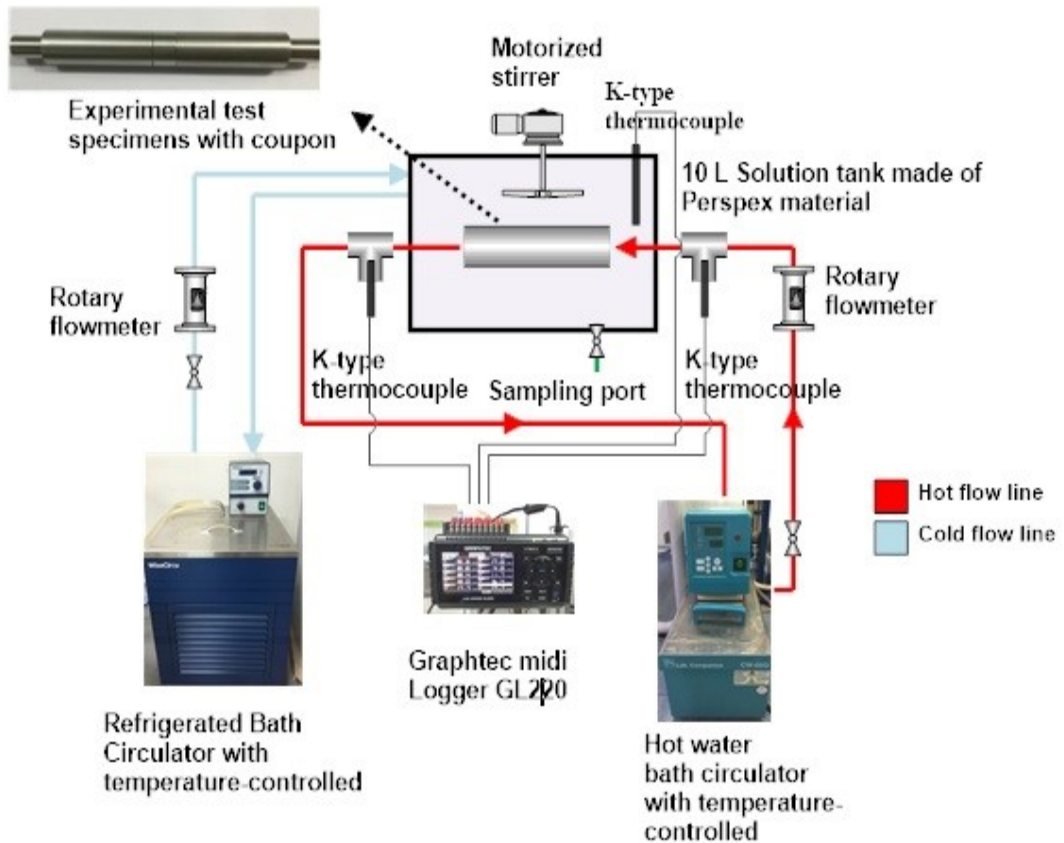


Figure 5.6: Schematic diagram of the experimental set-up.

5.2.4 Test Specimens

Every single piece of the experimental test tubing was 105 mm in total length and with 11 mm and 15 mm for inner and outer diameter respectively. The same dimensions of metal pipes (stainless steel SS-316) were used throughout the experiment. Cleaning of the smooth test specimens was performed in the first place by rubbing with a water-soaked cloth and flushing with hot water in order to remove any deposits of grease, oil or other impurities before being installed in the test rig. Stainless steel coupons that

were 10 mm long were installed in the middle of the test pipes. Characterized on the coupons were performed before and after the scaling tests to understand the fouling deposition rate.

5.2.5 Experimental Procedures

Experiments were conducted to identify the fouling rates, fouling resistances, and heat transfer rates for SS316 heat exchanger surfaces. Furthermore, the effectiveness of the MWCNT-DTPA additive (environment-friendly means) in mitigating the fouling deposition rate was studied in this research. Leakage tests were conducted prior to the experimental runs to ensure smooth flow conditions. The experimental test rig was cleaned by incorporating chemical cleaning agents and distilled water after each of the experimental runs to ensure the reproducibility of the data of the system. In order to accelerate the scaling effect, a supersaturated solution of salts in water was prepared and used in all of the tests. Artificial hard water was prepared by dissolving a mixture of calcium chloride (CaCl_2) and sodium bicarbonate (NaHCO_3) powders in distilled water. Calcium carbonate was formed by the reaction of CaCl_2 with NaHCO_3 , as shown in Equation 5.1.



The temperatures of the flow loops were set at 60 °C and the bulk temperature of 7 L of solution fluid remained at 25 °C by regulating the chiller. EDTA complexometric titration method was used to maintaining the constant hardness of the solution throughout the experimental process. The stirrer was regular at 200 rpm to ensure good mixing and 5 min intervals of the data recording was accomplished by the data acquisition system

5.2.6 Measurement and Characterization

All of the stainless steel coupons were weighed before and after the scaling tests. The measurement of deposited calcium carbonate scale on the coupon was calculated by using the accompanying Equation 5. 2:

$$W_s = W_f - W_I \quad (5.2)$$

where W_s , W_f , and W_I are the weights of the deposited scale, the fouled coupon, and the initial coupon, respectively. The morphologies of the scale deposits were characterized by scanning electron microscopy (SEM), and the elemental analysis was determined by energy dispersive spectroscopy (EDS). Photographic and optical images were obtained to visually differentiate the effect of the additives on the scaling that occurred on the surfaces.

5.2.7 Fouling Characteristics

A number of experiments were performed to study the effect of MWCNT-DTPA concentration on CaCO_3 crystallization fouling .The fouling resistance R_f on the SS316 surfaces under all cases were calculated using the Equation 5.3.

$$R_f = \frac{1}{U_{fouled}} - \frac{1}{U_{initial}} \quad (5.3)$$

where U_{fouled} is the overall heat transfer coefficient for the fouled case, while $U_{initial}$ is the overall heat transfer coefficient for the initial clean condition. These overall coefficients of heat transfer were calculated using the Equation 5.4.

$$Q = UA\Delta T_D \quad (5.4)$$

where ΔT_D (Equation 5.5) is the temperature difference which was determined from average temperature at the surface (T_S) and bulk solution(T_B):

$$\Delta T_D = T_S - T_B \quad (5.5)$$

$$Q = MC_p(T_o - T_i) \quad (5.6)$$

where Q is the rate of heat gained by the solution (Equation 5.6), M is the solution mass flow rate, T_i and T_o are the inlet and outlet temperature respectively and C_p is the specific heat of the solution (Baig, Antar, & Zubair, 2011).

5.3 Results and Discussion

5.3.1 Effect Concentration of the EDTA and MWCNT-EDTA

Figure 5.7 shows the fouling deposition under the effect of an additive. The results showed that fouling was reduced as the percentage of the additive was increased in the fouling solution. EDTA had a key role as a chelating agent and had a promising ability to sequester metal ions, such as Ca^{2+} and Fe^{3+} (D. H. Troup & J. A. Richardson, 1978). They are used effectively as anti-scalants in boiler feed water treatment. However, the efficiency of the EDTA chelating effect is not promising and uneconomical when hardness levels are high (D. Troup & J. Richardson, 1978). In this study, MWCNT-OH was first decorated with EDTA, and the product that was obtained was being bound by EDTA and sequestering Ca^{2+} , thereby reducing in the decreased reactivity of the metal ions. Again, it can be seen that there is a downward connection between weight deposition and concentration of MWCNT-EDTA. The higher extent of EDTA functionalities (or active chain for sequestering Ca^{2+}) in the presence of higher MWCNT-EDTA concentration can explain the above-mentioned decrease in the weight of scale deposited. Also, Ca^{2+} ions remained in the base fluids after being bound by the EDTA loaded onto the surface of the MWCNT, indicating their reduced reactivity. It was observed that the products having a higher degree of carboxyl group prolonged the induction period for crystallization due to the ability of the anionic carboxylate groups to adsorb the Ca^{2+} . Several investigations have indicated that the polymers exhibit an inhibitory effect on the crystallization kinetics of soluble salts which could be highly substituted by the carboxyl group (Lioliou, Paraskeva, Koutsoukos, & Payatakes, 2006). Apparently a larger number of the carboxylate functional group increases the ionic

attractive interactions between the adsorbate ($-\text{COO}^-$) and positive sites (Ca^{2+}) at the solution interface. If the inhibitor ions are rapidly adsorbed, the nuclei remain subcritical and eventually disappear through dissolution. The inhibitor polyanions are then available for repeated adsorption at the edges of newly developing nuclei. This eventually leads to breakdown and disintegration of a number of available embryos before further growth can take place. Moreover, the presence of additional hydroxyl group in MWCNT-OH augments the adsorption of Ca^{2+} . It can be concluded that increasing of the concentration of EDTA-treated MWCNT could provide more EDTA and hydroxyl group with the effect of higher probability of sequestering Ca^{2+} . However, when high concentrations of MWCNT-EDTA are incorporated this will lead to corrosion. Kazi et al. reported the combined effect of fouling and corrosion on copper surfaces while being treated by CaSO_4 solution. Later he found the corrosion prevailed with fouling when he tried to mitigate fouling by adding natural fibres. Fouling and corrosion are simultaneously occurring in nature, though the effect is mild on SS surface. MWCNT treated suspending additives behave like a mitigating agent with limited side effects as corrosion on the base metal. As shown in Figure 5.8, a negative weight deposition reported due to the corrosion happened on the surfaces. Hence, it was concluded that 0.015 % concentration of the EDTA-treated MWCNT in the fouling solution incurs minimum corrosion with significant fouling mitigation effect in this experiment's findings. It's believed that a high concentration of MWCNT-EDTA will contribute in the oxidation process, leading to corrosion.

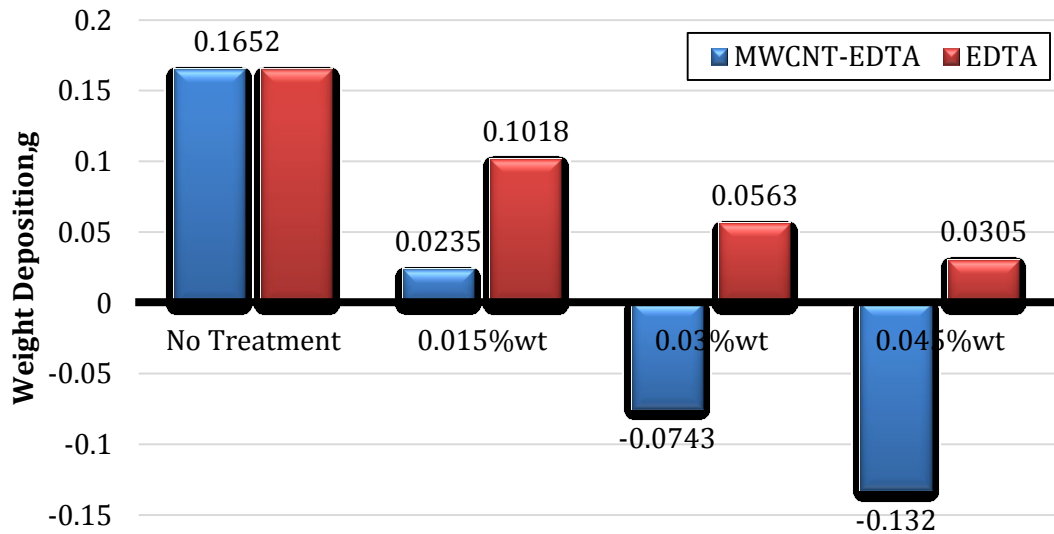


Figure 5.7: Deposition of fouling under effect of concentration at inlet temperature of 60 °C for EDTA and MWCNT-EDTA.

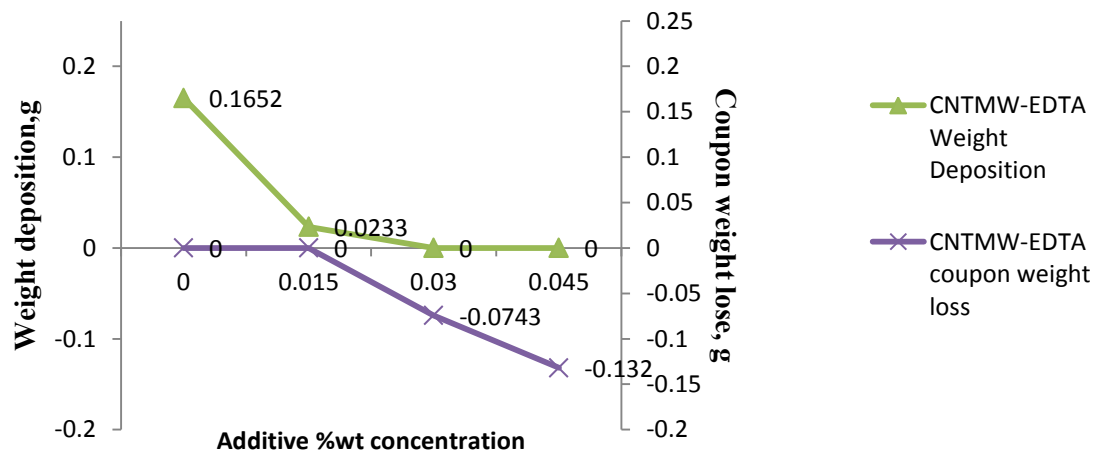


Figure 5.8: Deposition of fouling and corrosion effect under effect of additives MWCNT-EDTA treatment.

5.3.2 Effect Concentration of MWCNT-DTPA

Figure 5.9 indicates the effect of an additive on fouling deposition. The results obtained were compared to results from EDTA, MWCNT-EDTA and MWCNT-DTPA additives. It was shown that fouling was reduced as the percentage of the additive was increased in the fouling solution without corrosion effects. According to E. Altay, EDTA which contains four carboxylic and two amine groups is a well-known complexing agent of Ca^{2+} and its presence in a solution would consequently lower the number of free ions

thus decreasing the driving force towards nucleation (Altay et al., 2007). In these research works, DTPA with five carboxylic and three amine centres groups was considered as the fouling retardation additives. As a chelating agent, DTPA wraps around a metal ion by forming up to eight bonds.

The conjugate base of DTPA has a high affinity for metal cations. In this manner, the penta-anion DTPA^{5-} is potentially an octadentate ligand assuming that every nitrogen centre and each COO^- group counts as a centre for coordination. The formation constants for its complexes are about 100 greater than those for EDTA (J. Roger Hart, 2000). DTPA could perform much better than EDTA (D. H. Troup & J. A. Richardson, 1978). Hence, the effort on decorated MWCNT-OH with DTPA was introduced. The water soluble product obtained was being bound by DTPA and sequestering Ca^{2+} , thus reducing in the decreased reactivity of the Ca^{2+} ions.

Moreover, it can be seen that there is a descending connection between weight depositions under the effect of MWCNT-DTPA additives concentration. The higher amount of DTPA functionalities (or active chain for sequestering Ca^{2+}) in the presence of higher MWCNT-DTPA concentration can clarify the above-mentioned reduction in the weight of scale deposited. These findings are supported by several investigations which indicated that the induction period of crystallization could be prolonged by having a high degree of carboxyl group due to the ability of the anionic carboxylate groups to adsorb Ca^{2+} . The nuclei remain subcritical and eventually disappear through dissolution consequences of rapid adsorption of the inhibitor ions.

It can be concluded that the increasing of the concentration of DTPA-treated MWCNT which could provide more carboxylate group, with the effect of higher probability of sequestering Ca^{2+} without corrosion effect, is observed in these experiments findings.

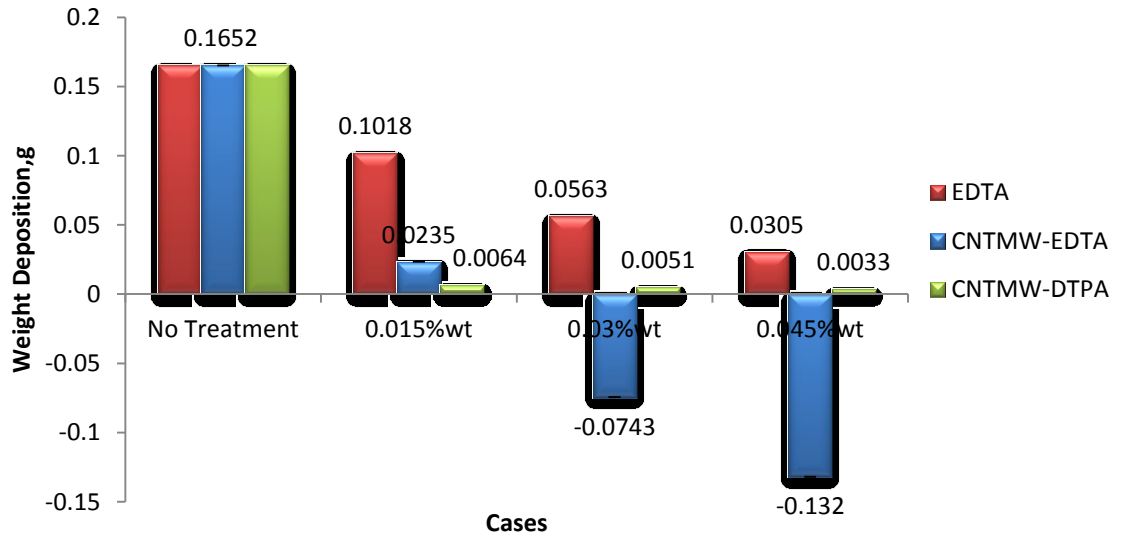


Figure 5.9: Deposition of fouling under effect of concentration at inlet temperature of 60 °C for MWCNT-DTPA.

5.3.3 Fouling Resistance

Figure 5.10 and Figure 5.11 show the results of the fouling test that were obtained by using a water hardness of 300 mgL⁻¹ and different concentrations of additives: EDTA and MWCNT-EDTA. According to Yang et al., the induction period can be defined as the time required for stable crystal nucleation to take place and to slowly spread out laterally until the heat transfer surface is fully covered with scale deposits (Yang et al., 2002). A straight horizontal line in the beginning of the fouling curve is usually used to describe this phenomenon.

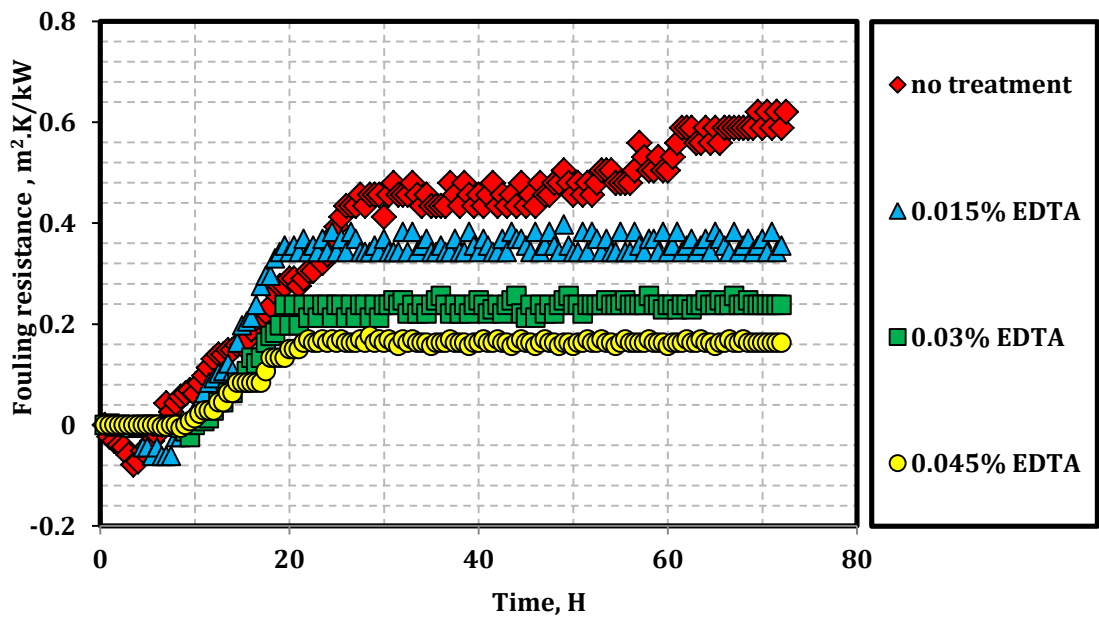


Figure 5.10: Fouling resistances under influence of EDTA additive at inlet temperature of 60 °C with 300 mg/l CaCO₃.

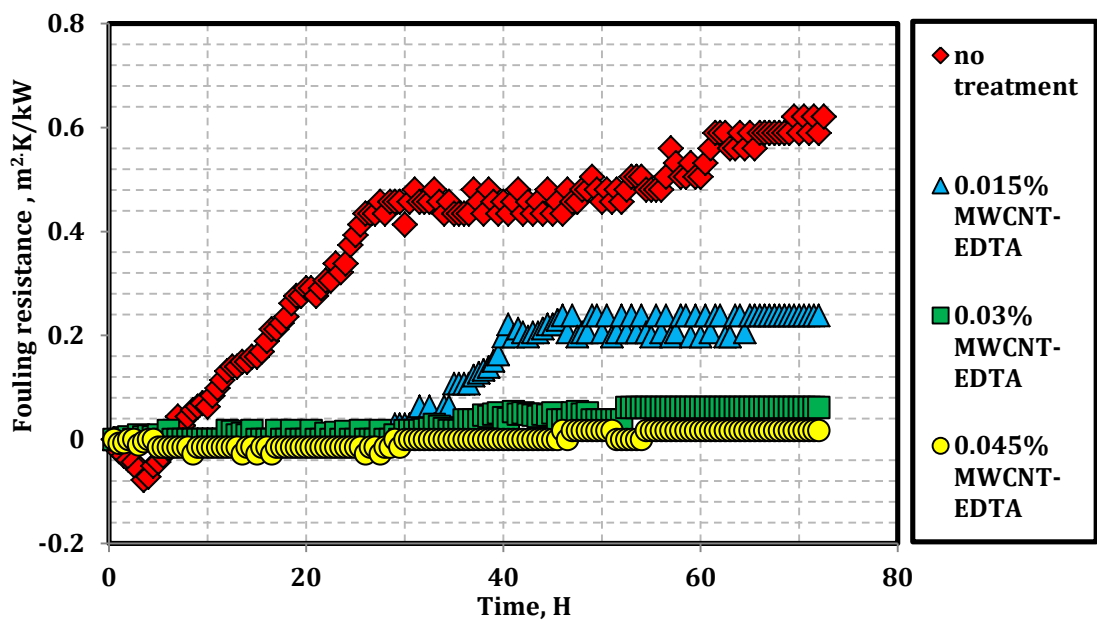


Figure 5.11: Fouling resistances under influence of additive at inlet temperature of 60 °C with 300 mg/l CaCO₃.

In this study, we observed that the induction period was increased by the increased concentration of additives due to the high absorption ability of the additives. The

additives sequestered vast numbers of calcium ions and retarded the formation of calcium carbonate crystals.

However, it was believed that the rapid reaction of the remaining calcium and bicarbonate ions in the bulk water with the hot heat transfer surface could be the key factor for the enhanced resistance to fouling after 10 h of testing. The scale deposition involves the cumulative effect of the direct diffusion of dissolved calcium ions to the heat transfer surface and the deposition of precipitated calcium salt particles due to the supersaturated condition and accelerated precipitation of calcium salts.

Without the additive, there was a step increase in fouling resistance in the first 12 h of operation, which indicated the precipitation of CaCO_3 and its adherence to the heat transfer surfaces. It was observed visually that the stainless steel tubes became fully covered in the first 6 h of the test, and the fouling resistance began to increase gradually in 12 h, reaching an asymptotic level, indicating significant deposition on the surfaces. In the tests without additives, a fouling layer of white deposits was observed visually, but the thickness of the deposits was not measured.

When the additives were used, similar fouling curves were observed for different concentrations of additives, but the induction period took a longer time and had a lower asymptotic value. It is believed that the additives had a significant role in retarding the formation of CaCO_3 on the surface.

As mentioned above, the results showed a reduction in fouling with the increase in the concentration of MWCNT-EDTA in the fouling solution. According to the previous results (J Roger Hart, 2000), EDTA has a key role in sequestering metal ions. Here, EDTA-treated MWCNT was used to sequester Ca^{2+} ions by diminishing their reactivity. MWCNT-EDTA loading in a base fluid, such as water, has two advantages, i.e., i) increasing the heat transfer rate by increasing the thermal conductivity of the base fluid

and subsequently enhancing convective heat transfer (Heris, Fallahi, Shanbedi, & Amiri, 2015; Shanbedi, Heris, Amiri, & Baniadam, 2014) and ii) diminishing the reactivity of heavy metal ions, such as Ca^{2+} , which results in the mitigation of fouling on the surfaces of heat exchangers. Based on the results, higher weight concentrations of EDTA-treated MWCNT in the base fluid can enhance the probability of sequestering a larger quantity of Ca^{2+} ions.

Figure 5.12 reports the fouling resistances under the effect of different concentrations of MWCNT-DTPA. Observation shows that the induction period was dramatically increased by the increased concentration of additives due to the high absorption ability of the additives, similar to MWCNT-EDTA. It is believed the MWCNT-DTPA additives had the same role in sequestering vast numbers of calcium ions, modified the crystal structure and retarded the formation of calcium carbonate crystals.

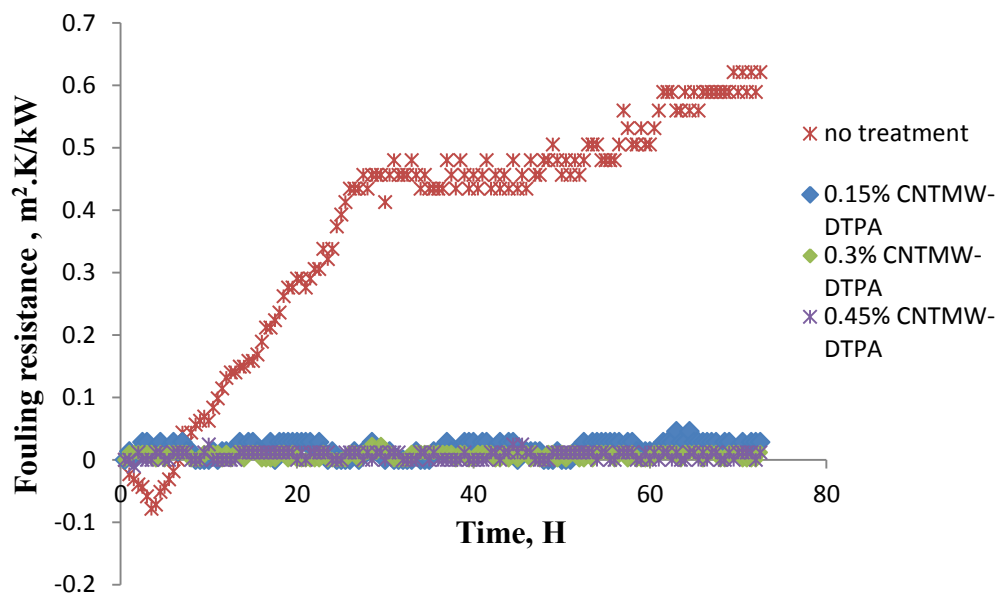


Figure 5.12: Fouling resistances under influence of additive at inlet temperature of 60 °C with 300 mg/l CaCO_3 .

As mentioned above, the results showed a reduction in fouling with the increase in the concentration of MWCNT-DTPA in the fouling solution. According to the previous

results (J Roger Hart, 2000), EDTA and MWCNT-EDTA are capable of sequestering metal ions. However, MWCNT-EDTA reported a corrosion phenomenon. At present, DTPA-treated MWCNT was used to sequester Ca^{2+} ions by diminishing their reactivity without any corrosion on the heat exchanger surfaces. MWCNT-DTPA loading in a base fluid, such as water, has two advantages, i.e., i) enhancement of heat transfer rate by increasing the thermal conductivity of the base fluid and subsequently enhancing convective heat transfer (Shanbedi et al., 2014; Shanbedi, Heris, Amiri, & Eshghi, 2015) and ii) diminishing the reactivity of heavy metal ions, such as Ca^{2+} , which results in the mitigation of fouling on the surfaces of heat exchangers without corrosion effect. Based on the results, higher weight concentrations of DTPA-treated MWCNT in the base fluid can enhance the probability of sequestering a larger quantity of Ca^{2+} ions.

5.3.4 Effect of Additives on the Scale Morphology of CaCO_3 Crystal

5.3.4.1 Comparison between MWCNT-EDTA, MWCNT-DTPA and No Treatment Case

Figures 5.13 and 5.14 show SEM images (taken at 250-1000 x) of the CaCO_3 scale that was obtained with and without additives of MWCNT-EDTA. Examination of the SEM images indicated that the additives affected the growth of crystals and their microstructure. Figure 5.13 shows a no-additive case in which sharp, pointed, needle-like crystals formed with larger crystal sizes. The amorphous CaCO_3 appear to be metastable and aggregate into larger spherical particles (about 20 μm). The crystals simultaneously grow larger and accumulate to form a layer a CaCO_3 fouling layer.

Figure 5.14 shows that, in the presence of additives, there were flatter and duller surfaces than in the case without additives. This indicated that using additives resulted in an accumulation of small-sized crystallites, importantly indicating that the growth rate when additives were used was relatively slow compared to the case without

additives. Similar findings have been reported in the literature regarding the use of additives for the purpose of mitigating fouling (El-Shall, Abdel-Aal, & Moudgil, 2000; S.-T. Liu & Nancollas, 1973; F. Manoli, Kanakis, Malkaj, & Dalas, 2002).

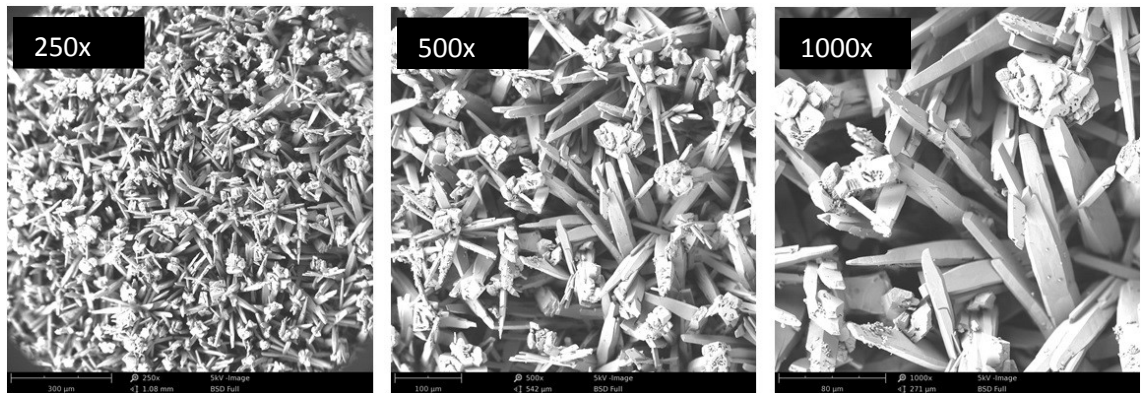


Figure 5.13: SEM images of 250–1000x of calcium carbonate crystal under no treatment case.

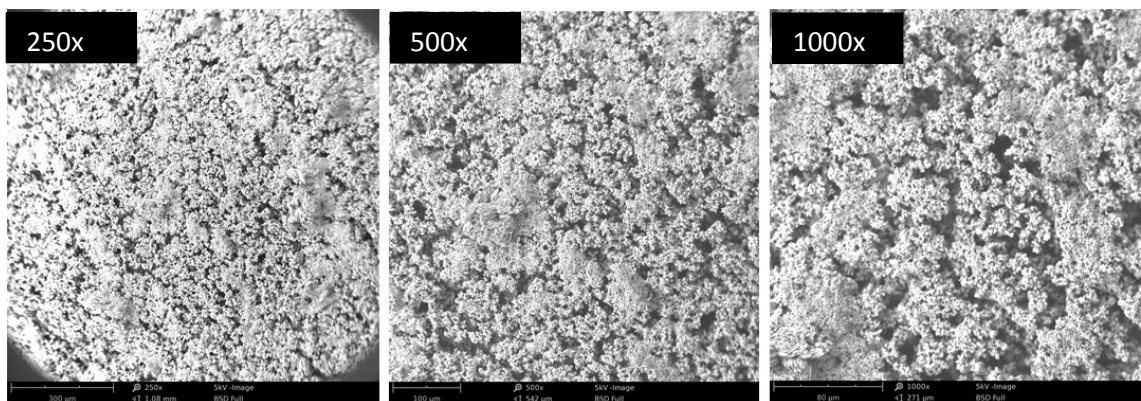


Figure 5.14: SEM images of 250-1000x of calcium carbonate crystal under effect of 0.015% MWCNT-EDTA.

Figure 5.15 shows SEM images of the CaCO_3 scale formation under effect of 0.015%wt MWCNT-DTPA additive. With the additives treatment, it can be seen clearly, the crystal morphology is distorted, irregular shape and relative smaller crystal size (about 16 μm) is observed. As a consequence of inhibition by MWCNT-DTPA, new crystal faces were develop and the crystals become more distorted.

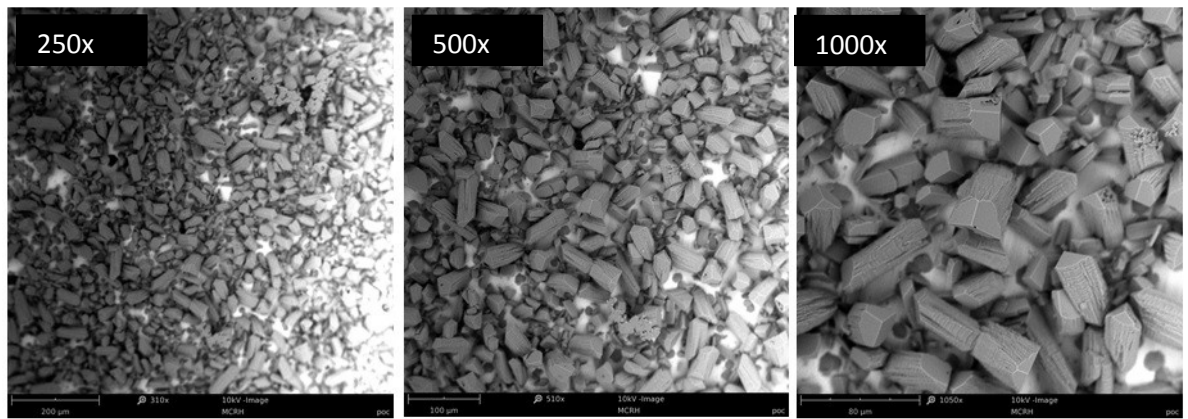


Figure 5.15: SEM images of 250-1000x of calcium carbonate crystal under effect of 0.015 wt% MWCNT-DTPA.

These SEM images indicated that the additives affected the crystals' growth and microstructure. Incorporating additives resulted in an accumulation of distorted and small-sized crystallites, prominently indicating that the growth rate, when additives were used, was relatively slow compared to the case without additives (Verch, Gebauer, Antonietti, & Colfen, 2011). In addition, it is preventing the formation of a regular, crystalline lattice and the build-up of an adherent scale. Related findings have been stated in the literature regarding the practice of additives for the driving of mitigating fouling (El-Shall et al., 2000; S.-T. Liu & Nancollas, 1973; F. Manoli et al., 2002; Volkmer, Fricke, Huber, & Sewald, 2004).

Crystals are formed during the CaCO_3 fouling experiments in the no-additives and presence of the additives cases. Figure 5.16 illustrates that CaCO_3 crystals are $<15 \mu\text{m}$ in size, defect near the crystal wall structure in 0.03 %wt concentration. When 0.045 %wt additives concentration was incorporated in the inhibited system, it was observed that crystal structures are fewer in number, most are $<10 \mu\text{m}$ and significantly distorted as seen in Figure 5.17. Most importantly it was observed that there was no corrosion effect on all the test specimens for 3 different concentrations.

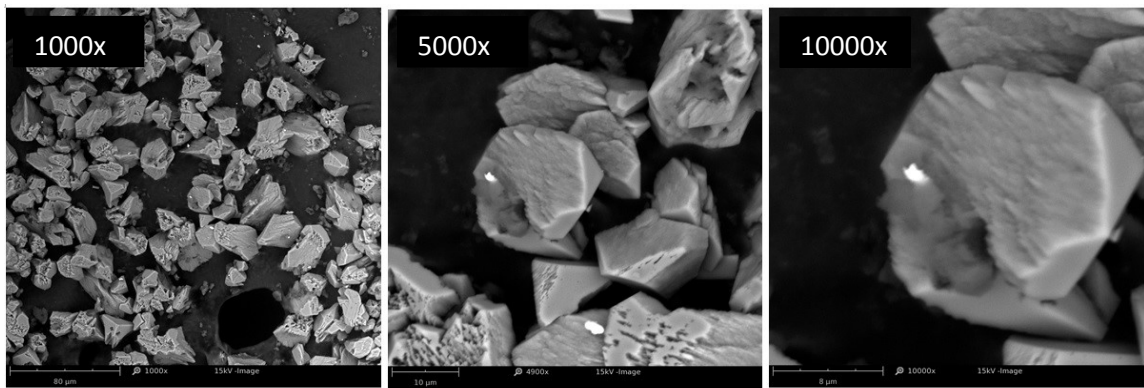


Figure 5.16: Crystal morphology of CaCO₃ under effect of 0.03 wt% additives concentration.

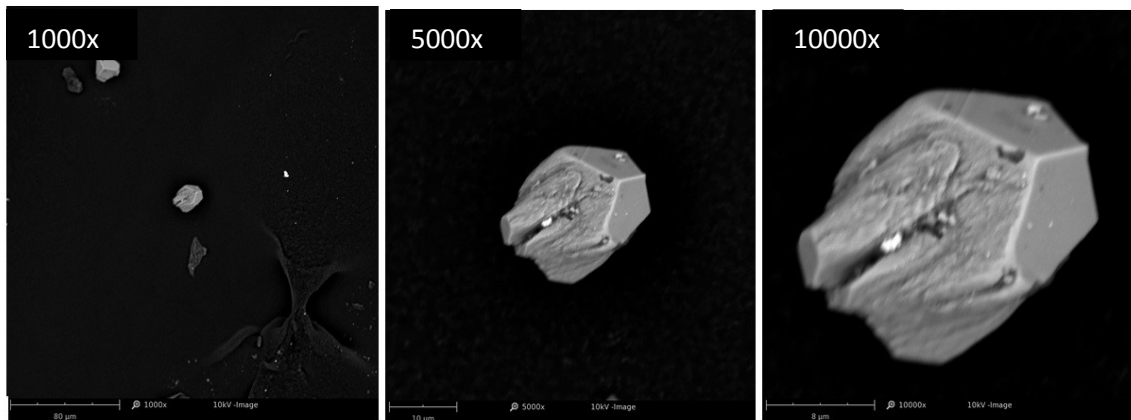


Figure 5.17: Crystal morphology of CaCO₃ under effect of 0.045 wt% additives concentration.

5.3.5 Thermal Analysis

Unsurprisingly, EDTA-treated MWCNT can easily disperse in aqueous media. The easily-miscible EDTA functionalities can describe the significant dispersion of MWCNT-EDTA. Regarding thermal study, Figure 5.18 illustrates the thermal conductivity of MWCNT-EDTA based water nanofluids for weight concentrations of 0.015 %, 0.03 % and 0.045 % at temperature range of 20-50 °C. In Figure 5.18, one can see that the thermal conductivity of water based nanofluids including MWCNT-EDTA is higher than that of DI-water. Also, the thermal conductivity shows a rising trend as the weight concentration of MWCNT in the base fluid increases. According to the previous results, the main mechanism of thermal conductivity enhancement in nanofluid was attributed to the Brownian motion of the particles, which itself is a dominating function of temperature (Amiri, Sadri, et al., 2015). On the other hand, the formation of

surface nanolayers can dominate the extent of energy transfer in the nanofluids. Liquid molecules create layers around the MWCNT, thereby increasing the local ordering of the liquid layer at the interface region. The liquid layer at the interface would reasonably have a higher thermal conductivity than the bulk liquid. In all samples with different concentrations, an increase in temperature results in an enhancement of thermal conductivity.

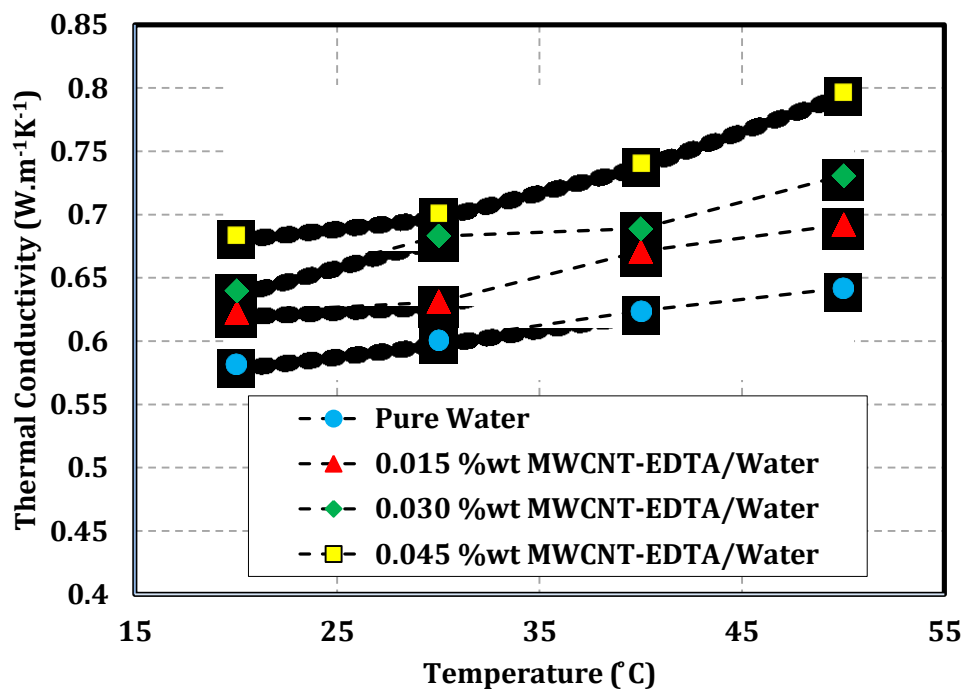


Figure 5.18: Thermal Conductivity of MWCNT-EDTA based water nanofluids at weight concentrations of 0.015, 0.030 and 0.045 %.

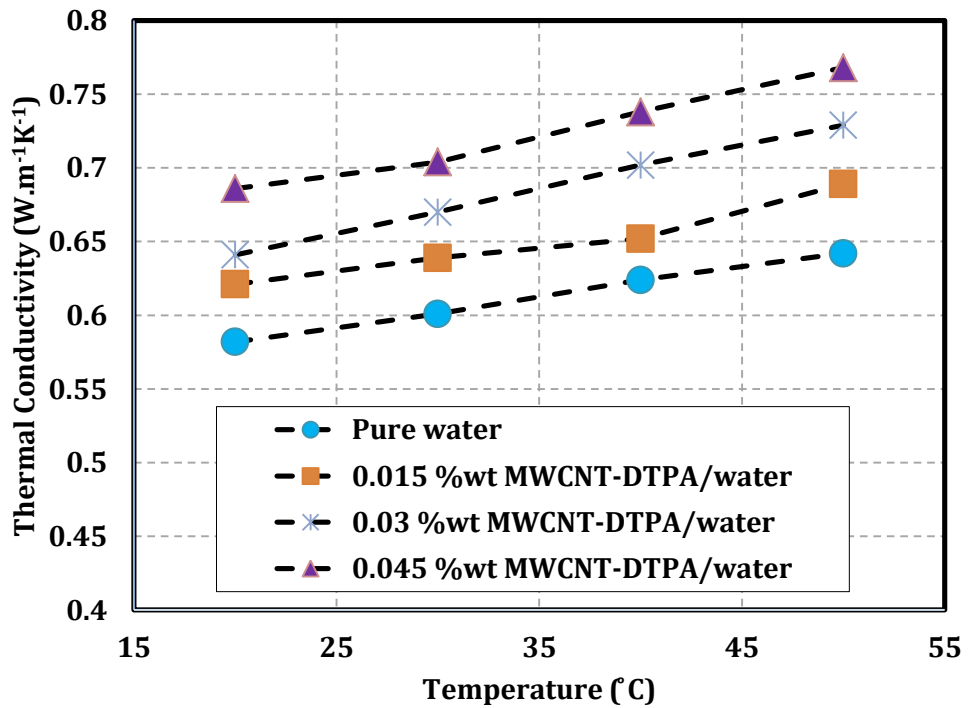


Figure 5.19: Thermal Conductivity of MWCNT-DTPA based water nanofluids at weight concentrations of 0.015, 0.030 and 0.045 %.

5.4 Summary

In these experiments, the comparing of fouling mitigation by using additives EDTA, MWCNT-EDTA and MWCNT-DTPA were studied systematically. Artificial hard water was prepared and used in this experimental setup to accelerate the occurrence of fouling. EDTA is a common chelating agent used to retard the rate of fouling. However, the efficiency is limited due to the corrosion effect because of a high concentration of additives in the solution. MWCNT-DTPA was incorporated in the system to mitigate fouling. A promising result with no corrosion effect is observed. Hence, the use of MWCNT-DTPA additive in the solution potentially retarded the formation of calcium carbonate crystals on the surface of the heat exchanger. These findings could be extended for use in designing systems and heat exchangers with enhanced performance and diminished adverse environmental consequences, which are topics that should be addressed in future research.

CHAPTER 6: IMPLEMENTATION OF A NON-INVASIVE SENSOR FOR ASSESSING WATER-HARDNESS IN HEAT EXCHANGERS IN REAL-TIME

6.1 Introduction

In this chapter, a non-invasive method for monitoring concentration of calcium hardness in heat exchanger cooling water was conducted with a 2.5 GHz electromagnetic (EM) cavity resonator designed and fabricated by Built Environment and Sustainable Technology (BEST) Research Institute for the experiment. The principle of electric dipole moment theories were used to analyse the sample solution that occurs as a function of calcium ion content. Artificial different concentrations of water hardness were prepared by mixing CaCl_2 in deionized water. The sample was centrally positioned in the electric field of the TM_{010} mode of a resonant cylindrical cavity. COMSOL simulation package was used to compare and validate the experimental cavity resonator frequency. Transmission signal (S_{21}) measurements via Vector Network Analyser (VNA) with different concentrations were observed as a linear relationship in amplitude with frequency changes. In addition, calcium absorption provides a first order change in material polarisation (i.e. real permittivity), and second-order transitions associated with dielectric losses (i.e. imaginary permittivity). These research findings introduce a novel technique of real time monitoring of water hardness concentration by using a non-invasive EM sensor.

6.2 Literature Review

6.2.1 Microwave Fundamentals

Electromagnetic waves (EM) can be categorised into x-rays, microwaves, visible light, ultraviolet light, infrared light, radio waves, and gamma rays which have a different frequency and wavelength as seen in Figure 6.1.

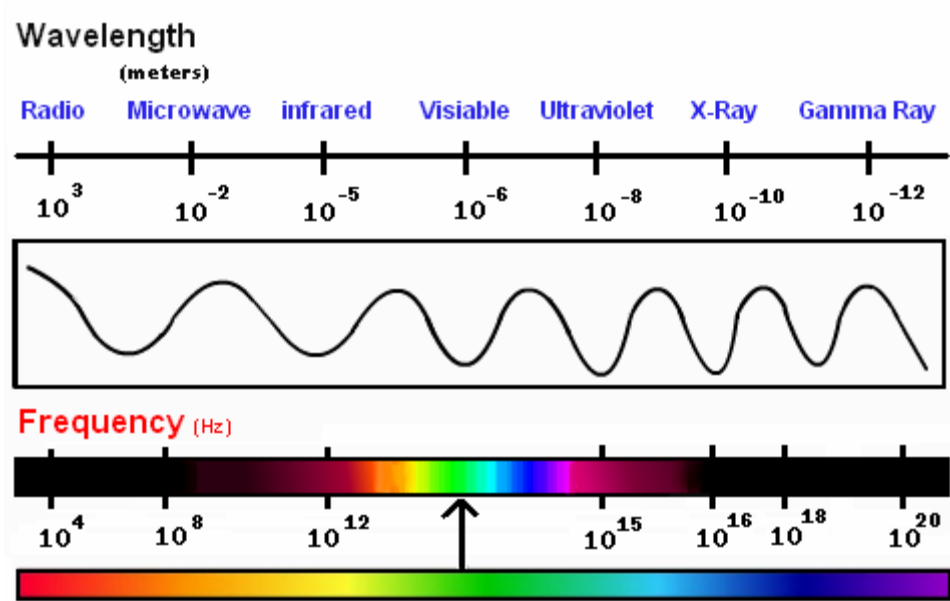


Figure 6.1: Electromagnetic spectrum. (Rao, 2015)

EM signals are often defined as the electromagnetic waves operating at a frequency ranging from 300 MHz to 300 GHz, with corresponding free space wavelengths between 1 m and 1 mm respectively. Microwaves are widely used in communication systems such as in wireless networks, mobile phones, military radar, and weather prediction. On the other hand, microwaves are also extensively used in global positioning systems, medical diagnostics, and industry measurement technologies (Hong & Lancaster, 2004).

6.2.2 On-line Monitoring of Water Quality

Accumulation of an insulated layer of deposit such as calcium carbonate, calcium sulphate and calcium phosphorus on piping surfaces in process plants and domestic equipment leads to a detrimental effect on plant operation and equipment performance . As a consequence, an effective monitoring method is crucial to ensure that the cooling water used in cooling equipment, boilers, or other industrial equipment is satisfactorily controlled so that the desired results, quality and efficiency are achieved to maintain plant operation performance (Hans, 2010). It is important to establish a monitoring

system for water quality in industrial plant. This is to ensure that the plant productivity is maintained, energy savings are achieved and the operation of the plant is compliant with the environmental regulations. The continuous monitoring also means reduced risks of sudden break down of boilers, heat exchangers and cooling towers during an industrial operation (H. Müller-Steinhagen et al., 2009). Contemporary practice is to use the traditional manual methods in industrial cooling water systems. A conventional monitoring typically comprises of plant operators or technicians conducting scheduled chemical tests and comparing the results to specified chemical control limits (Carducci, Verani, & Battistini, 2010). The scheduled tests can detect the properties such as pH, conductivity, suspended solids, alkalinity, hardness and others (J. S. Meyer et al., 1999). From the evaluation of the test results, the plant operator can manually regulate a chemical feed pump or broken down valve by estimating the necessary degree of changes to ensure the smooth production. From a sustainability point of view, a non-invasive on-line monitoring system can provide an automatic and continuous monitoring that is real time, faster, more efficient and reliable. Globally the industry is very much interested in finding an automated monitoring and control system for the quality of cooling water to replace the existing manual process. This will significantly contribute to the process and production of the industry (Ahmad & Reynolds, 1999). Hence, an automated continuous on-line monitoring method is much desired by the industry (K. Meyer, Kern, Zientek, Guthausen, & Maiwald, 2016).

Over the last decade, rapid technological developments have been noticed in electronics and microprocessor technology. There are wide ranges of instrumentation available to monitor the quality of cooling water, particularly calcium content, which is the main fouling ingredient. However, the existing technologies require highly skilled and trained workers and are costly to manufacture and maintain (Törer & Aytaç, 2016). Examples include ion chromatography, ion selective electrode and Flow Injection Analysis (FIA).

At present, there is no system which can completely fulfill needs of the industry, specifically, their requirement to carry out real time monitoring of the cooling water condition in an efficient and cost-effective way (Kovacs et al., 2016). Therefore, an effective and reliable real-time monitoring system is essential.

EM sensing technique has a potential to manage with present industrial real-time monitoring demand (Al-Shamma'a, Mason, & Shaw, 2010). It is an innovative technology and has been expeditiously developed over the last few decades to be used as a sensing and monitoring technique for various industrial applications. These include but are not limited to the detection of material moisture content and material characterization in the construction industry. Examples include moisture detection in concrete blocks, bitumen characterization (Jackson & Jayanthi, 2010; Kot et al., 2015), monitoring of fluid level in process industries (Boon & Brubaker, 2008), for continuous process monitoring of plants (Nacke et al., 2010), and in the healthcare industries, for example a real-time monitoring of glucose in diabetic patients (Korostynska et al., 2009) and for non-invasive monitoring of body fluids (Blakey, Mason, Al-Shamma'a, Rolph, & Bond, 2013).

Various research studies have been carried out on using EM sensors to detect the constituent concentrations in water solutions (Ortoneda-Pedrola, Korostynska, Mason, & Al-Shamma'a, 2013). Principally it is done by considering the variation in transmitted (S_{21}) microwave signals at discrete frequency intervals and linking it with the change in the composition of the solution under investigation. This change is realized through the change in the signal and the unique spectrum. The change in the hardness of water will affect its dielectric properties. It can be recognized by comparing the complex permittivity at several frequencies of the pure water and the one with higher water hardness concentration (Haggis, Hasted, & Buchanan, 1952). The EM wave technique could suit this application, coupled with reliability and cost-efficiency.

6.3 Experimental Design and Methodology

6.3.1 Microwave Theory and Application

Materials can be studied from the data of their interactions with electromagnetic waves. This interaction can be realized in the form of a unique signal spectrum known as reflection coefficient of networks (S_{11}) and transmission coefficient (S_{21}). Generally, these measurement quantities vary with the change in the parameter such as permittivity and conductivity of the materials (Rydosz, Maciak, Wincza, & Gruszczynski). Permittivity is a measurement of the response of a dielectric medium to the applied electromagnetic waves that can be detected through its changes in the electric field. It depends on the material's ability to polarise in response to the applied field (Ateeq, Shaw, Garrett, & Dickson, 2016). The two primary parameters that define permittivity are known as dielectric constant and dielectric loss of material (Huang, Shen, Chow, & Yang, 2001).

- i.) Dielectric constant (ϵ'): The phenomena of energy storage and reduction in the wave velocity when EM wave passes through the material which is always used to distinguish dielectric constant values of different materials. Different dielectric constant values are observed, because of the changes in polarisation inside the material.
- ii.) Dielectric loss (ϵ''): It is the loss of electromagnetic energy propagating inside a dielectric material. The reduction of the wave magnitude is due to the rotation and oscillation of the molecules in response to the applied electric field and loss of energy owing to the friction between the molecules.

Changes in the material's concentration, type, percentage etc. will be followed by the alteration of its permittivity yielding a unique signal spectrum when it comes in contact with electromagnetic wave. In this way, the material is characterised over the range of discrete frequencies.

6.3.2 Design of Cylindrical Microwave Cavity Resonator

The electromagnetic wave (EMW) cavity resonates at particular frequencies depending on the dimensions of the cavity. In addition, permittivity of the material (lossy / low loss materials) has an impact on the resonant peak generated and its quality inside the cavity. Resonance occurs when the magnetic and electric fields form a perpendicular/standing wave inside the cavity. This combination of an electric and a magnetic field inside the cavity is known as a mode. The term Transverse Electric (TE) and Transverse Magnetic (TM) are used to name each of the modes depending on the direction of its electric and magnetic components. Each mode has its own resonant peak/frequencies. Also, the cavity can have more than one mode depending on its design and dimensions. The cylindrical EM wave cavity resonator designed in this work along with the experimental setup is shown in Figure 6.2. It was fabricated from aluminium and has four parts (top, body and two ports to launch microwave inside the cavity). A sample solution was prepared in a low-loss quartz tube (outer diameter of 15 mm) with thin wall and inserted in the middle of cavity as in Figure 6.2. The cavity was designed such that its fundamental mode of operation (i.e. TM_{010}) occurs at close to 2.5 GHz. Equation 6.1 can be used to calculate the resonant frequency for a particular mode in a cylindrical cavity.

$$f_{nml} = \frac{c}{2\pi\sqrt{\mu_r\epsilon_r}} \sqrt{\left[\left(\frac{p_{mn}}{b}\right)^2 + \left(\frac{l\pi}{d}\right)^2\right]} \quad (6.1)$$

Where, c is the velocity of light, ϵ_r is the relative permittivity of the material, μ_r is the relative permeability of the material, p_{mn} is the m th root of the Bessel function of the n th order, b is the radius of the cavity and d is the depth of the cavity.

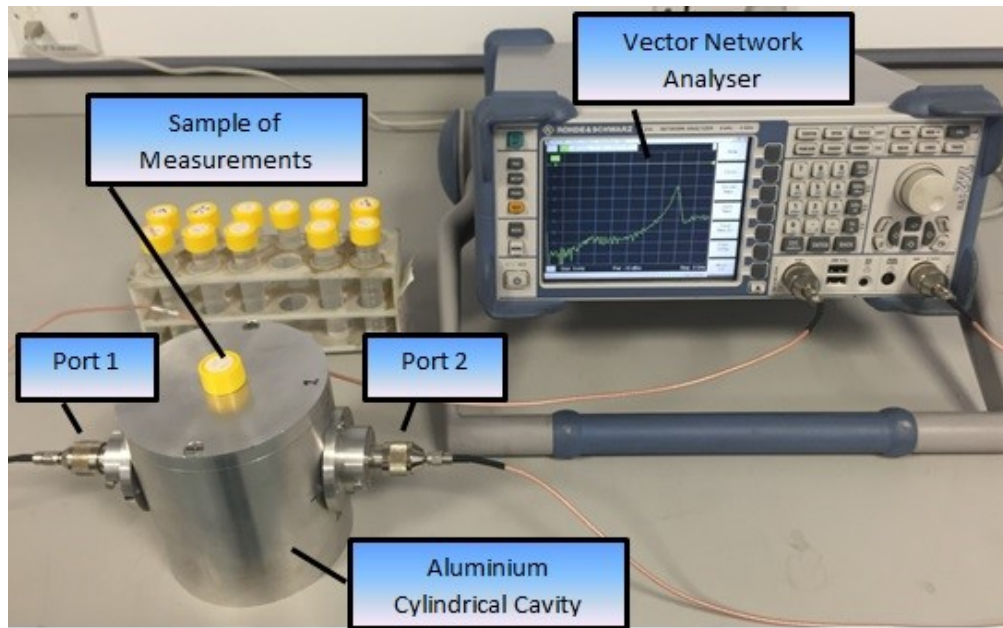


Figure 6.2: EMW cavity resonator measurement system used in experiment.

The fundamental mode enables high measurement sensitivity due to the strong fields inside the cavity. Each mode generates a resonant peak with a quality factor Q . A high Q indicates a sharp resonant peak that readily analyses the sample and hence improves the accuracy of the sensor. Furthermore, TM_{010} chosen in the current study for dielectric property measurement of the samples yields a high intensity, uniform electric field near the cavity's central axis. The electric field in this mode is normal to the direction of propagation of wave and parallel to the wall of the sample tube, resulting in only minor modification of the electric field when the quartz tube is introduced into the cavity (Hartley, Porch, & Jones, 2015). The distribution of electric field magnitude for the TM_{010} mode is shown in Figure 6.3. For maximum sensitivity of the dielectric property measurement, the sample needs to be placed in the region of maximum electric field (i.e. on axis) (Hartley et al., 2015). COMSOL simulation package was used to validate the cavity resonant mode and the frequency. COMSOL Multiphysics is a cross-platform finite element analysis, solver and multiphysics simulation software. It allows conventional physics-based user interfaces and coupled systems of partial differential equations (Gallien, Albaric, Duffar, Kakimoto, & M'Hamdi, 2017).

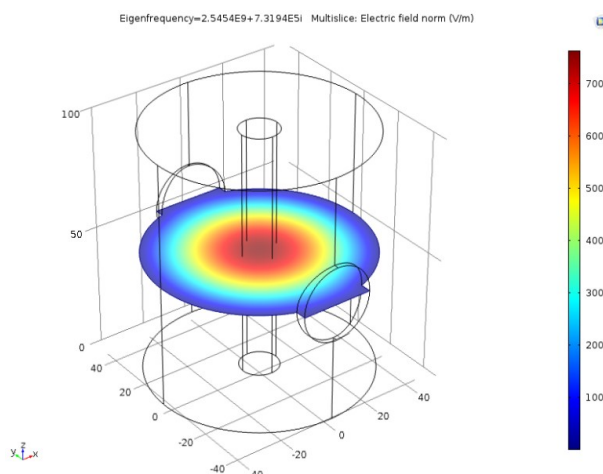


Figure 6.3: COMSOL model of the aluminium cavity resonator showing the distribution of the electric field magnitude in TM_{010} .

6.3.3 Sample Preparation

Experiments were conducted to detect varying concentrations of calcium hardness. Artificial hard water was prepared from a combination of de-ionized water and calcium chloride for various concentrations. In addition, different chemicals were introduced to understand the effects of anion and cation on the EMW measurements. Temperature measurements of samples were taken at room temperature (25 ± 0.5 °C), measured by using K-type thermocouple with Picolog recorder. Three sets of EMW measurements were taken and are listed below, the samples are presented in Tables 1, 2 and 3:

- i.) Measurement of different concentrations of calcium hardness in $CaCl_2$
- ii.) Measurement of varying cation effects on chloride contents.
- iii.) Measurement of varying anion effects on calcium hardness.

Table 6.1: List of samples for monitoring and analysis of water hardness.

Sample type	Concentration, Molar	Temperature, °C
Calcium Chloride ($CaCl_2$)	0	25 ± 0.5
	0.001	25 ± 0.5
	0.005	25 ± 0.5
	0.01	25 ± 0.5
	0.05	25 ± 0.5
	0.1	25 ± 0.5

Table 6.2: List of samples for monitoring and analysis of anion effects in water hardness.

Sample type	Concentration, Molar	Temperature, °C
Calcium Chloride (CaCl ₂)	0.1	25± 0.5
Calcium Bromide (CaBr ₂)	0.1	25± 0.5
Calcium Nitrate (CaNO ₃)	0.1	25± 0.5

Table 6.3: List of samples for monitoring and analysis of cation effects in water hardness.

Sample type	Concentration, Molar	Temperature, °C
Calcium Chloride (CaCl ₂)	0.1	25± 0.5
Sodium Chloride (NaCl)	0.1	25± 0.5
Potassium Chloride (KCl)	0.1	25± 0.5

6.3.4 Data Acquisition and Analysis

Experiments were conducted to measure samples with different concentrations and compositions of chemicals. All the EMW measurements were carried out as the transmission signal, S_{21} . R&S@ZVL Vector Network Analyser, 9 kHz – 6 GHz (Rohde & Schwarz) was used to transmit the microwave signal and capture the EMW response. The measurements were automated and were recorded by LabVIEW software (National Instrument). The R&S@ZVL is a vector network analyser (VNA) for use in research studies due to its powerful measurement capabilities and tremendous increase in the analysis efficiency. However, for the purpose of feeding the EMW energy to a commercial EM sensor, a more portable and cost-effective EM source can be developed which may deliver the necessary VNA functionalities alongside the range of the required measurement frequency. The EM wave input power of 1 mW (0 dBm) was launched into the cavity. Full two-port calibration was carried out to ensure the accuracy of the measurements.

To analyse the acquired samples data, first order cavity perturbation theory was used. It is required to calculate the dielectric constant and dielectric loss of the materials under test (MUT). Complex dielectric property (complex permittivity) of materials can be defined by the Equation 6.2.

$$\boldsymbol{\varepsilon} = \boldsymbol{\varepsilon}' - j\boldsymbol{\varepsilon}'' \quad (6.2)$$

Where, $\boldsymbol{\varepsilon}'$ is the dielectric constant of the material in an applied electric field and $\boldsymbol{\varepsilon}''$ is the dielectric loss of property of the material. The real and imaginary parts of the permittivity of MUT were determined by the frequency shift and change in Q-value presented in Equations 6.3, 6.4 and 6.5.

$$\boldsymbol{\varepsilon}' = 1 + 0.539 \left(\frac{V_c(f_o - f_s)}{V_s f_o} \right) \quad (6.3)$$

Where, $\boldsymbol{\varepsilon}'$ is the dielectric constant, V_c is the volume of the cavity, V_s is the volume of the sample under test dielectric sample, f_o is the resonant frequency of the empty cavity and f_s is the resonant of the loaded cavity.

$$\boldsymbol{\varepsilon}'' = 0.269 * \frac{V_c}{V_s} * \left(\frac{1}{Q_{LS}} - \frac{1}{Q_{L0}} \right) \quad (6.4)$$

$$Q = \frac{f_o}{\Delta f} \quad (6.5)$$

Where, $\boldsymbol{\varepsilon}''$ is the dielectric loss, Q_{LS} is the Q-value for the sample inside the cavity resonator, Q_{L0} is the Q-value for the empty cavity resonator loaded with coupling loop, f_o is the resonant frequency and Δf is the bandwidth or shift in the frequency (Li & Jiang, 2010).

6.3.5 Numerical Simulation

Numerical simulations were conducted by using the COMSOL simulation package. A numerical study was conducted to simulate the resonant frequency for the empty and sample filled cylindrical cavity. The simulation frequency range was set at 2.2–2.8 GHz at the interval of 0.001 steps to acquire a better resolution and accuracy of the simulated

results comparable to the experimental results. Details of the simulation will be explained in section 6.5.

6.4 Results and Discussion

6.4.1 Effect of Concentration

Transmission coefficient (S_{21}) measurements were obtained directly from the network analyser. Results of varying concentrations of CaCl_2 were obtained and shown in Figure 6.4. A close analysis of Figure 6.4 shows there is a change in the magnitude and frequency of the spectrum at around 2.5 GHz when different concentrations of samples were tested. The results also demonstrate the sensitivity of the designed sensor. The analysis of Figure 6.4 shows that the spectra of the samples with the molar concentration of 0 and 0.001 overlap each other making them indistinguishable. However, measurement of the difference molar concentration in CaCl_2 which are greater than 0.005 can be easily identified. Hence, an improvement is required in terms of detecting a minute change in the concentration equal or less than 0.001 molar.

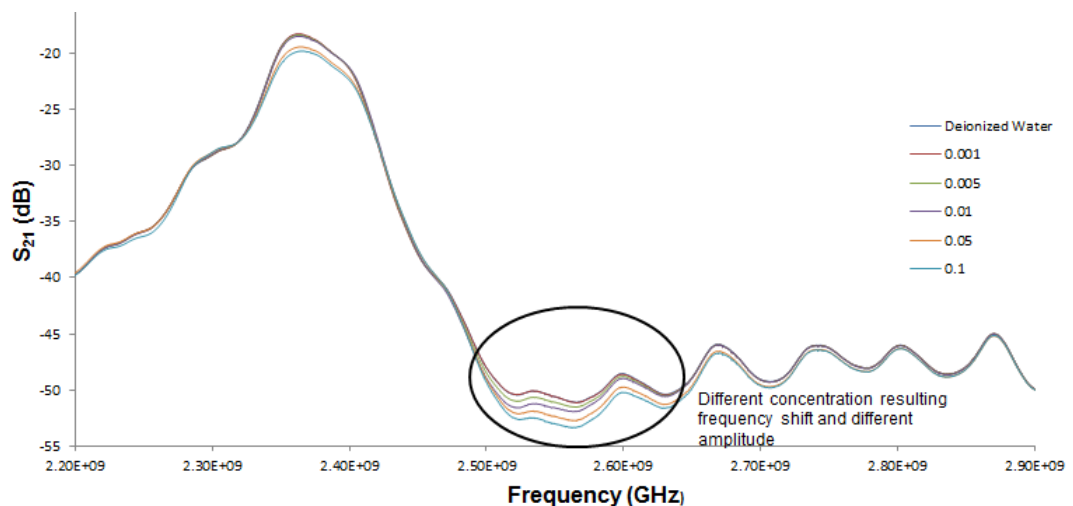


Figure 6.4: Microwave measurements under different CaCl_2 concentration.

Varying the step change in the concentration of CaCl_2 was used to show the sensitivity of the measurement sensor ranging from a small to a large change. To elaborate the

frequency shift and the amplitude change, the varying molar concentration was plotted against them. The results are shown in Figure 6.5 and Figure 6.6 respectively.

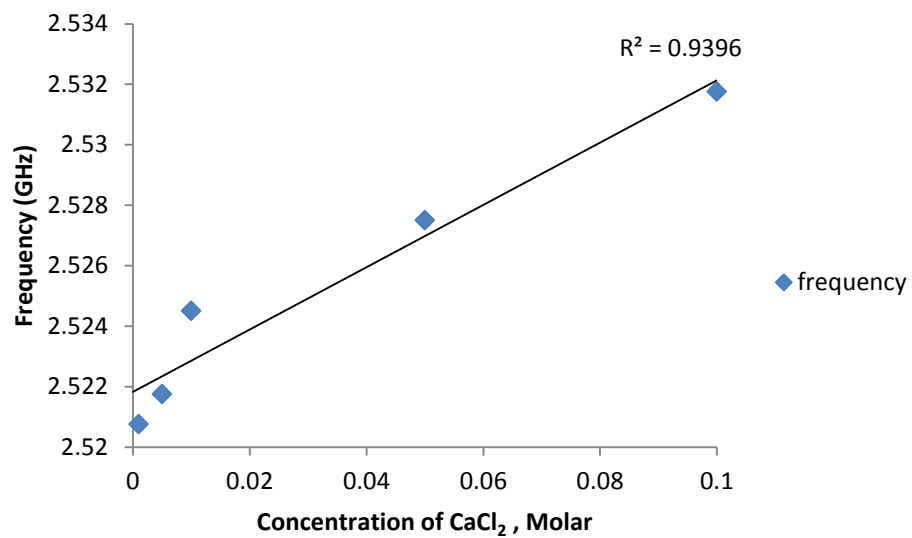


Figure 6.5: Frequency shifts at varying CaCl₂ concentrations.

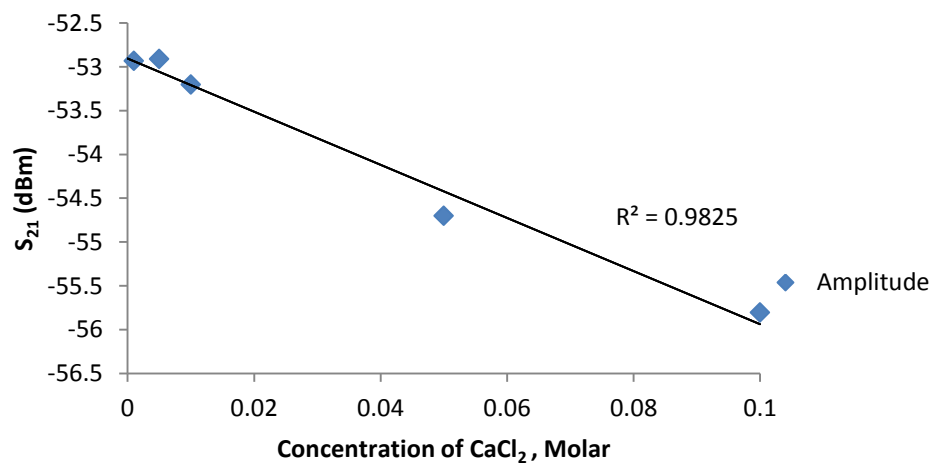


Figure 6.6: Amplitude changes for varying CaCl₂ concentration.

The results in Figures 6.5 & 6.6 show an acceptable change in both the frequencies and amplitudes for different samples. The R-square values demonstrate this with respect to the change in the concentrations. It shows a good linear regression for the measurements of change in concentration, hence showing the effectiveness of the microwave sensing technique.

In addition, permittivity measurements were used to strengthen the findings of the present investigation. Equations 6.3 & 6.4 were used to calculate both the dielectric constants and loss values of the various samples. Figure 6.7 shows the results of change in the dielectric constant of a solution. It illustrates a decrease in dielectric constant of a solution with the increase in its hardness.

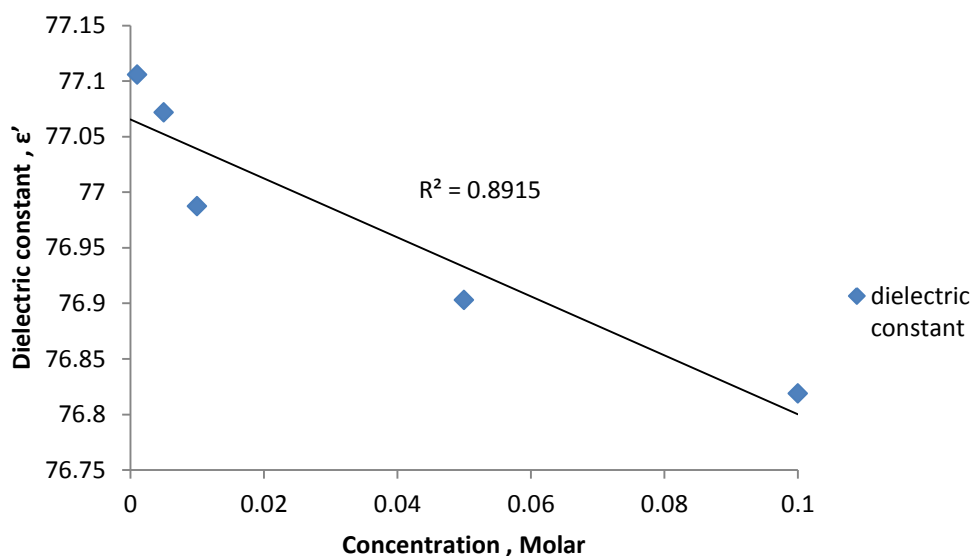


Figure 6.7: Variation of dielectric constants under different concentrations.

On the other hand, Figure 6.8 shows an increase in dielectric loss of solution with the increasing in the hardness of the solution, i.e. increase in the molar concentration of CaCl_2 . The change of a dielectric constant value with the concentration could be explained and it could be due to the electric field between calcium and chloride ions which dissociate in the solution (Valiskó & Boda, 2014). The electric field orients the polar water molecules resulting in oxygen facing towards the calcium ion and hydrogen facing towards the chloride ion. The orientation of these polar water molecules make its own electric field which cancels out most of the electric field that would exist, and effectively lowers the applied external field. This is the possible reason for the lowering of the dielectric constant as the concentration increases (Cheng et al., 2014).

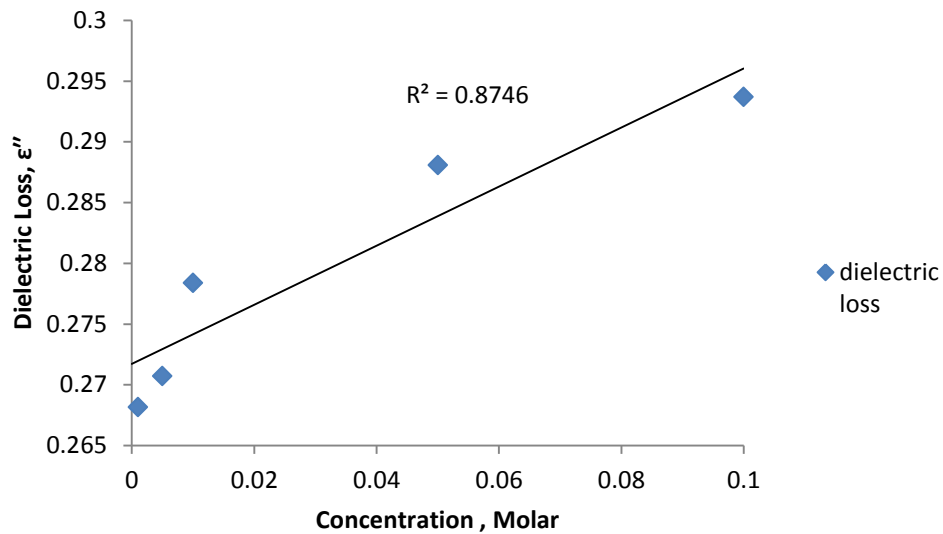


Figure 6.8: Variation of dielectric loss under different concentrations of CaCl₂.

With regards to the variation in the dielectric loss with concentration, it is believed that the motion of ions in the electrolyte solution is the key factor (Maglione & Subramanian, 2008). The dielectric loss increases with the increase in the concentration. This is supported by the fact that higher numbers of ions in the electrolyte solution burdens the dipole movement, and prevents the water molecules from oscillating freely at higher frequencies. In other words, it increases the drag to the rotation of the water molecules. This causes higher friction and results in the increase in dielectric loss value (Gadani, Rana, Bhatnagar, Prajapati, & Vyas, 2012).

6.4.2 Effect of Different Cations and Anions in Water Hardness

To enable people to draw a concrete conclusion on the potential of the EM technique to detect various hardness concentrations, an experimental work to analyse the effect of cation and anion on EM wave spectrum was performed. Figure 6.9 illustrates the EM spectrum under the effect of different cations with chloride based in the same molar concentration. Three chemicals namely, calcium chloride, sodium chloride and

potassium chloride were used in this investigation. The area of the interest is highlighted in Figure 6.9. It can be seen clearly that at the region around 2.5 GHz, amplitude and frequency changed when different cations were employed. However, no obvious change was observed at around 2.4 GHz frequency (highlighted in Figure 6.9).

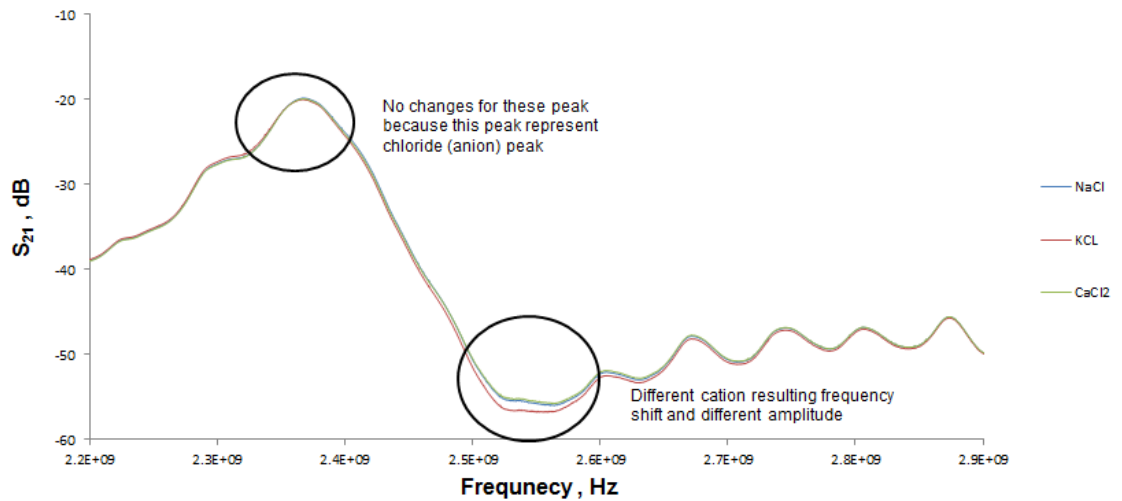


Figure 6.9: Frequency spectrum measurements for different chloride based cations.

Figure 6.10 demonstrates the EMW frequency spectra under the effect of different calcium based anions. The measurements were carried out using three different anions i.e. chloride, bromide and nitrate based anions. It is indicated at the highlighted region around 2.5 GHz that there are no changes in terms of amplitude and frequency for different calcium based anions. This emphasizes that the 2.5 GHz frequency region shows promising results in terms of using the EM sensing technique to monitor the hardness of the solution.

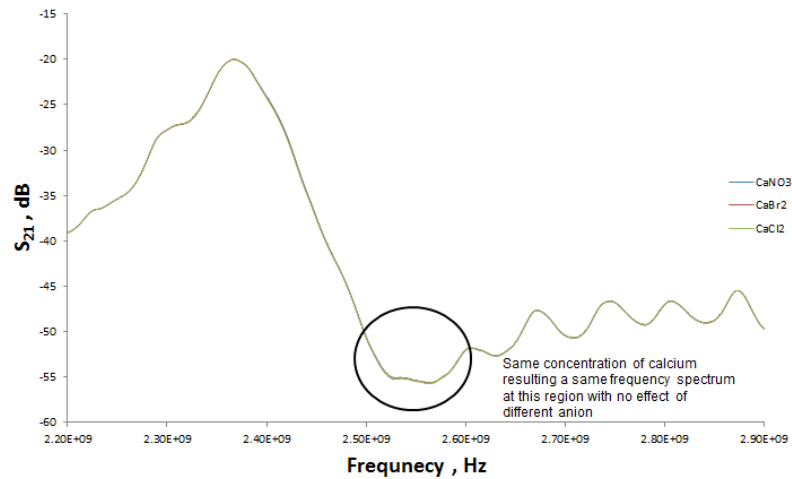


Figure 6.10: Frequency spectrum measurements for different calcium based anion.

6.4.3 Repeatability of the Technique and Validation of the Experiments

To validate the accuracy of the sensor, the simulated and experimental results were compared. COMSOL simulations were carried out to compare the simulated and experimental results of an empty and water-filled cavity. As seen in Figure 6.11, transmitted signals (S_{21}) were reported relatively comparable to the practical measurement. However, it is observed that the results could not exactly match because of the ideal environment in simulations. On the other hand, practically, the measurement instrumentations might experience energy loss while the signal is transported from port 1 to the cavity through a co-axial cable and received at port 2.

In addition the accuracy, reliability and consistency are important factors in any scientific measurement. For this purpose, a repetition test was performed by measuring the water sample 10 times over few days period. Root mean square (RMS) error was calculated and was found to be >99% for the repetition. Figure 6.12 shows the repetitive measurements for 10 de-ionized water measurements.

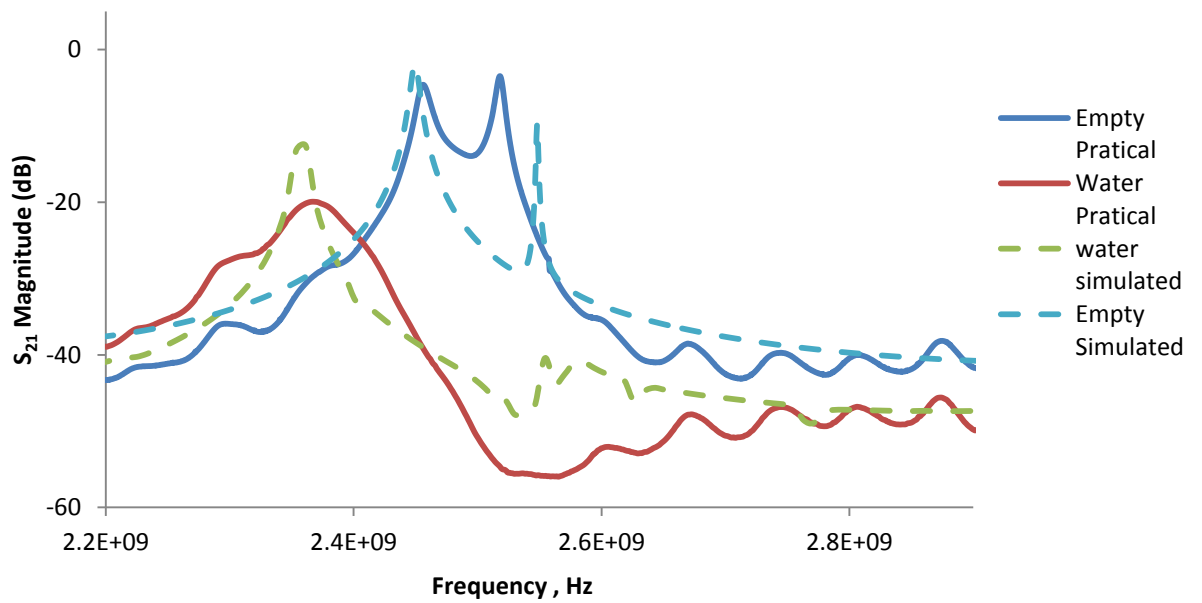


Figure 6.11: Comparison of simulated and experimental results.

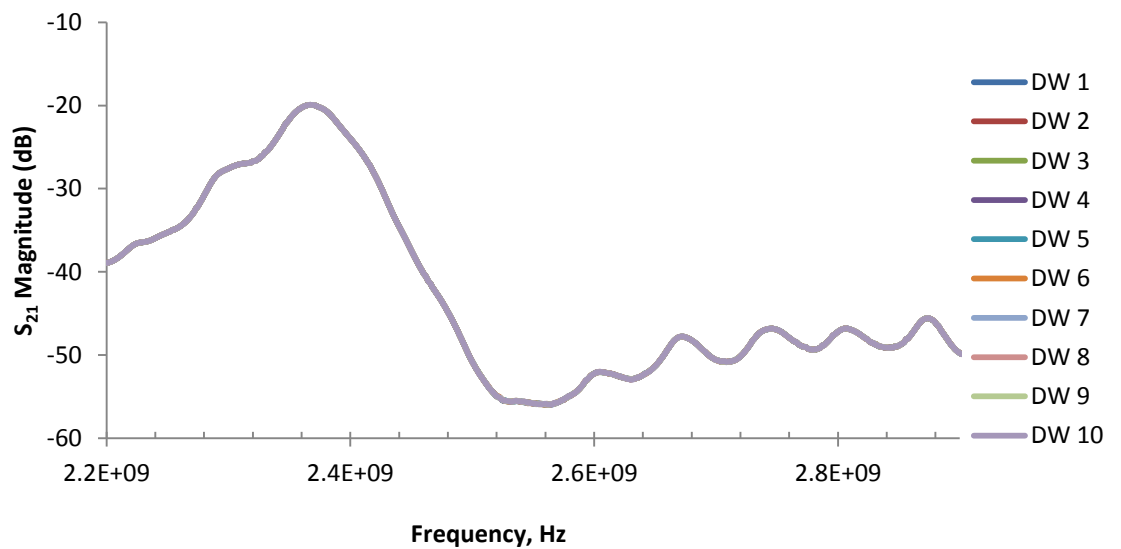


Figure 6.12: Repetitive of frequency measurements for de-ionized water.

6.5 Numerical Investigation on using EMW Sensor to Detect Water Hardness

6.5.1 Introduction

A numerical study using novel electromagnetic wave technique to detect water hardness concentration has been conducted. Simulation is a powerful and efficient engineering

method which allows a quick and accurate prediction of various engineering problems. The RF module is used in this research to predict and design electromagnetic wave propagation and resonance effects of a guided wave to detect water hardness concentration in terms of frequency domain, eigen frequency and mode analysis. A cylindrical cavity resonator is simulated and designed in the electric field of fundamental mode (TM_{010}). With the finite volume method, the three-dimensional governing equations were discretized. Boundary conditions for the simulation were the cavity materials as aluminum, two ports which include transmitting and receiving port, and assumption of vacuum inside the cavity. The designed model was successful to simulate a fundamental mode and extract S_{21} transmission signal within 2.1 GHz – 2.8 GHz regions. The signal spectrum under the effects of port selection technique and dielectric properties of different water concentrations were studied. It was observed that there was a linear reduction of magnitude in frequency domain when the concentration was increased. The numerical results were validated closely by the experimental available data. Hence, the conclusion of the available COMSOL simulation package is capable of providing acceptable data for microwave research.

Modelling of the system through the use of an available Radio Frequency (RF) modelling software package is a useful design tool for electromagnetic wave simulation. It can systematically describe how the system will perform (Huddar, Hampannavar, Patil, Shetty, & Savadi, 2015). The available interface can solve frequency dependent, time-harmonic and other electromagnetic-field distributions which are very useful to determine the performance of a system in the context of its application. Such a modelling tool can support various study types such as frequency domain, eigen frequency, mode analysis and boundary mode analysis to solve wave equation for the applied electric field (Xu et al., 2015). A simulation program is an important tool that can be used to:

- Predict the course and results of certain actions.
- Understand why observed events occur.
- Identify problem areas before physical design and implementation.
- Explore the effects of modifications and various factors.
- Confirm that all variables are known.
- Evaluate ideas and identify inefficiencies.
- Gain insight and stimulate creative thinking.
- Communicate the integrity and feasibility of your plans.

Electromagnetic wave sensing technology is an innovative, novel, non-invasive and on-line monitoring technique with a high potential to monitor water quality and subsequently performance of the cooling system (Korostynska, Mason, & Al-Shamma'a, 2012). In a laboratory environment, it uses a vector network analyser to measure the scattering parameter (S-parameter) to determine concentration of target chemicals. A simulation is conducted in this chapter to assist the design of a suitable microwave cavity resonator and to examine the feasibility of it for an industrial application.

6.5.2 Water Hardness Properties

In this experimental investigation, the relative permittivity of water with varying hardness was determined experimentally. A cylindrical microwave cavity resonator was designed to work along with the experimental setup. It was fabricated from aluminium and has 4 parts (the top, body and two ports to launch microwave inside the cavity). Sample solutions were prepared in a low-loss quartz tube (outer diameter of 15mm) with thin wall and inserted in the middle of cavity as in Figure 6.2. Electric conductivity of water with varying hardness was measured by using an AB200 pH/conductivity meter (Fisher Scientific) and tabulated in Table 6.4. A simulation model was constructed similar to the experimental cavity design by assigning aluminium as the cavity material and polyvinyl chloride as the tube material. The aluminium and

polyvinyl chloride properties were tabulated in Table 6.5. Material properties are investigated at a constant temperature, i.e. 25 ± 1 °C. All the experiments' results were assigned as user defined input into the simulation package to achieve reliable results.

Table 6.4: Electric conductivity and permittivity of different water hardness concentrations.

Water hardness concentration, Molar	Electric conductivity ($\mu\text{S/m}$) 25°C	Relative permittivity 25°C
0.0	5.500	77.2011
0.001	6.404	77.1055
0.005	9.396	77.07179
0.01	12.81	76.9876
0.05	42.11	76.9030
0.1	74.43	76.8186

Table 6.5: Relative permittivity, relative permeability and electrical conductivity of aluminum and polyvinyl chloride

	Aluminum	Polyvinyl chloride
Relative permittivity	1	3.2
Relative permeability	1	1
Electric conductivity (S/m)	36.9×10^9	0.1

6.5.3 Numerical Simulation

6.5.3.1 Model Geometry

RF module in COMSOL Multiphysics 5.1 has been used to investigate the eigen frequency inside a cylindrical cavity and response signal spectrum in a frequency domain to simulate the effect of hardness concentration. Figure 6.13 shows the model of

the cavity used in this study. The cylindrical cavity has a radius of 4.5cm and a height of 10cm.

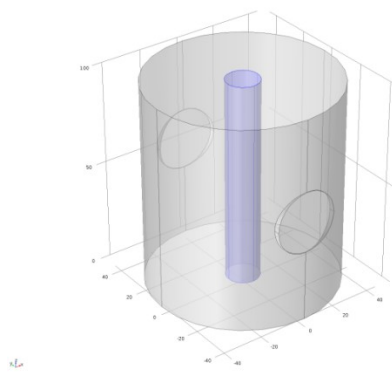


Figure 6.13: Model schematic of the cylindrical cavity.

6.5.4 Meshing Validation

6.5.4.1 Meshing

Modelling geometries with a high aspect ratio can be one of the challenging tasks for the finite element analysis. The appropriate mesh will improve the accuracy of the geometry and the resultant solution. In order to avoid excessive computation resources and time when solving models, meshing validation must be conducted to generate an efficient and accurate finite element meshed model for accurate simulation results.

Figure 6.14 shows different meshes used in this study simulation.

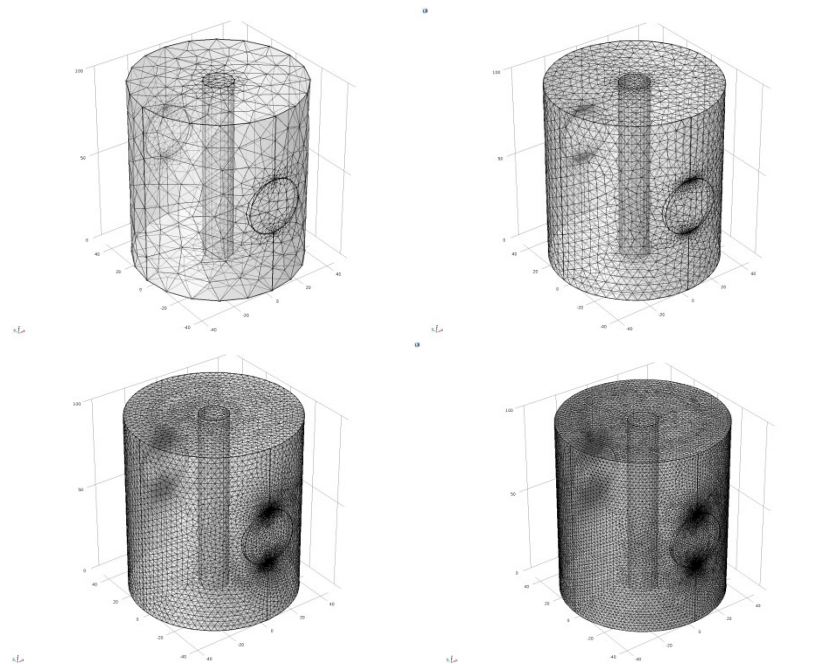


Figure 6.14: Different meshes used in this simulation, (a) coarse mesh, (b) normal mesh, (c) fine mesh, and (d) extra fine mesh

6.5.4.2 Grid Independence

The study of grid independence was done by using a few grid densities on the model with an empty cavity. The main purpose of conducting grid independence is to optimize the model mesh and total simulation time for a reliable result. The Q-factor for empty cavity was monitored to find the grid independence as shown in Table 6.6. It can be seen that there was no significant difference in the fine mesh and extra fine mesh with a relative percentage difference of 0.07 % for the peak frequency and 0.7 % for the Q-factor value. Hence, the fine mesh was used for the simulations.

Table 6.6: Grid independence tests inside an empty cavity for the electromagnetic wave model.

Types of mesh	Domain elements	Boundary elements	Edge elements	Q-factor value	Relative percentage difference (%)	Peak Frequency, f	Relative percentage difference (%)
Coarse	10189	2014	318	239.7	23.3	2.348	2.65
Normal	342375	14180	838	312.8	10.5	2.412	1.39
Fine	705502	22740	1044	349.5	0.7	2.446	0.08
Extra fine	1842550	41330	1358	352.3	-	2.448	-

6.5.5 Material Assignment and Boundary Condition

The wall was assigned an aluminium material and two ports were placed opposite to each other on both sides of the cavity (for transmission and reception of a signal). An impedance wall boundary was assigned as a perfect conductor to the aluminium wall as resistance to electromagnetic wave and has a perfect reflection within the cavity. The working cooling fluid temperature ranges in industrial applications is around 25 °C .Therefore, the temperature of 298 K (25 °C) was maintained within the cavity and measuring samples for this experiment. The samples used in this study were pure water and different concentrations of water hardness. Boundary conditions of the simulation setup are illustrated in Figure 6.15.

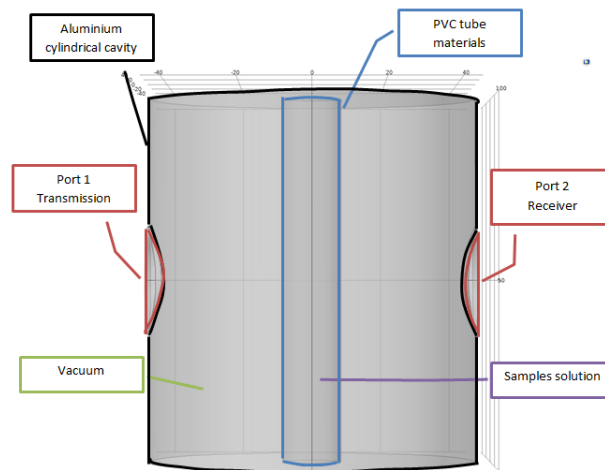


Figure 6.15: Boundary conditions for the analysed model.

6.5.6 Numerical Procedure

In order to solve the partial differential equations governing the propagation of the electromagnetic field inside a cavity resonator, an RF simulation module in COMSOL Multiphysics was used with user defined physical properties of samples. These included properties such as relative permeability, relative permittivity, electric conductivity and temperature.

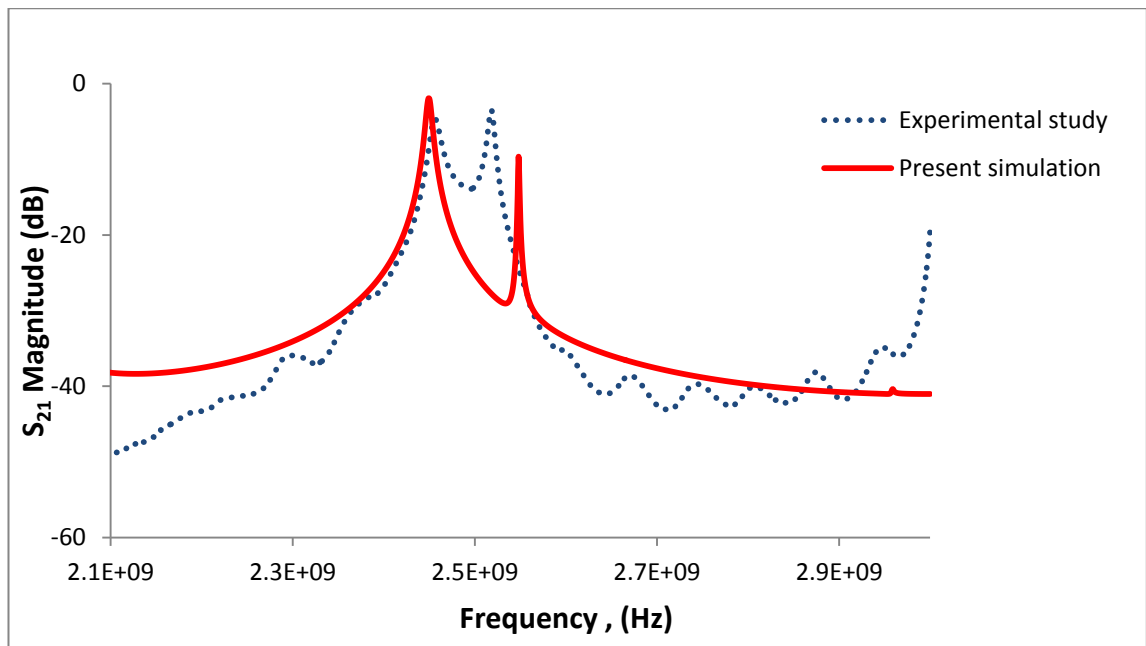


Figure 6.16: Comparison of simulated frequency spectrum data with experimental frequency spectrum data.

Figure 6.16 shows the difference of the frequency spectrum between the experimental and simulation measurements. It is clearly demonstrated that the simulated S_{21} magnitude in the empty cavity was relatively larger than the experimental S_{21} magnitude. This difference could be explained by the way the ports are modelled and the ideal simulation environments in comparison to the experimental measurements where there is a possibility of instrumentation errors during the experiment such as power dissipation in the coaxial cables, vacuum inside the cavity, etc. Based on the amount of difference in the results it can be concluded that the simulated and experimental measurements are comparable in terms of their accuracy when an electromagnetic wave is propagated inside the designed cavity.

6.5.7 Results and Discussion

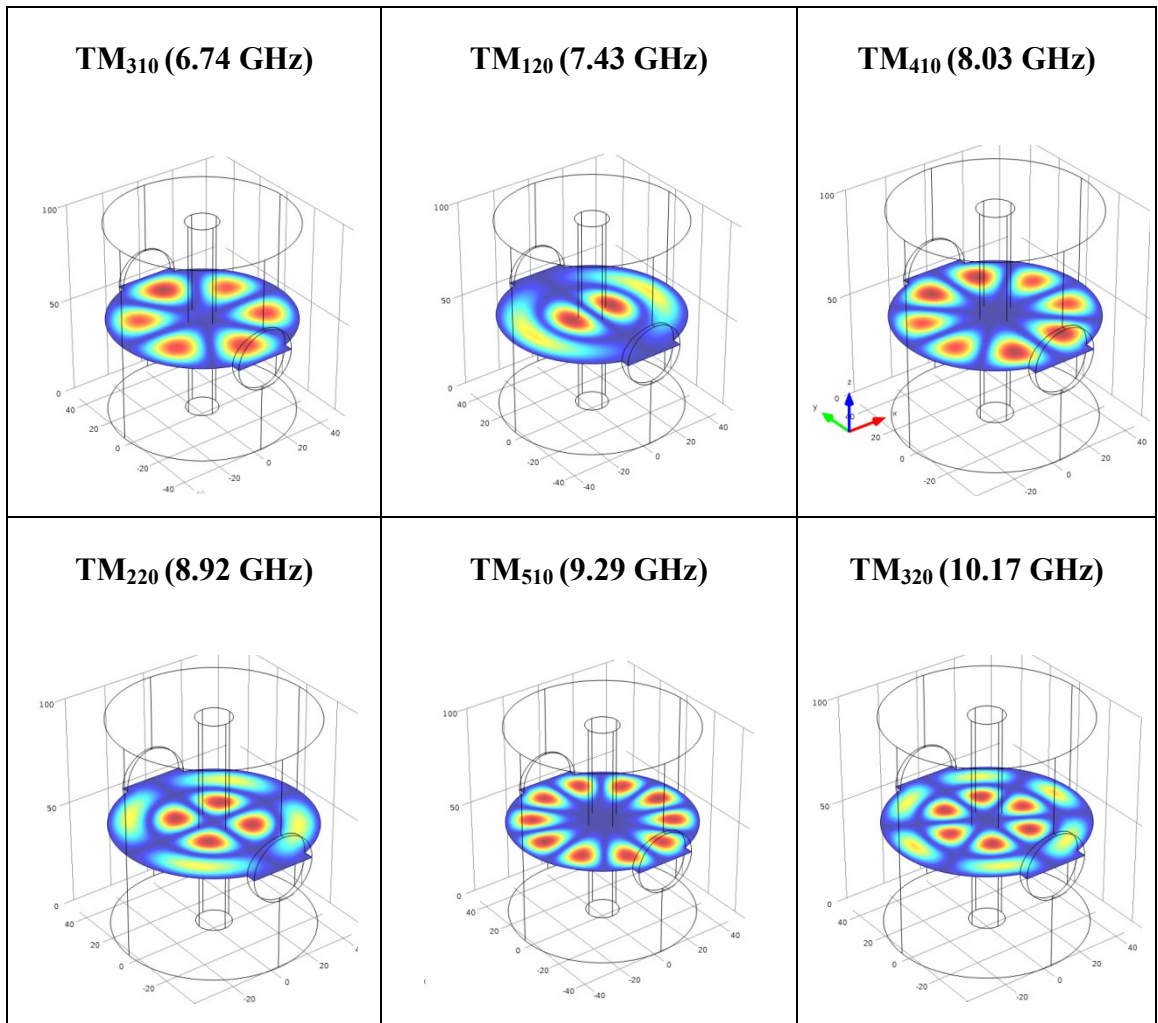
6.5.7.1 Eigen Frequency Analysis of Cylindrical Cavity Resonator

The COMSOL simulation package was used to analyse the eigen frequency inside the cavity resonator and its associated mode for the input frequency. The microwave cavity

resonator was designed such that its fundamental mode of operation (i.e. TM_{010}) occurs at approximately 2.5GHz. Fundamental mode enables the propagation of the wave strongly across the sample and yields a sensitive measurement of samples. This mode will generate a resonant peak with a quality factor (Q). A high Q indicates a sharp resonant peak that will be more readily analysed and improve the accuracy of the sensor. Table 6.7 shows the modes formed inside the cylindrical cavity and each mode's resonant frequency (in the range of 1 GHz–11 GHz approximately). These results show the homogeneous waveguide that transmits an electromagnetic wave from an input port to the output port (receiver port) at different frequencies and results in a different mode. The indicated frequency and the modes formed inside the cavity could be a good starting point to design a cylindrical cavity waveguide for a desired engineering application.

Table 6.7: Modes formed in the cylindrical cavity and their associated eigen frequencies

Mode of Operation		
TM_{010} (2.55 GHz)	TM_{110} (4.05 GHz)	TM_{210} (5.44 GHz)



6.5.7.2 Effect of the Water Hardness on the Signal Spectrum

Figure 6.17 shows the effect of the concentration of calcium hardness on the S_{21} output signal where an input microwave power of 1 mW rms (0 dBm) and the frequency range of 2.2–2.8 GHz was used. The results present a clear distinction in the amplitude of the signals with change in the sample hardness concentration. The amplitude of the spectrum for the higher concentration samples yields a relatively larger magnitude in comparison to the lower concentration. The observed phenomena can be explained as the result of the increased activity of soluble ionic compounds in the solution. The atoms absorb the EM wave and perturb it. As a result, a combination of higher quantity of different states atoms will settle into an excited state with a higher energy state. Hence, a higher absorption of energy in higher concentration solutions was observed as shown in Figure 6.17.

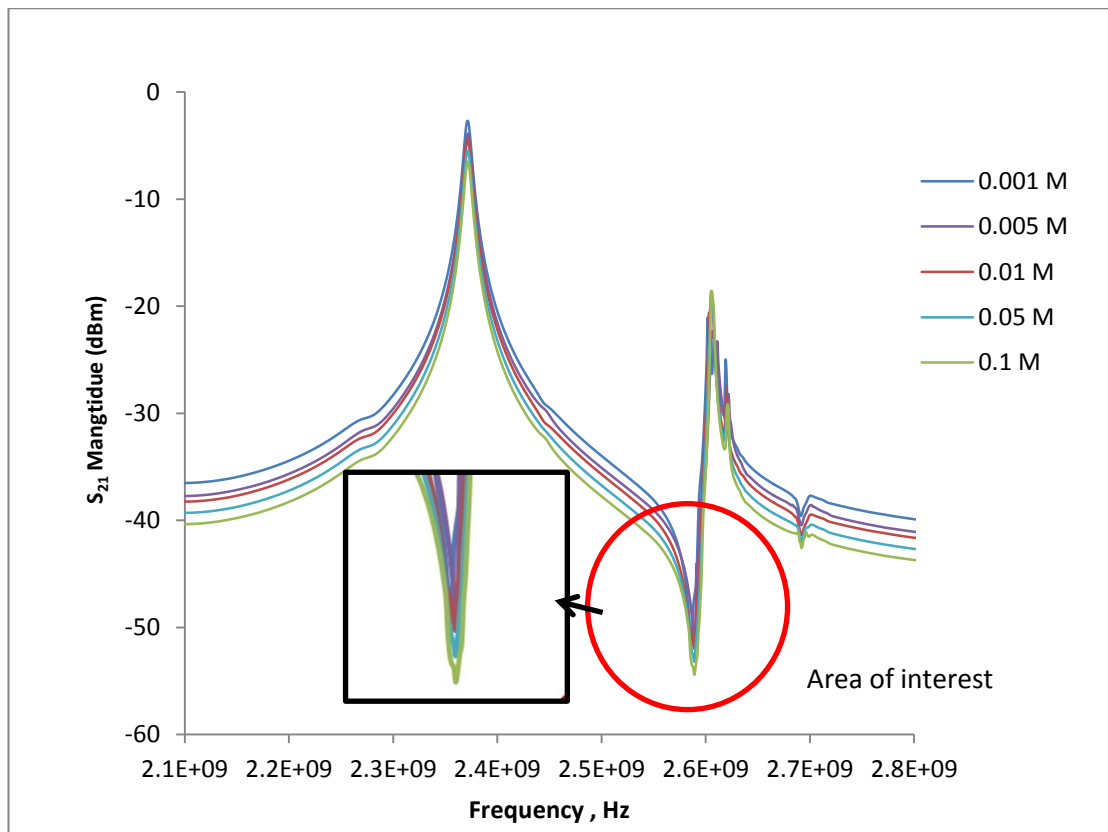


Figure 6.17: S_{21} spectrum analysis for different hardness concentrations in the solution.

6.5.7.3 Effect of Water Hardness Concentrations on the Signal Magnitude

Figure 6.18 shows the simulated and experimental results for the amplitude changes caused by different hardness concentrations in the solution. The simulated results demonstrate R-square values with respect to the change in the concentrations. It shows a good linear regression for the change in the hardness concentration in the solution. In addition, the experimental results show less than 5% error when compared to the simulated results. These results demonstrate the reliability of the simulation package to carry out Microwave based design activities & research. Overall, the simulated results shown are relatively higher than the experimental results; it is believed that the ideal condition which includes the power input, power loss and vacuum condition results in slightly different experimental results and simulation results.

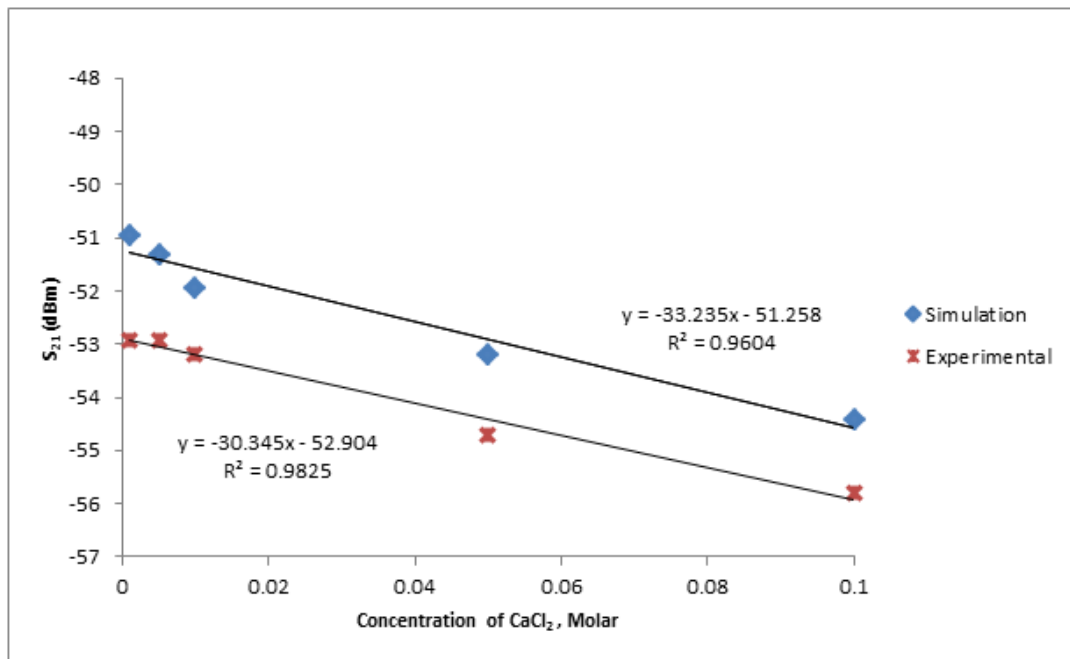


Figure 6.18: Comparison amplitude changes of simulated and experimental results under effect of different concentration of CaCl₂.

6.6 Summary

In these experiments, a microwave cavity resonator has been successfully designed and simulations show that it's theoretical and real practical data are well validated. On the top of it, a novel non-invasive real time electromagnetic wave sensor for assessing water-hardness was taken into consideration. In summary, it is observed that an electromagnetic wave sensor acts successfully for water-hardness monitoring in industrial applications. In addition, this electromagnetic wave sensor technique could be potentially the finger print for the chemical elements which could be addressed in the future research. These incredible findings could be a good practice for real-time monitoring systems for cooling-water assessments in industrial heat exchangers.

A numerical investigation on the eigen frequency and different water hardness concentrations were successfully performed. A range of frequency from 2.2 GHz to 2.8GHz with 4000 data points and 5 different calcium concentrations were considered in this numerical study. COMSOL Multiphysics simulation packages, RF module

functions based on a finite element method and Maxwell equations model were used for simulations. The simulations setup was benchmarked against conducted experimental results. The simulated data have been evaluated and the results indicated close resemblances to the experimental results.

The fundamental mode of operation, TM_{010} , was successfully modelled at the frequency of around 2.5 GHz. This fundamental mode enables the wave propagation across the sample in the middle of the cavity and yields a sensitive measurement of samples which validate the experimental results. On the other hand, the spectrum results show a good linear regression for different calcium concentrations. In conclusion, COMSOL Multiphysics simulation package is efficient and reliable to simulate an EM wave model for the prediction of chemical compounds across a range of industries.

CHAPTER 7:
TWO PHASE FLOW HEAT TRANSFER AND FOULING EXPERIMENT
UNDER NON-BOILING CONDITION

7.1 Introduction

Single phase flow heat exchanger design and analysis has been made in understanding the underlying mechanisms of mineral fouling in single-phase flows. However, the interactive effect of two-phase flows and fouling mechanisms are poorly understood (Wibisono, 2014). Many of the industrial heat exchangers in refining and petrochemical processing operate under multiphase flow condition with varying flow regimes. There are situations where there is phase-change (condensation or vaporizing) of fluids on heat exchanger fluids (Zalba, Marín, Cabeza, & Mehling, 2003). Hence, it is of interest to investigate heat transfer and fouling under this condition.

Over the past, fouling data are generally obtained with single phase flow fouling units (Sadık Kakaç, Shah, & Aung, 1987). Such fouling data or an empirical correlation based on these data cannot be directly applied to exchangers with two-phase flows. Therefore, an effort has been made to investigate the two phase flow phenomena under piping system and fouling effect under two phase flow condition. It is believed air flow effect plays a significant role in reducing the fouling deposition on the surfaces due to the shear force generated near the boundary wall of surfaces (Febrero, Granada, Regueiro, & Míguez, 2015).

On top of that, an appropriate monitoring method plays an important role in this investigation. Numerous researchers were suggested many different experimental setups for fouling deposition research (H. Müller-Steinhagen, M. Malayeri, & A. Watkinson, 2009; Hans Müller-Steinhagen et al., 2005). The monitoring approach was well developed to monitor the overall process of industrial parameters such as water flow rate, temperature, differential pressure, etc (Sarfraz & Bach, 2016). However, due to the complexity of the fouling deposition process which involves multi parameter variations

such as multiphase flow and foulant concentration for real-time scale formation, an automated control system is yet to be designed and further improved and implemented to perform this task.

This chapter aims to describe an overview of a monitoring and automation control system in two-phase flow fouling research. Validation has been conducted to verify the reliability of the fabricated experimental test rig. The designed LabVIEW system was used to monitor and control the system which was very useful as a reference to design and fabricate an experimental system for fouling research. Furthermore, heat transfer and fouling deposition under water-air phase condition were discussed. The research output has potential to be used as a reference for future complex fouling research such as co-precipitation, tri-precipitation or complex multi-phase flow fouling research.

Following that, a detection of gas-liquid two-phase flow regimes using a non-intrusive microwave cylindrical cavity sensor has been reported by Sean. A further research was conducted by using the same microwave cylindrical cavity sensor to investigate effect of gas-liquid fraction in heat transfer performance and fouling deposition on the piping surface.

7.2 Literature Review

7.2.1 Multiphase Flow Patterns

From a practical engineering point of view, one of the major design difficulties dealing with multiphase in heat exchanger is the heat transfer rate within the flow. The complexity of this presents a new challenge in the study of multiphase flows in heat transfer rate and fouling deposition on heat exchanger surfaces. Up to date, there are very little evidence has been found associating multiphase flow into heat transfer and deposition studies (S Kakaç & Pramuanjaroenkij, 2016).

A flow pattern or flow regime is used to define a particular type of geometric distribution of the component inside the piping. Generally, the flow pattern is recognized by visual inspection. In single-phase flow, it can be classified according to the characteristic of the flow into laminar (following streamlines) or turbulent (exhibiting fluctuations and chaotic motions). Whereas for the multiphase flow is classified according to the internal phase distributions. For a two-phase mixture of gas and liquid flowing together in a channel, different internal flow geometries can occur depending on the size or orientation of the flow channel, the magnitudes of the gas and liquid flow parameters, and the relative magnitudes of these flow parameters (Gupta, Nayak, Kandar, & Nair, 2016).

In current research, focus is given on the different flow regimes for horizontal flow. The various regimes are bubble flow, plug flow, stratified flow, wavy flow, slug flow and annular flow as seen in Figure 7.1.

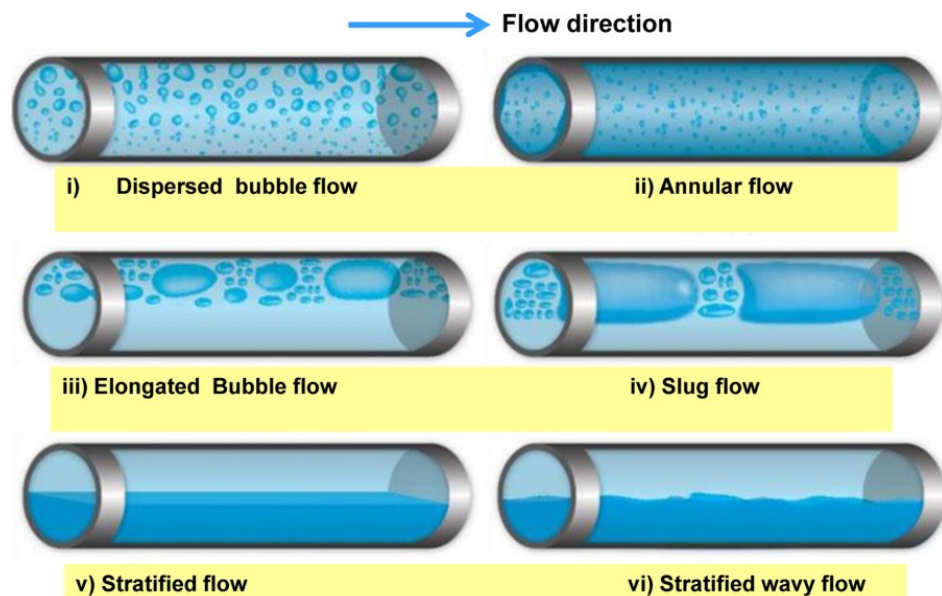


Figure 7.1: Different flow regimes for horizontal flow. (Flouros, Iatrou, Yakinthos, Cottier, & Hirschmann, 2015)

7.2.2 Detection of Two-Phase Flow Regimes

The past decade has seen the rapid development of different measurement techniques to measure the different flow regimes (Bertola, 2003). These include microwave (Ashton

et al., 1994), direct imaging by electric impedance techniques (Hervieu & Junior, 1999), gamma-rays (Nazemi, Fegghi, Roshani, Gholipour Peyvandi, & Setayeshi, 2016) and tomography process (Dyakowski, 1996), which required high skills, inaccurate and expensive. In 2012, Z. Zakaria et al. reported that magnetic induction tomography is a novel non-invasive imaging technique which was interested in mapping passive electrical properties that are conductivity, permittivity and permeability of a material (Zakaria et al., 2012). However, the error for low conductivity material measurement is limited its application. The research team at Radio Frequency & Microwave (RFM) of Liverpool John Moores University had previously attempted to use an electromagnetic wave sensor (EMW) for two-phase flow monitoring in which microwave attenuation was introduced. The technique is cost effective, robust and easy to be fabricated (C. S. Oon et al., 2016).

7.3 Description of the Experiment

7.3.1 Experimental System

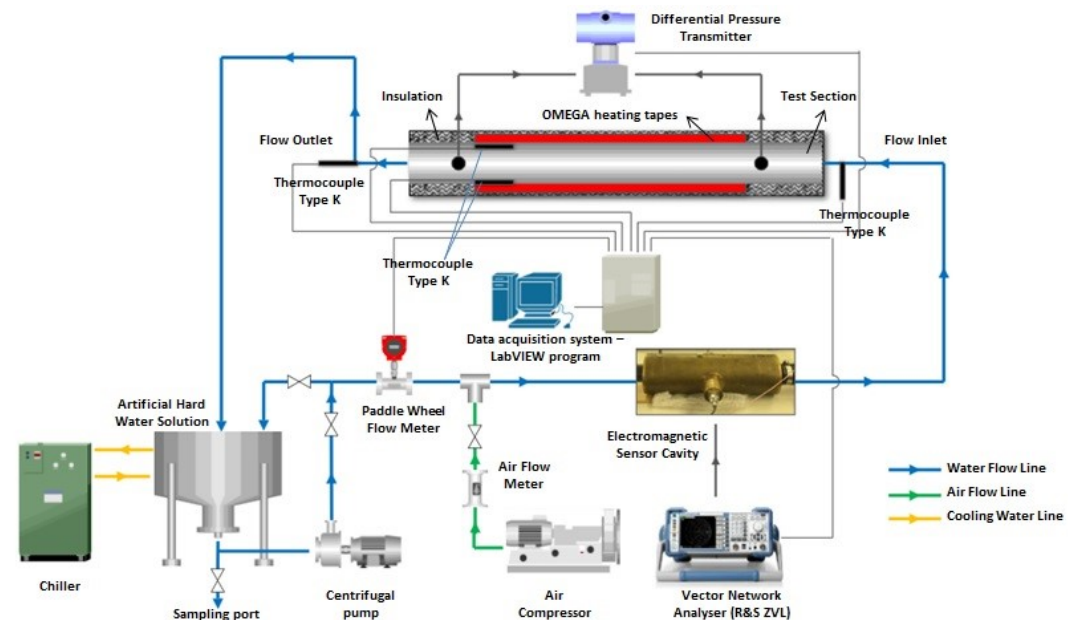


Figure 7.2: Schematic layout of two-phase flow experimental system.

The schematic layout of the experimental apparatus is presented in Figure 7.2. It consists of a water flow loop, air flow loop, heated test section, cooling section, measuring instrument, data acquisition and control units. The water flow loop includes a magnetic driven pump, a rotary flow meter, a reservoir tank, a differential pressure transmitter, microwave cavity sensor, cooling section and a test section. On the other hand, air flow loop includes a nitrogen (oxygen free) cylindrical tank, air flow meter and a regulator. The water flow and air flow were regulated at 0.1-1 m/s and 0.2-0.6 m/s respectively to achieve different flow regimes. The flow rate and pressure loss were measured using a Burkett rotary flow meter and an OMEGA differential pressure transmitter, respectively. In this experiment, a National Instruments control system was used and LabVIEW software was used for control, recording and analysis of the data. The surface temperature is maintained at 45 ± 1 °C by controlling the heater operation. On the other hand, the bulk solution is maintained at 25 °C by regulating the chiller.

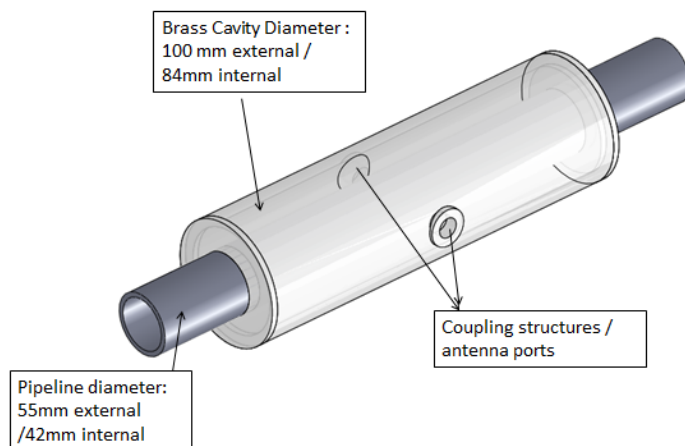
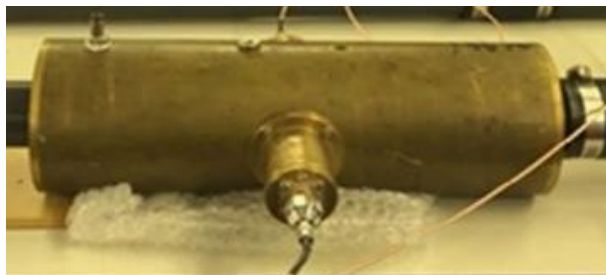
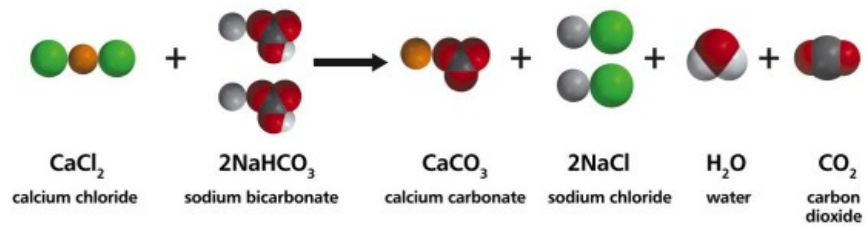


Figure 7.3: Schematic representation of the cavity sensor along with the coupling structures.

The electromagnetic wave sensor was designed and fabricated as open at both ends and larger in diameter as compared to the PVC pipe running through as seen in Figure 7.3. The main purpose of this design is to allow coupling structures to be separated from the pipeline and the flowing liquid which will advantage the non-intrusive measuring methods. The sensor's cavity was made out of brass. Being electrically conductive, the cavity was used to create the resonant modes when the microwaves were inserted into the cavity. The measurements were carried out by capturing the S_{21} parameter for each of the gas–water fractions. The data were captured to measure the percentage change in the gas–water fraction, influence of the temperature change on the measurement technique, different types of flows and influence of water hardness variation. A resonant peak was obtained representing the response of the gas–water fraction to the applied microwaves. In addition to measuring the resonant peaks, the change in the amplitude of the signal with change in the temperature, water fraction, flow type and rate was also observed. Both the resonant peaks and change in the amplitudes were used to represent the above set of measurement parameters. In addition, statistical analysis was also carried out to model the change in the S_{21} with change in the water fraction.

During the pipe flow experimental process, water was pumped from a 30 L capacity plastic tank by a (magnetic drive pump) at a flow rate of (0.1 – 1 m/s). On top of that, artificial two-phase flow condition was operated by immersing air flow inside the system by regulating the nitrogen (oxygen free) cylindrical tank. The main reasons of the nitrogen (oxygen free) being selected is to generate desired bubble flow to investigate the air velocity on fouling mitigation. A heat transfer research was further extended by using artificial hard water for fouling research under two phase condition. In fouling research, artificial hard water was prepared by mixing calcium chloride and sodium bicarbonate as seen in Equation 7.1.

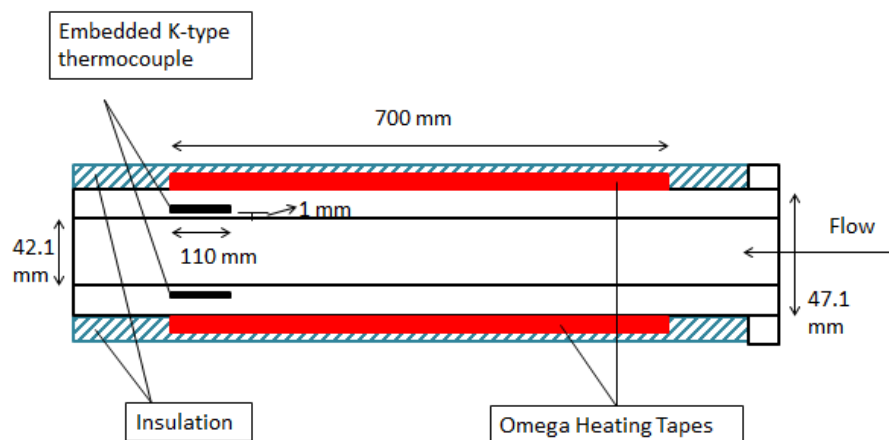


(7.1)

The LabVIEW program is designed and implemented for data acquisition and control. Fouling experiments is a long-term continuous process for the deposition formation. In order to improving the accuracy of the fouling research, a controlled environment is crucial for fouling research such as the temperature difference between the heating wall and the solution, calcium carbonate concentration, velocity, etc. LabVIEW software was successfully designed for controlling constant heat flux on heating wall surface, allowable tolerance for calcium carbonate concentration and velocity. In addition, analysis of heat transfer data, velocity, pressure drop and transmitted signal data were collecting by the designed data acquisition system (Appendix B).

7.3.2 Heat Transfer Test Section

The heat transfer test section was designed and constructed at the Liverpool John Moores University. Figure 8.4 illustrates the sectional view of the experimental test section.



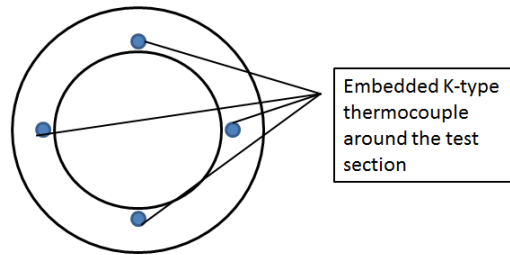


Figure 7.4: Sectional view of the experimental test section.

The heat transfer test section is a 700 mm length of 42.1 mm internal diameter with 2.5 mm thickness mild steel. Four grooves were cut along the section that was to be heated starting from the discharge end of the heated section and proceeding up to 110 mm inside along the section. These longitudinal grooves were used to house the thermocouples.

The grooves were cut as deep as possible while ensuring that the inside surface of the pipe was not disturbed. The distance between groove surface and inner surface of the tube was maintained at 1 mm. Then to keep the thermocouple in location four stainless steel 1.5 mm diameter thermo-wells were installed. Stainless-steel capillary tube thermo-wells were laid in the grooves downstream from the heated section with one end exiting outside the pipe wall. The grooves were filled with (ASTM B32-58T-50A) solder to fix the thermo-wells in location and to reduce the contact resistance.

Four 0.5 mm diameter Omega type-K sub-miniature thermocouples were inserted up to the end of the capillary tubes to obtain the wall temperature at a point approximately 110 mm from the discharge end of the heated section. Two sets of pressure tapings, one across the before the heating test section and the other after the heater at downstream return line, are connected to OMEGA differential pressure transducers to obtain friction loss measurements.

7.3.3 Component Used

7.3.3.1 Heating Elements

A high temperature dual element heating tapes (OMEGA, UK) was used to heat up the test section as seen in Figure 7.5. It is a highly flexible heating element that provides even heat across the tape. It is reinforced with high temperature fiberglass for added strength and durability. The specification of heating elements used is tabulated in Table 7.1.



Figure 7.5: High temperature heating tapes wrapping around test section for constant heat flux (Edwards & Bindra, 2017).

Table 7.1: Specification of flexible heating element

Model No.	Size	Wattage	Volts
DHT-102060LD	25.4 mm X 1.83m	936	240

7.3.3.2 Ion-Selective Electrodes

A calcium electrode was employed to monitor the calcium carbonate concentration throughout the experiment as seen in Figure 7.6. In order to control the calcium concentration which are the main calcium carbonate ions in the fouling research, a calcium selective electrode used as a data collecting instrument to be a references for controlling the peristaltic pump to feed in chemical from time to time to maintain the concentration of the solution. Calcium selective electrodes are membrane electrodes that produce a potential by converting the activity of ions dissolved in a solution. The

potential can be measured using a pH meter or voltmeter. It will improve the precision of the fouling experiment results as concentration effect is one of the critical parameters.

The main advantage of a calcium selective electrode being selected is because of the linear response of electrode toward the concentration in ppm against mV. It has a short response time and is unaffected by colour or turbidity.



Figure 7.6: PerfectION combination calcium electrode used in our experimental set-up (Athavale et al., 2017).

7.3.3.3 Peristaltic Pump

Two peristaltic pumps as seen in Figure 7.7 were used to feed in calcium chloride and sodium bicarbonate in solution form to maintain 500 mg/l calcium carbonate concentration throughout the experiment. The peristaltic pump is controlled by the desired concentration value in which uses detected mV value as a reference. The peristaltic pumps are quick, simple to maintain, operate and control which make it drive gains in process efficiency. In addition, the feeding chemicals only come into contact with the inside of a hose or tube elements which eliminates errors in the feeding chemicals amounts.



Figure 7.7: Peristaltic pumps used to feed chemical to maintain 500mg/l calcium carbonate concentration throughout experiment.

7.3.3.4 Vector Network Analyser (VNA)

The vector network analyser, VNA (RSZVL 9 kHz – 6 GHz) shown in Figure 7.8 is a form of RF network analyser widely used for RF applications. A vector network analyser is a test system that enables the RF performance of radio frequency (RF) and microwave devices to be characterised in terms of network scattering parameters, or S parameters. The information provided by the vector network analyser VNA is then used to analyse the two-phase flow condition inside the pipe and also fouling behaviour.



Figure 7.8: VNA used to analyse the transmitted signal under effect of two-phase and fouling condition.

7.3.3.5 Data Acquisition System

The data acquisition unit used in this experiment is the interface system between LabVIEW programs with the hardware. The data acquisition unit is supported by Ni-DAQ unit which is provided by National Instruments Hardware. This module performs single-ended or differential analog inputs, with four programmable input ranges for each. It is an effective combination of channel count and speed at a reasonable price for an economical multifunction system. Figure 7.9 illustrates the NI-9205 (analog input/output module for pressure transducer), NI-9211 (thermocouple transducer) and NI-9401 (digital input/output for heater) were used for the experimental setup.

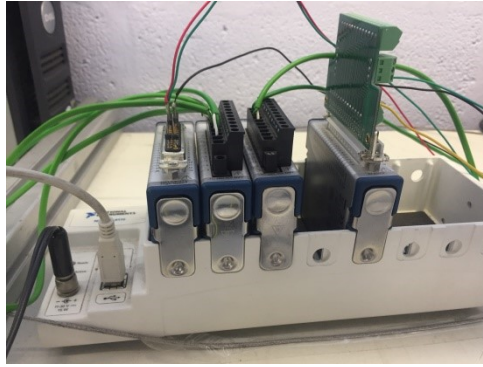


Figure 7.9: Ni hardware for LabVIEW program.

7.3.3.6 Data Collecting

LabVIEW is programmed to collecting all the experimental data for further analysis. In this research, temperature values from all the thermocouples, differential pressure, water flow velocity, concentration and EMW transmitted signal data are crucial for accurate heat transfer and fouling analysis. Hence, data collecting for analysis is set for every 1.5 ± 1 s throughout the experiment. The LabVIEW interface for data collection can be seen in Appendix B.

7.3.3.7 Automation Heater Control

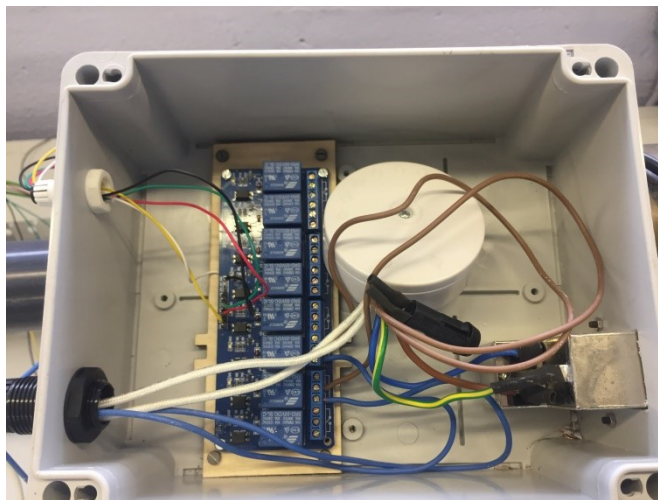


Figure 7.10: Control panel for constant wall temperature control.

A control panel associated with the LabVIEW program is designed and fabricated to control the heater operation as seen in Figure 7.10. A reference of average surface

temperature measured by K-type thermocouples imbedded on the test section surface is pre-set at 45 ± 1 °C for the control. The temperature range was set between 44.5 °C – 45.5 °C for the error tolerance. Figure shows the control panel unit used for the heater control.

7.3.3.8 Automation Concentration Control

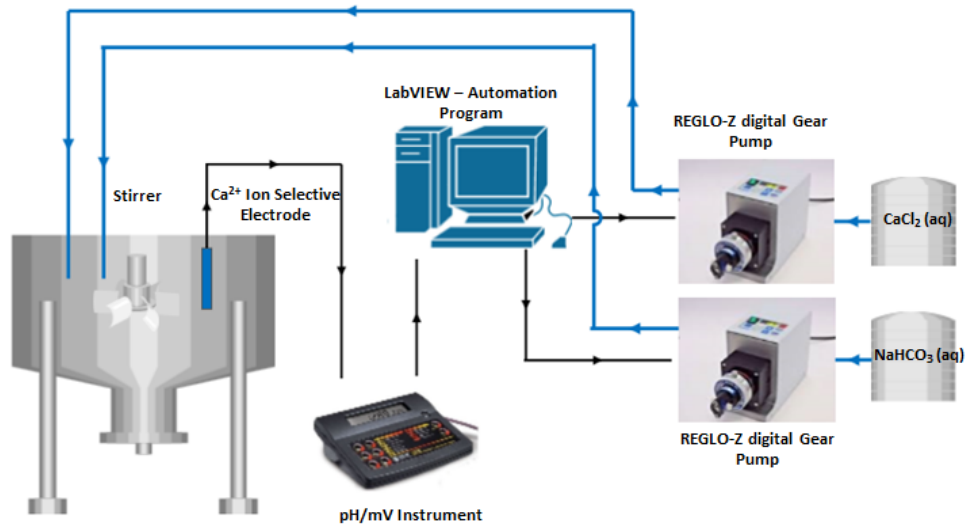


Figure 7.11: Automation chemicals dosing system

As can be seen from the Figure 7.11, an automation program was designed and fabricated to maintain the foulant concentration at 500 ± 10 mg/l to enhance the accuracy of fouling research. A Ca^{2+} Ion selective electrode was used to measure the concentration throughout the experiment. The ISE transmit millivolt signal which can be correlated with calcium concentration. The calibration and validation can see in Appendix B. At 500 mg/l, ISE transmits a signal of -15 ± 1 mV. The signal is sent to the LabVIEW program as a control reference. When the signal is below -15 mV, the pumps will activate to feed in CaCl_2 and NaHCO_3 in aqueous form and stop when the signal is above -15 mV. The feeding chemicals are prepared in solution form to ensure the homogeneity of the mixed solution.

7.4 Results and Discussion

7.4.1 Test Rig Validation

Figure 7.12 shows the validation of current experimental data with the standard equation such as Gneski, Dittus and boelter, Mangai and Pak and Choy for turbulent flow. Prior to carrying out the set of detailed experiments on the two-phase flow heat transfer, a set of initial experiments were performed for water as the base fluids, in order to assess the accuracy and reliability of the experimental setup. The experimental results for DW at constant heat flux conditions were compared with the results from the standard equations. The empirical correlations of Gnielinsky, Mangai, pak&choy and DittuseBoelter were selected for comparison with the obtained results especially for testing the accuracy of the setup in the turbulent region. The experimental data and classical correlations agree well. Data from the Gnielinski equation and the experimental data for distilled water are better than the data from other equations and validate the accuracy of the experimental setup with an error rate of less than 10%.

Figure 7.13 illustrates the experimental friction factor comparison with standard correlation from the measurements of the pressure drop along the length of the test section. To verify the friction factor data, the experimental results for DW are validated by the Blasius equation, the Power law and Petukhov correlation. Among all equations Power law showed the more accuracy with DW data. The Power law equation is the most simple equation for solving the Darcy friction factor. Because the Power law Equation (has no term for pipe roughness, it is valid only to smooth pipes). However, the Blasius equation is sometimes used in rough pipe because of its simplicity. The Power law Equation is valid up to the Reynolds number 10^5 .

$$f = 0.184RE^{0.2}$$

The validation of the friction loss data from the experimental investigation has an error rate of less than 10%.

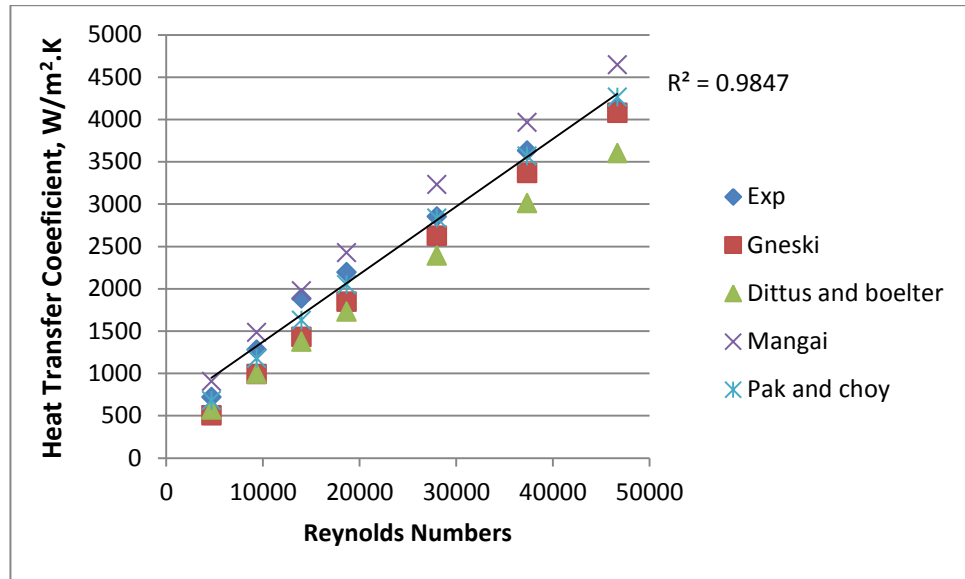


Figure 7.12: Validation of heat transfer coefficient with available literature review.

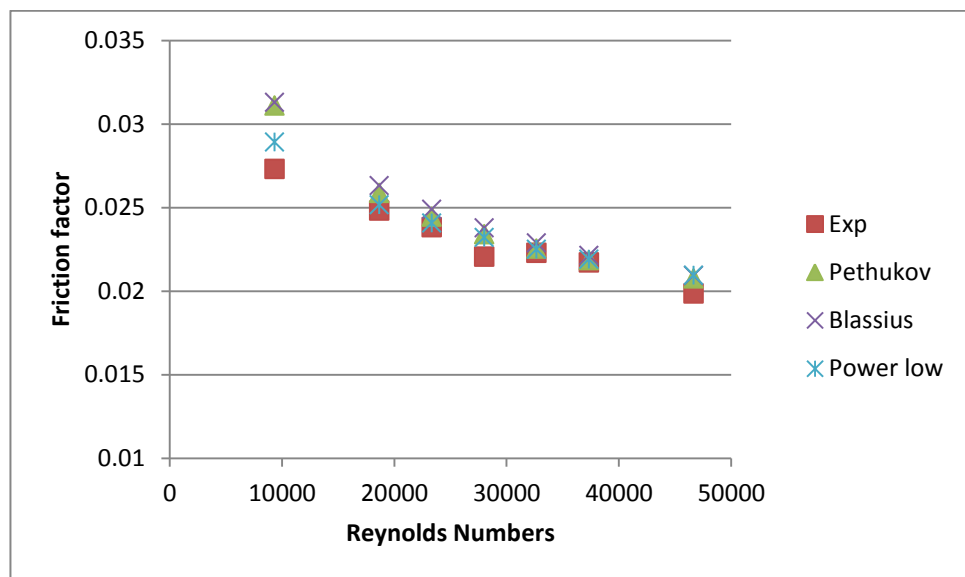


Figure 7.13: Validation of friction factor with available literature review.

7.4.2 Two-Phase Flow Experiment

7.4.2.1 Repetitive Results – Full Pipe Water Run (1-6 GHz)

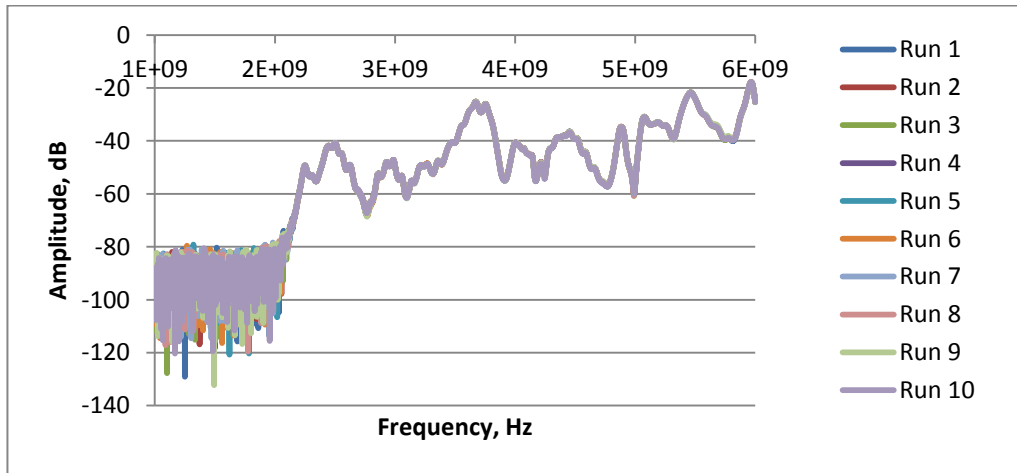


Figure 7.14: Repetitive for single phase flow by using EMW sensor.

Figure 7.14 provides the results obtained from the repeat experiment under single phase flow condition. There is a very good reproducibility of the signal spectrum from 2 GHz onward. It is believed due to the design constraints of the sensor cavity, the signal below 2 GHz contains strong interfering frequency component and contributed a strong noise.

7.4.2.2 Different Water Fractions

7.4.2.2.1 (Water & Air) (1-6 GHz) – Identify for Detection Region

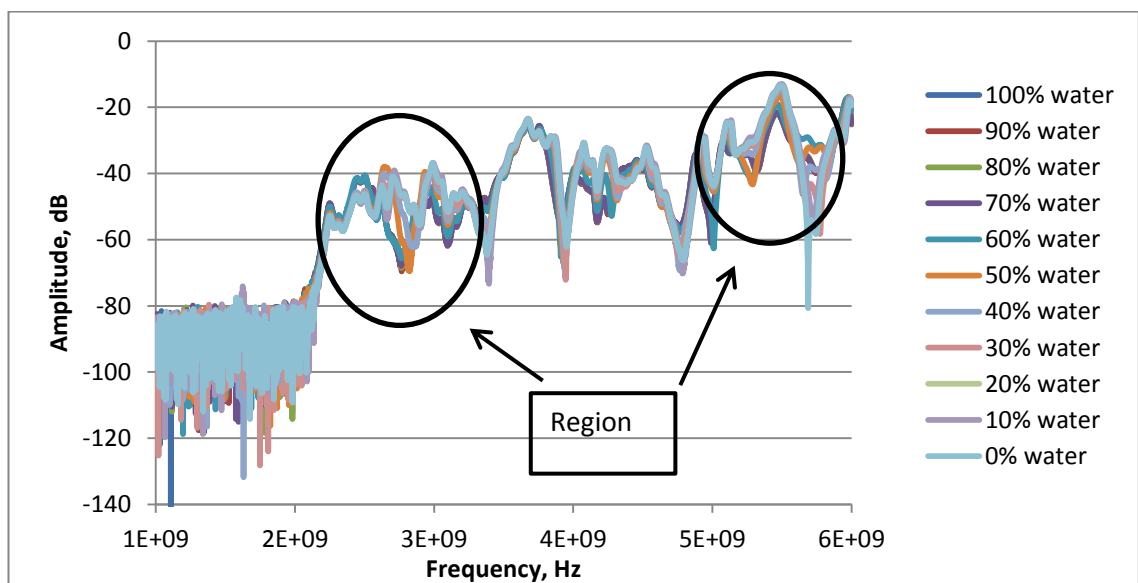


Figure 7.15: S₂₁ signal spectrum for different water fractions from 1-6 GHz in 4000 points

7.4.2.2.2 (Water & Air) (2-3 GHz)

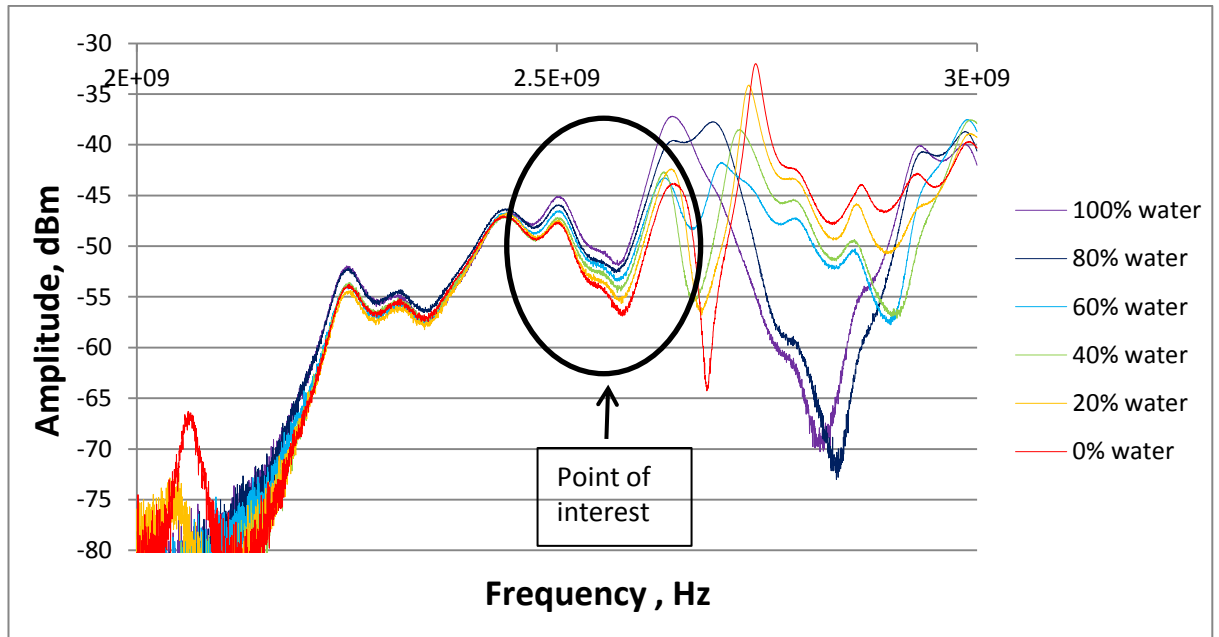


Figure 7.16: S_{21} signal spectrum for different water fractions from 2-3 GHz in 4000 points

7.4.2.2.3 (Water & Air) (4-6GHz)

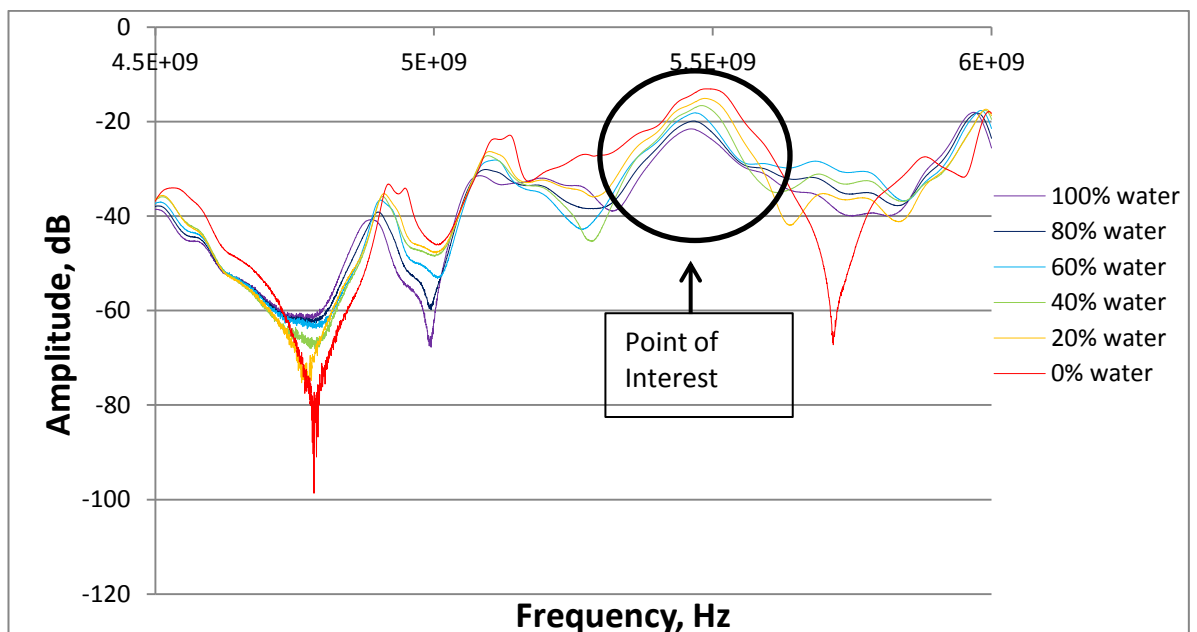


Figure 7.17: S_{21} signal spectrum for different water fractions from 4.5 - 6 GHz in 4000 points.

As seen from Figure 7.15, different water fractions were monitored from 1-6 GHz in 4000 data points. There are two areas showing significant changes which are good to identify different water fractions. In order to improve accuracy for the sensible spectrum for different water fractions, the frequency range was focused on 2-3 GHz and 4.5-6 GHz as seen in Figure 7.16 and Figure 7.17 respectively.

7.4.2.3 Temperature Effect

7.4.2.3.1 (Water & Air) (2-3 GHz)

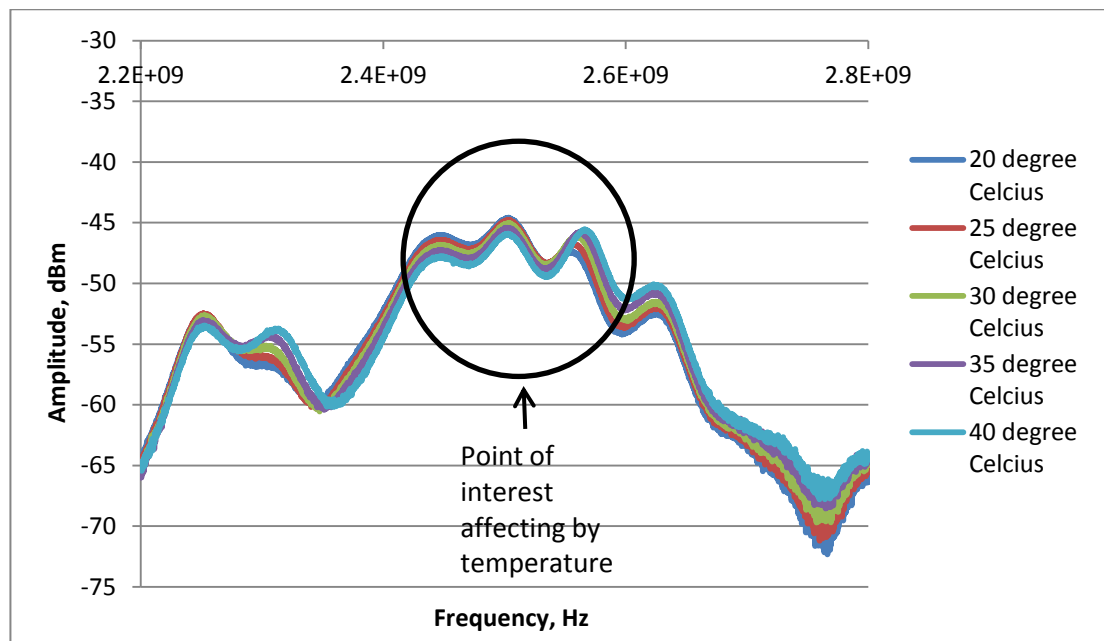


Figure 7.18: S_{21} spectrum signal under effect of temperature from 2.2 – 2.8 GHz

7.4.2.3.2 (Water & air) (5-6 GHz)

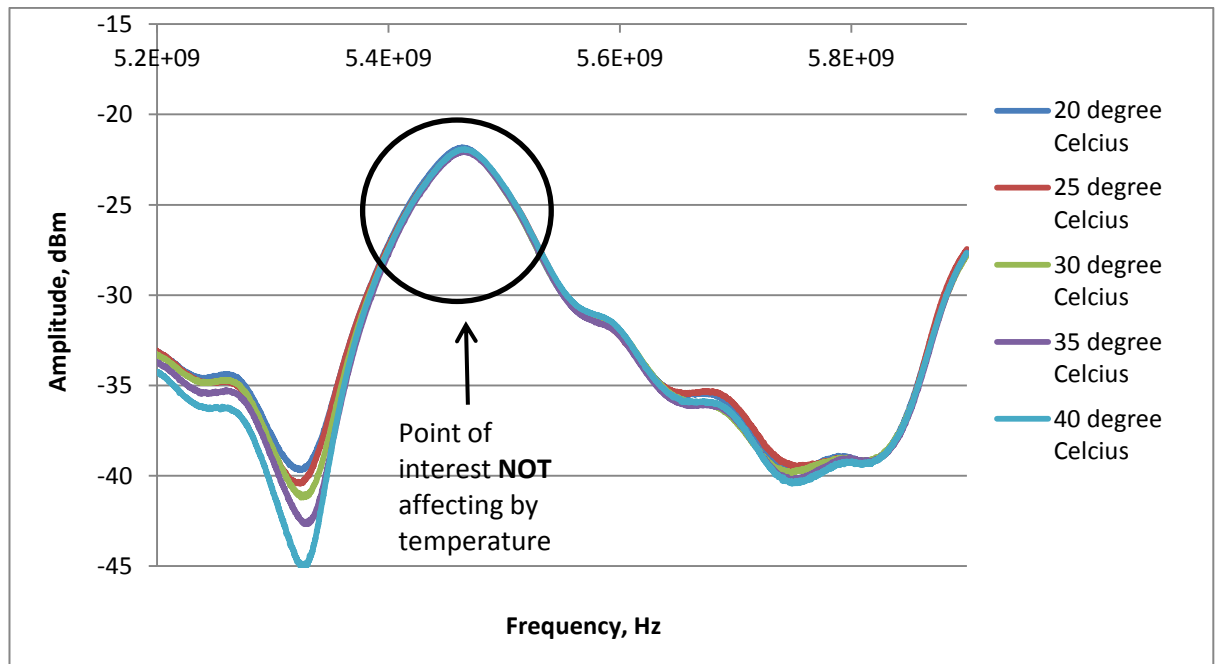


Figure 7.19: S_{21} spectrum signal under effect of temperature from 5.2-5.9 GHz.

From the Figure 7.18, the signal spectrum is affected by temperature variation at 2.55 GHz. This is unsurprisingly because the nature of electromagnetic wave is affected by temperature, particularly in 2.55 GHz which is the fundamental mode, TM_{010} . Interestingly, the results of the Figure 7.19 show there are no changes on signal spectrum at frequency range of 5.45 GHz for different temperatures. A possible explanation for this might be due to the different overlapping modes such as TE_{414} and TM_{023} negating the temperature effect, as in adjacent frequency ranges (Cheen Sean Oon et al., 2016). These results further support the idea of detecting chemical elements regardless of temperature. Further research should be undertaken to investigate the design of a microwave sensor unaffected by temperature.

The results of the correlations analysis of water fractions with amplitude are shown in Figure 7.20. It shows a very good linear regression. These findings suggest that EMW could have great potential as a sensing instrument in two-phase flow application.

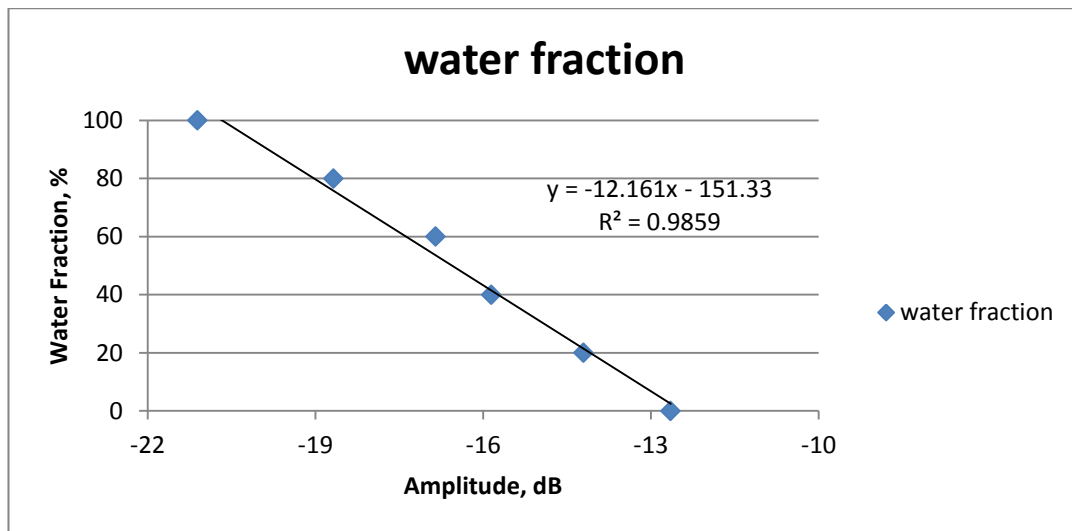


Figure 7.20: Statistical analysis results for different water fraction at 5.45 GHz.

7.4.3 Two-Phase Flow System with Different Regimes

In the present research, 3 different flow regimes were illustrated by maintaining the water velocity at 0.2 m/s constant and varying air velocity from 0.1 – 0.3 m/s. These flow regimes are plug flow, semi-slug flow and slug flow as seen in Figure 7.21. The change of amplitude was recorded every 1.2 s and the changes of the percentage of water inside the pipe were observed. Figure 7.22 shows the maximum and minimum level of water flowing inside the pipe over time. The amplitude oscillated is observed to be approximately 80-100 % indicating the plug flow. Figure 7.23 and Figure 7.24 show the semi-slug and slug flow respectively.

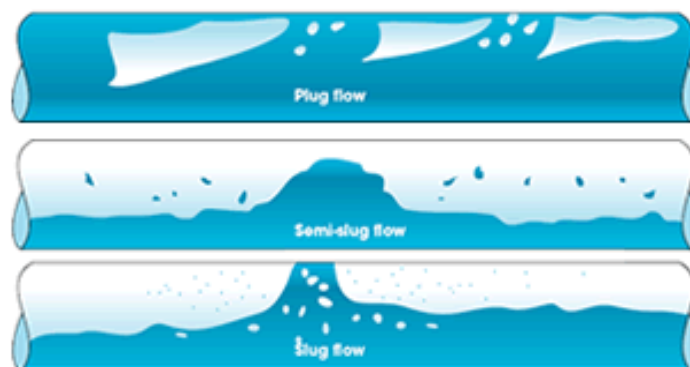


Figure 7.21: 3 different flow regimes of plug, semi-slug and slug flow.

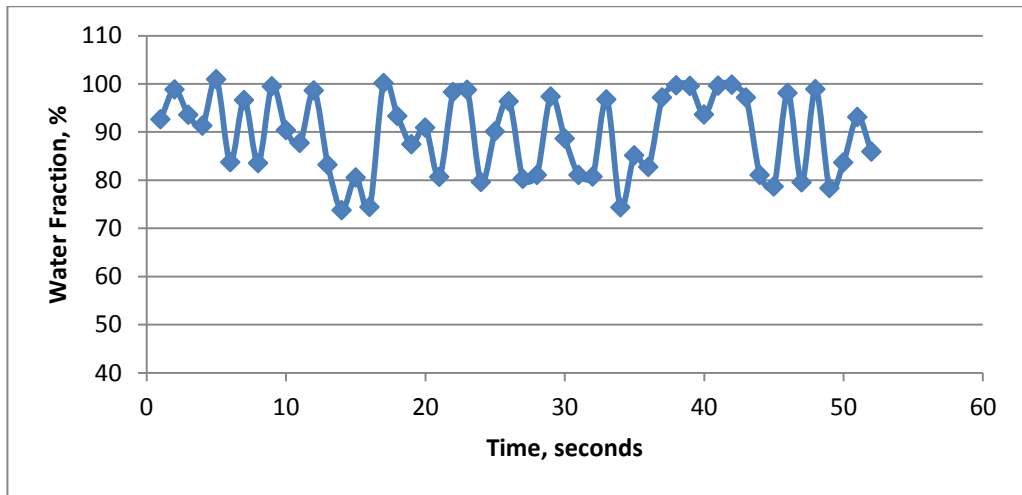


Figure 7.22: S_{21} signal under effect of 0.2 m/s water velocity and 0.1 m/s air velocity (Plug Flow)

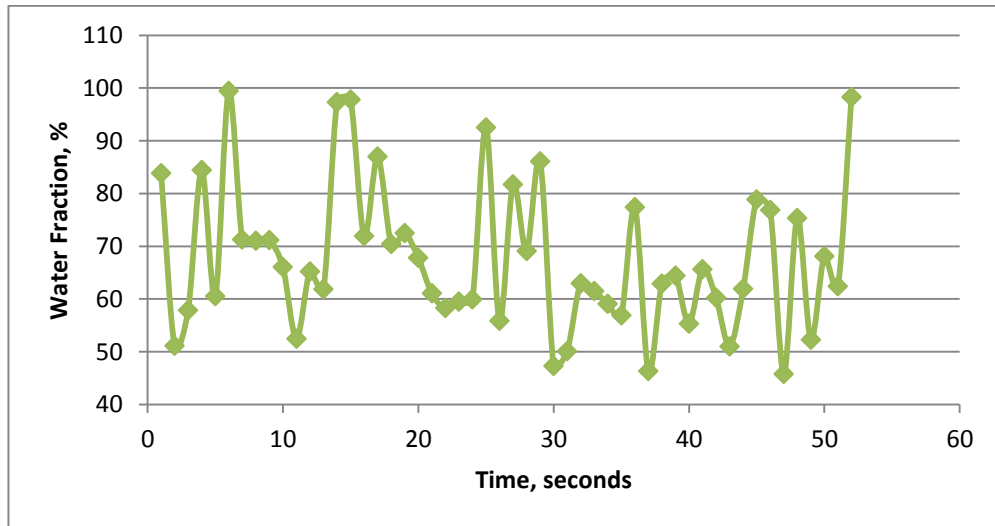


Figure 7.23: S_{21} signal under effect of 0.2 m/s water velocity and 0.2 m/s air velocity (Semi-Slug Flow)

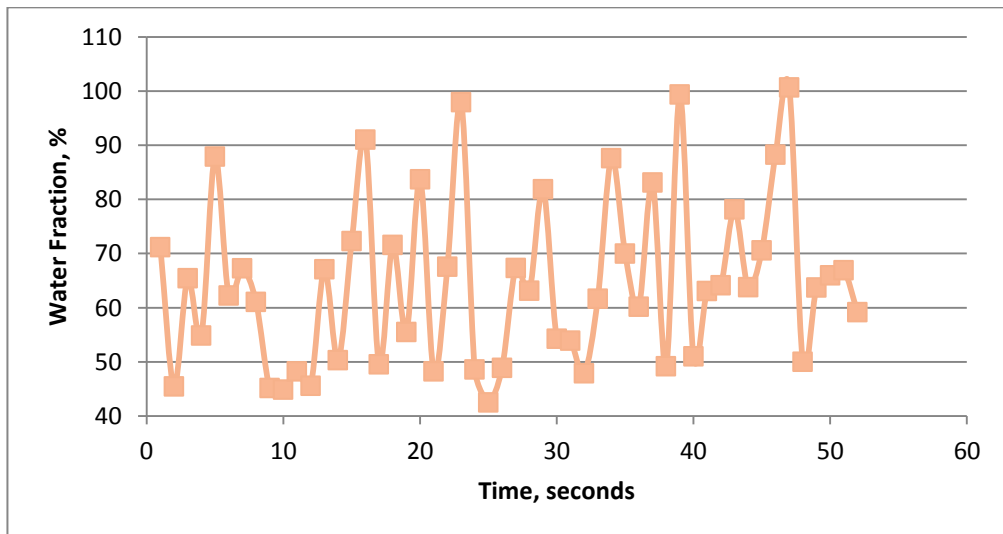


Figure 7.24: S_{21} signal under effect of 0.2 m/s water velocity and 0.3 m/s air velocity (Slug Flow)

7.5 Two Phase Flow Heat Transfer

7.5.1 Constant Average Wall Temperature of 45 °C and 0.2 m/s Water Velocity

The present research is further developed by examining the heat transfer performance under different flow regimes. The distribution of vapour in a constant heat flux system affects both the heat transfer and the flow properties of the fluid. A number of flow pattern or “flow regimes” have been observed experimentally by viewing flow or liquid-vapour mixtures through transparent tubes. Three different flow patterns were successfully created by varying the input of air flow velocity by maintaining the water flow velocity. Two-phase flow heat transfer was conducted to examine the flow regime effect on the heat transfer coefficient by maintaining the constant heat flux across the test section.

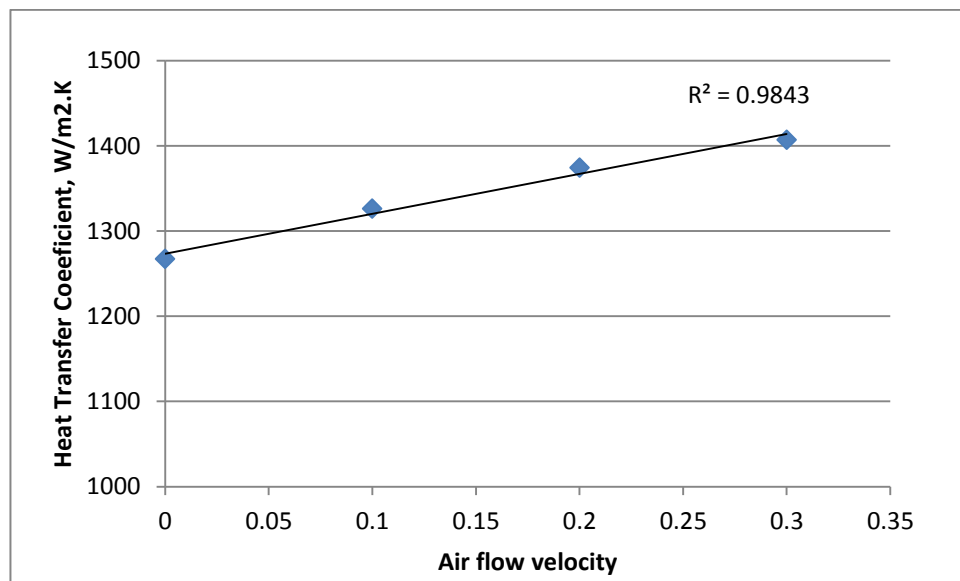


Figure 7.25: Overall Heat Transfer Coefficient against air flow velocity curve.

As clearly seen in Figure 7.25, the heat transfer coefficient is increased linearly with the air flow velocity. At air flow velocity equal to zero, there is no bubble formation within the flowing line. The heat transfer is by single-phase forced convection and is a strong function of fluid velocity (mass flux) and temperature. When air flow is introduced to

the flowing line, bubbles gaps begin forming across the flowing line and are generally associated with pits or crevices on the heated surface. As a result the bubbles grow and depart the surface they carry the heat, as well as generating increased turbulence and mixing which increase the overall heat transfer rate. Similar results were reported by Afshin Ghajar and Clement C. Tang has been conducted an intensive research in non-boiling heat transfer to two-phase flow in pipes (Ghajar & Tang, 2009).

7.6 Two-Phase Flow Fouling

7.6.1 Fouling Resistance and Total Deposition

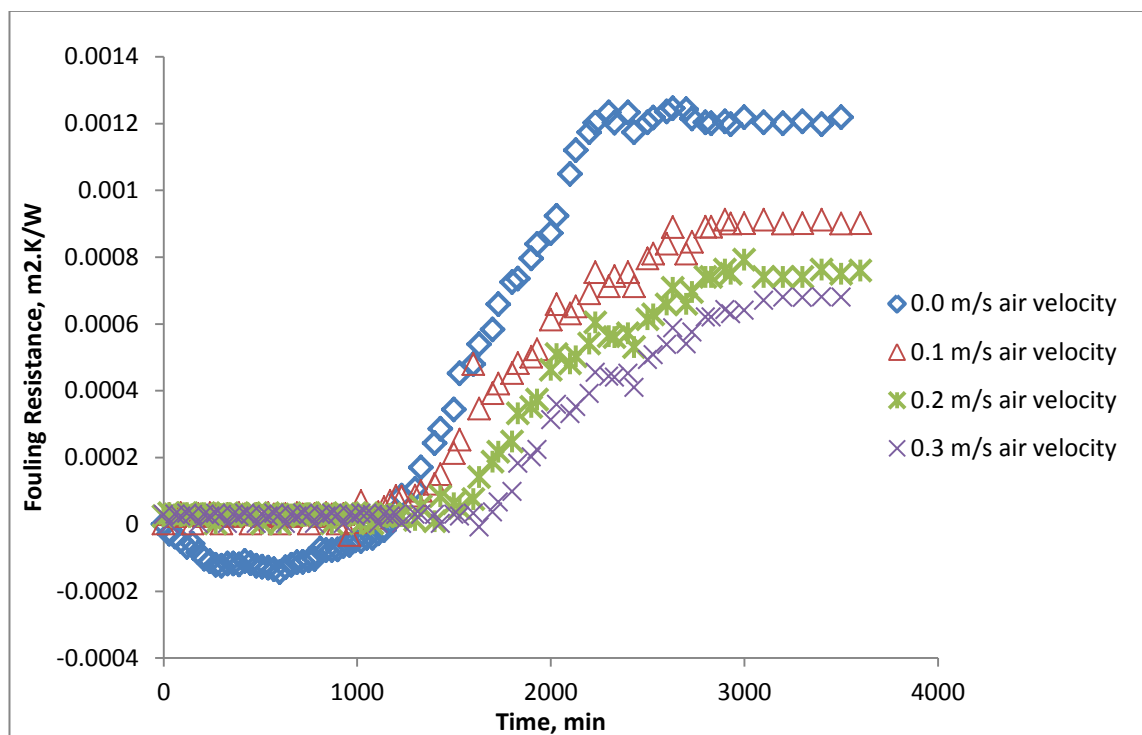


Figure 7.26: Fouling resistance as the function of time based on different air velocity input at constant $\Delta T = 15\text{ }^{\circ}\text{C}$, 0.2 m/s water flow and 500 mg/l concentration.

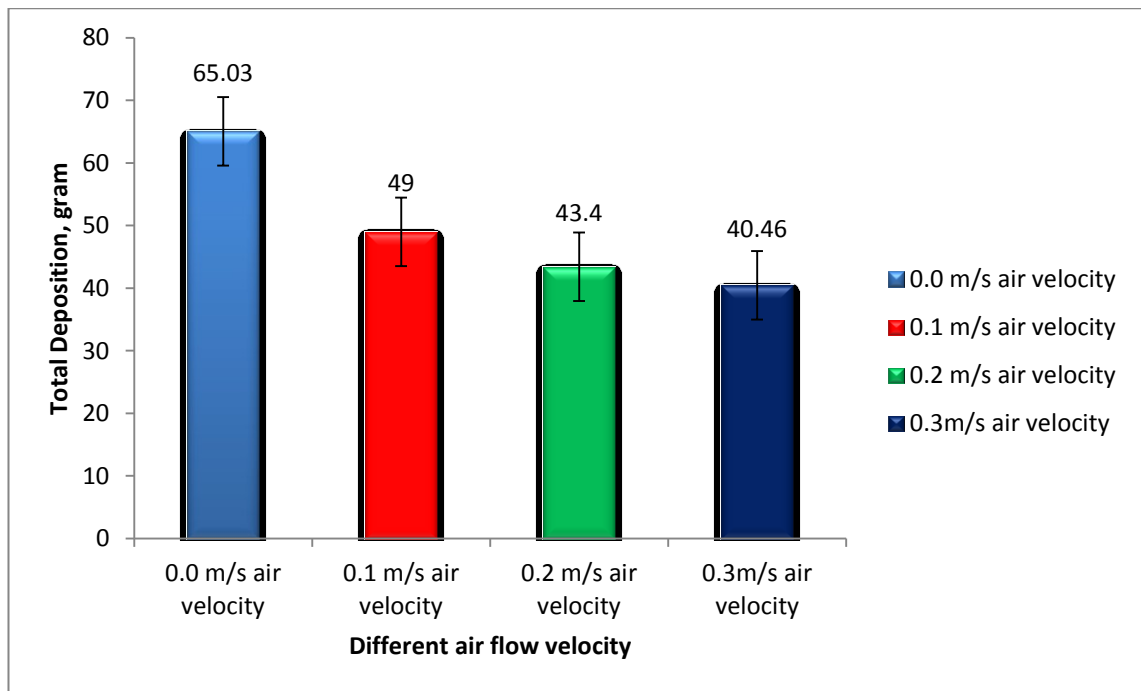


Figure 7.27: Total deposition on test section surface under effect of air velocity input, at constant $\Delta T = 15\text{ }^{\circ}\text{C}$, 0.2 m/s water flow and 500 mg/l concentration.

Figure 7.26 illustrates the fouling resistance curve under effect of different air flow velocity input. It is clearly seen that the induction period increases as the air velocity increases. The induction periods were observed at about 1020 min and 1600 min for 0 air velocity and 0.3 m/s air velocity respectively. It is believed due to the shear force generated by air velocity is great enough to prevent the nucleation near the heat transfer surface. In nature, once the stable crystal nucleation takes place, the accumulation is slowly spreads out laterally until it completely covers the heat transfer surface with scale deposition. In the present study, these phenomena could be observed by the step increase in fouling resistance after 1100 min. It is due to the vast number of calcium and bicarbonates ions in bulk water, it reacted quickly to hot heat transfer surface, indicating that CaCO_3 precipitates and continuously adheres to the heat transfer surface. As observed in 0 air velocity case, the fouling resistance gradually reaches an asymptotic level about 2320 min. On the other hand, as observed in 0.3 m/s air velocity case, it observed the asymptotic level about 3200 min, suggesting that shear force of air flow

significantly removes the particle fouling in which represent the net results of the fouling. In addition, the asymptotic fouling resistance value decreases as the air velocity increases.

On the other hand, Figure 7.27 shows the amount of CaCO_3 deposited on the heat transfer surface at different air velocities. It showed that the amount of deposition is reduced when air velocity is increased from 0 m/s to 0.3 m/s. This is because at higher air velocity, the shear force near the boundary resulting higher removal rate.

7.6.2 Visualization of Fouled Test Section



Figure 7.28: Deposition on test section surface under effect of air velocity input [(a) clean pipe surface, (b) 0.0 m/s air velocity & (c) 0.3 m/s air velocity], at constant $\Delta T = 15^\circ\text{C}$, 0.2 m/s water flow and 500 mg/l concentration .

Figure 7.28 shows general photographs of fouling deposition on the mild steel pipe heat transfer surface at CaCO_3 concentration of 500 mg/l at clean pipe, 0 m/s air velocity and 0.3 m/s air velocity respectively. Figure 7.28 (c) show less deposition on top surface in comparison to Figure 7.28 (b). It is believed that due to the air velocity at the input promoting the slug flow phenomena which contributing higher shear force and turbulence at top of the heat transfer surface. In addition, the deposits show similar form as in general visualization. Unfortunately, characterization of deposited CaCO_3 was not conducted in this case due to the deposition in middle of the inner pipe surfaces.

7.7 Summary

This chapter explored the application of electromagnetic wave sensor for two phase flow detection. Furthermore, the introduction of small air flow rate into the water flow resulted an increase of the heat transfer coefficient up to 5-8 %. Moreover, input of small air flow potential to retard mineral fouling on heat transfer piping system. Even though the rate of heat transfer is improved as small amount of input air flow into the heat transfer system, the bubbles' movement critical to be investigate in future research, which may significantly reduce the localize heat transfer performance and increase pressure drop. It is suggested to find the optimum flow pattern to be used in non-boiling heat transfer in industrial use which will enhance the overall performance as well as retard the fouling deposition.

CHAPTER 8: CONCLUSIONS AND RECOMMENDATION

An experimental test rig was designed and fabricated to conduct fouling and fouling mitigation research. This research work focused on calcium carbonate (CaCO_3) fouling and fouling mitigation by catalytic materials and green additives. In current research, investigation of mineral (CaCO_3) fouling on heated pipe surfaces shows augmentation of fouling with an increase in the concentration of fouling ingredients in solution, a lowering of flow velocity, and an increase in surface to bulk temperature difference. In the mentioned all cases augmentation of the fouling resistance occurred due to the enhanced driving force for mass transfer. Implementation of catalytic material composed of zinc and tourmaline causes a reduction in the rate of growth of the fouling deposit. Catalytic material modifies the onset of deposition by transforming the calcium carbonate deposition from calcite form into aragonite form. Calcite is reported to be the most thermodynamically stable phase at room temperature and under normal atmospheric pressure. Under non-PWT cases, a metastable calcite form of deposit was observed on the metal surfaces of approximately 15 μm size. In comparison to the PWT-treatment case, the deposited calcium carbonate appears in aragonite form which is often reported to be the first phase to precipitate out of solution. The crystal structure size of the deposited calcium carbonate in aragonite form (about 2 μm) on the hot transfer surface is significantly smaller compared to the non-PWT case.

In addition, fouling on different metal surfaces and its mitigation with EDTA, MWCNT-EDTA and MWCNT-DTPA have been systematically conducted in the present research scope. The fouling deposition increases with the increase of thermal conductivity of the material. The sequence of deposition is copper > aluminium > carbon steel > brass > stainless steel. Fouling deposition on a substrate increases with increasing roughness and enhances initial deposition by providing a site for more crystal

nucleation. The increasing of deposition rate on a metal surface also increases the size of crystals accumulated in the scale. The addition of EDTA, MWCNT-EDTA and MWCNT-DTPA are promising to alter the crystal structure and retard the rate of crystal growth.

Moreover, a non-invasive-monitoring of the concentration of calcium hardness in heat exchanger cooling water is successfully demonstrated. The electromagnetic wave sensor technique could be potentially the finger print for the chemical elements which could be addressed in future research. These findings could be a good practice for real-time monitoring systems for cooling-water assessments in industrial heat exchangers.

Highlights of the present research outcome emerge with an approach in designing systems and heat exchangers with enhanced performance and diminished adverse environmental consequences. A benign means of industrial mineral fouling mitigation technique is presented as an alternative to conventional fouling mitigation strategies.

Recommendations for Future Work

The present works have highlighted several new insights toward pursuing fouling mitigation techniques which are benign to environment and new technology for fouling monitoring. The knowledge acquired in the study particularly on crystal morphology of fouling particles, and chemical and morphological structure of synthesis of nanofluids for fouling mitigation, would become a good platform for devising a better strategy to achieve much higher mitigating ability. At present, there is a significant discrepancy in fouling resistance data under the effect of different mitigation approaches. For the practical application, these discrepancies should be eliminated by systematically investigating the effect of some parameters such as mitigating fouling which is composed of a combination of calcium carbonate, calcium sulphate, silicate etc. in

nature. In line with practical applications in industry, future research work should include the followings:

- 1.) Fouling deposition is uneven due to the nature of the phenomenon. It is because of fouling deposition is a very complex and inconsistent process. The fouling deposition varies based on the surface roughness, concentration, temperature difference, etc. So, it will develop more deposition at the beginning of the foulant solution process due to the high concentration and temperature difference. In addition, higher temperature difference will yield higher deposition. Once the nucleation starts, it will transport and accumulate toward that particular spot. Hence, it creates an uneven deposition thickness throughout the test section. Details of the study of the point corresponding to the onset of heat transfer reduction in fouling are recommended in future research.
- 2.) Extended study of fouling deposition mechanism of different salts such as $\text{Ca}_3(\text{PO}_4)_2$, CaSiO_3 , MgSiO_3 , MgCO_3 , etc. and combinations and their mitigation by adding green additives would provide new insights and help combat fouling deposition in practical situations in industry.
- 3.) The effect of fouling mitigation could be studied on non-metal surfaces in a manner similar to metal surfaces by adding green additives to the aqueous fouling solution. This could help in selecting tube coating materials for heat exchanger surfaces.
- 4.) Extension of the work could include a regeneration method for catalytic material to maintain the efficiency of the materials to mitigate fouling.
- 5.) In this study only one type of functionalized nanofluids was investigated, hence other different types of functionalized nanofluids should be investigated.
- 6.) The implementation of the sensor cavity in industry is yet to be achieved. The research is at the verification of the concept stage. In this particular research,

Ca^{2+} has been focused, which is the main foulant compounded with carbonate. Extensive researches have to be introduced to investigate different chemical compounds / pollutants on the effect of signal spectrum. Data have to be collected and a further machine oriented method can be implemented to predict the unknown solution by identifying the unique signal of each of the chemicals.

- 7.) The present numerical approach can be extended by increasing the dimensionalities within the computational domain. This may include reformulating the propagation port to suit the higher dimensional requirements. It is also interesting to adopt the chemical reaction within the prepared solution for analysis to compare with the existing experimental test specimen. The challenges remain to physically model the chemical reaction interaction within the computational domain to fully understand the actual phenomena.
- 8.) The designed LabVIEW system used to monitor and control the system is very useful as reference to design and fabricate an experimental system for fouling research. Full automation and accuracy enhancement are recommended for future complex fouling research such as co-precipitation, tri-precipitation or complex multi-phase flow fouling research.

REFERENCES

- Ahmad, S., & Reynolds, D. (1999). Monitoring of water quality using fluorescence technique: prospect of on-line process control. *Water Research*, 33(9), 2069-2074.
- Al-Shamma'a, A., Mason, A., & Shaw, A. (2010). Non-Invasive Monitoring Device: Google Patents.
- Alahmad, M. (2004). Experimental Study of Scale Formation in Sea Water Environment. *J. King Saud Univ*, 17(1), 73-88.
- Alahmad, M. (2008). Factors Affecting Scale Formation in Sea Water Environments – An Experimental Approach. *Chemical engineering & technology*, 31(1), 149-156.
- Altay, E., Shahwan, T., & Tanoğlu, M. (2007). Morphosynthesis of CaCO₃ at different reaction temperatures and the effects of PDDA, CTAB, and EDTA on the particle morphology and polymorph stability. *Powder Technology*, 178(3), 194-202.
- Amiri, A., Ahmadi, G., Shanbedi, M., Savari, M., Kazi, S., & Chew, B. (2015). Microwave-Assisted Synthesis of Highly-Crumpled, Few-Layered Graphene and Nitrogen-Doped Graphene for Use as High-Performance Electrodes in Capacitive Deionization. *Scientific reports*, 5.
- Amiri, A., Sadri, R., Shanbedi, M., Ahmadi, G., Chew, B., Kazi, S., & Dahari, M. (2015). Performance dependence of thermosyphon on the functionalization approaches: An experimental study on thermo-physical properties of graphene nanoplatelet-based water nanofluids. *Energy conversion and management*, 92, 322-330.
- Amiri, A., Shanbedi, M., Yarmand, H., Arzani, H. K., Gharekhani, S., Montazer, E., . . . Kazi, S. (2015). Laminar convective heat transfer of hexylamine-treated MWCNTs-based turbine oil nanofluid. *Energy conversion and management*, 105, 355-367.
- Amjad, Z. (2000). Controlling Metal Ion Fouling in Industrial Water Systems. *UltraPure Water*, 17(4), 31-40.
- Amjad, Z. (2006). Influence of Natural and Synthetic Additives on Calcium Carbonate Precipitation and Crystal Morphology. *Tenside Surfactants Detergents*, 43(4), 184-191.
- Amjad, Z. (2007). Controlling metal ion fouling in industrial water systems: Citeseer.
- Amjad, Z., & Zuhl, R. (2008). An evaluation of silica scale control additives for industrial water systems. *NACE International, New Orleans*.
- Arhancet, G. B. (1999). Compositions and methods for inhibiting fouling of vinyl monomers: Google Patents.

- Ashraf, M. A., Hussain, M., Mahmood, K., Wajid, A., Yusof, M., Alias, Y., & Yusoff, I. (2013). Removal of acid yellow-17 dye from aqueous solution using eco-friendly biosorbent. *Desalination and Water Treatment*, 51(22-24), 4530-4545.
- Ashton, S., Cutmore, N., Roach, G., Watt, J., Zastawny, H., & McEwan, A. (1994). *Development and trial of microwave techniques for measurement of multiphase flow of oil, water and gas*. Paper presented at the SPE Asia Pacific Oil and Gas Conference.
- Ateeq, M., Shaw, A., Garrett, R., & Dickson, P. (2016). Feasibility study on using microwave sensing technique to analyse silver-based products. *Journal of Electromagnetic Waves and Applications*, 30(7), 928-944.
- Athavale, R., Dinkel, C., Wehrli, B., Bakker, E., Crespo, G. A., & Brand, A. (2017). Robust Solid-Contact Ion Selective Electrodes for High-Resolution In Situ Measurements in Fresh Water Systems. *Environmental Science & Technology Letters*, 4(7), 286-291.
- Awad, M. M. (2011). *Fouling of heat transfer surfaces*: INTECH Open Access Publisher.
- Awad, M. M., El-Samad, S. A., Gad, H., & Asfour, F. Effect of Flow Velocity on the Surface Fouling. *Mansoura Engineering Journal (MEJ)*, 32, M27-M37.
- B. Thonon, S. G. C. J. (1999). Effect of Geometry and Flow Conditions on Particulate Fouling in Plate Heat Exchangers. *Heat Transfer Engineering*, 20(3), 12-24.
- Baig, H., Antar, M. A., & Zubair, S. M. (2011). Performance evaluation of a once-through multi-stage flash distillation system: Impact of brine heater fouling. *Energy conversion and management*, 52(2), 1414-1425.
- Bansal, B., & Muller-Steinhagen, H. (1993). Crystallization fouling in plate heat exchangers. *Journal of heat transfer*, 115(3), 584-591.
- Bertola, V. (2003). Two-Phase Flow Measurement Techniques. In V. Bertola (Ed.), *Modelling and Experimentation in Two-Phase Flow* (pp. 281-323). Vienna: Springer Vienna.
- Blakey, R., Mason, A., Al-Shamma'a, A., Rolph, C., & Bond, G. (2013). Dielectric characterisation of lipid droplet suspensions using the small perturbation technique *Advancement in Sensing Technology* (pp. 81-91): Springer.
- Bohnet, M. (1987). Fouling of heat transfer surfaces. *Chemical engineering & technology*, 10(1), 113-125.
- Boon, J. D., & Brubaker, J. M. (2008). *Acoustic-microwave water level sensor comparisons in an estuarine environment*. Paper presented at the OCEANS 2008.
- Bott, T. R. (1990). Fouling Notebook. *Institution of Chemical Engineering, Rugby, UK*.
- Bott, T. R. (1995). *Fouling of heat exchangers*: Elsevier.

- Bott, T. R. (1997). Aspects of crystallization fouling. *Experimental Thermal and Fluid Science*, 14(4), 356-360.
- Brar, T., France, P., & Smirniotis, P. G. (2001). Heterogeneous versus Homogeneous Nucleation and Growth of Zeolite A. *The Journal of Physical Chemistry B*, 105(23), 5383-5390.
- Brown, N. (1988). Crystallization of sodium oxalate on metal surfaces. *Journal of crystal growth*, 87(2), 287-294.
- Budz, J., Karpiński, P., & Nuruć, Z. (1985). Effect of temperature on crystallization and dissolution processes in a fluidized bed. *AIChE journal*, 31(2), 259-268.
- Bunaciu, A. A., UdrişTioiu, E. G., & Aboul-Enein, H. Y. (2015). X-ray diffraction: instrumentation and applications. *Critical reviews in analytical chemistry*, 45(4), 289-299.
- Buongiorno, J., Venerus, D. C., Prabhat, N., McKrell, T., Townsend, J., Christianson, R., . . . Alvarado, J. L. (2009). A benchmark study on the thermal conductivity of nanofluids. *Journal of Applied Physics*, 106(9), 094312.
- Burton, W.-K., Cabrera, N., & Frank, F. (1951). The growth of crystals and the equilibrium structure of their surfaces. *Philosophical Transactions of the Royal Society of London A: Mathematical, Physical and Engineering Sciences*, 243(866), 299-358.
- Carducci, A., Verani, M., & Battistini, R. (2010). Legionella in industrial cooling towers: monitoring and control strategies. *Letters in applied microbiology*, 50(1), 24-29.
- Ceylan, K., & Kelbaliyev, G. (2003). The roughness effects on friction and heat transfer in the fully developed turbulent flow in pipes. *Applied Thermal Engineering*, 23(5), 557-570.
- Chen, T., Neville, A., & Yuan, M. (2005). Calcium carbonate scale formation—assessing the initial stages of precipitation and deposition. *Journal of Petroleum Science and Engineering*, 46(3), 185-194.
- Chen, X. D., Li, D. X., Lin, S. X., & Özkan, N. (2004). On-line fouling/cleaning detection by measuring electric resistance—equipment development and application to milk fouling detection and chemical cleaning monitoring. *Journal of Food Engineering*, 61(2), 181-189.
- Cheng, E., Fareq, M., Shahrman, A., Afendi, M., Zulkarnay, Z., Khor, S., . . . Noorpi, N. (2014). Development of low cost microwave detection system for salinity and sugar detection. *International Journal of Mechanical & Mechatronics Engineering*, 14(5), 59-71.
- Chenoweth, J. M. (1990). Final Report of the HTRI/TEMA Joint Committee to Review the Fouling Section of the TEMA Standards. *Heat Transfer Engineering*, 11(1), 73-107.

- Chigondo, M., & Chigondo, F. (2016). Recent Natural Corrosion Inhibitors for Mild Steel: An Overview. *Journal of Chemistry*, 2016, 7.
- Cho, Y. I., Lee, S., Kim, W., & Suh, S. (2004). Physical Water Treatment for the Mitigation of Mineral Fouling in Cooling-Tower Water Applications.
- Choi, D.-J., You, S.-J., & Kim, J.-G. (2002). Development of an environmentally safe corrosion, scale, and microorganism inhibitor for open recirculating cooling systems. *Materials Science and Engineering: A*, 335(1–2), 228-235.
- Clavenna, L., Cody, I., Cooper, A., Colgrove, S., Greaney, M., Bruno, T., . . . Chun, C. (2006). Method for reducing fouling in a refinery: Google Patents.
- Collett, B. M. (2007). Scanning electron microscopy: A review and report of research in wood science. *Wood and Fiber Science*, 2(2), 113-133.
- Davey, R., & Garside, J. (2000). *From molecules to crystallizers*: Oxford University Press.
- de Leeuw, N. H., & Parker, S. C. (1998). Surface structure and morphology of calcium carbonate polymorphs calcite, aragonite, and vaterite: an atomistic approach. *The Journal of Physical Chemistry B*, 102(16), 2914-2922.
- De Yoreo, J. J., & Vekilov, P. G. (2003). Principles of crystal nucleation and growth. *Reviews in mineralogy and geochemistry*, 54(1), 57-93.
- Demadis, K. D. (2003). Combating heat exchanger fouling and corrosion phenomena in process waters. *Compact Heat Exchangers and Enhancement Technology for the Process Industries*, 483-490.
- Demény, A., Németh, P., Czuppon, G., Leél-Össy, S., Szabó, M., Judik, K., . . . Stieber, J. (2016). Formation of amorphous calcium carbonate in caves and its implications for speleothem research. *Scientific reports*, 6, 39602.
- Dittus, F., & Boelter, L. (1985). Heat transfer in automobile radiators of the tubular type. *International communications in heat and mass transfer*, 12(1), 3-22.
- Dyakowski, T. (1996). Process tomography applied to multi-phase flow measurement. *Measurement Science and Technology*, 7(3), 343.
- Dydo, P., Turek, M., & Ciba, J. (2003). Scaling analysis of nanofiltration systems fed with saturated calcium sulfate solutions in the presence of carbonate ions. *Desalination*, 159(3), 245-251.
- Edwards, J., & Bindra, H. (2017). An experimental study on storing thermal energy in packed beds with saturated steam as heat transfer fluid. *Solar Energy*, 157, 456-461.
- El-Shall, H., Abdel-Aal, E. A., & Moudgil, B. M. (2000). Effect of Surfactants on Phosphogypsum Crystallization and Filtration during Wet-Process Phosphoric Acid Production. *Separation Science and Technology*, 35(3), 395-410.

- El Bécaye Maïga, S., Tam Nguyen, C., Galanis, N., Roy, G., Maré, T., & Coqueux, M. (2006). Heat transfer enhancement in turbulent tube flow using Al₂O₃ nanoparticle suspension. *International Journal of Numerical Methods for Heat & Fluid Flow*, 16(3), 275-292.
- Epstein, N. (1981). Fundamentals of heat transfer surface fouling : With special emphasis on laminar flow, in Reynolds Number Flow Heat Exchangers. S. Kakac, R. K. Shah, and A. E. Bergles (eds.), Hemisphere, New York.
- Epstein, N. (1983). Thinking about Heat Transfer Fouling: A 5 × 5 Matrix. *Heat Transfer Engineering*, 4(1), 43-56.
- Febrero, L., Granada, E., Regueiro, A., & Míguez, J. L. (2015). Influence of combustion parameters on fouling composition after wood pellet burning in a lab-scale low-power boiler. *Energies*, 8(9), 9794-9816.
- Flouros, M., Iatrou, G., Yakinthos, K., Cottier, F., & Hirschmann, M. (2015). Two-Phase Flow Heat Transfer and Pressure Drop in Horizontal Scavenge Pipes in an Aero-engine. *Journal of Engineering for Gas Turbines and Power*, 137(8), 081901-081901-081911.
- Frenier, W. W., & Ziauddin, N. . *Formation, removal, and inhibition of inorganic scale in the oilfield environment*.
- Gadani, D., Rana, V., Bhatnagar, S., Prajapati, A., & Vyas, A. (2012). Effect of salinity on the dielectric properties of water. *Indian Journal of Pure and Applied Physics*, 50(6), 405-410.
- Gallien, B., Albaric, M., Duffar, T., Kakimoto, K., & M'Hamdi, M. (2017). Study on the usage of a commercial software (Comsol-Multiphysics®) for dislocation multiplication model. *Journal of crystal growth*, 457, 60-64.
- Geddert, T., Augustin, W., & Scholl, S. (2011). Induction time in crystallization fouling on heat transfer surfaces. *Chemical engineering & technology*, 34(8), 1303-1310.
- Ghaffour, N., Missimer, T. M., & Amy, G. L. (2013). Technical review and evaluation of the economics of water desalination: Current and future challenges for better water supply sustainability. *Desalination*, 309(0), 197-207.
- Ghajar, A. J., & Tang, C. C. (2009). Advances in void fraction, flow pattern maps and non-boiling heat transfer two-phase flow in pipes with various inclinations. *Advances in Multiphase Flow and Heat Transfer*, 1, 1-52.
- Gibbs, J. W. (1961). *Thermodynamics* (Vol. 1): Dover Publications.
- Giulietti, M., Seckler, M., Derenzo, S., Ré, M., & Cekinski, E. (2001). Industrial crystallization and precipitation from solutions: state of the technique. *Brazilian Journal of Chemical Engineering*, 18(4), 423-440.
- Gleick, P. H. (2003). Global freshwater resources: soft-path solutions for the 21st century. *Science*, 302(5650), 1524-1528.

- Gnielinski, V. (1975). New equations for heat and mass transfer in the turbulent flow in pipes and channels. *NASA STI/recon technical report A*, 75, 22028.
- Goldstein, J., Newbury, D. E., Echlin, P., Joy, D. C., Romig Jr, A. D., Lyman, C. E., . . . Lifshin, E. (2012). *Scanning electron microscopy and X-ray microanalysis: a text for biologists, materials scientists, and geologists*: Springer Science & Business Media.
- Gopi, S. P., & Subramanian, V. (2012). Polymorphism in CaCO₃—Effect of temperature under the influence of EDTA (di sodium salt). *Desalination*, 297, 38-47.
- Gros, N. (2013). Ion chromatographic analyses of sea waters, brines and related samples. *Water*, 5(2), 659-676.
- Gunn, D. J. (1980). Effect of surface roughness on the nucleation and growth of calcium sulphate on metal surfaces. *Journal of crystal growth*, 50(2), 533-537.
- Guo, W., Ngo, H.-H., & Li, J. (2012). A mini-review on membrane fouling. *Bioresource technology*, 122, 27-34.
- Gupta, B., Nayak, A., Kandar, T., & Nair, S. (2016). Investigation of air–water two phase flow through a venturi. *Experimental Thermal and Fluid Science*, 70, 148-154.
- Haggis, G., Hasted, J., & Buchanan, T. (1952). The dielectric properties of water in solutions. *The Journal of Chemical Physics*, 20(9), 1452-1465.
- Hans, M.-S. (2010). C4 Fouling of Heat Exchanger Surfaces *VDI Heat Atlas* (pp. 79-104): Springer Berlin Heidelberg.
- Hart, J. R. (2000). Ethylenediaminetetraacetic Acid and Related Chelating Agents *Ullmann's Encyclopedia of Industrial Chemistry*: Wiley-VCH Verlag GmbH & Co. KGaA.
- Hart, J. R. (2000). Ethylenediaminetetraacetic acid and related chelating agents. *Ullmann's Encyclopedia of Industrial Chemistry*.
- Hartley, J., Porch, A., & Jones, M. (2015). A non-invasive microwave method for assessing solid-state ammonia storage. *Sensors and Actuators B: Chemical*, 210, 726-730.
- Hasson, D., Avriel, M., Resnick, W., Rozenman, T., & Windreich, S. (1968). Mechanism of calcium carbonate scale deposition on heat-transfer surfaces. *Industrial & Engineering Chemistry Fundamentals*, 7(1), 59-65.
- Hasson, D., Shemer, H., & Sher, A. (2011). State of the art of friendly “green” scale control inhibitors: a review article. *Industrial & Engineering Chemistry Research*, 50(12), 7601-7607.
- Heat Exchangers. (2013) *Heat Exchanger Design Handbook, Second Edition* (pp. 1-38): CRC Press.

- Helalizadeh, A., Müller-Steinhagen, H., & Jamialahmadi, M. (2000). Mixed salt crystallisation fouling. *Chemical Engineering and Processing: Process Intensification*, 39(1), 29-43.
- Henry, C., Minier, J.-P., & Lefèvre, G. (2012). Towards a description of particulate fouling: From single particle deposition to clogging. *Advances in Colloid and Interface Science*, 185–186(0), 34-76.
- Heris, S. Z., Fallahi, M., Shanbedi, M., & Amiri, A. (2015). Heat transfer performance of two-phase closed thermosyphon with oxidized CNT/water nanofluids. *Heat and Mass Transfer*, 1-9.
- Hervieu, E., & Junior, P. S. (1999). *Direct imaging of two-phase flows by electrical impedance measurements*. Paper presented at the Proceedings of the First World Congress on Industrial Process Tomography, Buxton, UK.
- Herz, A., Malayeri, M., & Müller-Steinhagen, H. (2008). Fouling of roughened stainless steel surfaces during convective heat transfer to aqueous solutions. *Energy conversion and management*, 49(11), 3381-3386.
- Hoang, T. A., Ang, H. M., & Rohl, A. L. (2009). Effects of organic additives on calcium sulfate scaling in pipes. *Australian journal of chemistry*, 62(8), 927-933.
- Hoang, T. A., Ang, M., & Rohl, A. L. (2011). Effects of process parameters on gypsum scale formation in pipes. *Chemical engineering & technology*, 34(6), 1003-1009.
- Höfling, V., Augustin, W., & Bohnet, M. (2004). Crystallization fouling of the aqueous two-component system CaSO₄/CaCO₃. *Heat Exchanger Fouling and Cleaning: Fundamentals and Applications*, 7.
- Hong, J.-S. G., & Lancaster, M. J. (2004). *Microstrip filters for RF/microwave applications* (Vol. 167): John Wiley & Sons.
- Hou, H., Wang, B., Hu, S.-Y., Wang, M.-Y., Feng, J., Xie, P.-P., & Yin, D.-C. An investigation on the effect of surface roughness of crystallization plate on protein crystallization. *Journal of crystal growth*.
- Huang, M., Shen, D., Chow, L. M., & Yang, M. (2001). Correlations of the impedance parameters and conductivity and permittivity of liquid and gel phases in a series piezoelectric quartz crystal sensor. *Sensors and Actuators B: Chemical*, 72(1), 21-27.
- Huddar, S., Hampannavar, V., Patil, P., Shetty, K., & Savadi, R. (2015). Design of Electrostatic RF Switch using COMSOL. *Current Trends in Signal Processing*, 5(1), 13-16.
- Ishihara, K., Nakayama, M., Ohara, S., & Yamamoto, H. (2002). Direct ester condensation from a 1:1 mixture of carboxylic acids and alcohols catalyzed by hafnium(IV) or zirconium(IV) salts. *Tetrahedron*, 58(41), 8179-8188.

- Jackson, B., & Jayanthi, T. (2010). *A novel method for water impurity concentration using microstrip resonator sensor*. Paper presented at the Recent Advances in Space Technology Services and Climate Change (RSTSCC), 2010.
- Kakaç, S., & Pramuanjaroenkij, A. (2016). Analysis of Convective Heat Transfer Enhancement by Nanofluids: Single-Phase and Two-Phase Treatments. *Journal of Engineering Physics and Thermophysics*, 89(3), 758-793.
- Kakaç, S., Shah, R. K., & Aung, W. (1987). *Handbook of single-phase convective heat transfer*: Wiley New York et al.
- Karagiannis, I. C., & Soldatos, P. G. (2008). Water desalination cost literature: review and assessment. *Desalination*, 223(1–3), 448-456.
- Kavitha, A., Vasudevan, T., & Prabu, H. G. (2011). Evaluation of synthesized antiscalants for cooling water system application. *Desalination*, 268(1), 38-45.
- Kazi, S. (2012). *Fouling and fouling mitigation on heat exchanger surfaces*: INTECH Open Access Publisher.
- Kazi, S., Duffy, G., & Chen, X. (2009). *Fouling and fouling mitigation on different heat exchanging surfaces*. Paper presented at the Proceedings of International Conference on Heat Exchanger Fouling and Cleaning.
- Kazi, S., Duffy, G., & Chen, X. (2012). Fouling and fouling mitigation on heated metal surfaces. *Desalination*, 288, 126-134.
- Kazi, S. N., Duffy, G. G., & Chen, X. D. (2010). Mineral scale formation and mitigation on metals and a polymeric heat exchanger surface. *Applied Thermal Engineering*, 30(14–15), 2236-2242.
- Kazi, S. N., Duffy, G. G., & Chen, X. D. (2012). Fouling and fouling mitigation on heated metal surfaces. *Desalination*, 288(0), 126-134.
- Kazi, S. N., Duffy, G. G., & Chen, X. D. (2013). Fouling mitigation of heat exchangers with natural fibres. *Applied Thermal Engineering*, 50(1), 1142-1148.
- Korostynska, O., Arshak, A., Creedon, P., Arshak, K., Wendling, L., Al-Shamma, A., & O'Keefe, S. (2009). *Glucose monitoring using electromagnetic waves and microsensor with interdigitated electrodes*. Paper presented at the Sensors Applications Symposium, 2009. SAS 2009. IEEE.
- Korostynska, O., Mason, A., & Al-Shamma'a, A. (2012). Monitoring of nitrates and phosphates in wastewater: current technologies and further challenges. *International journal on smart sensing and intelligent systems*, 5(1), 149-176.
- Kot, P., Shaw, A., Jones, K. O., Cullen, J. D., Mason, A., & Al-Shamma'a, A. I. (2015, 8-10 Dec. 2015). *The feasibility of electromagnetic waves in determining the moisture content of concrete blocks*. Paper presented at the 2015 9th International Conference on Sensing Technology (ICST).

- Kovacs, Z., Bázár, G., Oshima, M., Shigeoka, S., Tanaka, M., Furukawa, A., . . . Tsenkova, R. (2016). Water spectral pattern as holistic marker for water quality monitoring. *Talanta*, *147*, 598-608.
- Kukulka, D. J., & Devgun, M. (2007). Fluid temperature and velocity effect on fouling. *Applied Thermal Engineering*, *27*(16), 2732-2744.
- Kukulka, P., Kukulka, D. J., & Devgun, M. (2007). Evaluation of Surface Roughness on the Fouling of Surfaces. *Chem. Eng. Trans*, *12*, 537.
- Lacmann, R. (1998). Crystallization, JW MULLIN, Butterworth-Heinemann, Oxford 1997, 527 Seiten, zahlr. Abb. und ISBN 0-7506-3759-5. *Chemie Ingenieur Technik*, *70*(11), 1468-1468.
- Lau, W.-J., & Ismail, A. F. (2009). Polymeric nanofiltration membranes for textile dye wastewater treatment: preparation, performance evaluation, transport modelling, and fouling control—a review. *Desalination*, *245*(1), 321-348.
- Lee, G. J., Tijging, L. D., Pak, B. C., Baek, B. J., & Cho, Y. I. (2006). Use of catalytic materials for the mitigation of mineral fouling. *International communications in heat and mass transfer*, *33*(1), 14-23.
- Lee, S. H., & Cho, Y. I. (2002). Velocity effect on electronic-antifouling technology to mitigate mineral fouling in enhanced-tube heat exchanger. *International Journal of Heat and Mass Transfer*, *45*(20), 4163-4174.
- Li, X., & Jiang, Y. (2010). Design of a Cylindrical Cavity Resonator for Measurements of Electrical Properties of Dielectric Materials.
- Lin, S., & Chen, X. (2007). A laboratory investigation of milk fouling under the influence of ultrasound. *Food and bioproducts processing*, *85*(1), 57-62.
- Lin, Y.-P., & Singer, P. C. (2005). Inhibition of calcite crystal growth by polyphosphates. *Water Research*, *39*(19), 4835-4843.
- Lioliou, M. G., Paraskeva, C. A., Koutsoukos, P. G., & Payatakes, A. C. (2006). Calcium sulfate precipitation in the presence of water-soluble polymers. *Journal of colloid and interface science*, *303*(1), 164-170.
- Liu, S.-T., & Nancollas, G. H. (1970). The kinetics of crystal growth of calcium sulfate dihydrate. *Journal of crystal growth*, *6*(3), 281-289.
- Liu, S.-T., & Nancollas, G. H. (1973). The crystal growth of calcium sulfate dihydrate in the presence of additives. *Journal of colloid and interface science*, *44*(3), 422-429.
- Liu, X., Chen, T., Chen, P., Montgomerie, H., Hagen, T. H., Wang, B., & Yang, X. (2012). *Understanding Mechanisms of Scale Inhibition Using Newly Developed Test Method and Developing Synergistic Combined Scale Inhibitors*. Paper presented at the SPE International Conference on Oilfield Scale.

- Lyklema, J. (2005). *Fundamentals of interface and colloid science: soft colloids* (Vol. 5): Academic press.
- Macadam, J., & Parsons, S. (2004). Calcium carbonate scale control, effect of material and inhibitors. *Water Science and Technology*, 49(2), 153-159.
- Macadam, J., & Parsons, S. (2004). Calcium carbonate scale control, effect of material and inhibitors. *Water Science & Technology*, 49(2), 153-159.
- MacAdam, J., & Parsons, S. (2004). Calcium carbonate scale formation and control. *Re/Views in Environmental Science & Bio/Technology*, 3(2), 159-169.
- Madaeni, S., & Samieirad, S. (2010). Chemical cleaning of reverse osmosis membrane fouled by wastewater. *Desalination*, 257(1), 80-86.
- Maglione, M., & Subramanian, M. A. (2008). Dielectric and polarization experiments in high loss dielectrics: A word of caution. *Applied Physics Letters*, 93(3), 032902.
- Manoli, F., & Dalas, E. (2000). Spontaneous precipitation of calcium carbonate in the presence of ethanol, isopropanol and diethylene glycol. *Journal of crystal growth*, 218(2), 359-364.
- Manoli, F., Kanakis, J., Malkaj, P., & Dalas, E. (2002). The effect of aminoacids on the crystal growth of calcium carbonate. *Journal of crystal growth*, 236(1-3), 363-370.
- Mehrali, M., Sadeghinezhad, E., Latibari, S. T., Kazi, S. N., Mehrali, M., Zubir, M. N. B. M., & Metselaar, H. S. C. (2014). Investigation of thermal conductivity and rheological properties of nanofluids containing graphene nanoplatelets. *Nanoscale Research Letters*, 9(1), 15.
- Meyer, J. S., Santore, R. C., Bobbitt, J. P., DeBrey, L. D., Boese, C. J., Paquin, P. R., . . . DiToro, D. M. (1999). Binding of nickel and copper to fish gills predicts toxicity when water hardness varies, but free-ion activity does not. *Environmental science & technology*, 33(6), 913-916.
- Meyer, K., Kern, S., Zientek, N., Guthausen, G., & Maiwald, M. (2016). Process control with compact NMR. *TrAC Trends in Analytical Chemistry*.
- Middis, J., Paul, S., Müller-Steinhagen, H., & Duffy, G. (1998). Reduction of heat transfer fouling by the addition of wood pulp fibers. *Heat Transfer Engineering*, 19(2), 36-44.
- Morra, M. (2000). On the molecular basis of fouling resistance. *Journal of Biomaterials Science, Polymer Edition*, 11(6), 547-569.
- Morse, J. W., Arvidson, R. S., & Lüttge, A. (2007). Calcium Carbonate Formation and Dissolution. *Chemical Reviews*, 107(2), 342-381.
- Morse, R. W., & Knudsen, J. G. (1977). Effect of alkalinity on the scaling of simulated cooling tower water. *The Canadian Journal of Chemical Engineering*, 55(3), 272-278.

- Müller-Steinhagen, H. (2000). *Heat Exchanger Fouling: Mitigation and Cleaning Techniques*: IChemE.
- Müller-Steinhagen, H. (2010). C4 Fouling of Heat Exchanger Surfaces *VDI Heat Atlas* (pp. 79-104). Berlin, Heidelberg: Springer Berlin Heidelberg.
- Müller-Steinhagen, H. (2011). Heat Transfer Fouling: 50 Years After the Kern and Seaton Model. *Heat Transfer Engineering*, 32(1), 1-13.
- Müller-Steinhagen, H., Malayeri, M., & Watkinson, A. (2009). Heat exchanger fouling: environmental impacts: Taylor & Francis.
- Müller-Steinhagen, H., Malayeri, M., & Watkinson, A. (2011). Heat exchanger fouling: mitigation and cleaning strategies. *Heat Transfer Engineering*, 32(3-4), 189-196.
- Müller-Steinhagen, H., Malayeri, M. R., & Watkinson, A. (2005). Fouling of heat exchangers-new approaches to solve an old problem. *Heat Transfer Engineering*, 26(1), 1-4.
- MÜLLER-Steinhagen, H., Malayeri, M. R., & Watkinson, A. P. (2005). Fouling of Heat Exchangers-New Approaches to Solve an Old Problem. *Heat Transfer Engineering*, 26(1), 1-4.
- Müller-Steinhagen, H., Malayeri, M. R., & Watkinson, A. P. (2009). Heat Exchanger Fouling: Environmental Impacts. *Heat Transfer Engineering*, 30(10-11), 773-776.
- Mullin, J. W. (2001a). 5 - Nucleation. In J. W. Mullin (Ed.), *Crystallization (Fourth Edition)* (pp. 181-215). Oxford: Butterworth-Heinemann.
- Mullin, J. W. (2001b). 6 - Crystal growth *Crystallization (Fourth Edition)* (pp. 216-288). Oxford: Butterworth-Heinemann.
- Mullin, J. W. (2001). *Crystallisation* (4th ed.). London,UK: Butterworth-Heineman.
- Muryanto, S. (2002). The role of impurities and additives in the crystallisation of gypsum.
- Nacke, T., Barthel, A., Pflieger, C., Pliquet, U., Beckmann, D., & Göller, A. (2010). *Continuous process monitoring for biogas plants using microwave sensors*. Paper presented at the Electronics Conference (BEC), 2010 12th Biennial Baltic.
- Nazemi, E., Fegghi, S. A. H., Roshani, G. H., Gholipour Peyvandi, R., & Setayeshi, S. (2016). Precise Void Fraction Measurement in Two-phase Flows Independent of the Flow Regime Using Gamma-ray Attenuation. *Nuclear Engineering and Technology*, 48(1), 64-71.
- Nguyen, T., Roddick, F. A., & Fan, L. (2012). Biofouling of water treatment membranes: a review of the underlying causes, monitoring techniques and control measures. *Membranes*, 2(4), 804-840.

- Noyes, A. A., & Whitney, W. R. (1897). The rate of solution of solid substances in their own solutions. *Journal of the American Chemical Society*, 19(12), 930-934.
- Ohara, M., & Reid, R. C. (1973). *Modeling crystal growth rates from solution*: Prentice-Hall.
- Oon, C. S., Ateeq, M., Shaw, A., Al-Shamma'a, A., Kazi, S. N., & Badarudin, A. (2016). Experimental study on a feasibility of using electromagnetic wave cylindrical cavity sensor to monitor the percentage of water fraction in a two phase system. *Sensors and Actuators A: Physical*, 245, 140-149.
- Oon, C. S., Ateeq, M., Shaw, A., Wylie, S., Al-Shamma'a, A., & Kazi, S. N. (2016). Detection of the gas-liquid two-phase flow regimes using non-intrusive microwave cylindrical cavity sensor. *Journal of Electromagnetic Waves and Applications*, 30(17), 2241-2255.
- Ortoneda-Pedrola, M., Korostynska, O., Mason, A., & Al-Shamma'A, A. (2013). *Real-time sensing of NaCl solution concentration at microwave frequencies using novel Ag patterns printed on flexible substrates*. Paper presented at the Journal of Physics: Conference Series.
- Pääkkönen, T. M., Riihimäki, M., Simonson, C. J., Muurinen, E., & Keiski, R. L. (2012). Crystallization fouling of CaCO₃ – Analysis of experimental thermal resistance and its uncertainty. *International Journal of Heat and Mass Transfer*, 55(23–24), 6927-6937.
- Packer, A. (1968). The precipitation of sparingly soluble alkaline-earth metal and lead salts: nucleation and growth orders during the induction period. *Journal of the Chemical Society A: Inorganic, Physical, Theoretical*, 859-862.
- Pak, B. C., & Cho, Y. I. (1998). Hydrodynamic and heat transfer study of dispersed fluids with submicron metallic oxide particles. *Experimental Heat Transfer an International Journal*, 11(2), 151-170.
- Palanisamy, K., Sanjiv Raj, K., Bhuvanewari, S., & Subramanian, V. (2016). A novel phenomenon of effect of metal on calcium carbonate scale, morphology, polymorphism and its deposition. *Materials Research Innovations*, 1-10.
- Park, J.-S., Lee, H.-J., Choi, S.-J., Geckeler, K. E., Cho, J., & Moon, S.-H. (2003). Fouling mitigation of anion exchange membrane by zeta potential control. *Journal of colloid and interface science*, 259(2), 293-300.
- Parson, S. A., S.J. Judd, Stephenson, T., S.Udol, & Wang, B. L. (1997). Magnetically augmented water treatment. *Process Safety and Environmental Protection, Transaction of the Institution of Chemical Engineering 75(Part B)*, 98-104.
- Parsons, S. A., Wang, B.-L., Judd, S. J., & Stephenson, T. (1997). Magnetic treatment of calcium carbonate scale—effect of pH control. *Water Research*, 31(2), 339-342.
- Patnaik, P. (2003). *Handbook of inorganic chemicals* (Vol. 28): McGraw-Hill New York.

- Paz, C., Suárez, E., Eiris, A., & Porteiro, J. (2012). Experimental evaluation of the critical local wall shear stress around cylindrical probes fouled by diesel exhaust gases. *Experimental Thermal and Fluid Science*, 38, 85-93.
- Pritchard, A. M., & Freyer, P. J. (1988). Cleaning of Fouled Surfaces: A Discussion. In L. F. Melo, T. R. Bott & C. A. Bernardo (Eds.), *Fouling Science and Technology* (pp. 721-726). Dordrecht: Springer Netherlands.
- Quan, Z., Chen, Y., & Ma, C. (2008). Experimental study of fouling on heat transfer surface during forced convective heat transfer. *Chinese Journal of Chemical Engineering*, 16(4), 535-540.
- R.Davey, J. G. (2000). *From Molecules to Crystallizers : an Introduction to Crystallization*. Oxford.
- Rajagopal, S., Van der Velde, G., Van der Gaag, M., & Jenner, H. A. (2003). How effective is intermittent chlorination to control adult mussel fouling in cooling water systems? *Water Research*, 37(2), 329-338.
- Rao, R. (2015). *Microwave engineering*: PHI Learning Pvt. Ltd.
- Roder, H. (1981). A transient hot wire thermal conductivity apparatus for fluids. *Journal of research of the National Bureau of Standards*, 86(5), 457-493.
- Rubasinghege, G., & Grassian, V. H. (2013). Role(s) of adsorbed water in the surface chemistry of environmental interfaces. *Chemical Communications*, 49(30), 3071-3094.
- Ruelo, M. T. G., Tijjing, L. D., Amarjargal, A., Park, C.-H., Kim, H. J., Pant, H. R., . . . Kim, C. S. (2013). Assessing the effect of catalytic materials on the scaling of carbon steel. *Desalination*, 313, 189-198.
- Rydosz, A., Maciak, E., Wincza, K., & Gruszczynski, S. Microwave-based sensors with phthalocyanine films for acetone, ethanol and methanol detection. *Sensors and Actuators B: Chemical*.
- Sadeghinezhad, E., Kazi, S. N., Dahari, M., Safaei, M. R., Sadri, R., & Badarudin, A. (2014). A comprehensive review of milk fouling on heated surfaces. *Critical Reviews in Food Science and Nutrition*, null-null.
- Sarfraz, O., & Bach, C. (2016). A Literature Review On Heat Exchanger Air Side Fouling In Heating, Ventilation And Air-conditioning (HVAC) Applications.
- Schoenitz, M., Grundemann, L., Augustin, W., & Scholl, S. (2015). Fouling in microstructured devices: a review. *Chemical Communications*, 51(39), 8213-8228.
- Shanbedi, M., Heris, S. Z., Amiri, A., & Baniadam, M. (2014). Improvement in heat transfer of a two-phased closed thermosyphon using silver-decorated MWCNT/water. *Journal of Dispersion Science and Technology*, 35(8), 1086-1096.

- Shanbedi, M., Heris, S. Z., Amiri, A., & Eshghi, H. (2015). Synthesis of water-soluble Fe-decorated multi-walled carbon nanotubes: A study on thermo-physical properties of ferromagnetic nanofluid. *Journal of the Taiwan Institute of Chemical Engineers*.
- Sheikholeslami, R. (1999). Fouling mitigation in membrane processes: Report on a Workshop held January 26–29, 1999, Technion — Israel Institute of Technology, Haifa, Israel. *Desalination*, 123(1), 45-53.
- Sheikholeslami, R. (2000). Composite fouling of heat transfer equipment in aqueous media-a review. *Heat Transfer Engineering*, 21(3), 34-42.
- Sheikholeslami, R., & Watkinson, A. (1986). Scaling of plain and externally finned heat exchanger tubes. *Journal of heat transfer*, 108(1), 147-152.
- Snoeyink, V. L., & Jenkins, D. (1980). *Water chemistry*: Wiley.
- Somerscales, E. (1990). Fouling of heat transfer surfaces: an historical review. *Heat Transfer Engineering*, 11(1), 19-36.
- Somerscales, E., & Knudsen, J. G. (1981). *Fouling of heat transfer equipment*: Hemisphere Pub.
- Somerscales, E. F. C. (1997). Fundamentals of corrosion fouling. *Experimental Thermal and Fluid Science*, 14(4), 335-355.
- Spicher, R. G., & Skrinde, R. T. (1963). Potassium permanganate oxidation of organic contaminants in water supplies. *Journal (American Water Works Association)*, 1174-1194.
- Steinhagen, R., Müller-Steinhagen, H., & Maani, K. (1993). Problems and costs due to heat exchanger fouling in New Zealand industries. *Heat Transfer Engineering*, 14(1), 19-30.
- Sudmalis, M., & Sheikholeslami, R. (2000). Coprecipitation of CaCO₃ and CaSO₄. *The Canadian Journal of Chemical Engineering*, 78(1), 21-31.
- Sunagawa, I. (2005). *Crystals Growth, Morphology, and Perfection*. Cambridge, UK: Cambridge University Press.
- Tai, C. Y., & Chien, W. C. (2003). Interpreting the effects of operating variables on the induction period of CaCl₂–Na₂CO₃ system by a cluster coagulation model. *Chemical engineering science*, 58(14), 3233-3241.
- Tang, Q. G., Meng, J. P., Liang, J. S., Nie, L., & Li, Y. X. (2010). Effects of copper based alloys on the nucleation and growth of calcium carbonate scale. *Journal of Alloys and Compounds*, 491(1–2), 242-247.
- Thomas, M. P. (2010). Calcium and Magnesium in Drinking-water: Public Health Significance. *International Journal of Environmental Studies*, 67(4), 612-613.

- Tijing, L., Ruelo, M., Park, C.-H., Amarjargal, A., Kim, H., Pant, H., . . . Kim, C. (2013). Efficacy of zinc and tourmaline in mitigating corrosion of carbon steel in non-flow mode. *Chemical Papers*, 67(10), 1304-1310.
- Tijing, L. D., Kim, H. Y., Lee, D. H., Kim, C. S., & Cho, Y. I. (2010). Physical water treatment using RF electric fields for the mitigation of CaCO₃ fouling in cooling water. *International Journal of Heat and Mass Transfer*, 53(7–8), 1426-1437.
- Tijing, L. D., Yu, M.-H., Kim, C.-H., Amarjargal, A., Lee, Y. C., Lee, D.-H., . . . Kim, C. S. (2011). Mitigation of scaling in heat exchangers by physical water treatment using zinc and tourmaline. *Applied Thermal Engineering*, 31(11–12), 2025-2031.
- Törer, N., & Aytac, Ö. (2016). Is the Routine Use of Impedance Analysis for the Diagnosis of Gastro-Esophageal Reflux Disease More Expensive than Conventional pH Monitoring? Cost Analysis of Two Procedures. *Indian Journal of Surgery*, 1-4.
- Troup, D., & Richardson, J. (1978). Scale nucleation on a heat transfer surface and its prevention. *Chemical Engineering Communications*, 2(4-5), 167-180.
- Troup, D. H., & Richardson, J. A. (1978). SCALE NUCLEATION ON A HEAT TRANSFER SURFACE AND ITS PREVENTION. *Chemical Engineering Communications*, 2(4-5), 167-180.
- Uyak, V., Akdagli, M., Cakmakci, M., & Koyuncu, I. (2014). Natural organic matter removal and fouling in a low pressure hybrid membrane systems. *The Scientific World Journal*, 2014.
- Valiskó, M., & Boda, D. (2014). The effect of concentration- and temperature-dependent dielectric constant on the activity coefficient of NaCl electrolyte solutions. *The Journal of Chemical Physics*, 140(23), 234508.
- Verch, A., Gebauer, D., Antonietti, M., & Colfen, H. (2011). How to control the scaling of CaCO₃: a "fingerprinting technique" to classify additives. *Physical Chemistry Chemical Physics*, 13(37), 16811-16820.
- Vidojkovic, S., Onjia, A., Matovic, B., Grahovac, N., Maksimovic, V., & Nastasovic, A. (2013). Extensive feedwater quality control and monitoring concept for preventing chemistry-related failures of boiler tubes in a subcritical thermal power plant. *Applied Thermal Engineering*, 59(1–2), 683-694.
- Volkmer, D., Fricke, M., Huber, T., & Sewald, N. (2004). Acidic peptides acting as growth modifiers of calcite crystals. *Chemical Communications*(16), 1872-1873.
- Walker, M. E., Safari, I., Theregowda, R. B., Hsieh, M.-K., Abbasian, J., Arastoopour, H., . . . Miller, D. C. (2012). Economic impact of condenser fouling in existing thermoelectric power plants. *Energy*, 44(1), 429-437.
- Walker, P., & Sheikholeslami, R. (2003). Assessment of the effect of velocity and residence time in CaSO₄ precipitating flow reaction. *Chemical engineering science*, 58(16), 3807-3816.

- Walker, P., & Sheikholeslami, R. (2003). Assessment of the effect of velocity and residence time in CaSO₄ precipitating flow reaction. *Chemical engineering science*, 58(16), 3807-3816.
- Wang, Y. (2005). *Composite Fouling of Calcium Sulfate and Calcium Carbonate in a Dynamic Seawater Reverse Osmosis Unit*. The University of New South Wales.
- Watkinson, A., & Wilson, D. (1997). Chemical reaction fouling: A review. *Experimental Thermal and Fluid Science*, 14(4), 361-374.
- Watkinson, A. P. (2007). Deposition from crude oils in heat exchangers. *Heat Transfer Engineering*, 28(3), 177-184.
- Watkinson, A. P., & Wilson, D. I. (1997). Chemical reaction fouling: A review. *Experimental Thermal and Fluid Science*, 14(4), 361-374.
- Wibisono, Y. (2014). *Two-phase flow for fouling control in membranes*: Universiteit Twente.
- Wilson, D. (2005). Challenges in cleaning: recent developments and future prospects. *Heat Transfer Engineering*, 26(1), 51-59.
- Xu, J., Jiang, X., Fang, N., Georget, E., Abdeddaim, R., Geffrin, J.-M., . . . Guenneau, S. (2015). Molding acoustic, electromagnetic and water waves with a single cloak. *Scientific reports*, 5.
- Yang, Q., Liu, Y., Gu, A., Ding, J., & Shen, Z. (2002). Investigation of induction period and morphology of CaCO₃ fouling on heated surface. *Chemical engineering science*, 57(6), 921-931.
- Yu, H. (2007). *Composite fouling on heat exchanger surfaces*: Nova Science Publishers, Inc., New York.
- Yuan, Y., & Lee, T. R. (2013). Contact angle and wetting properties *Surface science techniques* (pp. 3-34): Springer.
- Zakaria, Z., Zain, N. A. M., Balkis, I., Yaacob, S., Mansor, M. S. B., Rahim, R. A., & Ayob, N. M. N. (2012, 28-31 Oct. 2012). *Evaluation of square type electromagnetic field screen implementation on interference effects in magnetic induction tomography modality*. Paper presented at the 2012 IEEE Sensors.
- Zalba, B., Marín, J. M., Cabeza, L. F., & Mehling, H. (2003). Review on thermal energy storage with phase change: materials, heat transfer analysis and applications. *Applied Thermal Engineering*, 23(3), 251-283.
- Zhang, F., Hou, Z., Sheng, K., Deng, B., & Xie, L. (2006). Crystallization of calcium carbonate on polyethylene [gamma]-radiation-grafted with acrylic acid. *Journal of Materials Chemistry*, 16(13), 1215-1221.
- Zhao, X., & Chen, X. D. (2012). A Critical Review of Basic Crystallography to Salt Crystallization Fouling in Heat Exchangers. *Heat Transfer Engineering*, 34(8-9), 719-732.

Zhao, X., & Chen, X. D. (2013). A Critical Review of Basic Crystallography to Salt Crystallization Fouling in Heat Exchangers. *Heat Transfer Engineering*, 34(8-9), 719-732.

LIST OF PUBLICATIONS AND PAPERS PRESENTED

Journal Article

1. KH Solangi, SN Kazi, MR Luhur, A Badarudin, A Amiri, R Sadri, **KH Teng**. A comprehensive review of thermo-physical properties and convective heat transfer to nanofluids. *Energy* 89, 1065-1086 (Impact Factor:4.52)
2. SN Kazi, **KH Teng**, MS Zakaria, E Sadeghinezhad, MA Bakar. Study of mineral fouling mitigation on heat exchanger surface, *Desalination* 367, 248-254 (Impact Factor: 5.527)
3. **KH Teng**, RH Baharudin, MA Bakar, SN Kazi. Mitigation of heat exchanger fouling in industry using catalytic materials, *Desalination and Water Treatment* 57 (1), 22-27 (Impact Factor: 0.93)
4. **KH Teng**, A Amiri, SN Kazi, MA Bakar, BT Chew . Fouling mitigation on heat exchanger surfaces by EDTA-treated MWCNT-based water nanofluids. *Journal of the Taiwan Institute of Chemical Engineers* 60, 445-452 (Impact Factor: 4.217)
5. **KH Teng**, Ahmad Amiri, S. N. Kazi, M. A. Bakar, B. T. Chew, Al-Shamma'a A, Shaw A Retardation of Heat Exchanger Surfaces Mineral Fouling by Diethylenetriamine pentaacetate-treated MWCNT-based water nanofluids, *Applied Thermal Engineering* 110, 495-503 (Impact Factor: 3.356)
6. **KH Teng**, S. N. Kazi, Ahmad Amiri, A.F. Habali, M. A. Bakar, B. T. Chew, Al-Shamma'a A, Shaw A, K.H. Solangi, Ghulamulah Kha. Calcium Carbonate Fouling on Double-Pipe Heat Exchanger with Different Heat Exchanging Surfaces, *Powder Technology* 315 , 216-226 (Impact Factor: 2.942)
7. Ahmad Amiri, Mohd Nashrul Mohd Zubir, Ayrat M Dimiev, **KH Teng**, Mehdi Shanbedi, SN Kazi, Shaifulazuar Bin Rozali. Facile, Environmentally Friendly, Cost Effective and Scalable Production of Few-Layered Graphene, *Chemical Engineering Journal* 326, 1105-1115 (Impact Factor: 6.216)
8. **KH Teng**, M. Ateeq, Shaw A, Al-Shamma'a A., S. N. Kazi, B. T. Chew, Kot. P. Numerical Investigation on using an Electromagnetic Wave Sensor to Detect Water Hardness in Water Cooling System Industry, *International Journal of Electromagnetics and Applications* . (Accepted)

Book Chapter

1. **KH Teng**, S.N. Kazi, M.A. Bakar, Al-Shamma'a A, Shaw A. Industrial Heat Exchanger - Operation and Maintenance to Minimise Fouling and Corrosion. InTech in the book project tentatively titled "Heat Exchanger- Advanced Features and Applications ", ISBN: 978-953-51-4911-8.

Conferences

1. Postgraduate Faculty of Technology and Engineering Research Week 2017
2. 2nd Annual LJMU Graduate School Research Conference – (2017,Liverpool, United Kingdom) – Runner-up for poster competition
3. 19th International Conference on Smart Sensor and Information Engineering (ICSSIE – 2017, London, United Kingdom)
4. International Conference on Business, Economics, Energy and Environmental Sciences (ICBEEES 2014, Kuala Lumpur, Malaysia) – Best paper award

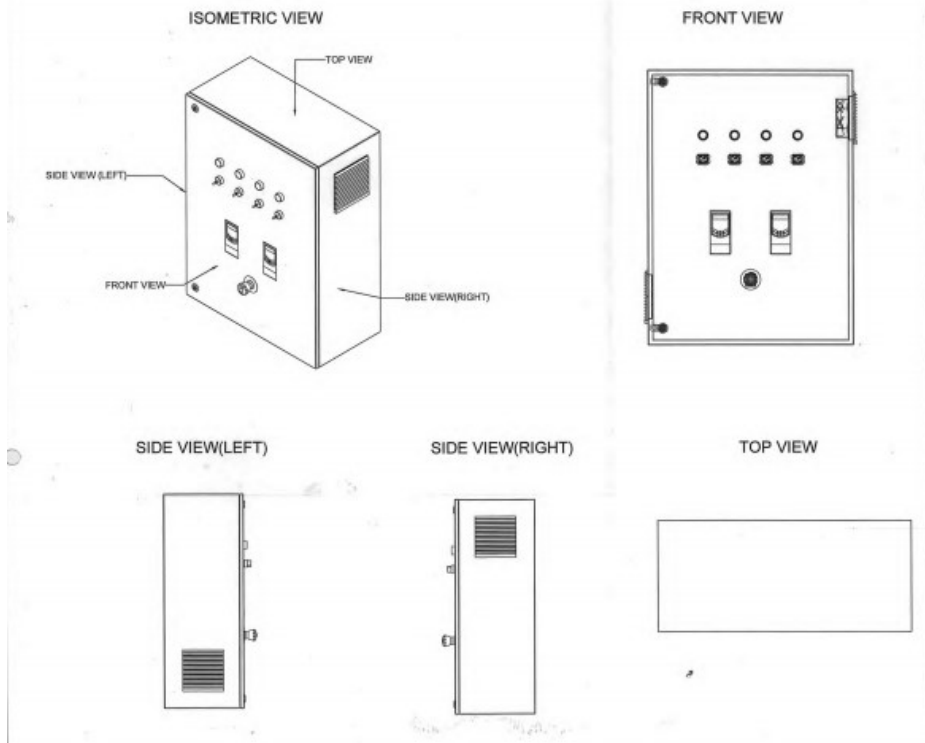
APPENDIX

Appendix A: Program-Logic-Control Overview and Power Distribution

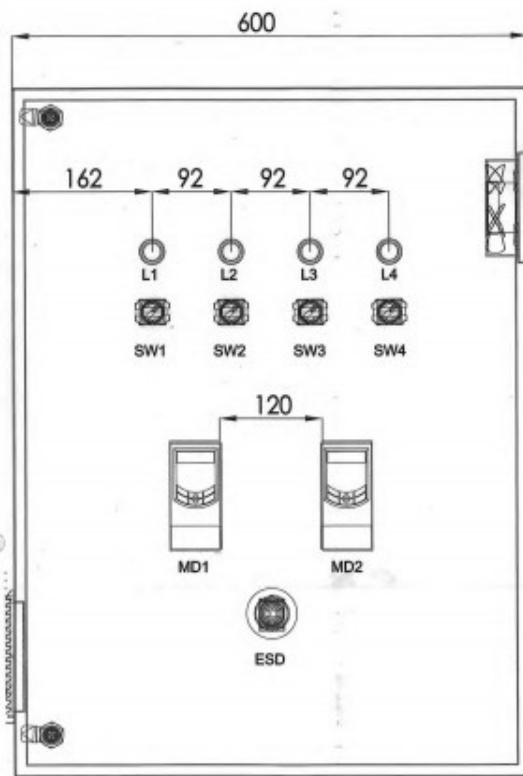
INDEX/LIST OF MATERIAL

NO.	MATERIAL	MANUFACTURER	QUANTITY	TAG NO.	MODEL	POWER SUPPLY
1	INDICATOR LIGHT(GREEN)	LED(TOSHI)	4 NOS	L1,L2,L3,L4	AD22-22DS	240V
2	SELECTOR SWITCH	CIKACHI	4 NOS	SW1,SW2,SW3,SW4	DR-120-24	240V
3	EMERGENCY STOP BUTTON	KOINO	1 NOS	ESD	KH-220-1ER	240V
4	DC POWER SUPPLY	MEAN WELL	1 NOS	P.S.U	DR-120-24	240V
5	ELCB 40A	ABB	1 NOS	ELCB	M40-363	240V
6	MCB C20 2P	ABB	3 NOS	MCB1,MCB2,MCB3	SH202L-C20	240V
7	MCB 6A 1P	ABB	2 NOS	MCB4,MCB5	MH40-106	240V
8	MAGNETIC CONTACTOR	FUJI	3 NOS	MC1,MC2,MC3,MC4	SC-03	240V
9	THYRISTOR POWER REGULATOR	SIPIN	1 NOS	PWR	W5	240V
10	MOTOR DRIVER	HUFFMAN MULLER	2 NOS	MD1,MD2	SC-03	240V
12	CPU-1214C (PLC)	SIEMENS	1 NOS	PLC1	6ES7214-1HG31-0XB0	24VDC
13	SM 1231 RTD (PLC)	SIEMENS	3 NOS	PLC2,PLC3,PLC4	6ES7231-5PF32-0XB0	24VDC
14	RELAY	OMRON	1 NOS	RLY	MY2N	24VDC

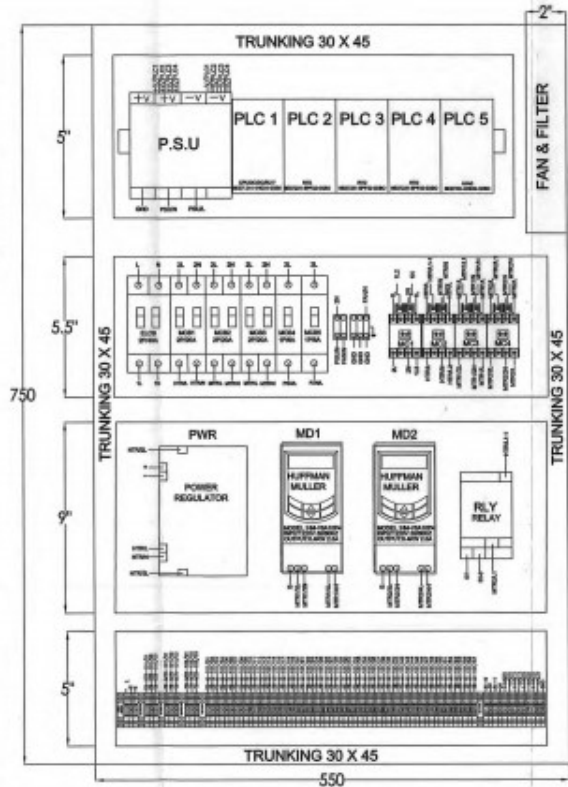
LOCAL PANEL STRUCTURE



PANEL FRONT VIEW

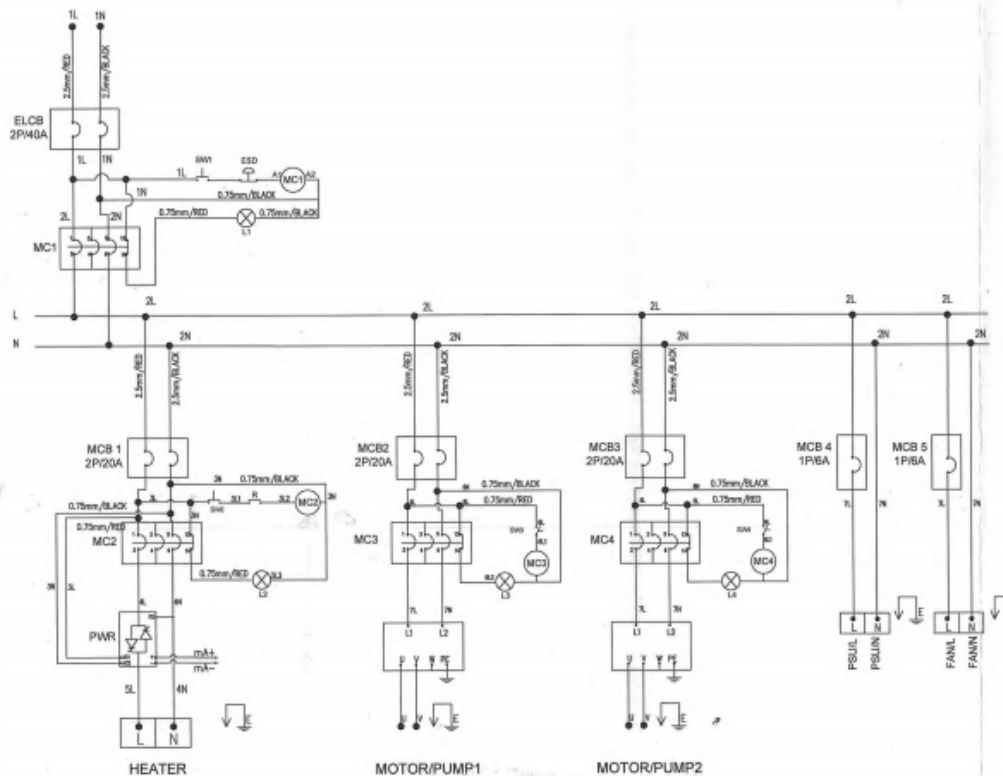


FRONT VIEW

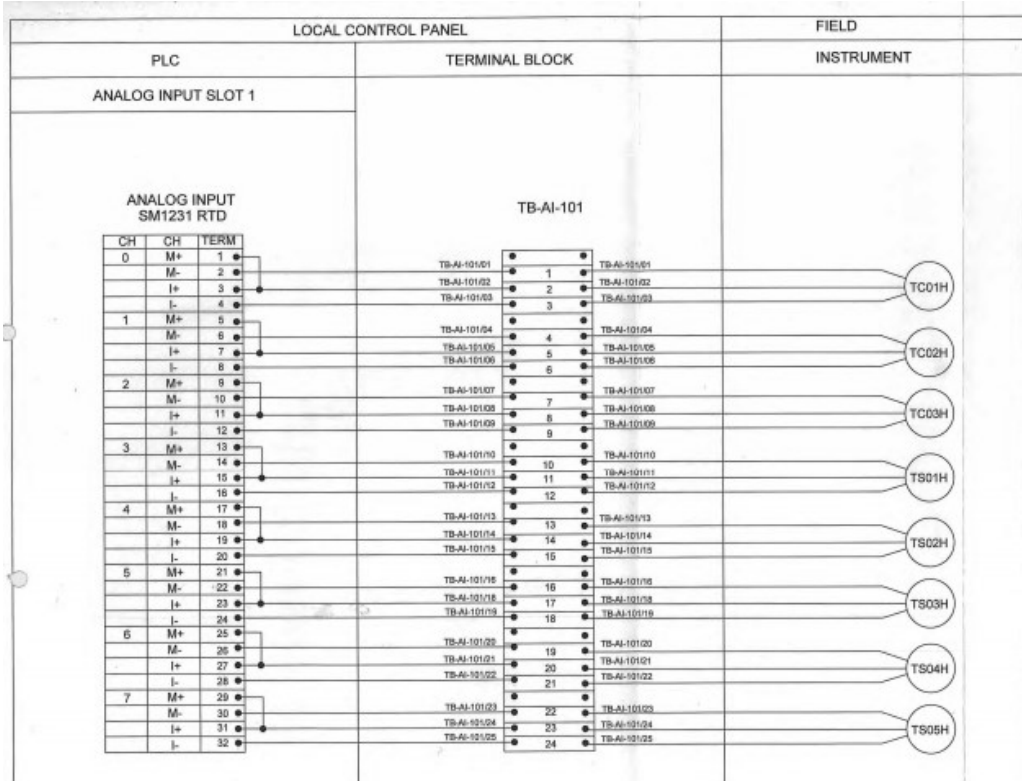
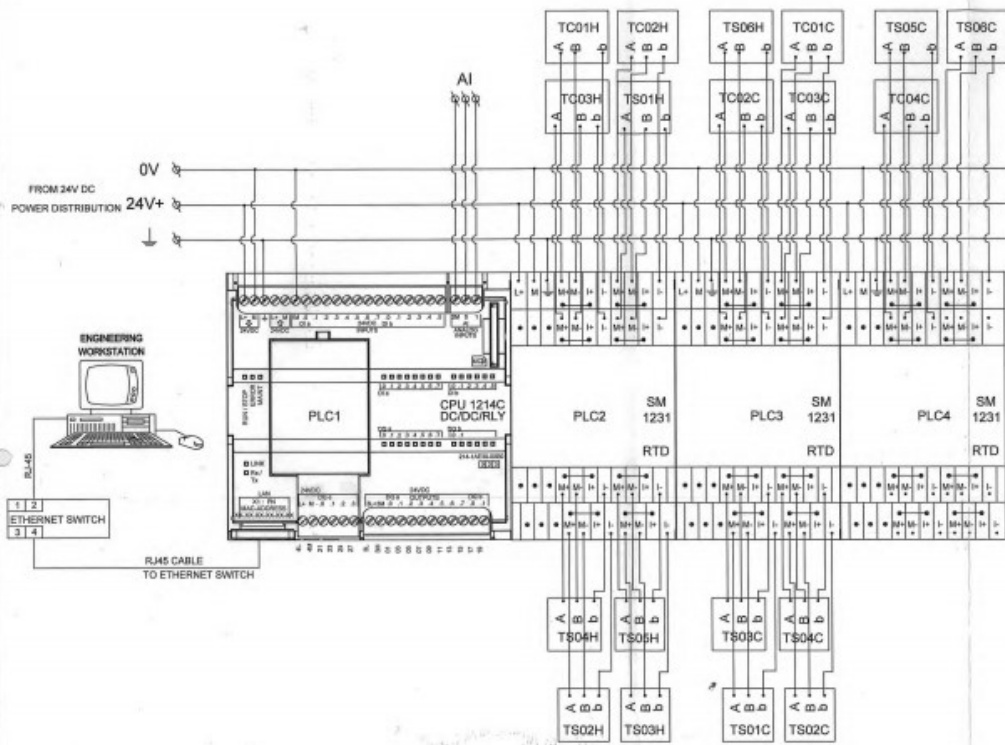


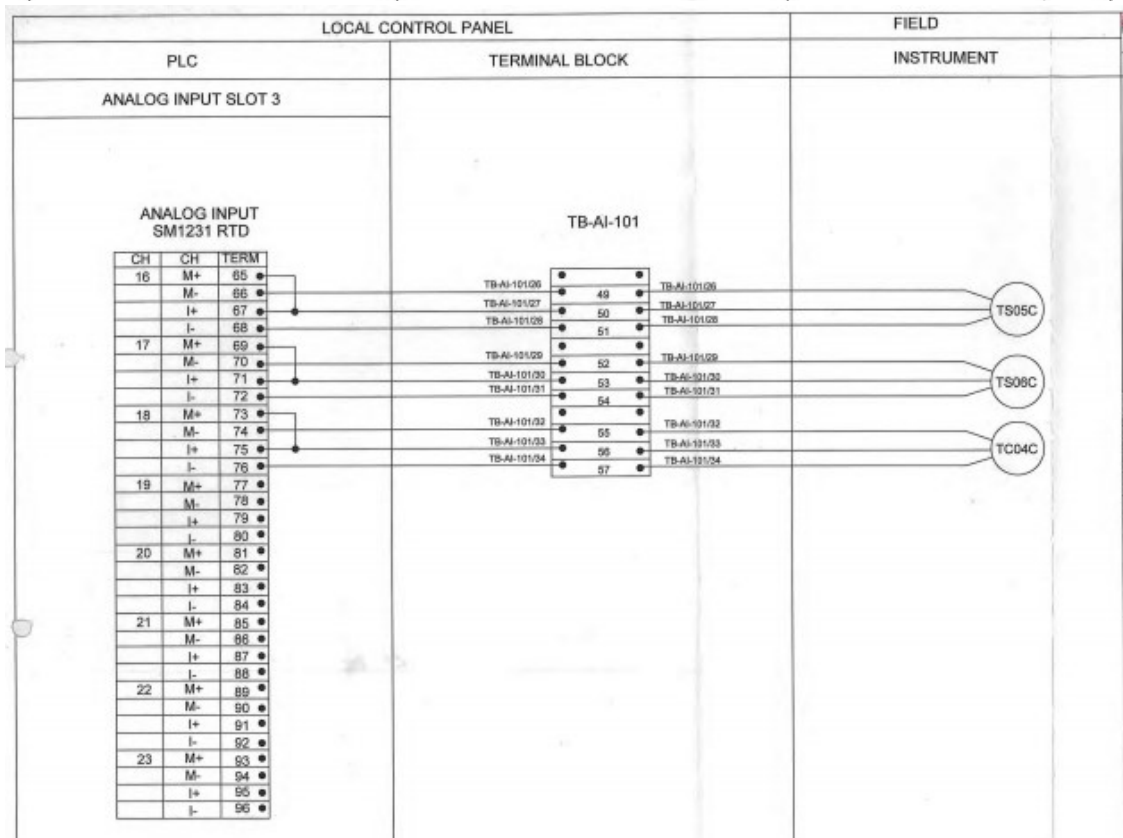
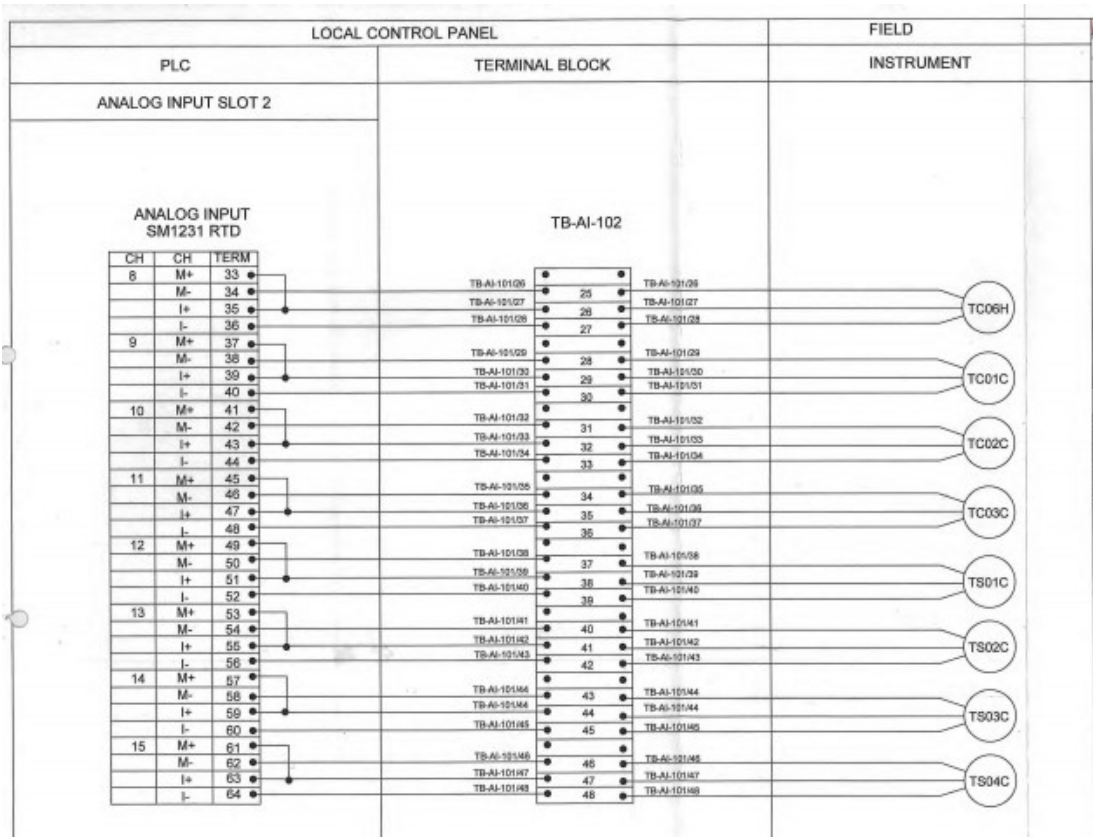
INTERNAL FRONT VIEW

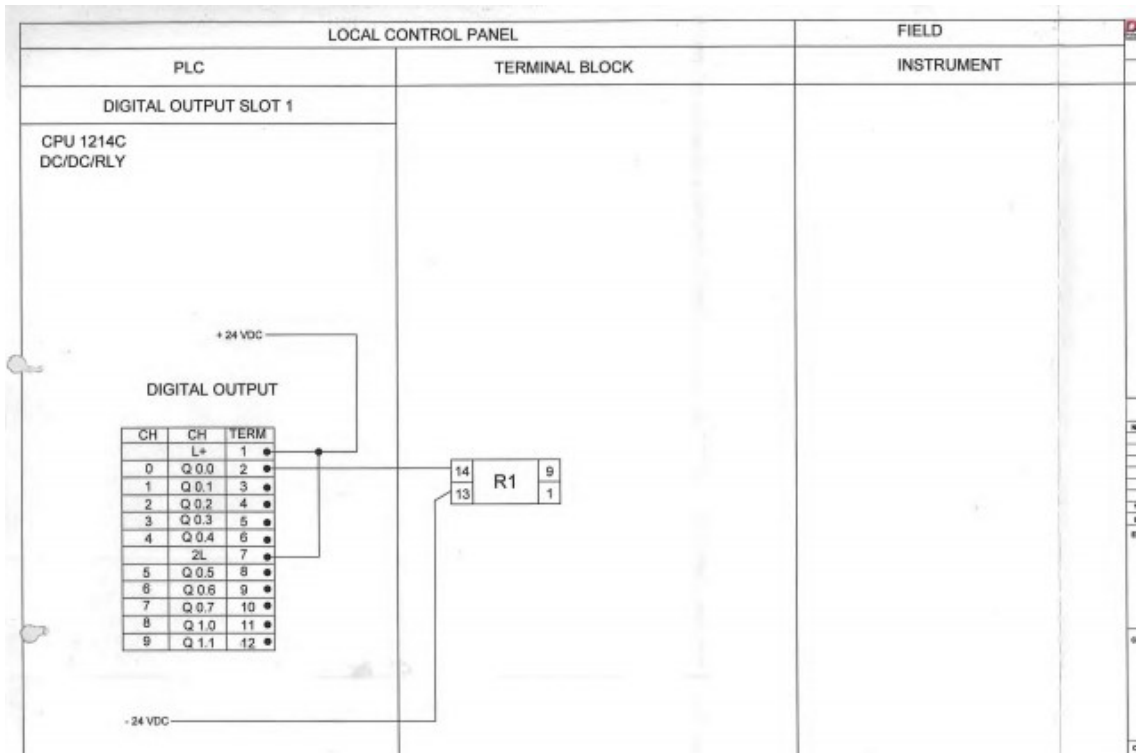
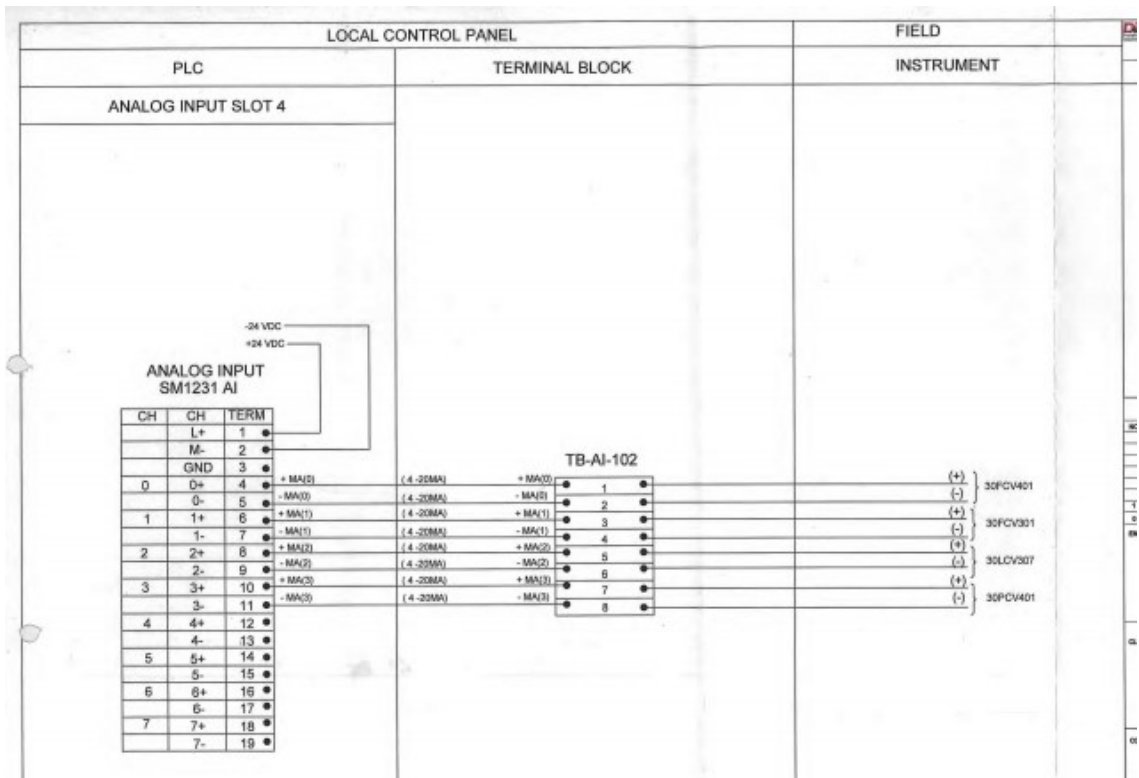
POWER DISTRIBUTION



PLC OVERVIEW







Appendix B: Data Acquisition and control in LabVIEW program

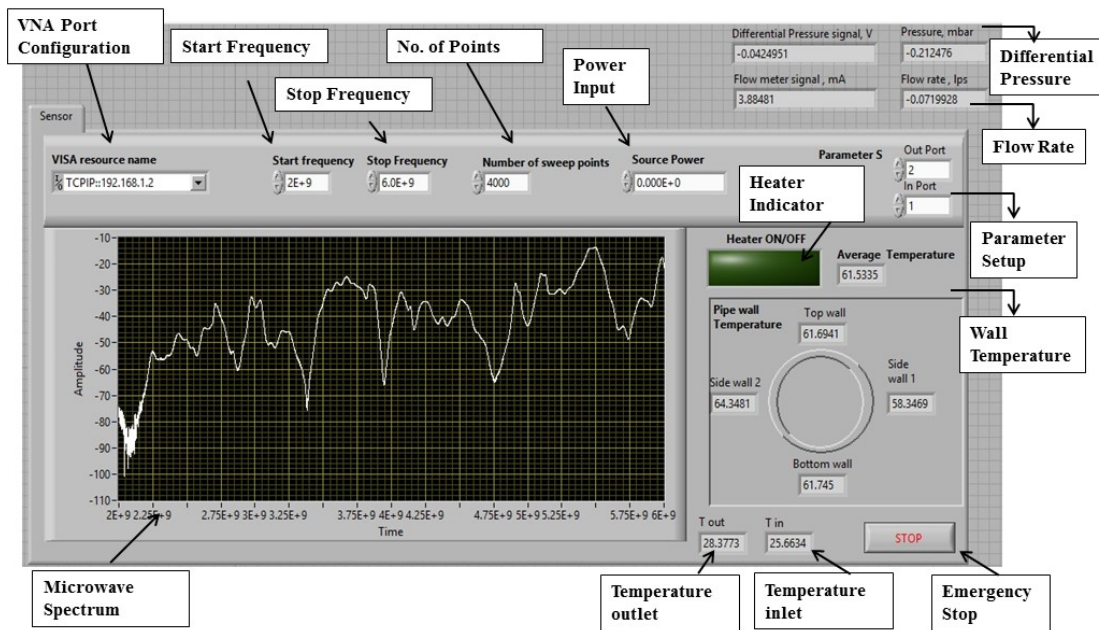


Figure B1: LabVIEW for data acquisition

Data has been displayed and collected via LabVIEW as indicated in Figure B1. Vector Network Analyser has been connected to workstation via cross over Ethernet cable. On top of that, thermocouples embedded around the test section wall, inlet and outlet were connected via Ni-DAQ unit (NI-9211). Differential pressure transmitter was connected via NI-9205 by transmitting 0-10V for data acquisition. Whereas flow meter transmitting 4-20mA output. On the other hand, heater is connected via NI-9401 to perform the control for constant wall temperature by the average temperature around the test section wall.

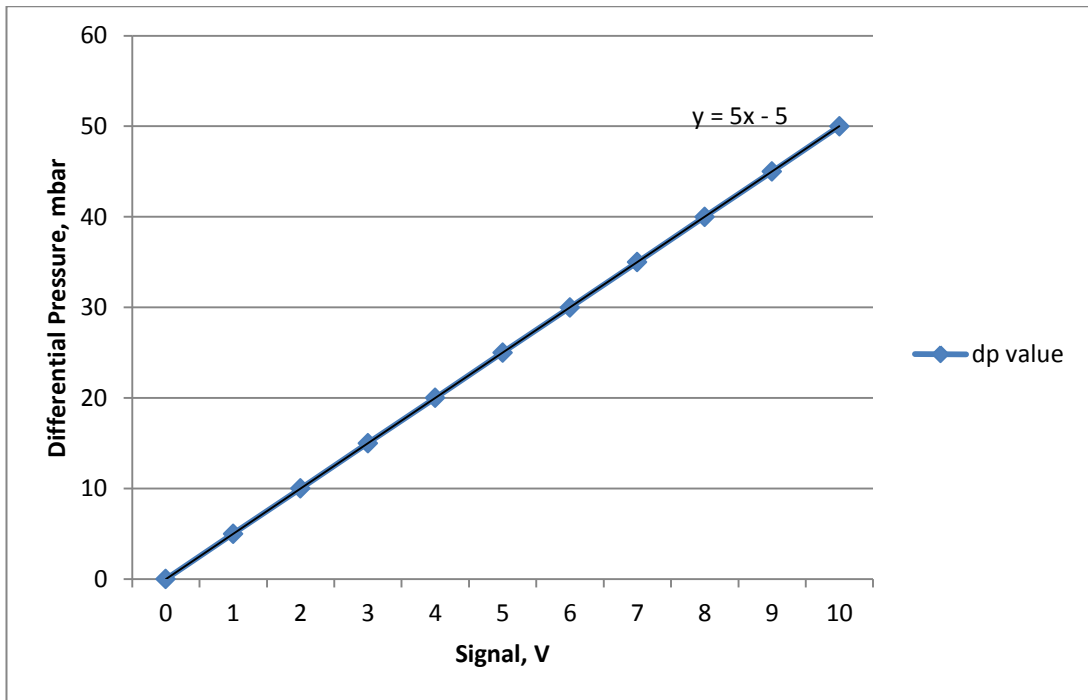


Figure B2: Differential pressure mbar as a function of voltage for differential pressure transducer used in two phase flow test rig.

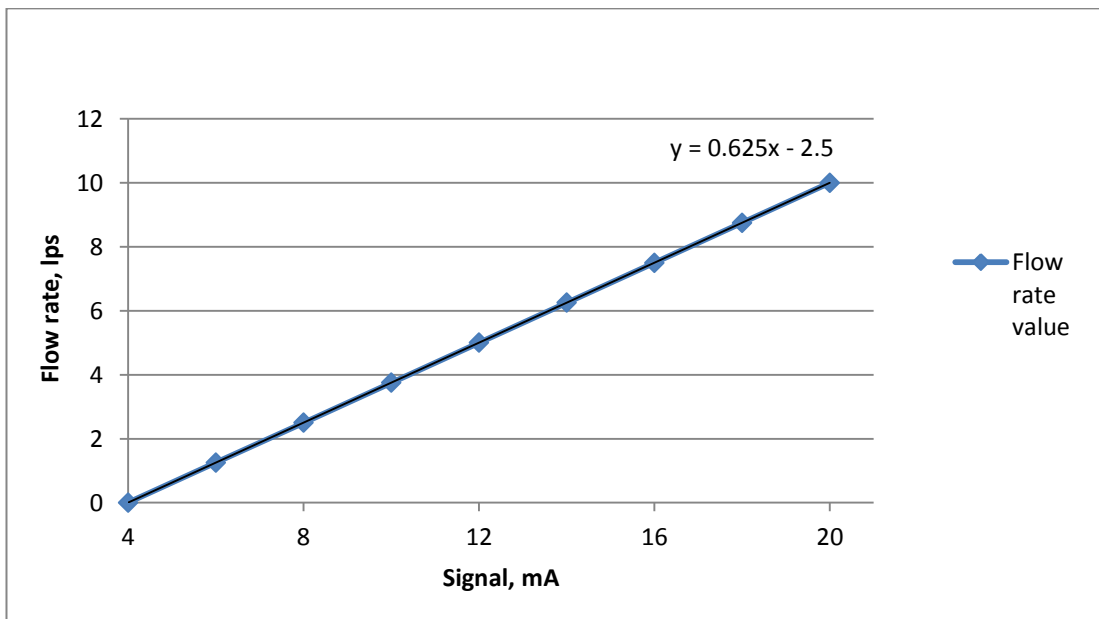


Figure B3: Flow rate lps as a function of mA for flow meter used in two phase flow test rig.

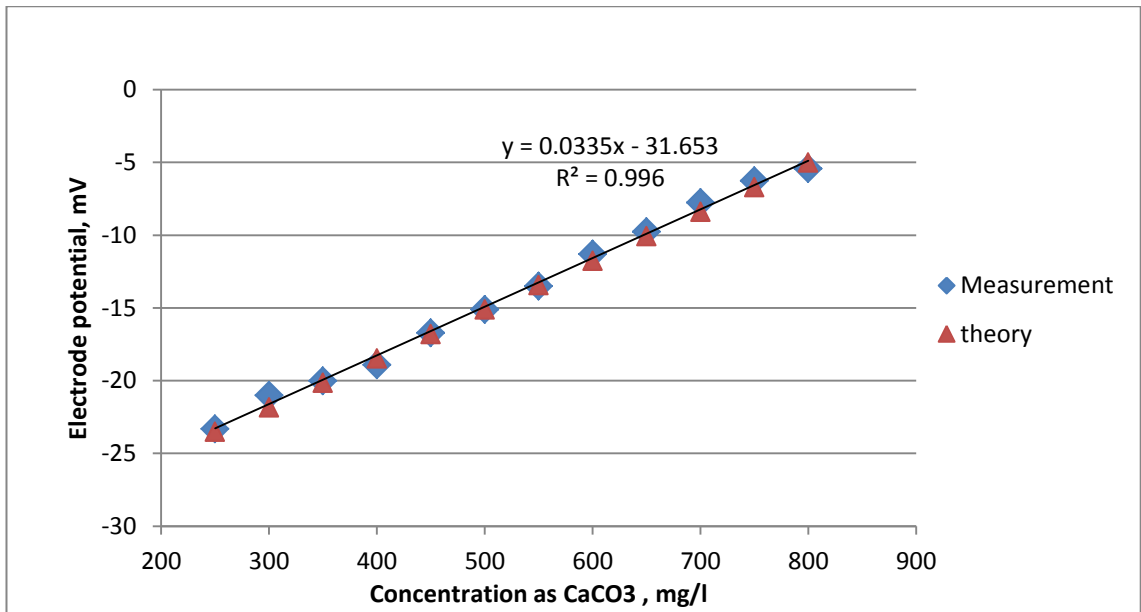


Figure B4: Concentration in mg/l as a function of mV for detection of calcium carbonate concentration in two phase flow test rig.

Figures B2 and B3 show the calibration of transmitted signal for pressure and flow rate respectively. In addition, Figure B4 shows the calibration of Ca²⁺ ion selective electrode probe. The equations for best fit curve in linear form for pressure and flow rate were obtained for data acquisition.

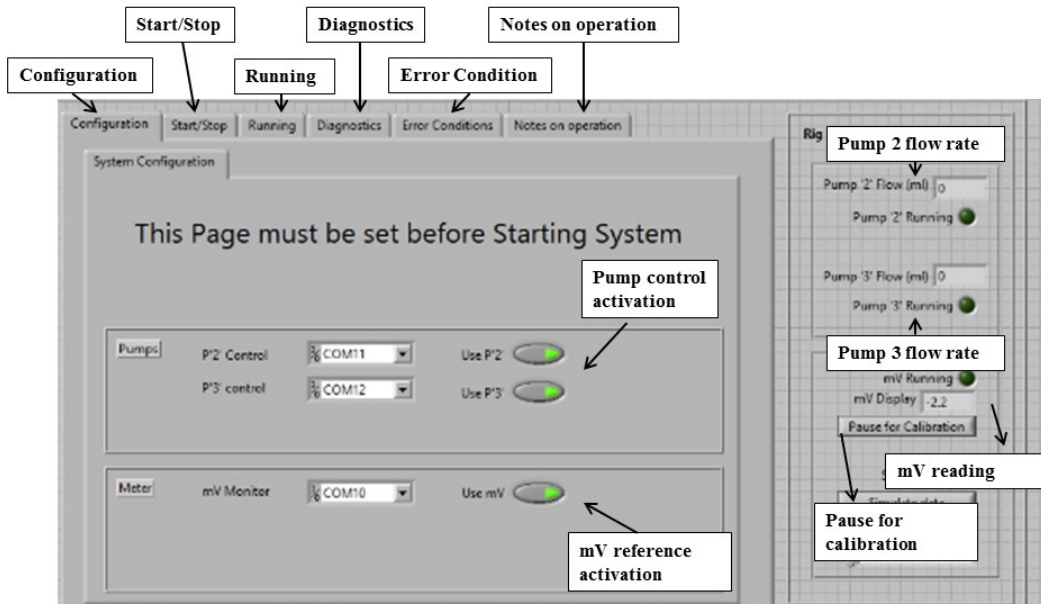


Figure B5: LabVIEW for control foulant concentration (configuration tab)

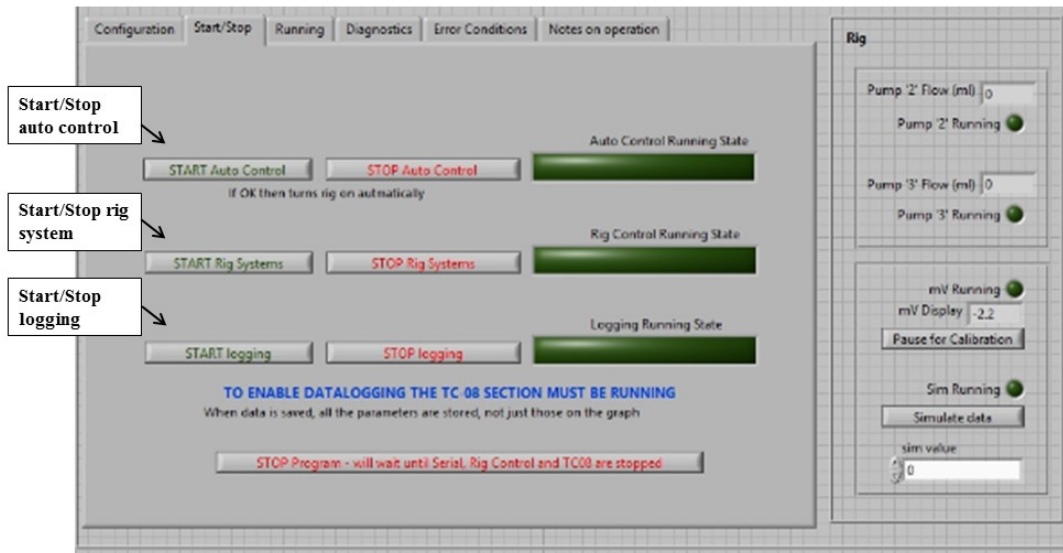


Figure B6: LabVIEW for control foulant concentration (start/stop tab)

Figures B5 and B6 demonstrated the LabVIEW interface to activate the control and logging system for foulant concentration. In addition, due to the limited operation hours of Ion Selective Electrode, the system is designed to pause during the operation for calibration purpose.

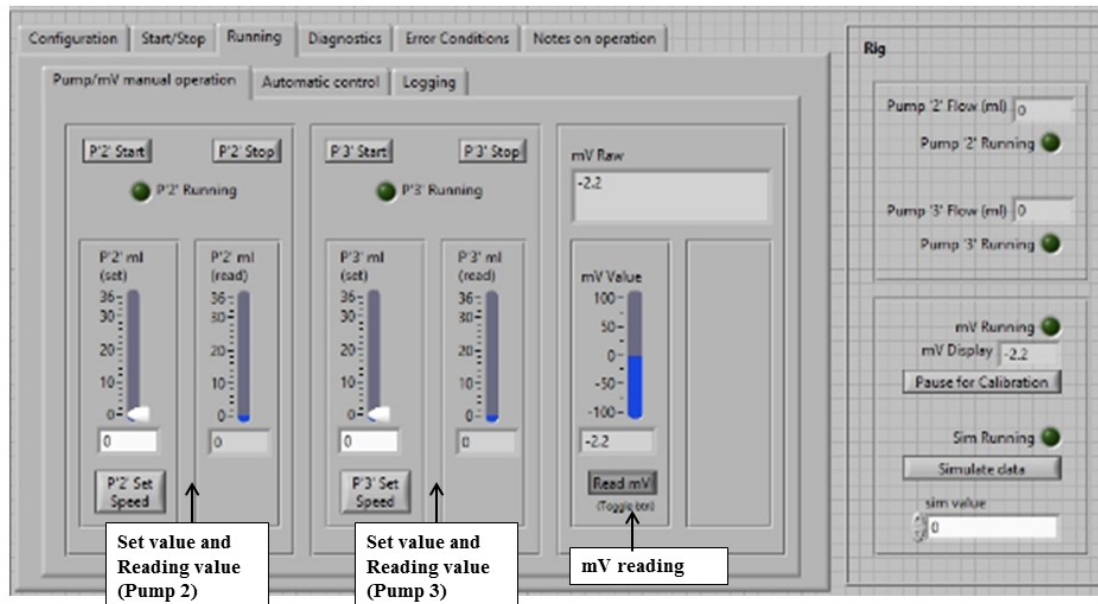


Figure B7: LabVIEW for control foulant concentration (running- Pump/mV manual operation tab)

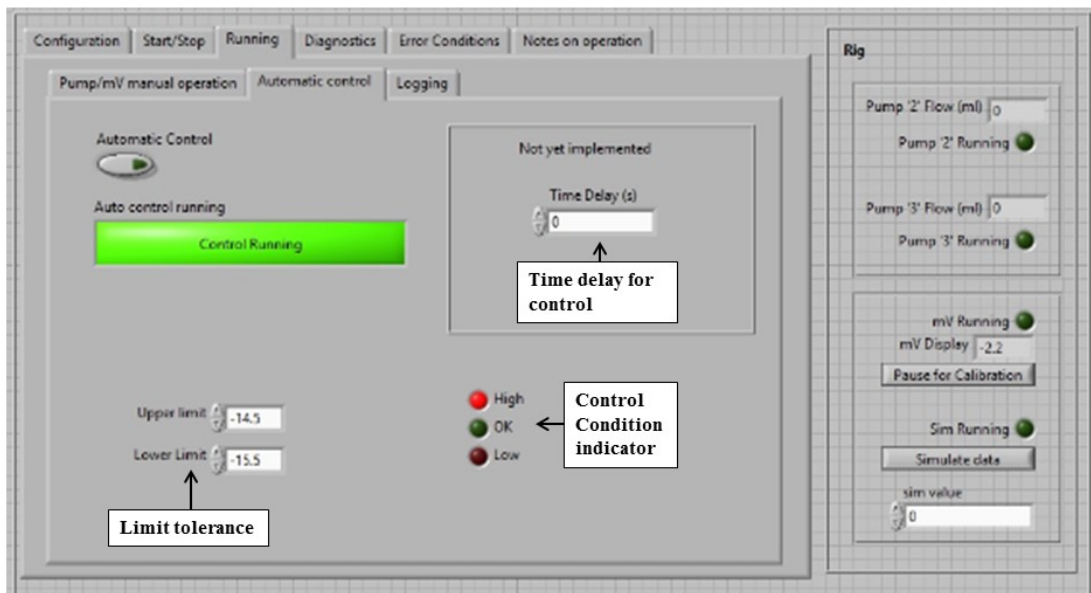


Figure B8: LabVIEW for control foulant concentration (running- Automatic control tab)

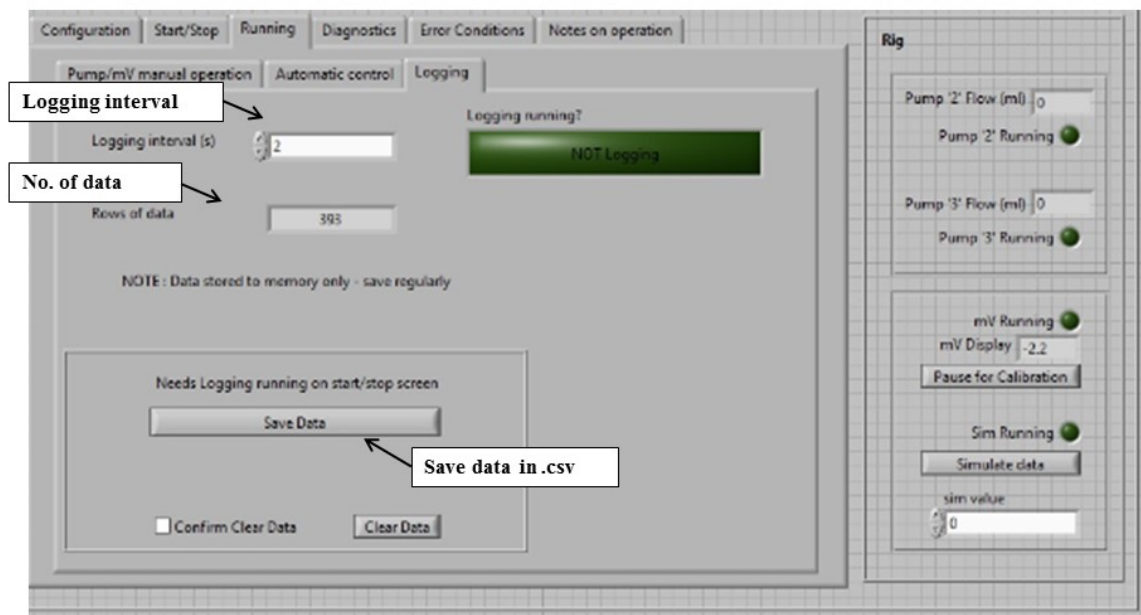


Figure B9: LabVIEW for control foulant concentration (running- Logging tab)

Figure B7 shows the display interface during the operation. It will show the flow rate for operation pump and mV detected by Ion Selective Electrode. Figure B8 illustrates the user setting for control limit of foulant concentration. Upper limit and lower limit are assigned to perform the control for constant foulant concentration throughout the

experiment. Figure B9 shows the logging setting for constant foulant concentration. All the collected data could be display in .csv file for further analysis.

Appendix C: Cleaning Procedure

After completion of each of the fouling tests, the test section will be removed and the loop will be drained completely and flushed several times to remove the remaining deposition. It is preferred in many cases to use an alternative solvent family which consists of the aqueous solution of the chelating agent. So, the agent should not have the potential to damage the equipment during or after cleaning process. Two chelating agents are used in this experiment as described in Table C1.

Table C1: List of chelating agents used in this experiments for cleaning purpose.

Chelating agent	Specification	Preparation procedure	Times of washing
Decon 90	Surface active cleaning agent and radioactive decontaminant which is suitable for laborator,, medical and industrial applications	Prepared a 2-5% solution of Decon 90 with water.	3 times
Degreaser cleaner + antifoam	Water-based formula dissolves grease and grime from almost any surface	Prepare a 4% solution with water	3 times

During the cleaning process, a steady solution temperature of 30°C was maintained. Decon 90 and Degreaser Cleaner + antifoam pumped into the system separately several times. After each run, the loops were cleaned and flushed by using filtered tap water three times and finally with DW two times, each of the duration was of 20 minutes. In order to ensure that there are no surface modifications or fouling of the system, a DW run was once again performed and compared the data with the theoretical calculated

data. Figure C1 presents the heat transfer coefficient as a function of velocity before and after cleaning runs for a DW at a bulk temperature of 25°C. It is observed that the data are reproducible and the test rig status remains highly reproducible and attains an error of < 2 %.

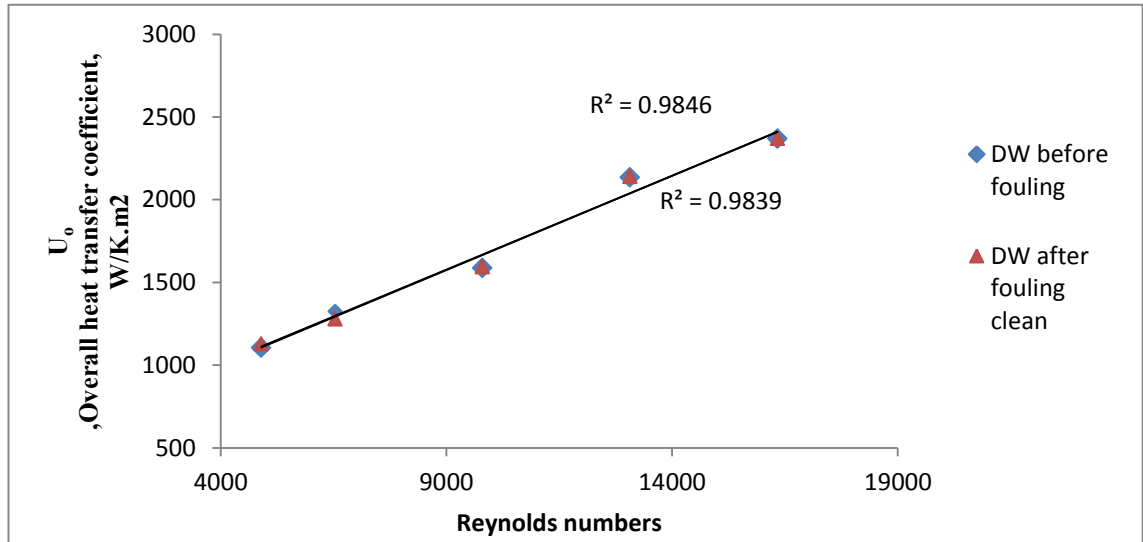


Figure C1: Variation of overall heat transfer coefficient with Reynolds numbers for DW retest.